Histopathological correlates of the biological variation in primary melanomas

Sally Jane O'Shea

Submitted in accordance with the requirements for the degree of Doctor of Philosophy

The University of Leeds

School of Medicine

Faculty of Medicine and Health

December 2016

The candidate confirms that the work submitted is her own, except where work which has formed part of jointly authored publications has been included. The contribution of the candidate and the other authors to this work has been explicitly indicated below. The candidate confirms that appropriate credit has been given within the thesis where reference has been made to the work of others.

Chapter 6 contains work from the following jointly authored publications:

Histopathology of melanocytic lesions in a family with an inherited BAP1 mutation. **O'Shea, SJ***, Mitra, A, Graham, JL, Charlton, R, Adlard, J, Merchant, W and Newton-Bishop, JA. Journal of Cutaneous Pathology 2016; 43(3): 287-289.
* first author

I wrote the paper, performed the literature review and summarised the clinical histories. I also performed a detailed histopathology review of the melanocytic lesions in the proband and family members and I interpreted the results.

Dr Angana Mitra, consultant dermatologist, obtained written informed consent for publication from the patients and contributed to the paper. Dr Will Merchant provided histopathology training, provided access to and reviewed the H&E sections, and contributed to the paper. Prof. Julia Newton-Bishop contributed to the paper. Dr Julian Adlard and Dr Ruth Charlton performed genetic testing. Dr Jennifer Louise Graham helped to capture the photomicrographs.

A population-based analysis of germline BAP1 mutations in melanoma. **O'Shea, SJ***, Robles-Espinoza, CD*, McLellan, L*, Harrigan, J, Jacq, X, Hewinson, J, Iyer, V, Merchant, W, Elliott, F, Harland, M, Bishop, DT, Newton-Bishop, JA and Adams, DJ. Human Molecular Genetics. 2017. 26(4):717–728.

* joint first author

I wrote the paper, performed a literature review and summarised the case histories. I performed the histopathological review of all of the cases reported, the statistical analyses of the associations between the histopathological appearances and the *BAP1* variants and cancer history data and I interpreted the data.

Dr Daniela Robles-Espinoza performed the statistical analyses of *BAP1* variants identified by SIFT and PolyPhen-2 in cases and controls, interpreted the data and contributed to the paper. Laura McLellan, Jeanine Harrigan and James Hewinson performed experiments. Vivek Iyer, Jeanine Harrigan and Dr Mark Harland performed analyses of *BAP1* variants in cases and controls. Dr Will Merchant provided histopathology training and reviewed the 9 cases with *BAP1* variants that were predicted to be deleterious. Faye Elliott provided statistical training and assisted in

statistical analyses. Xavier Jacq, Prof. D. Tim Bishop, Prof. Julia Newton-Bishop and Dr David Adams interpreted the data and contributed to the paper. Joanne Gascoyne compiled the cancer history data and drew the pedigrees. Deubiquitinase assays were performed by the team at the Sanger Institute, in collaboration with MISSION Therapeutics©.

Acknowledgements

Participants in the Leeds Melanoma Cohort (MREC 01/3/057) Study have been recruited since 2000 and ethical approval had already been granted before I started my PhD. I was involved in recent protocol amendments and subsequent applications for ethical approval.

I am very grateful to my colleagues in the Section of Epidemiology and Biostatistics Group who had previously recorded clinical data, taken histology sections from formalin-fixed paraffin embedded (FFPE) melanoma tumour blocks and stained them with haematoxylin and eosin (H&E), taken tissue microarray (TMA) cores and generated data on gene expression and tumour mutation status.

Statistical training was provided by Faye Elliott, statistician. Dr Jon Laye, senior research scientist, and Minttu Polso, research technician, provided training in histology sectioning, H&E staining, TMA sampling and RNA and DNA extraction. Dr Will Merchant, consultant dermatopathologist, provided histopathology training, reviewed some of the cases reported in the interobserver agreement analyses (Pathologist B, Chapter 3) and assessed cases where queries arose. Dr Sara Edwards had previously recorded a histopathology review using the Prof. Cook protocol and these data were analysed for interobserver agreement analyses (Pathologist A, Chapter 3). Minttu Polso and Tracey Mell, research technicians, assisted in the preparation of H&E slides for virtual pathology scanning. Michael Hale generated virtual pathology images from melanoma H&E research slides. Dr Darren Treanor, consultant histopathologist, provided access to and training in virtual pathology. Alex Wright, PhD student, provided training in and access to RandomSpot©.

I performed a detailed review of the melanoma H&E sections presented in this report: using the Prof. Cook protocol initially and then a virtual pathology protocol, which I developed in collaboration with my supervisors and Dr Treanor. I used a flatbed scanner to record the locations of black markings that corresponded to regions sampled using TMA biopsy needles. I annotated virtual pathology images and recorded a detailed histopathological review of primary melanoma tumours and of regions of the tumour from which TMA cores were taken for gene expression.

I undertook all of the statistical analyses reported, except where highlighted, with assistance from Faye Elliott, statistician. Faye Elliott performed the statistical analysis of the association between *BRAF/NRAS* mutation status and histological subtype and helped to format the tables presented in Chapter 5. Ernest Mangantig provided code for the transposition of data using R. Dr Jeremie Nsengimana, statistician, provided training in Cluster 3.0 and MetaCore™. I performed all of the unsupervised hierarchical

clustering analyses (except where highlighted) and MetaCore™ enrichment analyses of the transcriptomic data. Dr Jeremie Nsengimana performed unsupervised clustering of the immunome genes and generated the ESTIMATE scores using R. I used these data for analyses of the association between the ESTIMATE scores, the immunome and the percentage of stroma.

Joanne Gascoyne recorded cancer history data for the Leeds Melanoma Cohort Study, which I used for analyses in Chapter 6**,** and drew the pedigree presented in Chapter 6. May Chan, data manager, designed and patiently amended the FileMaker Pro© databases as they evolved, which I used to record my histopathology review. May Chan also extracted data from these databases, which I used for statistical analyses. I thank her for her kindness and support. Dr Jennifer Graham helped to capture photomicrographs of some of the histology images presented in Chapter 6. Dr David Adams, Senior Group Leader at the Sanger Institute, and his team performed sequencing of blood-derived DNA for the analysis of *BAP1* variants and SIFT and PolyPhen-2 analyses (presented in Chapter 6). Deubiquitinase assays were performed by the team at the Sanger Institute, in collaboration with MISSION Therapeutics© (Chapter 6).

I thank Dr Juliette Randerson-Moor for her assistance with proofreading and formatting my thesis, helping to salvage a corrupt file and for providing sound advice and encouragement.

I thank Cancer Research UK for funding this work. I thank Prof. D. Tim Bishop and Prof. Julia Newton-Bishop for taking a chance on me and for their kindness and support during my PhD. Thank you to Dr Jon Laye for his words of wisdom and encouragement. I thank each of my supervisors for providing feedback on my thesis. I thank Faye Elliott for her kindness and support, for crosschecking table entries and for providing feedback on my thesis.

I thank my parents and my family for their support, love and inspiration and for always believing in me. I thank my Dad, Barry, who taught me that I could achieve anything that I put my mind to. I thank my Mum, Karmen, for providing me with the practical support to do this and for giving me an early taste of University life. I thank my Dad, Barry, for visiting and helping me in Leeds when I needed him. I thank each of my siblings, Susan, Carol, Shelley, Kenneth, Bryan, Shane and Luke, for their support, love and friendship. I thank all of the people who have educated and supported me and enriched my life. I thank Mum, Dad, Shane, and Sharon O'Sullivan for proofreading my thesis.

I thank the patients for their inspiration, generosity in participating in research and for the privilege of reviewing their histology and histories. I hope this research will benefit people diagnosed with melanoma.

Abstract

Primary cutaneous melanoma is a highly heterogeneous tumour. My hypothesis is that the histopathological heterogeneity reflects biological variation, which is likely to have prognostic and predictive significance.

A histopathological review of 798 primary melanomas from the Leeds Melanoma Cohort Study was recorded using virtual pathology. The tumour blocks had previously been sampled using a tissue microarray needle, yielding a core from which RNA was extracted and assayed using Illumina® WG-DASL. This provided the opportunity to compare histopathological characteristics with gene expression data derived from consistently sampled regions. RandomSpot© was used to estimate the percentage of stroma (POS) within cored regions. Statistical analyses were performed using STATA v14.2. Inter- and intraobserver agreement were analysed and robust measures were retained.

Histopathological characteristics were analysed with respect to germline *BAP1* mutation status to assess whether they could predict germline *BAP1* mutation status. *BAP*-like histopathology was not significantly associated with germline *BAP1* mutation status (deleterious versus none, Fisher's exact test, p=0.1). A personal history of mesothelioma (Fisher's exact test, p=0.005), or a family history of meningioma (Fisher's exact test, p=0.005) or BCC (Fisher's exact test, p=0.02) was associated with deleterious, germline *BAP1* mutations. Cancer history appeared to be a better indicator of germline *BAP1* mutation status than *BAP*-like histopathology.

Several histopathological factors were predictive of melanoma-specific survival, including the POS. The area under the curve increased by 3% when the POS and AJCC stage were combined in ROC curve analysis. The POS was an independent predictor of melanoma-specific survival (HR 0.99, 95% CI 0.98-0.99, Cox proportional hazards model, p=0.005), even adjusting for known prognostic factors. *SDF1* gene expression was significantly associated with the POS and was independently protective for melanoma-specific death (HR 0.8, 95% CI 0.68-0.94, Cox proportional hazards model, p=0.005) in adjusted analyses. The POS and *SDF1* could represent novel predictive and prognostic biomarkers.

Table of Contents

Table of Figures

Table of Tables

Abbreviations

95% CI	95 per cent Confidence Interval
ABCDE	Asymmetry, Border, Colour, Diameter, Evolution
aCGH	Array-based Comparative Genomic Hybridization
AJCC	American Joint Committee on Cancer
AKT	Protein Kinase B
ALK	Anaplastic Lymphoma Kinase
ALK^{ATI}	ALK Alternative Transcriptional Initiation
ASXL1	Additional Sex combs Like 1
ATM	Ataxia Telangiectasia Mutated
BAD	Bcl2-Associated Death promoter
BAP1	BRCA1 Associated Protein-1
BARD1	BRCA1-Associated RING Domain protein 1
BCC	Basal Cell Carcinoma
BCG	Bacillus-Calmette-Guerin vaccine
BRAF	V-Raf murine sarcoma viral oncogene homolog B
BRCA1	Breast Cancer 1
C2ORF61	Chromosome 2 Open Reading Frame 61
CAF	Cancer-Associated Fibroblast
cAMP	Cyclic adenosine monophosphate
CD3	Cluster of Differentiation 3
CD34	Cluster of Differentiation 34
CD45	Cluster of Differentiation 45
cFos	Fos proto-oncogene
cJun	Jun proto-oncogene
CLIP1	CAP-GLY domain containing Linker Protein 1
COSD	Cancer Outcomes and Services Data set
CRYM	Crystallin Mu
CTLA4	Cytotoxic T Lymphocyte-Associated protein 4
CXCL12	C-X-C motif chemokine ligand 12
CXCR4	C-X-C chemokine Receptor type 4

CXCR7	C-X-C chemokine Receptor type 7
D2-40	Anti-D240 antibody (Podoplanin)
DASL	cDNA-mediated Annealing, Selection, extension and Ligation
DCTN1	Dynactin subunit 1
DNA	Deoxyribonucleic acid
E2F	E2F family of transcription factors
E2F1	E2F Transcription Factor 1
ECM	Extracellular Matrix
EML4	Echinoderm Microtubule Associated Protein Like 4
ENT	Ear, Nose and Throat
ESTIMATE	Estimation of STromal and Immune cells in MAlignant Tumours using Expression data
FAP	Fibroblast Activation Protein-alpha
FDR	False Discovery Rate
FFPE	Formalin-Fixed, Paraffin-Embedded
FISH	Fluorescence In Situ Hybridisation
FOXP3	Forkhead Box P3
FYN	Gene which encodes Fyn, a tyrosine kinase
GTF3C2	General Transcription Factor IIIC Subunit 2
H&E	Haematoxylin and Eosin
H2A	Histone 2A
H2A-Ub	Ubiquityl Histone 2A
H3	Histone 3
H4	Histone 4
HCFC1	Host Cell Factor C1
HPF	High Power Field
HR	Hazard Ratio
HRAS	Harvey Rat Sarcoma viral oncogene homolog
HRT	Hormone Replacement Therapy
IFN	Interferon-alpha
IHC	Immunohistochemistry
IL	Interleukin

IL-6	Interleukin-6
JPEG	Joint Photographic Experts Group
KCNQ5	Potassium voltage-gated Channel KQT-like subfamily member 5
KIT	Mast/stem cell growth factor receptor (also known as CD117)
LCK	Lymphocyte-specific protein tyrosine kinase
LDH	Lactate Dehydrogenase
LMC	Leeds Melanoma Cohort
LOF	Loss-Of-Function
LOH	Loss Of Heterozygosity
LYN	LCK/YES Novel tyrosine kinase
MAPK	Mitogen-Activated Protein Kinase
MBAITs	Melanocytic *BAP1*-mutated Atypical Intradermal Tumours
MELTUMP	Melanocytic Tumour of Uncertain Malignant Potential
MET	MET proto-oncogene, receptor tyrosine kinase
MIA	Melanoma Institute of Australia
MITF	Microphthalmia-associated Transcription Factor
mm	Millimetre
MPATH-Dx	Melanocytic Pathology Assessment Tool and Hierarchy for Diagnosis
MREC	Medical Research and Ethics Committee
MRI	Magnetic Resonance Imaging
mRNA	Messenger RNA
MSH	Melanocyte Stimulating Hormone
mTOR	Mammalian Target Of Rapamycin
N	Number of cases
NA	Not Applicable
NC	Not Calculable
NEMMPs	Nevoid Melanoma-like Melanocytic Proliferations
NF1	Neurofibromin 1
NFKB	Nuclear Factor Kappa-light-chain-enhancer of activated B cells
NMP1	Nuclear Matrix Protein 1
NRAS	Neuroblastoma RAS viral oncogene homolog

NTRK1	Neurotropic receptor Tyrosine Kinase 1
NTRK3	Neurotropic receptor Tyrosine Kinase 3
OCP	Oral Contraceptive Pill
ONS	Office for National Statistics
OS	Overall Survival
P53	Tumour protein P53
PD1	Programmed cell Death 1
PDL1	Programmed Death Ligand 1
pHH3	Phosphohistone H3 antibody
PI3K	Phosphatidylinositol-3-kinase
PKA	Protein Kinase A
PKN	Protein Kinase N
POS	Percentage Of Stroma
PRC1	Polycomb Repressive Complex 1
PRC2	Polycomb Repressive Complex 2
PTEN	Phosphatase and Tensin homolog
RAD51	RAD51 recombinase
RET	RET proto-oncogene (rearranged during transfection)
RFS	Relapse-Free Survival
Rho	Spearman correlation coefficient
RNA	Ribonucleic acid
ROC curve	Receiver Operator Characteristic curve
ROS1	ROS proto-oncogene 1, receptor tyrosine kinase
RT-PCR	Reverse Transcription-Polymerase Chain Reaction
SD	Standard Deviation
SDF1	Stromal cell-Derived Factor 1
SFRP2	Secreted Frizzled-Related Protein 2
SIFT	Sorting Intolerant From Tolerant
SNB (SLNB)	Sentinel (Lymph) Node Biopsy
STRN	Striatin
STUMP	Spitzoid Tumour of Uncertain Malignant Potential

SVD	Singular Value Decomposition
SVS	The file format for digital images that is generated by scanning slides using the Aperio AT2® scanner
SYK	Spleen-associated tyrosine kinase
TCGA	The Cancer Genome Atlas
TERT	Telomerase Reverse Transcriptase
TILs	Tumour-Infiltrating Lymphocytes
TIMs	Tumour-Infiltrating Macrophages/Melanophages
TMA	Tissue Microarray
TNM	Tumour, Node, Metastasis
TP53	Tumour protein P53
TPM1	Tropomyosin 1 alpha
TPR1	Translocated Promoter Region 1
Ub	Ubiquitin
UK	United Kingdom
USP	Ubiquitin Specific Peptidase
UVR	Ultraviolet Radiation
VEGF-A	Vascular Endothelial Growth Factor-A
VGP	Vertical Growth Phase
XML	Extensible Markup Language; an output file format for recording annotations using ImageScope©
YY1	Yin Yang 1

A table providing additional information regarding the complex histological and statistical definitions used throughout the thesis is given in Appendix A.

Chapter 1 Introduction

1.1 Cutaneous melanoma

Cutaneous melanoma is a form of skin cancer that develops from melanocytes, the pigment-producing cells of the skin. Normal melanocytes predominantly reside in the basal layer of the epidermis [1]. Skin cancer prevention is a considerable public health concern, with 15419 new cases of melanoma diagnosed in 2014 in the United Kingdom (UK) and a rising incidence, especially in people over the age of 60 [2, 3]. Cancer among young people is unusual but melanoma is indiscriminate of age after puberty. Between 2012 and 2014, an estimated 50% of cases were diagnosed in those aged 65 years and older in the UK [2].

Melanoma is a complex and diverse condition. There is remarkable variability in its clinical presentation: some being pigmented and flat while others are amelanotic and exophytic. It stands to reason that the biology of these tumours could be different.

1.2 The clinical diversity of melanoma

The most frequent presentation of primary cutaneous melanoma is of a changing mole (naevus) with one or more of the following features: asymmetry, change of colour, shape or size, bleeding or itch. Indeed, this is the basis of the Asymmetry Border Colour Diameter Evolution (ABCDE) public health awareness campaign [4]. These characteristics most closely relate to the commonest melanoma subtype: superficial spreading melanoma rather than nodular and amelanotic melanomas. It is the tendency of melanoma to “stand out from the crowd” (relative to benign naevi) that facilitates its clinical diagnosis.

Multiple factors lead a pathologist to suspect melanoma upon microscopic examination, including the relative absence of benign features, e.g. lack of uniform nuclei and maturation [5]. Atypical features are also variably present: asymmetrical architecture, abnormal melanocytes spreading upwards through the epidermis (“pagetoid spread”), variability of the size and shape of nuclei (“pleomorphism”) and nuclear cell division (“mitoses”) [5].

1.3 Melanoma survival/prognosis

1.3.1 Factors associated with melanoma-specific survival

In terms of survival, age, sex and tumour site predict survival as well as histopathological characteristics of the tumour.

1.3.2 Age at diagnosis and melanoma

Melanoma onset before 20 years of age has a favourable outcome despite aggressive histopathological features and a diathesis to sentinel node metastasis [6, 7]. The worse prognosis in those aged >70 years has been attributed to a tendency to have melanomas with poor prognostic features but a lower rate of sentinel lymph node positivity and higher mortality which might imply a greater likelihood of haematogenous spread [6, 7]. Moreover, Weiss *et al.* reported that older patients were significantly more likely to be male and to have an increased risk of death due to melanoma, compared with their younger counterparts [8]. A rising incidence in melanoma has been reported, which is most marked in men aged 70 years and older [9, 10]. Advancing age has also been linked to decreased self-detection [11] and immunosenescence [12]. Furthermore, older patients are significantly less likely to have a dense immune cell infiltrate, consisting of brisk tumour-infiltrating lymphocytes, within their primary melanomas [8], suggesting a decreased ability to mount an appropriate anti-tumour response. In essence, there is evidence that older people have a worse prognosis, partly due to later presentation, although age is an independent predictor of melanoma death. Some have reported evidence that relative immune insufficiency is seen with age and that could be causal.

1.3.3 Sex disparity and melanoma

Men have been shown to be at greater risk of death from melanoma [13]. Biological differences in the type of tumour could account for some of this increased risk, e.g. men are prone to ulcerated primaries with a worse prognosis [14-16]. Conversely, mitotic count does not appear to predict sex-based differences in survival [17]. Variation in care-seeking behaviour might explain some of the sex disparity [18] but Joosse *et al.* have identified sex as an independent risk factor for melanoma death, even after lymph node metastasis [19]. Men have an increased propensity to visceral metastases [19] and a higher mutation burden in their metastases, compared with women [20]. It is well recognised that men are less likely to use sun protection [21], however, the observed differences in mutation burden cannot be attributed to

ultraviolet radiation (UVR) [20], which supports the view that genuine biological differences exist in melanomas between the sexes.

Several studies have confirmed the independent, protective effect of female sex [22-24], while others have not substantiated this finding [22, 25-27]. In a study of 1998 melanoma cases with negative sentinel lymph node biopsies, sex was not independently predictive of outcome [28]. Furthermore, Mandala *et al.* evaluated 1524 cases of localised melanoma and did not find sex to be independently predictive of either relapse or death [26].

The underlying basis for the apparent sex disparity has not been fully elucidated, although several hypotheses have been proffered. Hormonal influences, including the effect of exogenous oestrogens, in the form of the oral contraceptive pill (OCP) or hormone replacement therapy (HRT), have been explored but there are conflicting results. In a retrospective study, MacKie *et al.* noted a survival advantage for female melanoma patients who received HRT, compared with those who did not, however, ulceration was more frequent in the latter group [29]. Conversely, a meta-analysis of case-control studies of OCP use and melanoma, showed no significant difference in outcome between women who did and did not receive the OCP [30]. However, there is some evidence to suggest that the protective effect of female sex reduces after the menopause [14]. Alternative hypotheses for the sex disparity in mortality include differences in immune function, response to oxidative stress and the expression of X-linked genes but none of these studies has been conclusive [31].

1.3.4 Body site and melanoma

Historically, the most common site for melanoma has been the trunk for men and the lower limb for women [2]. Truncal primaries are becoming more common among younger females, possibly reflecting changes in fashion (and, hence, uncovered skin) or sun exposure [32]. The site of primary melanoma has been shown to be an independent predictor of outcome, with melanomas located at an axial site (trunk, head and neck) having a significantly increased risk of sentinel lymph node positivity [33] and death, compared with melanomas on the extremities [28, 34]. This is not as yet biologically understood, although it is possible that biological differences could exist between tumours located at different sites. For example, mutation status is influenced by body site, with *BRAF* mutations more frequently associated with sites of intermittent sun-exposure, *NRAS* with sites that are continuously exposed [35] and *KIT* in acral and mucosal melanomas, and some melanomas occurring on chronically-sun damaged skin [36]. However, there is little evidence that driver mutation status *per se* is a determinant of outcome [37]. Furthermore, melanomas located at acral sites tend to

have a poor prognosis [38, 39], which most likely reflects late detection, at least in part. Similarly, melanomas that occur in locations that are not readily visualised, including genital and rectal melanomas, tend to have low survival rates [40, 41].

1.3.5 Histopathological classification of melanoma

Melanoma is classified after surgical resection, by histopathological examination. Light microscopy is used to identify characteristic cellular features from cross-sectional profiles of the tumour. The distinction between radial and vertical growth phases and of *in situ* from invasive disease is of paramount importance. The established view is that the radial growth phase (RGP) precedes the vertical growth phase (VGP) in most melanomas. Vertical growth phase melanomas carry the risk of metastasis, possibly due to their proximity to blood and lymphatic vessels. Advancing thickness is also likely to reflect a more biologically aggressive tumour.

Multiple subtypes of invasive melanoma have been described, each with characteristic (and somewhat subjective) histopathological features. In addition, each subtype may well demonstrate distinct biological behaviour. For example, nodular melanoma is regarded as a more foreboding tumour, often lacking classical clinical features as discussed and tending to present thicker [42]. Superficial spreading melanomas may contain a nodular component, making subtype distinctions less clear.

1.3.6 Histopathological factors associated with prognosis

Here I describe the recognised histopathological factors impacting on survival from melanoma, some of which are incorporated into the 7th edition American Joint Committee on Cancer (AJCC) staging system (see Table 1.1) [43]. There are additional well-recognised features, e.g. cellular morphology, of unknown biological and prognostic significance.

1.3.7 Breslow thickness

Breslow thickness is a well-established, independent prognostic factor [23, 25, 26, 43, 44] and is superior to Clark's level of invasion in predicting outcome from melanoma [23]. Breslow compared the depth of invasion, tumour diameter and cross-sectional area in a cohort of 98 melanomas and established that thickness was the best predictor of outcome, with metastases developing only after a depth of 0.76mm [45]. The Breslow thickness cut-off point for stage IA (T1a N0 M0, Table 1.1) in the AJCC 7th edition staging is 1.0mm [43], however, a cut-off point of 0.8mm will be used in the forthcoming AJCC 8th edition (in press).

1.3.8 Microscopic ulceration

Microscopic ulceration is a key prognostic variable in the AJCC staging of cutaneous melanoma [43]. Although ulceration occurs more frequently in thicker tumours, it is an independent predictor of outcome and confers an increased risk of metastasis compared to non-ulcerated melanomas of equivalent thicknesses [46-49]. Higher mitotic counts have been recorded in ulcerated tumours, suggesting intrinsically aggressive behaviour [48, 49]. Recent evidence suggests an association between ulcerated primaries and sun-protected sites, nodular subtype, lymphovascular invasion, microvessel density and macrophage infiltration [49, 50].

The presence of microscopic ulceration is clearly important for prognosis; however, its detection is somewhat challenging. The Royal College of Pathologists define ulceration as “a full-thickness epidermal defect”, associated with “reactive changes” (e.g. fibrin, neutrophils) and “thinning, effacement or reactive hyperplasia of the surrounding epidermis” in the absence of trauma or surgery [51]. Yet, the distinction of true from artefactual ulceration is subject to interobserver variation [52].

In addition to its presence, the extent of ulceration appears to provide additional prognostic information but there is no consensus about the optimal cut-off point. In a study of 4661 cases, ulceration alone conferred a HR of 1.55 for melanoma-specific death, whereas for ≤5mm ulceration and >5mm ulceration, the HRs were 1.39 and 2.03, respectively [53]. By contrast, a study of 235 melanoma patients reported that ulceration of as little as 5% of the lesional diameter was hazardous [54]. Day *et al.* suggested using a cut-off point of 3mm for ulceration width, as their study of 596 patients showed no significant difference in survival between cases with ≤3mm ulceration and without ulceration [55]. In a study of 365 melanomas, the extent of the largest ulcer, type of ulceration and involvement of adjacent epidermis were recorded [56]. The extent of ulceration was expressed as a percentage of the lesional diameter and a cut-off point of 70% was used to define “minimal/moderate” and “excessive” ulceration groups [56]. Using a previously published classification, ulceration was deemed to be infiltrative when the epidermis was infiltrated and eroded by melanoma cells and as attenuative when a melanoma nodule expanded the epidermis resulting in a defect with minimal infiltration [57]. Excessive ulceration (≥70%) and attenuative type were independent risk factors for melanoma death (HR 3.57, 95%CI 2.01 - 6.36, $p<0.0001$; and HR 3.02, 95%CI 1.82 - 5.01, $p<0.0001$, respectively) and an ulceration width >3mm was significantly hazardous [56].

Table 1.1: TNM staging of melanoma (on which the 7th edition AJCC staging system is based).

Adapted from reference [43].

Primary tumor (T) Melanoma	
T1	T1a: ≤ 1.0 mm in thickness without ulceration, mitoses < 1/mm^2 T1b: ≤ 1.0 mm in thickness with ulceration or mitoses ≥ 1/mm^2
T2	T2a: 1.01-2.0 mm in thickness without ulceration T2b: 1.01-2.0 mm in thickness with ulceration
T3	T3a: 2.01-4.0 mm in thickness without ulceration T3b: 2.01-4.0 mm in thickness with ulceration
T4	T4a: >4.0 mm in thickness without ulceration T4b: >4.0 mm in thickness with ulceration
Regional lymph nodes (N)	
N0	No regional metastases detected
N1	N1a: Micrometastases in one lymph node N1b: Macrometastases in one lymph node
N2	N2a: Micrometastases in 2-3 lymph nodes N2b: Macrometastases in 2-3 lymph nodes N2c: In-transit metastases/satellites without metastatic lymph nodes
N3	≥ 4 metastatic lymph nodes, or matted lymph nodes, or in-transit metastases/satellites with metastatic lymph node(s)
Distant metastasis (M)	
M0	No evidence of distant metastases
M1a	Metastases to the skin, subcutaneous tissue, or distant lymph nodes, normal serum lactate dehydrogenase (LDH) level
M1b	Lung metastases, normal LDH level
M1c	Metastases to all other visceral sites or distant metastases to any site combined with an elevated serum LDH level

1.3.9 Mitotic count

For primary melanomas, a mitotic count (as measured by counting the presence of mitotic figures within tumour nuclei) of ≥1/mm^2 has been found to be an independent, poor prognostic factor for stage I melanoma (T1b N0 M0, Table 1.1) [43]. This forms part of the AJCC 7th edition staging, to stratify tumours with a thickness of ≤1mm (Table 1.1) [43], although no longer a criterion to define stage IB (T1b N0 M0, Table 1.1), in the forthcoming AJCC 8th edition (in press).

Several studies have explored the optimum cut-off point for mitotic count and whether it might also provide additional prognostic information for thicker melanomas. Roach *et al.* analysed mitotic count in 551 melanomas >1mm thick and found that the presence ≥6 mitoses was associated with an increased risk of relapse and death, although it was not an independent predictor [58]. In a study of 313 T2 melanomas with negative sentinel lymph node biopsies, Baker *et al.* reported that a mitotic count ≥1 was significantly hazardous for melanoma relapse and death [59]. However, Speijers *et al.* explored various cut-off points and analysed mitotic count as a continuous variable for 453 cases with a Breslow thickness >1mm and failed to show an independent effect for mitotic count [22]. Conversely, in a study of 13,296 stage I and II patients (T1a-T4b N0 M0), Thompson *et al.* reported mitotic count to be the most significant prognostic factor, after Breslow thickness, with an increasing mitotic count being significantly inversely associated with survival [23]. Recently, Mandala *et al.* reported that a mitotic count ≥3 was an independent predictor of relapse and death, compared to <3 mitoses, for melanomas >1mm in thickness (n=1524) [26]. Moreover, mitotically active tumours are less likely to have brisk tumour-infiltrating lymphocytes [26] and are more likely to be thicker and ulcerated [22, 58, 59]. The presence of mitoses is regarded to be a marker of a proliferating, aggressive tumour that is more likely to metastasise [23].

1.3.10 Tumour-infiltrating lymphocytes

Standard histopathology reporting of melanoma includes a description of tumour-infiltrating lymphocytes (TILs), derived from a classification developed by Clark *et al.* as absent, non-brisk or brisk [60] (Figure 1.1). This classification has been shown to correlate with disease-free and overall survival in some studies; brisk TILs having the best prognosis [27, 60-63]. Others have not confirmed an independent survival advantage [25, 64-67]. TILs have not been incorporated into AJCC staging [43]. Absent TILs may increase the likelihood of a positive sentinel node biopsy [24, 64] but there are conflicting results [68]. The reason for this variation is unclear but may reflect the subjective nature of the current classification. This has led to the development of alternative grading systems for TILs. In 1996, Clemente *et al.* proposed a modified

version of Clark's classification, showing a prognostic significance [61]. The Melanoma Institute of Australia (MIA) proposed a modified classification of TILs, with grades ranging from 0 to 3, incorporating the distribution and density of the infiltrate [24]. This correlated with melanoma-specific survival [24].

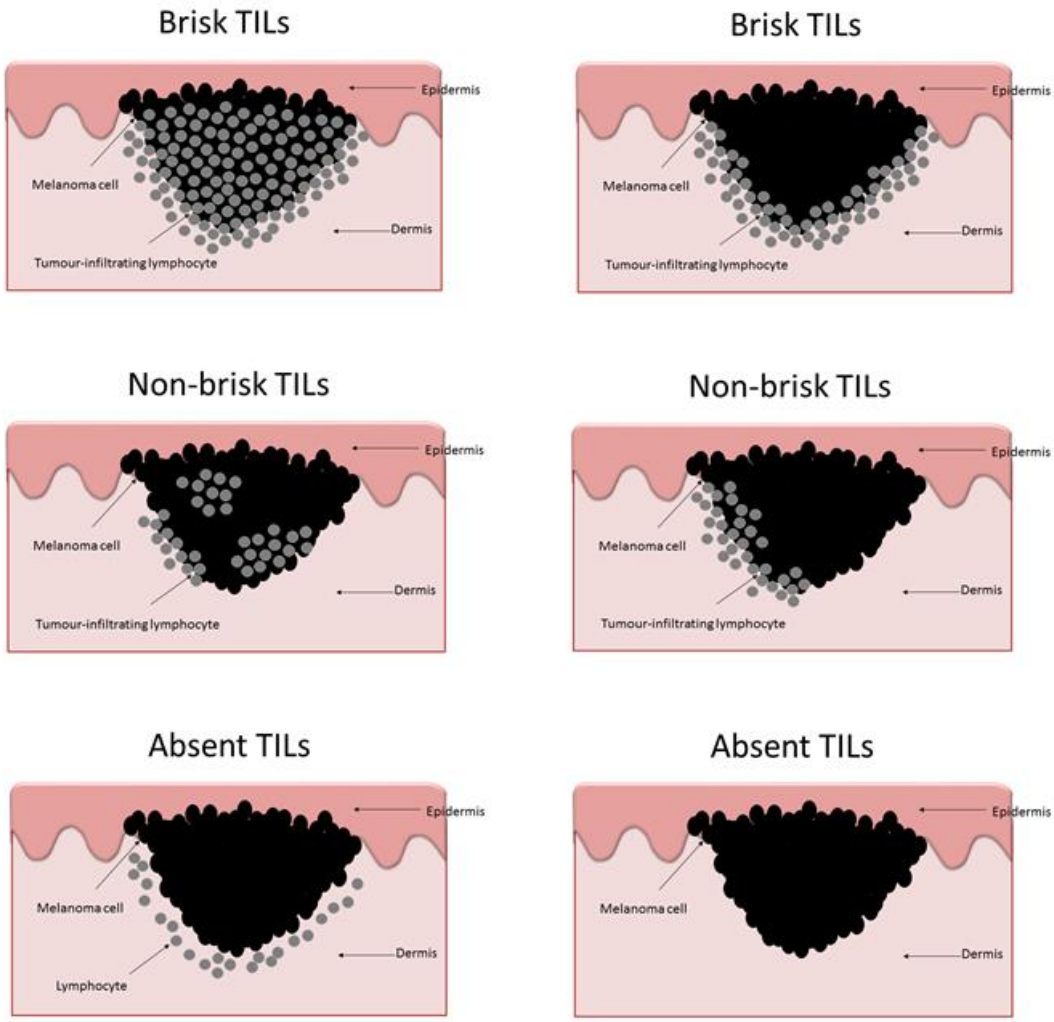

Figure 1.1: Clark's classification of tumour-infiltrating lymphocytes (TILs)

> Lymphocytes involving the radial growth phase do not have prognostic significance; therefore, to qualify as TILs, lymphocytes must surround and disrupt tumour cells in the vertical growth phase [60]

TILs have also been reported to vary according to Breslow thickness [24, 27, 33, 61, 69]. Clemente *et al.* noted that brisk TILs were most frequent in melanomas ≤2mm thick [61]. In a study of 3,330 primary melanomas from the Genes, Environment and Melanoma Study, there was an inverse association between brisk TILs and Breslow thickness [27]. Similarly, Azimi *et al.* reviewed 1865 melanomas from the MIA database and reported that a higher TIL grade was inversely associated with Breslow thickness,

ulceration and mitoses [24]. Moreover, a study of melanomas with a thickness ≥4mm or regional nodal metastases at diagnosis, did not replicate the association between TILs and survival [70].

Immunohistochemistry (IHC) is an alternative approach that can be used to quantify TILs [69]. Weiss *et al.* assessed whether or not IHC could improve the predictive power of TILs, by evaluating the immunohistochemical expression of the lymphocyte markers, CD3, CD45 and FOXP3, in 184 primary melanomas [69]. They enumerated intratumoural and peritumoural lymphocytes within one high power field of the highest regions of expression of CD3, CD45 or FOXP3 [69]. There was no independent predictive power for IHC-quantified TILs [69]. Furthermore, there was no significant difference in either the pattern of lymphocytes (absent, non-brisk and brisk) or in survival by the expression of FOXP3, a marker of inhibitory T-regulatory lymphocytes (Tregs) [69]. Moreover, the authors evaluated the transcriptomic expression of 579 immune genes in 67 melanomas and found that brisk TILs appeared to be biologically distinct, with a greater number of differentially expressed genes, compared with non-brisk and absent TILs [69]. The top biological pathways associated with brisk TILs were related to immune cell activation and cytokine signalling [69]. Therefore, the grading of the pattern of TILs by histopathologists using H&E-stained sections appears to be of superior prognostic value to IHC, although transcriptomic studies could provide further insight into the biological basis for such patterns.

1.3.11 Regression

Regression, that is the replacement of tumour cells by fibrosis and/or an immune cell infiltrate, is thought to result from host-mediated immune responses to melanoma [71, 72]. An alternative hypothesis is that regression represents a type of tumour remodelling, triggered by the accumulation of a critical burden of chromosomal abnormalities and resulting in apoptosis [73]. Although regression is reported to occur more frequently in thin melanomas, an association with poor prognostic factors, including male sex, older age at diagnosis and an axial site of primary melanoma, has also been noted [74].

The histopathological definition is variable [72, 75] and includes the presence of a mixed immune cell infiltrate composed of lymphocytes and melanophages, which may be accompanied by epidermal atrophy [76]. Kaur *et al.* described regression as a segment of melanoma that is lost and replaced by fibrosis, with evidence of increased vascularity and infiltration by melanophages and lymphocytes [77]. Zurac *et al.* classified regression as: segmentary, partial and mixed [75]. Segmentary regression was defined by the complete loss of tumour within a segment of the melanoma, while

partial regression was characterised by patchy loss of tumour cells [75]. The authors also reported a trend for regressing tumours to lack ulceration and to have a lower tumour mitotic count [75]. Furthermore, different phases of regression have been described, including an early “inflammatory” phase, which may be difficult to distinguish from TILs, and a later phase associated with dense fibrosis [76]. Moreover, others have classified regression as partial (involving <50% of the melanoma) or extensive (≥50%) [78].

The prognostic effect of regression is an area of intense debate. Regression is considered to be favourable by some, reflecting anti-tumour immunity [74, 79]. Kaur *et al.* studied the association between regression and sentinel lymph node status [77]. They noted a trend towards decreased nodal disease among regressing tumours [77]. Other studies have shown no association between regression and survival [80, 81]. A recent meta-analysis showed that the presence of regression was associated with a reduced risk of sentinel lymph node positivity [72].

Conversely, some authors report a worse prognosis and an increased propensity to metastasise [82-86] and it has been speculated that regression could have led to underestimation of the true Breslow thickness and, thereby erroneous down-staging of the tumour [71, 80]. Rubenstein *et al.* reported that 16% of 252 primary melanomas ≤1mm showed evidence of regression and although it was not predictive of nodal metastases, the presence of regression was significantly associated with a false-negative sentinel lymph node biopsy and subsequent nodal recurrence [71]. The authors proposed that similar mechanisms underlying regression in the primary might have led to regression in the lymph node [71]. In a study of 2243 melanomas, Maurichi *et al.* reported that the presence of ≥50% regression was associated with a significantly increased risk of death, again thought to be due to underestimation of the original Breslow thickness [78].

1.3.12 Lymphovascular invasion

The presence of tumour cells in vessel lumina predicts the likelihood of sentinel node metastasis [87] and drainage to multiple sentinel lymph nodes [88]. Furthermore, lymphovascular invasion is associated with a higher Breslow thickness, ulceration, mitoses and a nodular subtype [89]. Detection is improved by the use of immunohistochemical stains to more clearly delineate vessel walls, including the vascular marker CD34 and the lymphatic endothelial marker D2-40, and this has prognostic significance in some studies [89-91]. Others have not found an association with survival [87].

1.3.13 Perineural invasion

The majority of melanomas with evidence of perineural invasion are located in the head and neck region, typically occurring in older men and composed of spindle cells [92-95]. Cases with perineural invasion may be more likely to recur, which could be related to the mode of spread and, therefore, adequate margins of excision are required to reduce the risk of recurrence [95].

1.3.14 Microsatellites

A microsatellite is deemed to be present if there is a “discontinuous nest of metastatic cells” >0.05mm, beneath the invasive melanoma and separated from it by ≥0.3mm of normal tissue [43]. The current Cancer Outcomes and Services Data set (COSD) minimum requirements for the reporting of primary melanomas includes microsatellites, as their presence indicates stage III melanoma and a worse prognosis [96]. The current approach is to exclude microsatellites from the Breslow thickness measurement [51].

1.4 Histopathological factors of uncertain biological significance

1.4.1 Melanoma cell shape

Histopathologists have long noticed and reported differences in cellular shape between primary melanomas. Epithelioid cells are one of these distinct cell types, consisting of large, round cells with abundant, often eosinophilic cytoplasm and conspicuous eosinophilic nucleoli [97]. Spindle cells have an elongated or fusiform appearance and are often seen in lentigo maligna, acral and mucosal melanomas [98].

Cellular shape has been reported to impact on survival. Desmoplastic melanomas, which are ill-defined spindle cell tumours characterised by the presence of an abundance of collagen-rich stroma [5], are reported to recur locally but to metastasise less frequently than tumours of other cell types [99, 100]. In a study of 212 melanoma cases with a Breslow thickness <1mm, 86.6% of recurrences were in patients with melanomas of epithelioid cell-type [101]. Epithelioid cell melanomas have been shown to have more DNA ploidy abnormalities [102]. A study of 669 melanomas revealed spindle cells, marked pigmentation and a low mitotic count were indicative of a better prognosis [103]. Melanomas of mixed cell type and low mitotic count were the most frequent finding [103].

Cellular shape might predict response to treatment. In a trial of 44 patients with advanced melanoma, who received a polyvalent vaccine plus Bacillus-Calmette Guerin (BCG) or BCG plus placebo, 9/11 (81.8%) patients who died within 6 months had epithelioid cell-type melanomas [101]. Ascierto *et al.* performed retrospective studies of low or intermediate dose interferon among a small cohort of melanoma patients and showed that the majority of relapsers, 73.1% and 87.5% respectively, had tumours of an epithelioid cell-type [101].

In the process of metastasis, melanoma cells physically migrate from the skin, and it has been postulated that motility varies according to cell shape. Two patterns of melanoma cell migration, influenced by alterations in the cytoskeleton and actomyosin contractility, have been demonstrated *in vitro*: a rounded or “amoeboid” type and an elongated or “mesenchymal” type [104-106]. Melanoma cells are considered to be highly plastic, with a propensity to alternate in a switch-like fashion between the two patterns [104]. In cell migration assays, the amoeboid mode of movement was faster and these cells have been noted at the invasive front of some melanomas [106, 107].

A number of groups have reported the biological basis of differences in cellular shape between melanomas. Viros *et al.* performed an analysis of 302 melanomas and defined 4 shapes: round, ovoid, elongated and spindle [108]. They showed that *BRAF*-mutated melanomas consist of larger, rounder, pigmented cells [108]. Research in melanoma cell lines demonstrated that *PTEN* loss was associated with elongated cells [109].

1.4.2 Primary tumour architecture

The way in which primary melanoma cells are organised in the skin contributes to the histopathological subtyping: nesting being typical of superficial spreading melanoma whilst junctional clefts are often seen in Spitzoid lesions [110]. There is evidence that the nature of the driver mutations (Section 1.6.1) is reflected in tumour morphology: *BRAF*-mutated melanomas are associated with epidermal hyperkeratosis, pagetoid spread and intraepidermal nesting [108]. Spindle cells tend to arrange in fascicles [98]. This might reflect differences in the pliability of the stroma or intrinsic factors related to cell shape, as elongated cells degrade collagen I less efficiently than rounded cells [105].

1.4.3 Melanoma cell pigmentation

Melanin pigment production (“melanogenesis”) is a hallmark of melanocytes and this occurs within structures called melanosomes [1]. Melanin protects the skin from UVR and is a marker of melanocyte differentiation [111]. One of the most striking clinical

characteristics of melanoma is irregularity of pigmentation [112], and the lack thereof contributes to difficulty in diagnosing amelanotic melanomas [113]. It is possible that differences in the degree of melanocyte differentiation might contribute to variation in melanoma cell pigmentation. Furthermore, heterogeneity in melanoma cell pigmentation is a prominent histopathological feature of cutaneous melanoma [108]. This curious phenomenon might reflect biological variation. Viros *et al.* performed a detailed histopathological assessment of melanoma cell pigmentation within 298 primary melanomas and showed that pigmented melanomas were more likely to harbour *BRAF* mutations [108].

Moreover, pigmentation might affect the ability of melanoma cells to invade. Sarna *et al.* showed an inverse association between pigmentation and both melanoma cell elasticity and transmigration *in vitro* [114]. They concluded that melanosomes contributed to the rigidity of pigmented melanoma cells [114]. These findings suggest that the loss of pigmentation could promote melanoma cell invasion.

The prognostic implications of pigmentation have been reported in small studies. Brozyna *et al.* studied the melanin content of 73 primary melanomas and 42 matched lymph node metastases and did not find any overall difference in survival, based on the presence or absence of pigmentation [111]. In a subset analysis of cases that developed metastases, there was a reduced interval to relapse and death in cases with pigmented, compared with amelanotic, primaries [111]. In a subsequent study, Brozyna *et al.* assessed the pigmentation of 57 melanoma metastases and 84 primary melanomas and noted that there was less pigment in thicker primaries [115]. Yet, they noted a higher level of pigmentation among the thick melanomas that metastasised, compared with primary melanomas that did not metastasise [115]. Furthermore, they reported that cases with amelanotic metastases, treated with radiotherapy, tended to survive longer compared to cases with pigmented metastases [115]. However, the radioprotective effect of melanin might have been contributory.

The relationship between primary and metastatic melanoma cell pigmentation appears to be complex. Pinner *et al.* reported that melanoma cells undergo reversible “switching” between levels of high and low pigmentation, adopting a less pigmented, less differentiated phenotype in the process of metastasis [116]. These motile, less pigmented cells adopted a rounded morphology and moved rapidly [116]. Therefore, the classification of melanoma cell pigmentation within primary melanomas is of interest, however, the corresponding metastatic potential is uncertain.

1.4.4 Melanoma heterogeneity

Primary cutaneous melanoma displays remarkable variation in its clinical appearance, both within and between tumours [1]. Just as features of the ABCDE [112] prompt a dermatologist to recognise melanoma, asymmetry, the lack of melanocyte maturation and the presence of mitoses assist a pathologist in diagnosing melanoma [5]. At a histopathological level, heterogeneity reflects diversity in cellular size, shape, pigmentation [117] and differences in the pattern of immune cell infiltration [60]. Even within the same tumour, some melanocytes elicit a lymphocytic response, while others lack an inflammatory infiltrate, so-called “non-brisk” TILs [60]. Some melanomas arise within pre-existing naevi, while others do not [5].

At a biological level, heterogeneity might result from genetic variation both within and between tumours, with heterogeneous primary tumours having multiple subpopulations or subclones [118]. Harbst *et al.* examined intra-tumoural heterogeneity within 41 melanoma biopsies from 8 cases and reported that a higher level of mutational heterogeneity was associated with a worse prognosis [119]. Mutational heterogeneity was not associated with recognisable morphological characteristics and just 12% of driver mutations displayed intra-tumoural heterogeneity [119]. Furthermore, in a study of 63 melanomas from 28 cases, discordant gene-expression profiles were reported within different tumours from the same patient in half of cases [120]. Despite such variation, *BRAF* and *NRAS* mutations appeared to be conserved in subsequent metastases, when identified in the first metastasis [120]. Sanborn *et al.* reported that in 6/8 (75%) cases, melanoma metastases within the same patient were derived from different subclones within the primary tumour and that the metastases developed at various anatomic sites in a parallel fashion [121]. Intra-tumoural heterogeneity has also been shown to contribute to the development of resistance to targeted therapy, via selection for resistant subclones [118]. An integrated taxonomy of melanoma is in evolution, combining descriptive terminology, related to morphology, with the molecular inferences of such traits [122], which could help to inform therapeutic decisions.

1.4.5 Dominant nodule

As previously discussed, histological subtypes are defined by somewhat subjective characteristics. For instance, a nodular component can occur within a superficial spreading melanoma, which could reflect the positive selection of a clone of tumour cells during melanoma evolution. Rao *et al.* performed a histopathological review of 293 primary melanomas >4mm in thickness and noted the presence of a “dominant nodule” in 18% (53/293) of cases [70]. They defined a dominant nodule as an expansile nodule, consisting of homogeneous cells with either a naevoid or

pleomorphic appearance, and proposed that it might represent a clonal expansion of tumour cells [70]. Furthermore, the presence of a dominant nodule was significantly associated with an increased risk of relapse, with almost 40% of cases with a dominant nodule having lymph node metastases, however, there was no significant difference in survival [70].

1.5 Host immunity

In addition to tumour-specific features, there is strong evidence for the role of the immune system in melanoma. Spontaneous regression has been reported [123], and the immune-mediated damage to normal melanocytes (vitiligo) is a good prognostic factor in patients being treated with chemotherapy [124]. A case report by MacKie *et al.* is an anecdotal record of the importance of immunosuppression in host responses to melanoma [125]. In this report, two renal transplant recipients developed melanoma, one metastatic and the other locally at the donor kidney site [125]. The donor, who had a history of melanoma 16 years before, was common to both cases [125]. The implication is that metastases had survived for 16 years within the kidneys of the donor, only to grow and metastasise under the influence of immunosuppression of the recipient.

Successful responses to immune-checkpoint blockade, e.g. ipilimumab [126], anti-PD1 [127] and anti-PDL1 [128] agents, highlight the importance of the immune system in suppressing melanoma. Melanomas with an immune-related gene expression signature pre-treatment with the anti-CTLA4 agent, ipilimumab, appear to exhibit better clinical responses [129].

1.5.1 The melanoma microenvironment

The overall histopathological appearance of a melanoma embodies features intrinsic to its constituent melanoma cells, including cell shape, nuclear size, the distribution of chromatin and the degree of pigmentation. The blueprint formed by each melanoma is also a representation of its complex interaction with and integration of different components of its surrounding microenvironment. Therefore, melanoma stands, not alone, but within a framework of supportive infrastructure. This non-tumour component is often referred to as the stroma; yet, it is a variably defined entity. In breast cancer, Criscitiello *et al.* describe stroma as a composition of endothelial cells, fibroblasts, immune cells and extracellular matrix [130], whilst Moorman *et al.* define stroma as “the connective tissue that supports the deeper layer of breast tissue” [131]. Ruiter *et al.*

tabulated the various constituents of the melanoma stroma in detail, which included microvessels, inflammatory cells, fibroblast-like cells and extracellular matrix [132].

A complex, physical inter-relationship exists between the tumour and stroma, which suggests that it is an active rather than a passive process. Desmoplastic melanoma is a rare melanoma subtype, characterised by a dense collagenous stroma and paucicellular, spindle-shaped melanoma cells [133]. Notably, although prone to local recurrence, it rarely metastasises [99]. It provides anecdotal evidence of a favourable role for the stroma in melanoma. The significance of the tumour/stroma interaction can also be summarised by quantifying their respective amounts. Their relative proportions have been shown to provide prognostic information in several cancers [134-141]. In addition, increased expression of stromal genes has been shown to predict outcome in gastric cancer and was significantly associated with the estimated stromal content [142].

Previous work in cutaneous melanoma has demonstrated some interesting findings, for instance, the density and thickness of collagen have been shown to differ between melanomas and naevi [143]. In a small study, histopathological sections of 12 melanomas (>1mm thick) and 12 melanocytic naevi were stained with azan trichrome and analysed using automated imaging software [143]. Naevi contained more collagen than melanomas, whilst the latter tended to have thicker collagen bundles [143]. In a subsequent study of 267 Clark level III-IV melanomas, Smolle *et al.* measured the area, perimeter and diameter of pre-existing collagen bundles, which had been assimilated into the body of the tumours [144]. To ascertain these dimensions, a typical collagen fibre was marked and automated imaging applied to the H&E-stained sections [144]. Thicker melanomas had integrated more pre-existing collagen [144]. Interestingly, there was a significant inverse relationship between the area of collagen and both metastasis-free and overall survival in a univariable model [144]. The prognostic effect of collagen was lost after incorporating Breslow thickness in a multivariable analysis; however, the median follow-up was only 31 months [144]. Limitations of this study were that fine collagen, that was considered to represent the tumour stroma itself, was excluded from the measurements and the relative area occupied by melanoma cells was not recorded, thus it was not possible to infer the proportion of stroma [144]. The melanomas in this study were also restricted to the trunk and limbs, so that these results could not readily be applied to melanomas at other body sites [144].

Webster *et al.* utilised automated imaging software to determine the areas and percentages of tumour and stroma in lymphomas, melanomas and osteosarcomas [145]. For melanomas, muscle, connective tissue, epithelium, haemorrhage and

necrosis were counted as stroma [145]. The median percentage of stroma was 26% (range 0.21 – 93.24%) [145]. Algorithms had to be readjusted for melanomas due to their heterogeneity, yet measurements for 10/70 (24.3%) melanomas could not be computed [145]. Important histopathological and clinical parameters, e.g. Breslow thickness and ulceration, and survival data were not reported in this study [145]. During my PhD, I evaluated the percentage of stroma within primary melanomas and I analysed its effect on melanoma-specific survival. This work, on the nature and extent of the stroma within primary melanomas, is described in detail in Chapter 5.

1.6 The molecular biology of melanoma

1.6.1 Key pathways and genes implicated in melanoma

Altered signalling through the mitogen-activated protein kinase (MAPK) and phosphatidylinositol-3-kinase (PI3K) pathways frequently occurs in melanoma [146]. Two common "driver" mutations drive this signalling, in the *v-raf murine sarcoma viral oncogene homolog B1* (*BRAF*) and *neuroblastoma RAS viral gene homolog* (*NRAS*) genes (Figure 1.2) and these mutations are usually mutually exclusive [147]. Rarely mutations in *mast/stem cell growth factor receptor* (*KIT*) drive melanoma, usually in a small proportion of mucosal or acral subtypes.

1.6.2 Molecular profiles of melanoma

The AJCC staging is a powerful predictor of outcome [43] but unexplained variance of between 26% and 32% in survival exists [148][151], which researchers hope to reduce by better understanding the molecular diversity among tumours.

Due to difficulties in acquiring sufficient volumes of fresh primary melanomas, most studies relate to metastases. The melanoma transcriptome, i.e. the transcripts of all messenger RNA, can be divided into meaningful prognostic groups by statistical analysis. One such method is unsupervised hierarchical clustering. This agnostic approach produces a dendrogram that can be used to assign individuals to different groups, based on the degree of similarity of their gene expression profiles. Jönsson *et al*. applied this technique to stratify the transcriptomic profile of 57 metastatic melanomas into 4 categories, referred to as "high-immune", "proliferative", "pigmentation" and "normal-like", with the high-immune subtype having the best prognosis [149]. The names of the groups summarise the corresponding genes enriched within each category, e.g. *MITF* and other pigmentation genes in the

"pigmentation" subtype. These subtypes were replicated in 2 further data sets, which included 39 stage III melanomas.

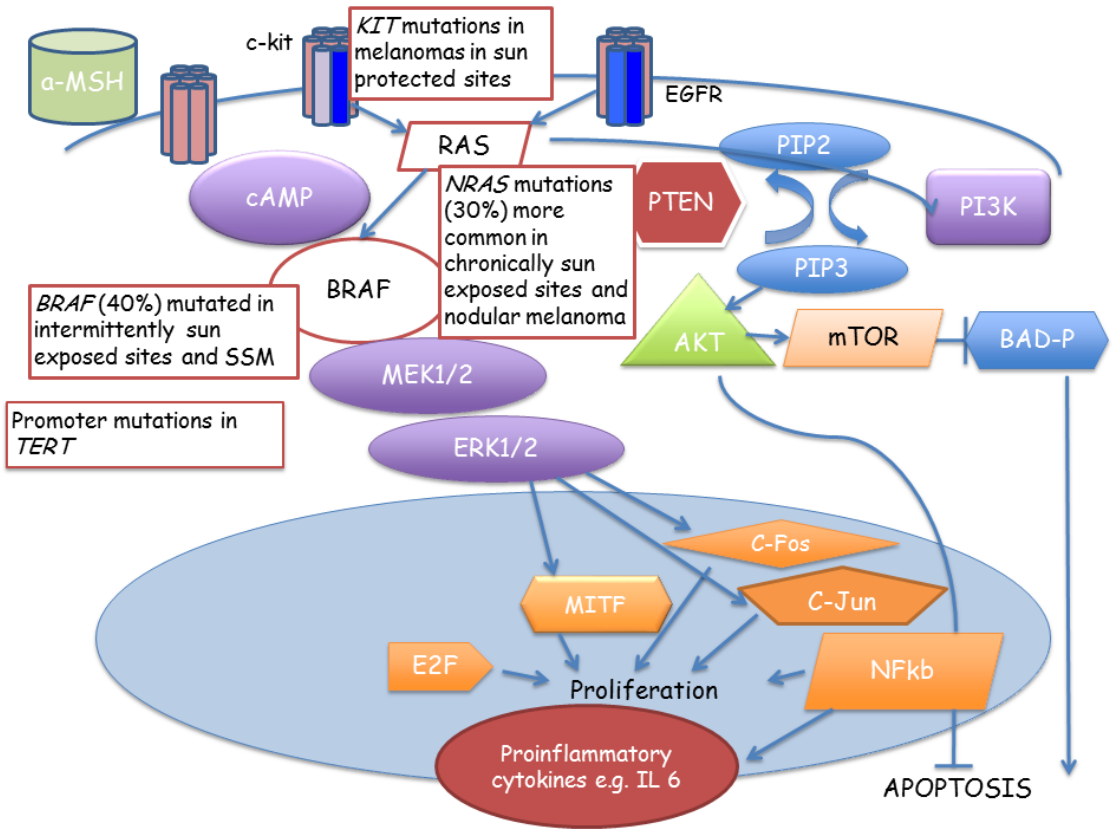

Figure 1.2: The mitogen-activated protein kinase (MAPK) pathway.

AKT: protein kinase B. α-MSH: alpha-melanocyte stimulating hormone. BAD: Bcl2 associated death promoter. *BRAF*: *V-raf murine sarcoma viral oncogene homolog B1*. cAMP: cyclic adenosine monophosphate. cFos: Fos proto-oncogene. cJun: Jun proto-oncogene. E2F: E2F family of transcription factors. EGFR: epidermal growth factor receptor. ERK: extracellular signal-related kinase. IL-6: interleukin 6. *KIT*: *Mast/stem cell growth factor receptor*. MEK: mitogen-activated protein kinase kinase. MITF: microphthalmia-associated transcription factor. mTOR: mammalian target of rapamycin. NF-κb: nuclear factor kappa-light-chain-enhancer of activated B cells. *NRAS*: *Neuroblastoma RAS viral gene homolog*. PI3K: phosphatidylinositol-3-kinase. PIP2: phosphatidylinositol biphosphate. PTEN: phosphatase and tensin homolog. *TERT*: *Telomerase reverse transcriptase*.

Using a similar approach, Harbst *et al.* validated these 4 subtypes in 223 primary melanoma tumours and 2 distinct prognostic subclasses evolved: high- and low-grade [150]. The pigmentation and proliferative subgroups were merged to form the high-

grade subclass whilst the low-grade subclass consisted of melanomas originally classified as high-immune and normal-like [150]. Melanomas with a high-grade signature tended to be thicker and nodular, to have a higher mitotic count and stage and displayed upregulation of cell cycle genes [150]. Conversely, melanomas with a low-grade signature were more likely to have brisk infiltration of TILs, *BRAF* mutations and were enriched for the expression of immune genes [150]. These two subclasses were validated in 29 stage III and 79 primary melanomas [150]. These subclasses were predictors of outcome, independent of stage [150]. This suggests that the transcriptome can provide additional prognostic information, both in early and advanced melanoma. In 2015, the Leeds group reported that these Jönsson subtypes could also be detected in samples from the Leeds Melanoma Cohort study and that 96% and 81% of the primaries could be classified using the 4-grade and 2-grade signatures, respectively [151].

Previous transcriptomic studies have largely focused on advanced and metastatic melanomas due to the limited availability of tumour tissue, particularly from thin melanomas. However, Gerami *et al.* sought to identify patients at risk of progression at an earlier stage of disease (stages I and II) [152]. They developed a binary classification, based on the expression of 28 genes that had previously been reported to be associated with metastasis [152]. Gene ontology software also predicted these genes to be involved in processes of epithelial differentiation and cell-cell junction, which were considered to be pertinent to the metastatic process [152]. This classification had a negative and positive predictive value for metastasis of 93% and 72%, respectively [152].

Clearly, a number of methods can be used to define subgroups within the transcriptome that have clinical and/or prognostic relevance. Selecting how to utilise this potentially powerful tool is in itself a challenge, as the transcriptome can potentially be interrogated in several ways to satisfy different aims. In my thesis, I will explore different techniques that I have adopted to address my aims, which are outlined at the beginning of each chapter.

1.6.3 Driver mutation status and melanoma

In addition to stratifying patients based on their transcriptomic profiles, recent evidence suggests that it is possible to make meaningful distinctions based on the principle driver mutation status. The Cancer Genome Atlas (TCGA) Network described a classification composed of 4 melanoma subtypes based upon these mutations: *BRAF*, *RAS*, *neurofibromin 1* (*NF1*) mutant and triple wild type [153]. However, this framework, based on 67 primary and 266 metastatic melanomas, failed to demonstrate an

association with outcome [153], indicating that although these cases were genetically distinct, they were not significantly different in their behaviour. Nonetheless, these molecular entities might have histopathological correlates.

Three-quarters of primary melanomas and, interestingly, 84% of metastases had a UV signature, i.e. a distinct set of somatic mutations attributable to ultraviolet radiation [153]. The mean mutation rate was high at 16.8/MB [153], relative to other cancers assessed within the TCGA data set [154]. Therefore, statistical algorithms were used to identify the most significantly mutated genes among the samples [153]. Patients with *BRAF*-mutated melanomas tended to be younger, while patients with *NF1*-mutated melanoma were older [153]. The triple wild type subgroup had a lower frequency of UV signatures (30%) and a diathesis to complex structural rearrangements [153].

Although there was no significant association between driver mutation status and survival, using unsupervised hierarchical clustering, it was possible to define 3 prognostic groups within the transcriptome: “immune”, “keratin” and “MITF-low” [153]. The immune group had increased expression of immune cell subsets, cytokines and chemokines and within this group, patients with regional metastases had a better outcome than those in the other 2 groups [153].

1.7 Histopathological consequences of variation in the molecular biology of melanoma

1.7.1 The presence of *BRAF* mutation and implications for histopathological appearance

Although diversity is typical of primary melanomas, it may be possible to sub-classify them by categorising their histopathological characteristics and there is some evidence for a relationship between biological and histopathological variation. Previous studies suggest a relationship between such features and the presence of a driver mutation. Viros *et al.* performed a histopathological review of 302 primary melanomas and found that *BRAF*-mutant melanomas tended to display more intra-epidermal scatter and nesting of melanocytes, which had a round, pigmented appearance [108]. Patients with a *BRAF* mutation also tended to be younger. The reproducibility of this scoring system was investigated by Broekaert *et al*., who reported an accuracy in prediction of *BRAF* status of up to 65.5%, with the best inter-observer agreement for pigmentation, intraepidermal scatter and solar elastosis [155]. *BRAF*-mutations have been reported in

superficial spreading melanomas, particularly on sites of intermittent sun exposure [156].

1.7.2 Kinase fusions and histopathological appearance

Apart from predicting the driver mutation status, Yeh *et al.* described characteristic histopathological appearances associated with kinase fusions involving *ALK* in a series of 32 Spitz tumours: plump, spindle-shaped melanocytes arranged in elongated nests, often with a wedge-shaped base [157]. In a further series of 17 cases with *ALK* fusions, a plexiform growth pattern was noted [158]. This suggests that recognising such features could be helpful in the identification of appropriate lesions for future molecular testing and the potential for more targeted treatment. This will be explored further in Chapter 6**.**

1.7.3 *BAP1* and histopathological appearance

An area of current speculation is whether or not germline mutations could be predicted based on the histopathological appearances of tumours. Wiesner *et al.* reported an autosomal dominant tumour predisposition syndrome associated with mutations in the *BAP1* gene in 2 families with uveal and cutaneous melanoma [159]. Cases had multiple pink naevi, which had a bland appearance clinically but had an unusual histopathological appearance; composed of pleomorphic, epithelioid melanocytes and lacking an epidermal component [159]. Multinucleated melanocytes and intranuclear pseudoinclusions have also been described in melanocytic lesions among cases [160, 161]. Various terms have been proposed for these lesions, including “Melanocytic *BAP1*-mutated Atypical Intradermal Tumours” (MBAITs) [162] and “NEvoid Melanoma-like Melanocytic Proliferations” (NEMMPs) [163]. The types of cancer to which these families are prone continue to expand but include mesothelioma [162], renal cell cancer and meningioma [164-166]. This will be discussed further in Chapter 6**.**

1.7.4 Ulceration and gene expression profiles

As mentioned, microscopic ulceration is one of the key prognostic indicators in melanoma, included in the current AJCC staging system and here I describe the evidence that ulceration reflects important biological differences [43]. Although the presence of ulceration strongly predicts melanoma death, somewhat paradoxically, a subgroup analysis of data from a trial of intermediate dose interferon-alpha-2b as adjuvant therapy for resected stage IIB and III melanoma suggested that ulceration

predicted benefit from interferon [167]. Patients with ulcerated melanomas who received the 25-month schedule were significantly less likely to die than those with non-ulcerated primaries (HR 0.59, p=0.0007) [167].

The mechanisms underlying ulceration are not fully understood. Rakosy *et al.* analysed the gene expression patterns of 36 primary melanomas and discovered that 1,080 genes distinguished ulcerated from non-ulcerated cases, 93 of which were upregulated [168]. The top pathways identified in ulcerated melanomas included p53, NFκB and Wnt/β-catenin [168]. Jewell *et al.* from the Leeds group explored this further by comparing the gene expression profiles of ulcerated and non-ulcerated melanomas in multiple data sets [49]. Ulceration occurred more frequently with advancing age, male sex and in melanomas on sun-protected sites [49]. The expression of 56 genes was significantly different between ulcerated and non-ulcerated cases in the test data set; the most prominent differences included downregulation of genes involved in cell adhesion and the upregulation of *Interleukin-6* (*IL-6*) and *Interleukin-8* (*IL-8*) [49]. These observations were confirmed in 2 validation sets [49]. When hierarchical clustering was applied, 2 distinct clusters were identified, the first of which had a higher proportion of ulcerated melanomas [49]. Differential expression of genes involved in wound healing discriminated between the non-ulcerated melanomas of clusters 1 and 2 and gene ontology revealed cell cycle and cell proliferation pathways to be enriched among ulcerated cases [49]. This suggests that ulceration is associated with a proliferative melanoma phenotype and that it appears to be associated with a pro-tumourigenic type of inflammation, which might be amenable to interferon therapy.

1.8 Molecular techniques for imputing stromal composition

1.8.1 ESTIMATE and tumour purity

Establishing the proportion of tumour present within a sample is important: it informs decisions about the contribution of the tumour to the transcriptomic profile. For example, one might infer that if RNA is extracted from a melanoma sample with a high tumour purity, then most of the resultant transcriptome is likely to have been derived from the melanoma cells themselves, whereas, the opposite could be true in cases of low tumour purity. Estimation of STromal and Immune cells in MAlignant Tumours using Expression data, is a method of quantifying the contribution of stromal and immune cells within a sample, based on the expression of a stromal and an immune gene signature [169]. Genes from the Cancer Genome Atlas and publicly available databases were filtered in order to construct these signatures [169]. The immune score

included genes that were both enriched in haematopoietic cells (relative to normal cells) and were associated with high immune cell infiltration in ovarian carcinoma [169]. Genes that were enriched in stromal tissue isolated by laser-capture microdissection from breast, ovarian and colorectal cancers were filtered to generate the stromal score: removing genes that had decreased expression in glioma stem cell-like cells and genes that showed little variability among cancer cell lines [169]. The tumour purity was subsequently derived from these scores [169]. The comparability of these transcriptomically-derived estimates of tumour purity, immune and stromal content with a histopathological assessment will be investigated in Chapter 5.

1.9 The "immunome"

The immune cell infiltrate within primary melanomas is an integral part of the melanoma microenvironment and is thought to represent a snapshot of the host response to foreign tumour tissue at a certain point in time. Several cell types contribute to this immune infiltrate, including T-lymphocytes, plasma cells, neutrophils, eosinophils and phagocytic cells, e.g. melanophages [170]. The immune cell response is complex: extensive discussion is beyond the scope of this thesis. Suffice it to say that there is considerable variation in the cell configuration and intensity of the immune cell infiltrate within primary melanomas: TILs being completely absent in some, whilst others display brisk TILs [60]. This is informative of the communication between melanoma and immune cells: potentially, the efficiency of the host immune response in eradicating the tumour and also escape mechanisms exploited by melanoma cells, in order to continue to proliferate and invade. Visual inspection of H&E-stained sections does not permit precise definition of the cellular composition, e.g. the pattern of TILs can be recorded but it is not possible to distinguish between cytotoxic- and T-helper cells, without ancillary tests, e.g. immunohistochemistry or multispectral imaging [171-173]. In order to better understand the key immune cell players and their respective numbers, it would therefore be helpful to be able to identify these features without sacrificing several sections of clinical tissue. Furthermore, it seems likely that much more detailed categorisation of the immune cell infiltrates into tumours would tell us much more about the nature of host/tumour interactions and the determinants of those interactions. As an approach to this, Bindea *et al.* developed a resource, consisting of 577 genes compiled from published literature, which could be used to map the presence of 28 immune cell subtypes [174]. This was initially applied to colorectal cancer but has since been validated in melanomas by the Leeds group. I am in receipt of these data, which I will implement to further interpret immune cell responses within

primary melanomas and the relationship between their histopathological and transcriptomic profiles.

1.10 Hypotheses

- Histopathological heterogeneity could be indicative of biological variation
- The presence of a dominant nodule could be indicative of the positive selection of a clone of melanoma cells and might represent a more aggressive melanoma, which could be reflected in increased risk of relapse or death from melanoma
- The immune system is important in determining outcome from melanoma and this can be measured histopathologically
- The percentage of stroma might be predictive of melanoma-specific survival
- *BAP*-like histopathology could help to predict germline *BAP1* mutation status

Chapter 2 Methods

My thesis was based on samples from the Leeds Melanoma Cohort, which is a long-term study; already mature at the beginning of my time in Leeds. Although 2184 participants were studied, my work focused on 798 tumour samples for which matching transcriptomes were ultimately available in 676 cases. I had access to the anonymized clinical and exposure data collected from participants, e.g. relapse data, etc.

At the beginning of my thesis, I trained in melanoma histopathology. I accomplished this by studying the literature and through regular one-to-one training with Dr Will Merchant, consultant dermatopathologist, using light microscopy. A protocol that had previously been developed by Prof. Martin Cook was initially utilised. In the process, I developed a list of key histopathological variables of putative prognostic and/or biological significance to be measured, based upon the literature. I worked under Dr Merchant's tutelage to define robust definitions for those variables. I carried out inter and intraobserver comparisons which are reported in Chapter 3.

During the first year, it became possible to use digitised images. I moved to this virtual pathology approach because of its advantages in annotating and digitally extracting specific regions of tumour. Additionally, images of the measurements could be captured, for future reference, e.g. for clarification with a consultant dermatopathologist or in my subsequent research.

2.1 Generation of H&E-stained sections, tumour mutation status, TMA core biopsies and whole-genome transcriptomes

By the time I started my PhD, ethical approval had already been granted for the Leeds Melanoma Cohort (LMC) Study (MREC 01/3/057), which began recruiting in 2000 and upon which my thesis is based. Participants were asked to consent to sampling of their stored primary tumour blocks. Histology sections (each 5 μm thick) were taken from their primary melanoma formalin-fixed, paraffin-embedded (FFPE) tumour blocks. Histology sections and staining with H&E were performed by staff in the Section of Epidemiology and Biostatistics. The H&E slide was examined by Prof. Julia Newton-Bishop and laboratory staff. A 0.6mm diameter circle of tumour was identified which was towards the advancing edge but was not so near the edge that sampling using a

tissue microarray (TMA) needle horizontally would miss the bulk of the tumour. The area selected contained the least inflammatory cell infiltrate and the least amount of stroma, so that the samples would be comparable. The site was marked with a marker pen and, subsequently, laboratory staff used this to guide sampling of the block using the TMA needle. For large tumours, the protocol allowed sampling twice. Where the tumour was judged too small to sample without destruction of the block (which might be needed subsequently by the patient for clinical testing) then no core was taken.

DNA and RNA were extracted from the TMA cores according to a previously published protocol [175, 176]. *BRAF* and *NRAS* mutation status were established from extracted DNA using pyrosequencing by section staff. The mRNA was assayed by an external service provider using the Whole-Genome DASL HT12v4 assay (Illumina®). This array was developed by Illumina® for use particularly in degraded RNA extracted from FFPE tissue. The use of archival FFPE tissue for RNA extraction can yield cross-linked, degraded fragments [177]. The Whole-Genome DASL® assay utilises random primers, which can bind small fragments of RNA (~50 nucleotides) [178]. The Whole-Genome DASL® assay has previously been shown to produce high quality transcriptomic data from RNA extracted from FFPE tissue [175, 178]. Data were extracted using GenomeStudio© software. The whole-genome gene expression data were quantile-normalised using Lumi R by Dr Jeremie Nsengimana [179]. Singular value decomposition (SVD) was used to assess the relationship between the top principal components of gene expression and technical variables, such as the batch, plate, chip, age of the tumour block and the date of RNA extraction using ‘swamp’ package [180]. Technical variables, found to significantly affect the data, were adjusted out. Significant variation disappeared when the data were adjusted for the chip used for each sample.

2.2 Histopathological review of H&E-stained sections using a light microscope

During the first ten months of the PhD, I used a Leica® *DMLB2* light microscope to learn about melanoma histopathology and to grade 158 primary melanomas for key prognostic factors. I utilised a protocol that had previously been developed by Prof. Cook for this analysis (please see Appendix B). I learned melanoma pathology through reading dermatopathology textbooks, to which Dr Merchant kindly provided access, and by reading the literature about melanoma pathology. Dr Merchant provided regular one-to-one histopathology training. In order to be able to use the detailed protocol that had been developed by Prof. Cook, it was necessary to learn about melanoma

pathology. I reviewed melanoma cases with Dr Merchant using a multi-headed light microscope. I learned how to record measurements, correcting for the appropriate magnification. I gained an appreciation of the criteria used to define histopathological factors, e.g. distinguishing artefactual from true ulceration. The Royal College of Pathology guidelines were used as a reference for histopathological definitions [51]. An approach was developed for measures that were not already defined, through discussion and review of cases with Dr Merchant. I gradually became more familiar with melanoma pathology, by reviewing melanoma H&E sections that had been made for research purposes (results for the histopathological assessment using the Prof. Cook protocol are provided in the Appendix B). Dr Merchant reviewed cases where queries arose or where verification was required.

The aims of the thesis were such that I needed to describe features of a whole slide, representative of the thickest part of the tumour, and features of the particular area within the tumour from which the TMA core was taken. Below, I describe how I identified the area of the tumour sampled for examination.

After training using the light microscope, I worked with digitized images of the histology slides (virtual pathology) and hence some of the definitions used relate to screen dimensions rather than fields. It is notable that at this time of transition, I adopted a different classification to define certain factors, e.g. tumour-infiltrating lymphocytes (TILs). A decision was also made to discontinue the recording of other factors, e.g. microsatellites due to limited interobserver reproducibility and to allow sufficient time to record novel measures introduced in the virtual pathology protocol.

The scoring variables outlined in Table 2.1 were applied for the protocol using the light microscope. The protocol was modified after discussion with my supervisor, Prof. Julia Newton-Bishop, and particularly with Dr Merchant, to derive definitions as seen in Table 2.3, which were used for the virtual pathology protocol.

Table 2.1: Properties of the Histopathological Scoring Variables for Whole-Tumour Measures using the Light Microscopy Protocol.

Microscopic diameter, ulceration width, Breslow thickness, thickness of regression and distance to the peripheral and deep margins were calculated using the measurement on the eyepiece graticule, multiplied by the relevant calibration factor for the microscope. In cases where the maximum microscopic diameter, ulceration width, Breslow thickness or distances to the peripheral and deep margins were outside of the field of view, even at the lowest magnification (2x on the microscope used), a ruler was used, however, this was a crude estimate and would give a value to the nearest millimetre only.

Scoring variable	Detail of Scoring Schema
Acral lentiginous melanoma	Melanoma occurring in the volar or subungual skin. The intraepidermal component is usually lentiginous in pattern with a “moth eaten” appearance.
Breslow thickness	Measured from the top of the granular layer of the epidermis to the deepest invading melanoma cell, ignoring melanoma cells that were apposed to adnexal structures or within vessels. In ulcerated cases, where the thickest part of the melanoma was beneath the ulcer, the Breslow thickness was measured from the ulcer base.
Clark level I	Melanoma confined to the epidermis.
Clark level II	Melanoma begins to encroach on but does not fill the papillary dermis.
Clark level III	Melanoma fills and expands the papillary dermis.
Clark level IV	Melanoma invades the reticular dermis.
Clark level V	Melanoma invades the subcutaneous fat.
Desmoplastic melanoma	Ill-defined and variably cellular melanoma composed of spindle cells associated with dense collagen and usually occurring on sun-damaged skin. Lentigo maligna may be seen in association.

Scoring variable	Detail of Scoring Schema
Epithelioid cells	Cells with a round nucleus, a prominent, pink nucleolus and variably eosinophilic and often abundant cytoplasm [97].
Histological subtype	As per definitions listed in Appendix A.
Lentiginous intraepidermal proliferation	Proliferation of melanoma cells along the basal layer of the epidermis.
Lentigo maligna	The *in situ* phase of lentigo maligna melanoma (i.e. radial growth phase; peri-adnexal involvement is frequent).
Lentigo maligna melanoma	Melanoma characterised by epidermal atrophy, a prominent intraepidermal lentiginous component, accompanied by evidence of actinic damage or solar elastosis and frequently involving adnexal structures.
Lymphovascular invasion	The presence of melanoma cells within lymphatic or blood vessels.
Maximum microscopic diameter (in mm)	The distance between the most lateral epidermal nest at either side of the melanoma, or where nests are absent, the distance between the furthest edges of the invasive component of the tumour. (This definition was developed following discussion with Dr Merchant).
Melanocytic lesion of unknown malignant potential	A melanocytic lesion where uncertainty exists regarding its biological behaviour and its propensity to metastasise is unclear. The behaviour may follow either a benign or a malignant course. Histopathological assessment tends to reflect a combination of features that can be seen in melanocytic naevi and in melanoma but fall short of a diagnosis of melanoma.
Microsatellites	The presence of melanoma nests >0.05mm in diameter, lying in the reticular dermis, panniculus or vessels, deep to the invasive melanoma and separated by normal tissue of at least 0.3mm on the section in which the Breslow thickness was measured [51, 181].

Scoring variable	Detail of Scoring Schema
Mitotic count (per mm^2)	The number of dermal mitoses within $1mm^2$ region of the “hot spot” (or area of apparently most numerous dermal mitoses), or in the absence of a hot spot, the number of dermal mitoses within $1mm^2$ of a representative dermal mitosis [43].
Naevoid melanoma minimal deviation	A subtype of melanoma characterised by the presence of a nodule composed of uniform melanocytes, with rare or absent mitoses and tending to lack a host response or necrosis [182].
Nested intraepidermal proliferation	The proliferation of melanocytes in nests within the epidermis.
Nodular melanoma	Melanoma characterised by a predominant vertical growth phase, with the lateral intraepidermal component extending no more than 3 rete ridges beyond the vertical growth phase component.
Pagetoid intraepidermal proliferation	Proliferation of melanocytes following a pagetoid spread pattern.
Pagetoid spread	Upward spread of atypical melanocytes into the epidermis.
Percentage regression	Calculated by dividing the horizontal diameter of regression by the maximum microscopic diameter of the lesion and multiplying by 100.
Perineural invasion	The presence of melanoma cells around a nerve.
Pigmentation	Initially graded as absent, mild, moderate and severe but subsequently modified and graded according to a protocol developed by Viros *et al.* as absent, faint, moderate, high and very high [108]. Later amended to record both the main and highest degree of pigmentation within the tumour as pigmentation was noted to vary significantly across the whole tumour.
Radial growth phase melanoma	Predominantly intraepidermal melanoma or if present, dermal nests consist of <15 cells, are no larger than intraepidermal nests and dermal mitoses are absent.

Scoring variable	Detail of Scoring Schema
Radial growth phase (*in situ*)	The presence of intraepidermal melanoma cells, singly or in nests [98].
Radial growth phase (microinvasive)	The presence of intraepidermal melanoma with involvement of the papillary dermis [98].
Regression	Replacement of melanoma cells by a variable lymphocytic infiltrate, melanophages, telangiectasia and fibrosis and often accompanied by epidermal atrophy [77]. • Stage 1 regression: some loss of dermal melanoma but preservation of the epidermal component [77]. • Stage 2 regression: loss of all dermal melanoma but a residual junctional component remains [77]. • Stage 3 regression: loss of junctional and dermal components of melanoma, with resultant dermal scarring [77]. Partial regression: loss of part of the tumour mass without complete replacement of tumour by inflammatory cells and fibrosis [75]. Segmentary regression: complete regression of a segment of melanoma [75].
Regression thickness	Measured from the top of the granular layer of the epidermis to the nearest melanoma cell (if present) lying deep to the regression. If no melanoma cells remained, the thickness was measured to the deepest estimated edge of regression.
Small/naevoid cells	Melanoma cells which have prominent nuclear hyperchromasia, sparse cytoplasm and resemble benign naevus cells.
Solar elastosis	The presence of elastotic fibres in the dermis, which may occur singly or may form clumps or amorphous masses [183]. Graded as follows: mild if single, scattered, elastotic fibres were present, moderate if there were clumped, elastotic fibres with normal intervening dermis and severe if amorphous masses of elastotic fibres were present or if the papillary dermis was replaced by clumped elastotic fibres [183].
Spindle cells	Cells with an elongated or fusiform appearance and a long axis proportionally larger than the short axis.

Scoring variable	Detail of Scoring Schema
Spitzoid cells	Melanoma cells within a spitzoid melanoma, which may be spindled and/or epithelioid in appearance [184].
Spitzoid melanoma	A melanoma that has features of a Spitz naevus, i.e. dome-shaped and consisting of spindle and/or epithelioid melanoma cells [184].
Subungual melanoma	Melanoma occurring underneath or in close proximity to a fingernail or toenail.
Superficial spreading melanoma	Characterised by a predominant nested pattern of melanoma but may contain a dermal nodule with a lateral intraepidermal component extending more than 3 rete ridges beyond the vertical growth phase melanoma. Pagetoid spread is common in this subtype.
Tumour-infiltrating lymphocytes (TILs)	Lymphocytes in the vertical growth phase that surround and disrupt melanoma cells [51]. • Absent TILs: no lymphocytes or if present, they do not infiltrate the vertical growth phase melanoma [60]. • Non-brisk TILs: lymphocytes infiltrate the invasive melanoma but only focally [60]. • Brisk TILs: lymphocytes diffusely infiltrate the entire base or the entire invasive component [60].
TILs pattern	The pattern of TILs was recorded as peripheral if present at the edge of the tumour only, central if present anywhere within the body of the vertical growth phase (VGP) of the tumour except the edge, and both if present in a combined pattern.

2.3 Preparation for the transition to virtual pathology

2.3.1 Ethical approval for virtual pathology

The opportunity arose to make virtual pathology images of H&E sections from the Leeds Melanoma Cohort (LMC) Study for analysis. This would permit digital measurements and annotations to be made on the virtual pathology images. These digital measurements and annotated images could then be saved for future reference. Thus, facilitating learning and interobserver studies, by enabling the review of differences in the measurements recorded between observers. Clarification was sought from the Ethics Committee, who permitted this. An official amendment was also submitted, detailing the storage of images, both on the secure Genetic-Epidemiology server and anonymised images on the Leeds virtual pathology website.

2.3.2 Recording the locations of TMA core biopsies

H&E sections of primary melanomas from the LMC study had already been assessed by Prof. Newton-Bishop and Dr Jon Laye (senior histology technician) for suitability for sampling using a TMA core biopsy needle. TMA core biopsies were extracted from tumours where sufficient melanoma would remain in the event that the specimen might be required for subsequent clinical testing. Therefore, there was a bias to sampling thicker tumours. Overall, more than 2000 slides were reviewed, in excess of 900 tumour blocks were sampled and RNA extracted. Unfortunately two plates of RNA samples were sent to the service provider and failed analysis due to reagent degradation. In total, 703 tumour transcriptomes were generated from the 2184 participants.

Glass slides containing H&E sections that had previously been marked for TMA coring using a black felt-tip pen, were scanned using a flatbed scanner (Canon® Canoscan LIDE 60) to retain a record of the markings that corresponded to the sites of TMA cores before cleaning (Figure 2.1A). JPEG images of the scanned slides were saved by study number on the secure Genetic-Epidemiology server.

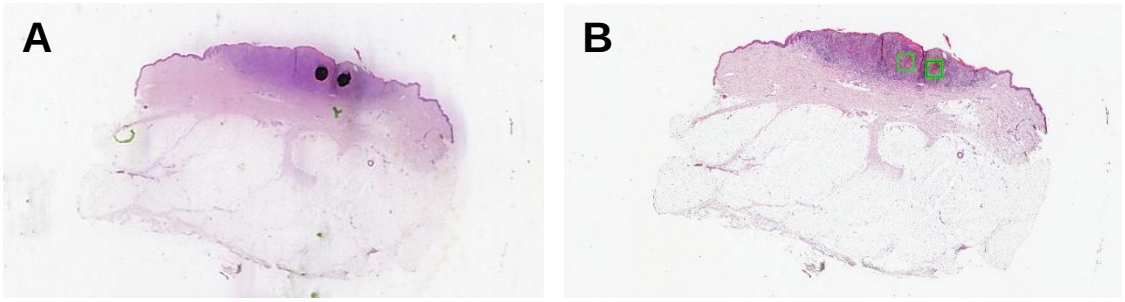

Figure 2.1: (A) Flatbed-scanned and (B) virtual pathology images showing cored regions

(A) The image on the left shows the sites that had been marked with a black felt-tip pen for sampling using a TMA biopsy needle. (B) The virtual pathology image on the right shows the corresponding annotated regions.

2.3.3 Slide scanning

Glass slides containing H&E sections of primary melanomas from the LMC study were cleaned using 100% ethanol and paper towel, with assistance from laboratory staff (Minttu Polso and Tracey Mell). Slides were then submitted for scanning using the Aperio AT2® slide scanner (performed by Michael Hale).

2.4 Pilot work using virtual pathology

Dr Darren Treanor, consultant histopathologist, provided initial virtual pathology training on the first scanned images, which were viewed on a large screen, known as the mini-wall (Figure 2.2). The cored regions were annotated as follows: the JPEG image from the flatbed scanner and the corresponding virtual pathology image were opened on parallel screens on the mini-wall. The images were adjusted to the same scale. A 600μm square (the same diameter as a TMA core needle) was overlaid onto the virtual pathology image in the cored region. This was repeated for subsequent cores from the same case (Figure 2.1B). After marking, an image of 2,426 pixels, at a resolution of 0.2473μm per pixel, was extracted (corresponding to a width of 600μm). Each virtual pathology image was assigned a unique SVS number and each case was saved on the secure Genetic-Epidemiology server as an .xml file.

Pilot work on measuring stromal content within the estimated cored regions and a representative area of the expansile vertical growth phase (VGP) of the tumour was performed on 10 cases. An outline of the representative tumour from which the core had been obtained was created, and the file was exported as an .xml file (Figure 2.3A).

Only the dermal, invasive component of the melanoma from which the core had been taken was incorporated into the outline, ignoring *in situ* components. I used a programme called RandomSpot© to estimate stromal content. This approach has previously been applied to other cancers, including colorectal [141] and breast cancer [136] for this purpose. A series of arrowheads or 'spots' are generated by the software. The observer then uploads the output onto the virtual slide, where the tissue identified by each arrowhead can be viewed at high magnification and the relevant cell or structure recorded (Figure 2.3B).

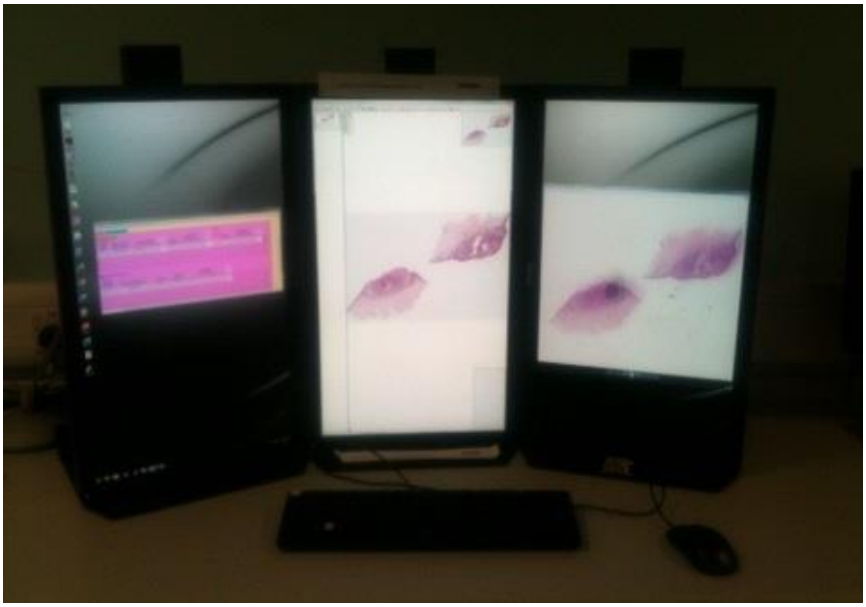

Figure 2.2 Photograph of the mini-wall used to perform the virtual pathology review

The mini-wall consists of 3 parallel screens connected to a single computer. The first screen was used to access files and to input information into the FileMaker Pro© database. The second screen was used to assess and to annotate the virtual pathology images. The third screen was used to visualise flatbed-scanned images of the glass slides, which contained black markings that corresponded to the sites of TMA core biopsies.

To superimpose a set of arrows onto the virtual images, RandomSpot©, bespoke virtual pathology software was used (http://129.11.65.182/RandomSpot/, developed by Alex Wright, Virtual Pathology Department, University of Leeds) [185].

The .xml files were uploaded separately: 50 spots (arrowheads) were selected for each estimated cored region and 300 spots for each of the representative tumour areas (Figure 2.3C).

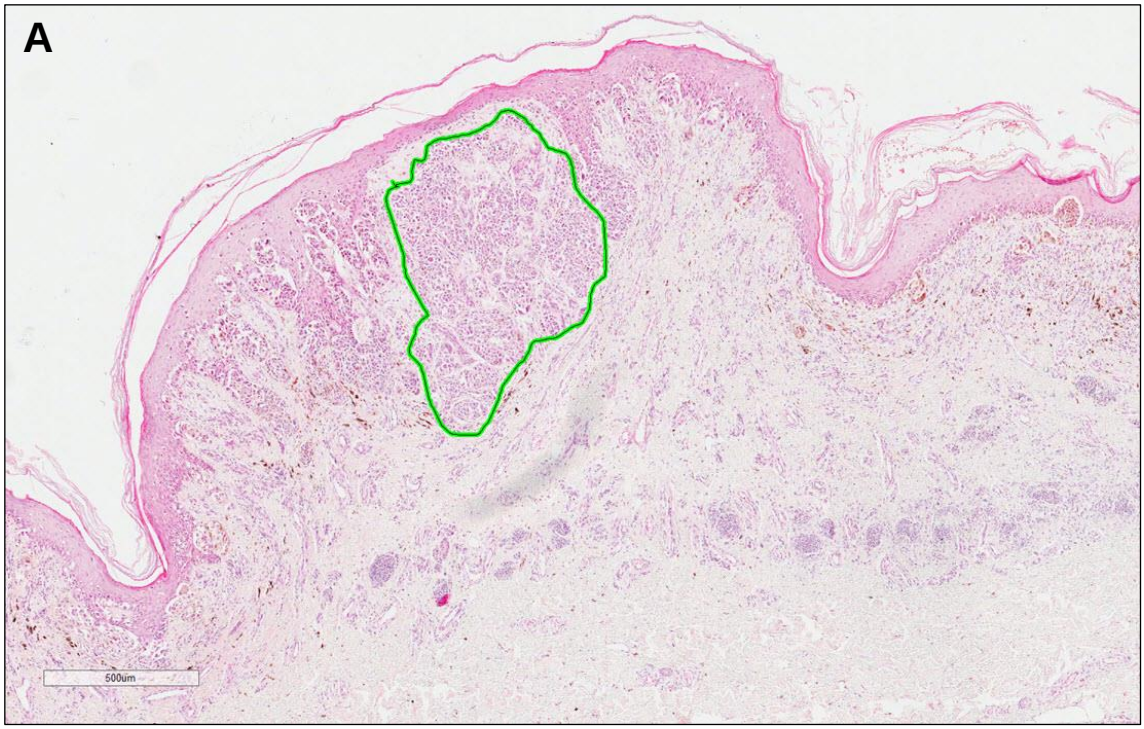
A
500um

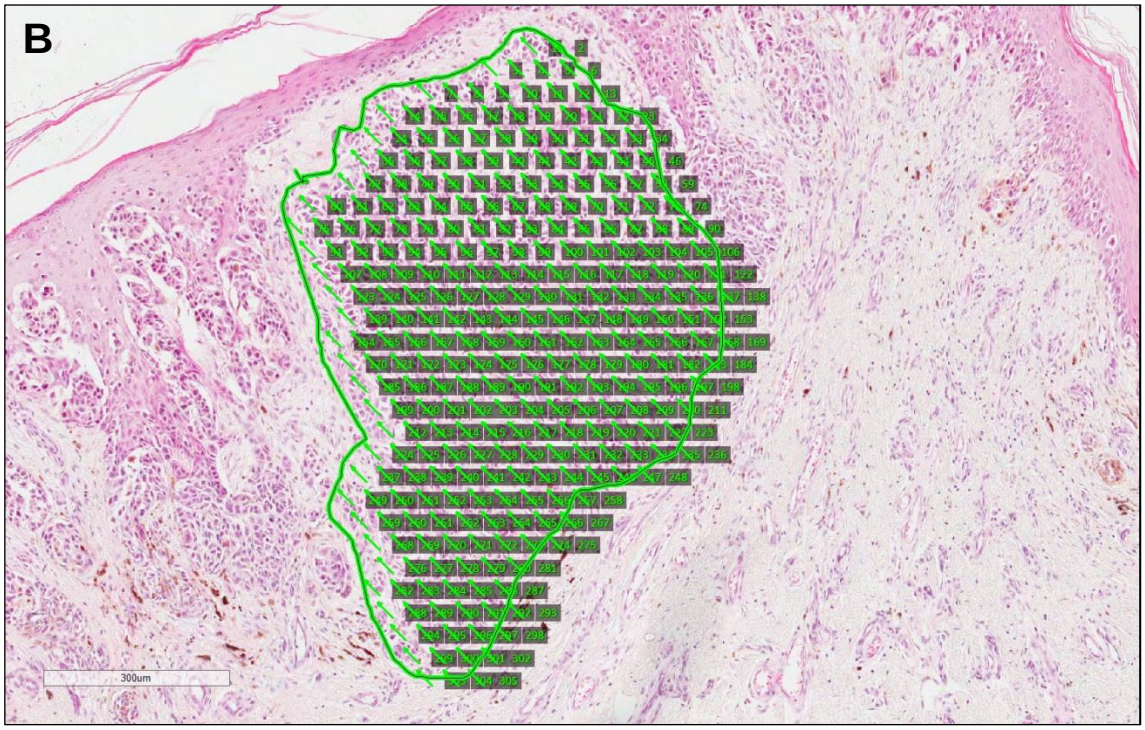
B
300um

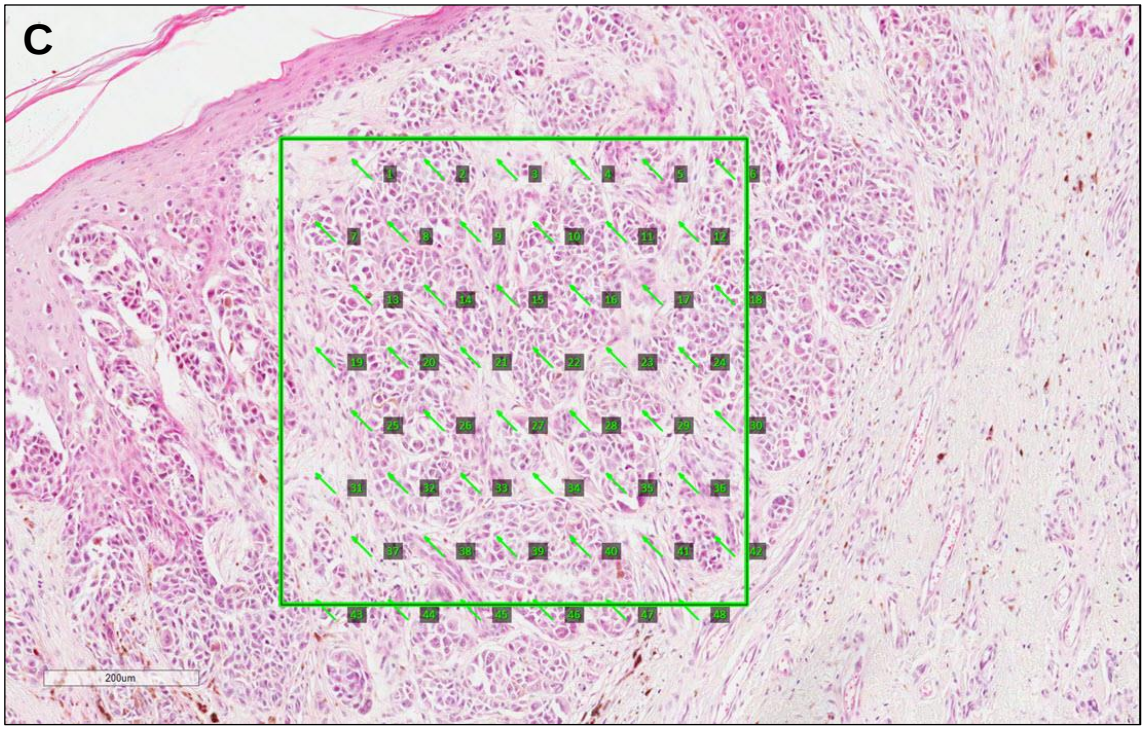

Figure 2.3: Virtual pathology images showing (A) the outline of the vertical growth phase melanoma, (B) spots imported from RandomSpot© onto the digital image within the vertical growth phase melanoma and (C) spots imported from RandomSpot© onto the cored region

(A) The outline of a representative region of the vertical growth phase melanoma is shown (x4 magnification), (B) 305 spots imported from RandomSpot© onto the digital image within the representative region of melanoma (x8 magnification). Please note that although 300 spots were selected, RandomSpot© allocates the approximate number of spots requested, and (C) 48 spots imported from RandomSpot© onto the 600 micron square which corresponded to the TMA biopsy site (50 spots had been requested).

Sections were scored with a “t” or “s” for each arrowhead that landed on tumour and stroma, respectively. Anything that was not tumour was recorded as stroma, i.e. immune cells, connective tissue, vascular structures. If an arrowhead landed on a non-informative area, “▪” was recorded. Similarly, squamous epithelium (including rete ridges and hair follicles) was excluded from the calculation by recording as “▪”.

Results were exported both as .xml and .xls/.xlsx files. Proportions of tumour and stroma were calculated using pivot tables in Microsoft Excel (2007) and the data were imported into the statistical software package STATA v.12.1 [186].

Regions on the virtual image that had been estimated to correspond to cored regions were analysed for the proportion of stroma. The percentage of stroma (POS) was

calculated for each core and was subsequently categorised into percentage groupings as follows: 0, 1-24, 25-49, 50-74, ≥75%. This was then compared with an eyeballed measure of the POS and the extent of agreement was calculated.

In order to assess the variance across the arrow count and the number of arrows required to accurately record the proportion of stroma in each estimated core, the moving average of the 50-arrow count was calculated for each estimated core. Line graphs were plotted of the moving average versus the arrow number (Appendix C). Lines for multiple cores within the same case were superimposed and, for patients with two cores, the frequency distributions of the moving average for each core were compared using a two-tailed T-test. Line graphs of the moving average for the 300-arrow count over the representative tumour region were plotted using the same method.

2.5 Virtual pathology protocol: whole tumour measures

Virtual pathology opened up new possibilities to record measurements hitherto infeasible using a light microscope, such as the use of a technology to facilitate the estimation of stromal content called RandomSpot©. The histopathology review was restricted to all available primary melanomas that had been sampled using a TMA needle to generate whole-genome transcriptomes. An iterative process ensued to develop a suitable protocol that would account for features of the primary melanoma as a whole and also characteristics particular to the locations selected for TMA sampling.

Slides were accessed from a personal folder within the Leeds virtual pathology website, using Internet Explorer version 9. The relevant batch was selected and the SVS of interest was opened in ImageScope© v12.2.1.5005. Separate files linking the study number, batch and SVS numbers and files containing details of which cases met the inclusion criteria (i.e. had been sampled using a TMA needle) were stored on the secure Genetic-Epidemiology server. These were consulted each time a case was assessed.

With respect to the whole tumour, Breslow thickness, microscopic ulceration, TILs and regression were retained as measures to be recorded. There were multiple H&E sections available for several cases. Each section was assessed. The method I applied to each parameter is described below. Briefly, a maximum of three measurements per section and a total of up to six measurements per case were recorded for Breslow thickness. The highest value for Breslow thickness on any section was recorded as the maximum Breslow thickness. Microscopic ulceration was deemed to be present if it was present on any section. A maximum of six measurements were recorded for the

extent (width) of ulceration in millimetres. These measurements could be distributed between different sections or could be recorded on a single section. The maximum value for the extent of ulceration was used as the value for the maximum extent of ulceration. Tumour-infiltrating lymphocytes (TILs) were assessed on the thickest section (i.e. the section where the maximum value for Breslow thickness had been recorded). TILs were recorded as non-evaluable if the base of the section was partially or entirely missing (e.g. due to a shave biopsy). If regression was present on any section, it was recorded as being present for that case. Up to six measurements were permitted for the depth of regression and the maximum value was recorded as the maximum depth of regression. The ruler icon in Aperio® ImageScope© was selected to record measurements in millimetres.

Whole-tumour measures were recorded in a FileMaker Pro© database, specifically designed for the study. A photograph was taken of the measurements made using the camera icon in ImageScope©. Annotations for each slide were exported as separate .xml files. These and the corresponding JPEG images were saved on the Genetic-Epidemiology server.

Several variables were dropped due to limited reproducibility (Chapter 3) and in an effort to utilise time as effectively as possible, while introducing new, detailed measures for the cored regions. These dropped variables included the histological subtype, the maximum microscopic diameter, percentage of ulceration, the growth phase, Clark's level, lymphovascular and perineural invasion, percentage and stage of regression, microsatellites, co-existent naevus, solar elastosis, distances to the deep and peripheral margins and the type of intraepidermal melanocytic proliferation. The recording of TILs was modified (please see below) and the mitotic count, predominant cell type and pigmentation of melanoma cells were recorded in the cored regions rather than within the whole tumour. I elected to enumerate mitoses within the cored region in preference to the whole tumour because this would permit subsequent comparisons with the transcriptomic data. These dropped measures had already been recorded from histology reports on the Section of Epidemiology and Biostatistics database.

Details of the scoring variables used and the scoring schema adopted are given in Table 2.2.

Table 2.2: Properties of the Histopathological Scoring Variables for Whole-Tumour Measures using the Virtual Pathology Protocol

Details of histopathological variables that were measured for cases reviewed using the virtual pathology protocol.

Scoring variable	Detail of Scoring Schema
Absent tumour-infiltrating lymphocytes (TILs) with a perifibrotic/regression pattern	TILs located mainly in a region of fibrosis or regression (with or without melanophages).
Absent tumour-infiltrating macrophages/melanophages (TIMs) with a perifibrotic/regression pattern	TIMs located mainly in a region of fibrosis.
Absent tumour-infiltrating lymphocytes (TILs) with a perivascular pattern	TILs situated predominantly around vascular structures.
Absent tumour-infiltrating macrophages/melanophages (TIMs) with a perivascular pattern	TIMs situated predominantly around vascular structures.
Breslow thickness (in mm)	The measurement between the top of the granular layer of the epidermis and the deepest point of invasion of melanoma, or where epidermal ulceration is present (and involves the thickest region of tumour), the measurement between the base of the ulcer and the deepest point of melanoma invasion. Melanoma cells apposed to adnexal structures or within vessels or microsatellites were excluded from the measurement.
Brisk diffuse TILs	TILs situated throughout the base of the vertical growth phase (VGP) melanoma and additionally infiltrating the body of the VGP to the extent that the majority of the VGP appears to be consumed by TILs.

Scoring variable	Detail of Scoring Schema
Brisk diffuse TIMs	TIMs situated throughout the base of the VGP melanoma and additionally infiltrating the body of the VGP to the extent that the majority of the VGP appears to be consumed by TILs.
Brisk peripheral TILs	TILs situated throughout the base of the VGP melanoma, which may infiltrate some of the body of the VGP to an extent that is less that of brisk diffuse TILs.
Brisk peripheral TIMs	TIMs situated throughout the base of the VGP melanoma that may infiltrate some of the body of the VGP to an extent that is less that of brisk diffuse TIMs.
Cumulative extent of ulceration	The sum total of width measurements for discontiguous ulcers on the same section of melanoma.
Deep tumour loss	A deficit within the melanoma VGP whose proximal aspect begins within the dermis but is not in direct contact with the dermo-epidermal junction.
Depth of tumour loss (mm)	Measured from the top of the granular layer of the epidermis to the deepest estimated edge of tumour loss, i.e. fibrosis or lymphohistiocytic infiltrate.
Dominant nodule	The presence of a nodule of melanoma, characterised by an abundance of melanoma cells accounting for an entire screen of the mini-wall at 10x magnification which may contain immune cells or blood vessels but not perceptible collagen or the following structures: nests, fascicles or dispersed.
Extent of ulceration (mm)	The distance between the most lateral points of the epidermal defect and associated reactive changes.
Focally absent biphasic VGP TILs	TILs present to some extent within one VGP component of the melanoma but lacking in another VGP component.
Focally absent biphasic VGP TIMs	TIMs present to some extent within one VGP component of the melanoma but lacking in another VGP component.
Microscopic ulceration	Full thickness epidermal defect, accompanied by reactive changes (including neutrophils and fibrin) and surrounding epidermal thinning or hyperplasia, in the absence of trauma or surgery.
Non-brisk sparse TILs	TILs that infiltrate the upper half of the VGP melanoma.
Non-brisk sparse TIMs	TIMs that infiltrate the body of the VGP melanoma in the absence of TIMs along the base of the VGP.

Scoring variable	Detail of Scoring Schema
Non-brisk peripheral TILs	TILs that infiltrate the VGP melanoma focally or subtotally and are absent from the upper half of the VGP melanoma.
Non-brisk peripheral TIMs	TIMs that infiltrate the VGP melanoma along the base in a focal or subtotal fashion.
Regression thickness (in mm)	Measured from the top of the granular layer of the epidermis to the nearest melanoma cell (if present) lying deep to the regression. If no melanoma cells remained, the thickness was measured to the deepest estimated edge of regression.
Superficial tumour loss	A deficit in the melanoma, detectable at 4x magnification, whose proximal aspect is situated in the dermis that is immediately in contact with the dermo-epidermal junction. This must not underlie a region of melanoma *in situ* without perceptible VGP melanoma beneath it or a region of microscopic ulceration.
Totally absent TILs	TILs that are not detectable at 10x magnification or do not infiltrate the VGP melanoma.
Totally absent TIMs	TIMs that are not detectable at 10x magnification or are not closely apposed to the VGP melanoma.
Tumour-infiltrating macrophages/melanophages (TIMs)	Macrophages/melanophages that infiltrate or are closely apposed to the VGP melanoma.
Tumour loss	A clear deficit within the silhouette of the melanoma at 4x magnification and composed of a variable presence of lymphocytes, melanophages and/or fibrous tissue.

2.5.1 Breslow thickness measurement

For non-ulcerated cases, Breslow thickness was calculated by selecting the ruler icon in Aperio® ImageScope© and drawing a line from the top of the granular cell layer of the epidermis to the deepest point of melanoma invasion (excluding adnexal or lymphovascular involvement or microsatellites) (Figure 2.4). A maximum of three measurements were permitted on one section and a maximum of six measurements were recorded in total per slide (i.e. some slides contained multiple sections).

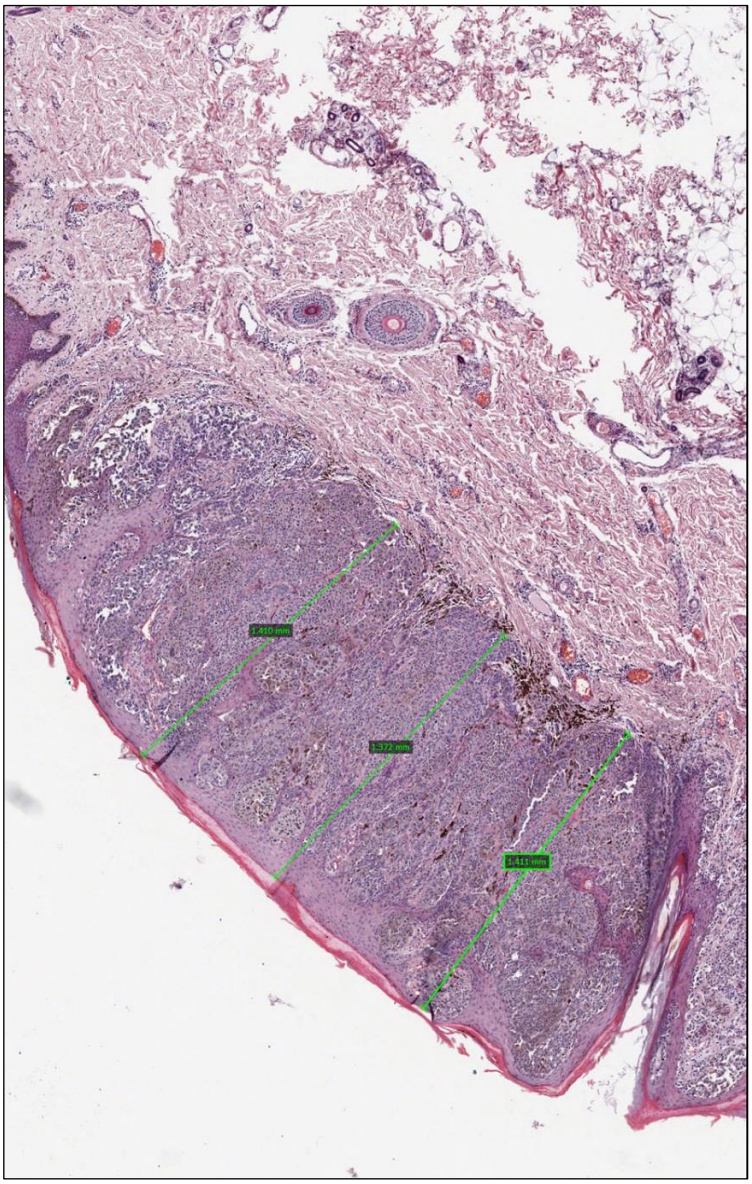

Figure 2.4 Virtual pathology image showing a melanoma with annotated Breslow thickness measurements

Histopathological findings (low power view) show a melanoma with 3 annotated Breslow thickness measurements. The greatest tumour thickness on any section for a single case was taken to be the definitive Breslow thickness.

2.5.2 Dominant nodule

Superficial spreading melanoma is characterised by the presence of a nested arrangement of melanoma cells; however, some of these may have a prominent nodular component. In contrast, nodular melanoma adopts a nodular configuration and is said to lack a radial growth phase [182]. The histological definition, however, permits the presence of intraepidermal melanoma cells lateral to the nodule for up to 3 rete ridges [187]. If melanoma cells extend laterally beyond this limit, then superficial spreading melanoma is recorded. Therefore, there is a degree of overlap between these two categories, the cut-off point for which is somewhat arbitrary.

Rao *et al.* noted that a "dominant nodule" was present in some thick melanomas [70]. They defined a dominant nodule as "an expansile nodule composed of morphologically homogeneous cells of naevoid or pleomorphic morphologic features" and considered that it might reflect a clonal expansion of melanoma cells [70]. Its presence was shown to influence relapse-free survival [70]. Therefore, the presence of a prominent nodular component, regardless of its histological subtype appeared to be noteworthy. Accordingly, I opted to record the presence or absence of a dominant nodule (recorded as yes or no). This initially appeared to be a simple measure, however, it became clear that its interpretation could be altered by the magnification used. Although Rao *et al.* recommended that low-power magnification be used to determine the presence of a dominant nodule, it became clear that melanomas with significant nesting could be still be captured by this definition (as nesting might not be fully appreciable at low-power). The definition was adapted in order to record the presence of a confluent nodule, which I considered most likely to represent the positive selection of a clonal expansion of melanoma cells, dominating over other subpopulations. The final definition necessitated that each section of melanoma be assessed at 10x magnification. A dominant nodule was deemed to be present if melanoma cells occupied the entirety of a single computer screen of the mini-wall. The presence of lymphocytes, macrophages, plasma cells, neutrophils, eosinophils, vascular or lymphatic vessels was permitted within the dominant nodule of the melanoma. Squamous epithelium, rete ridges, normal dermis or subcutaneous fat had to be excluded from the field of vision. A dominant nodule was absent if these elements could not be excluded from the screen, if the melanoma was too small to fill the entire screen, if collagen or a clear structural pattern of melanoma, other than sheets (Table 2.1 and Table 2.2), could be appreciated at this magnification. Whether or not the TMA biopsy was taken from the dominant nodule was also recorded as yes, no or not applicable.

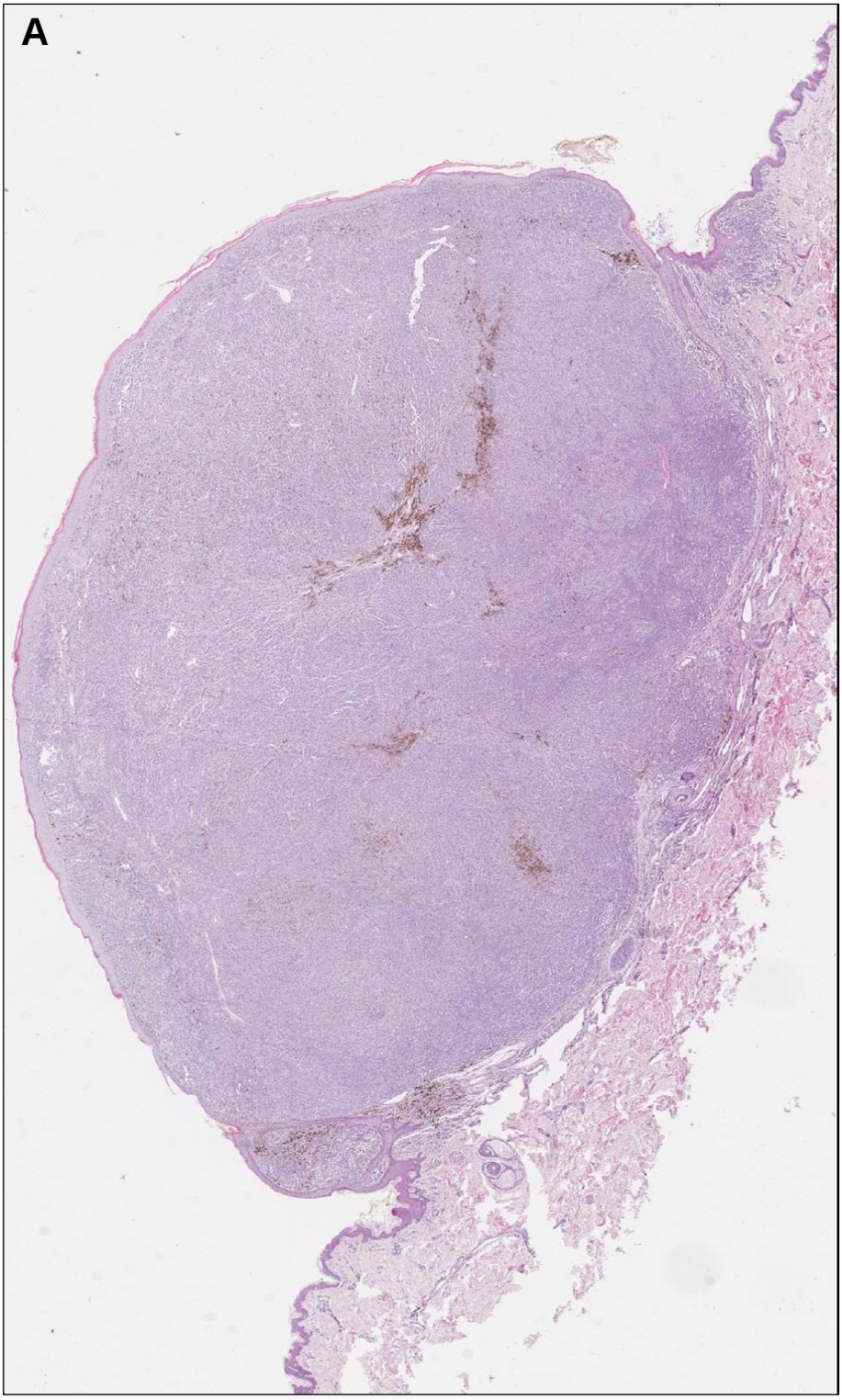
A

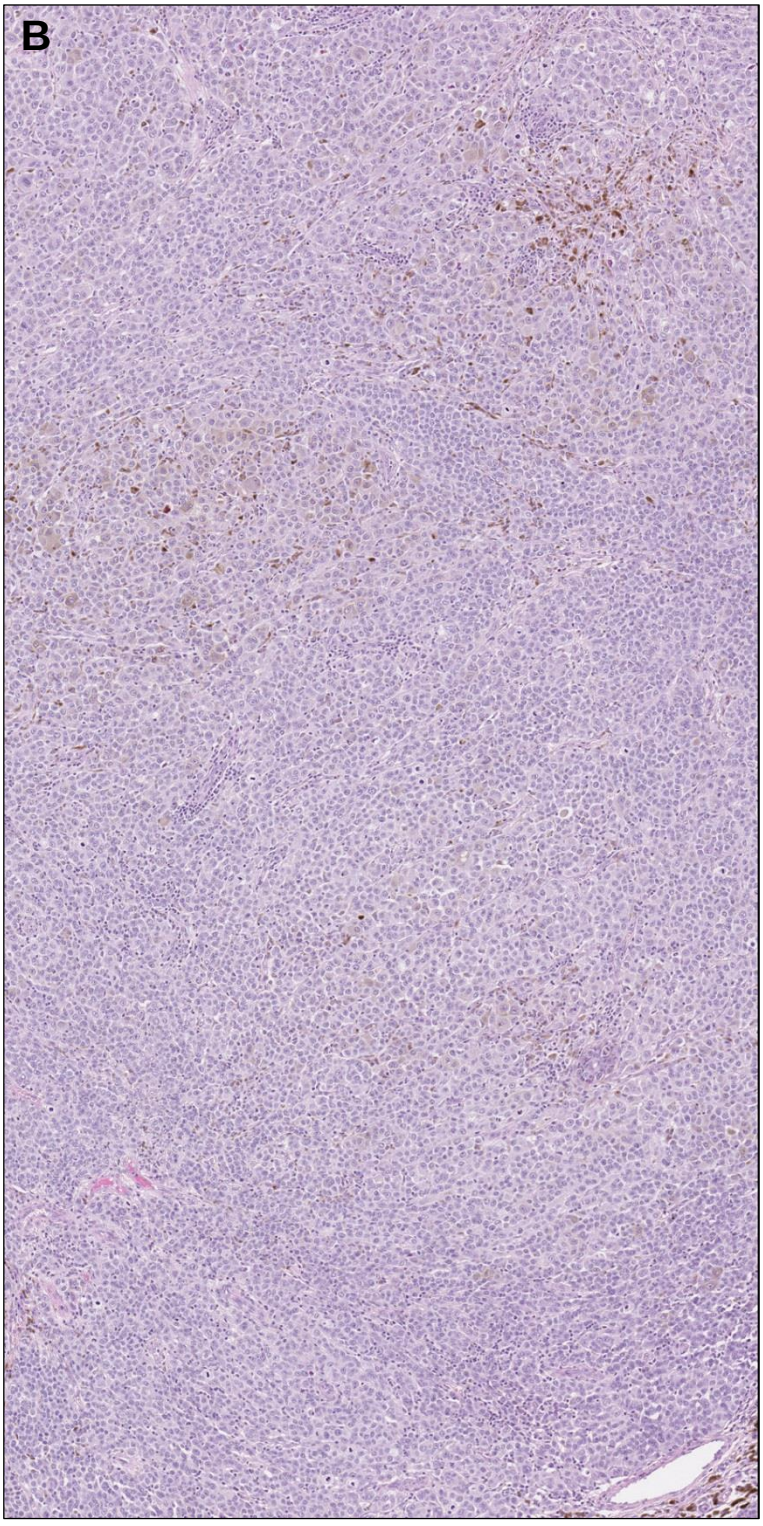

Figure 2.5: Virtual pathology images (A) and (B) of a melanoma containing a dominant nodule

The histopathological appearance (A) at low power (x2 magnification) is suggestive of the presence of a dominant nodule, however, the findings (B) at x10 magnification confirm that this meets the criteria for a dominant nodule. One entire screen of the mini-wall was occupied by melanoma at this magnification and the appearance was relatively structureless with minimal connective tissue.

2.5.3 Microscopic ulceration and measurement of its extent

If ulceration was present on any section, it was deemed to be present. Where present, the extent of ulceration was measured by drawing a line (using the ruler icon) between the two most lateral points of ulceration with the computer cursor (Figure 2.6A). A total of six separate measurements could be made, on either the same or different sections. The largest value recorded on any slide for the same case was the maximum extent of ulceration for that case. For melanomas with multiple, discontiguous ulcers, the cumulative extent of ulceration was also calculated, by the addition of measurements for up to six ulcers on the same section (Figure 2.6B). The maximum cumulative extent of ulceration for a case was the maximum value for the sum of these discontinuous ulcers within the same section.

2.5.4 Grading tumour-infiltrating lymphocytes

TILs were graded at 10x magnification on the thickest section of melanoma. A modified version of Clemente *et al.*'s approach was employed [61] (Figure 2.7).

Figure 2.6 (on following page): Virtual pathology images (A) and (B) showing melanomas with annotated measurements for the extent of microscopic ulceration

Histopathological findings (low power view) show (A) a continuous ulcer measuring 10.99mm (annotated in yellow). Measurements for Breslow thickness are annotated in green. The maximum thickness was used for the definitive Breslow thickness. (B) Four discontiguous, focal ulcers (annotated in yellow). The largest ulcer (340 microns) was used for the definitive extent of ulceration, while the cumulative extent of ulceration was calculated by summing the measurements of all four ulcers on this section (to give a cumulative extent of ulceration of 0.965mm). The extent of ulceration was used for statistical analyses, as the cumulative extent of ulceration was present in a minority of cases.

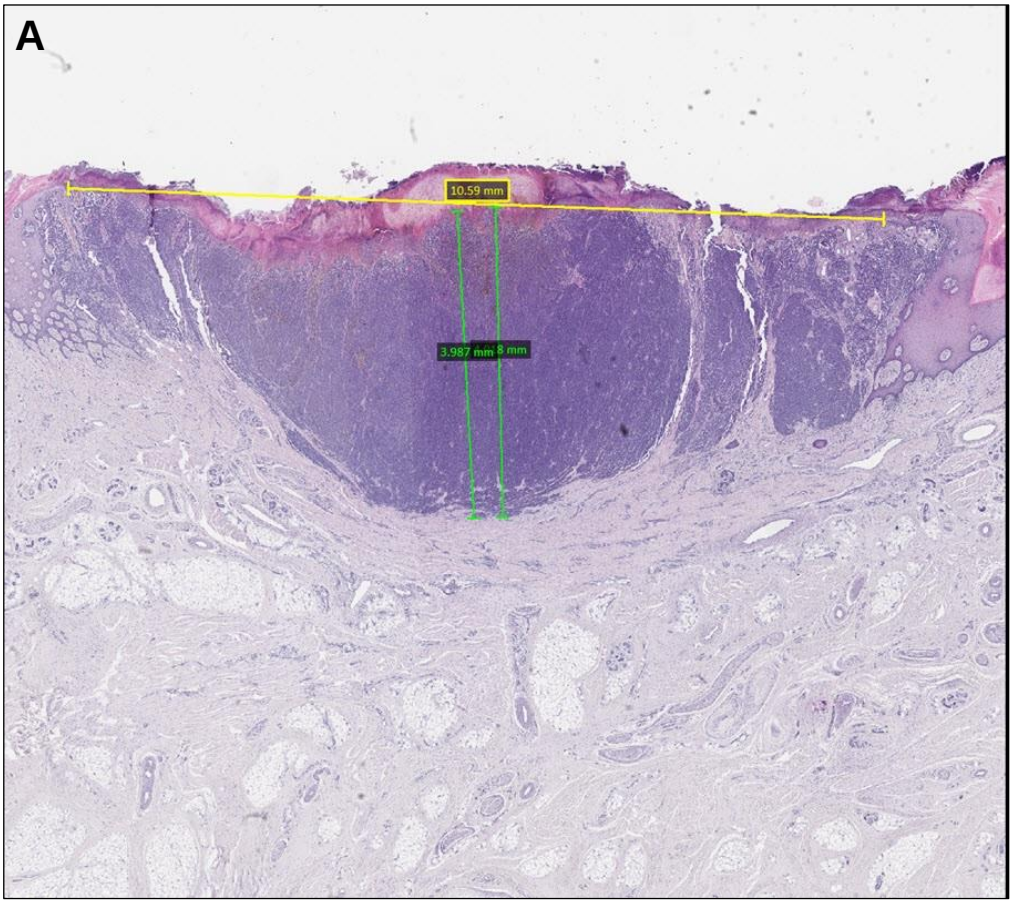
A
10.59 mm
3.987 mm
8 mm

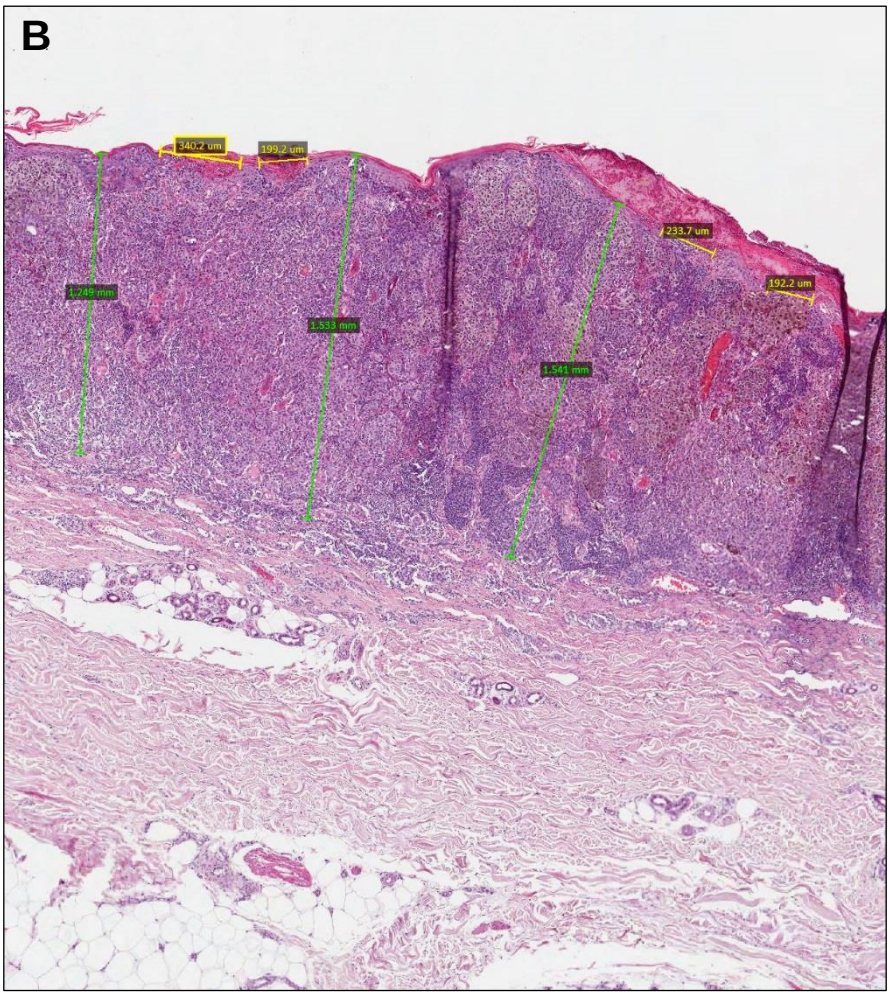
B
340.2 um
199.2 um
1.749 mm
1.533 mm
1.541 mm
233.7 um
192.2 um

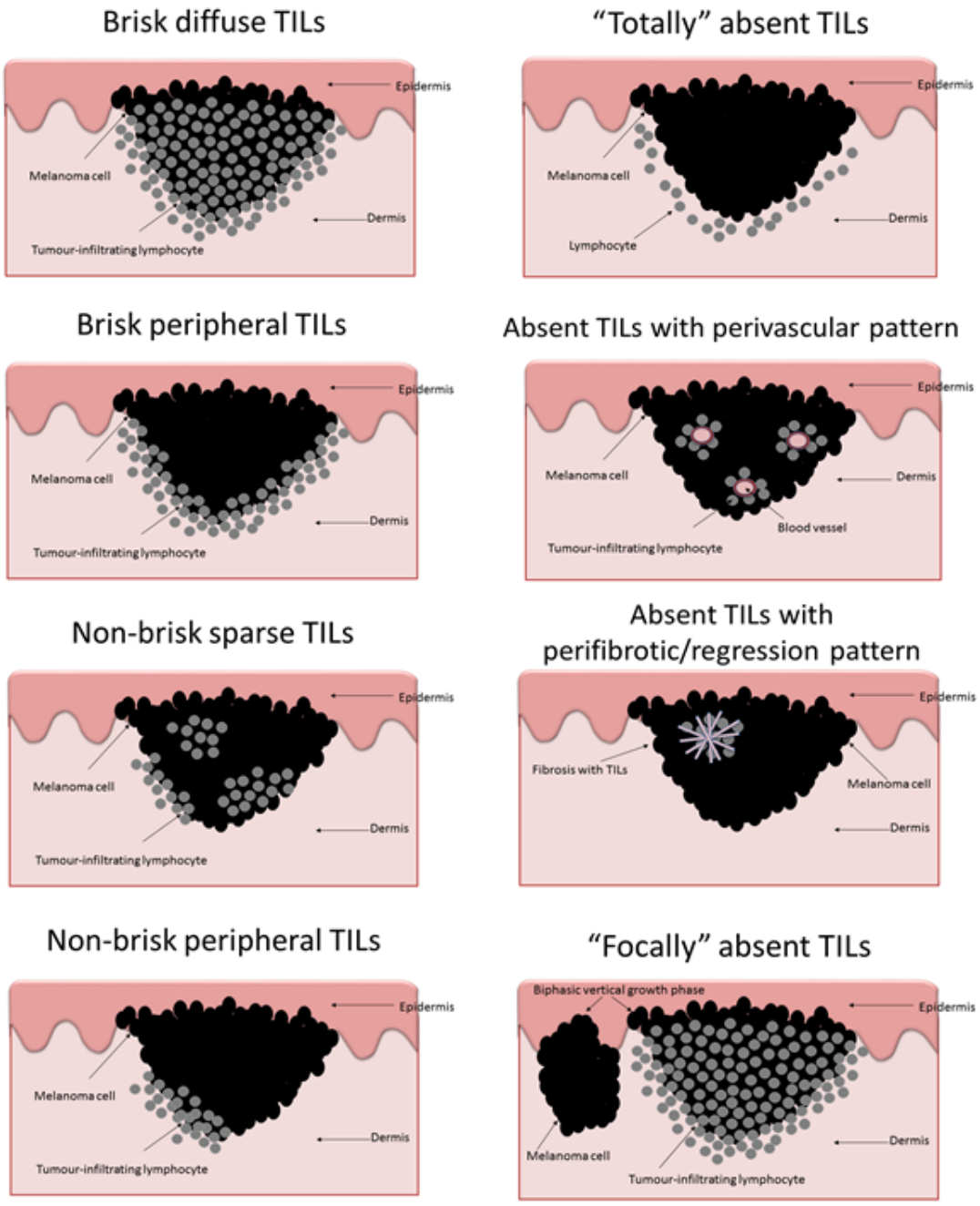

Figure 2.7: Clemente's classification of TILs [61], modelled on Clark's original classification.

Brisk TILs were subclassified as diffuse and peripheral. Non-brisk TILs were subclassified as sparse and peripheral. TILs were considered to be "totally" absent if lymphocytes were present but did not infiltrate the vertical growth phase (VGP). TILs were "focally" absent if they infiltrated only one part of a biphasic VGP melanoma. TILs occurring in a perivascular pattern or associated with a region of fibrosis were regarded as being absent.

Examples of TIL infiltration patterns are shown in (Figure 2.8 A-G). “Brisk peripheral” was assigned if TILs infiltrated the entire base of the vertical growth phase (VGP) melanoma. TILs were deemed to be “brisk diffuse” if they met the criteria for “brisk peripheral” and additionally infiltrated the VGP melanoma centrally, to the extent that the VGP melanoma appeared to be consumed or heavily infiltrated by TILs. If TILs were located within the upper half of the VGP and were not distributed in a brisk pattern, then they were regarded as “non-brisk sparse” TILs, irrespective of focal infiltration of the VGP base. Even small clusters of TILs in the upper half of the VGP were sufficient to be categorised in this way. “Non-brisk peripheral” was recorded if TILs infiltrated the base of the VGP focally or in an incomplete manner. TILs were considered to be “totally absent” if there was no lymphocytic infiltrate noted at 10x magnification or if lymphocytes were located elsewhere in the skin, including near but separate to the base, i.e. not infiltrating the VGP. TILs were graded as “absent with a perivascular pattern” if they did not meet the criteria for brisk or non-brisk but instead congregated in clusters surrounding blood vessels within the VGP. TILs were graded as “absent with a perifibrotic/regression pattern” if they did not meet the criteria for brisk or non-brisk and were located predominantly within a region demonstrating fibrosis or regression (with or without a variable infiltrate of melanophages). “Focally absent biphasic VGP” was selected if the melanoma had more than one VGP component and if TILs infiltrated only one of these VGPs, regardless of the pattern of TILs in the infiltrated VGP component. A series of sequenced questions was developed to determine the categorisation in a systematic way (Figure 2.9).

Figure 2.8 Virtual pathology images (A-G) showing melanomas with different patterns of tumour-infiltrating lymphocytes (TILs)

Histopathological findings (x10 magnification) show (A) TILs extensively infiltrating the base and the body of the melanoma. TILs were classified as brisk diffuse. (B) A brisk lymphocytic infiltrate at the invasive margin of the melanoma. TILs were classified as brisk peripheral. The superficial part of the melanoma was not heavily infiltrated by TILs (not shown). (C) Small clusters of lymphocytes can be seen focally infiltrating the superficial aspect and the invasive margin of the melanoma. TILs were classified as non-brisk sparse. (D) Focal infiltration of the invasive margin of the melanoma but sparing of the superficial aspect of the melanoma. TILs were classified as non-brisk peripheral. (E) TILs are not apparent within this melanoma and were classified as totally absent. (F) Absent TILs with a perivascular pattern. (G) TILs within a region of fibrosis, classified as absent TILs with a perifibrotic/regression pattern.

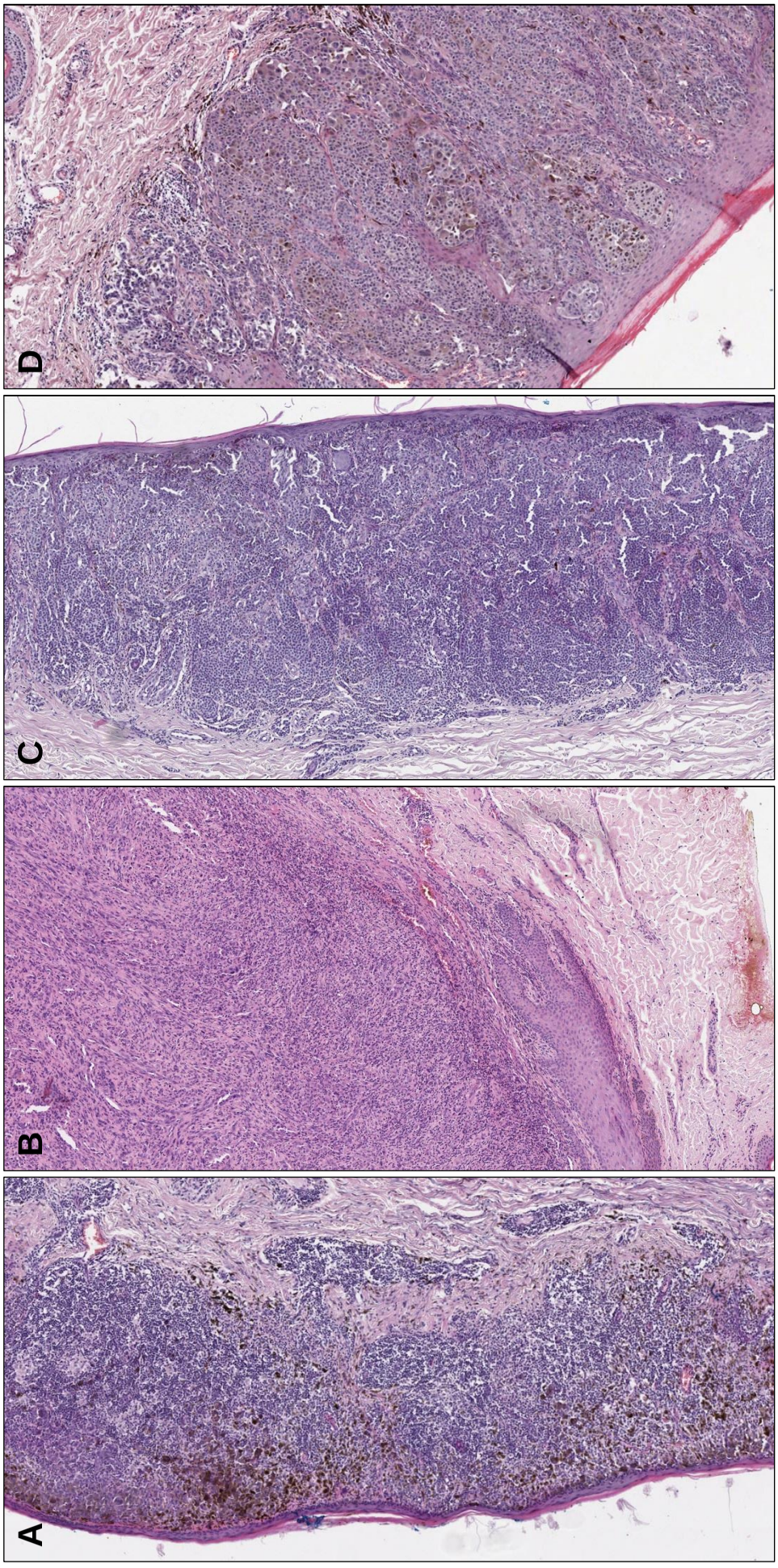
D
C
B
A

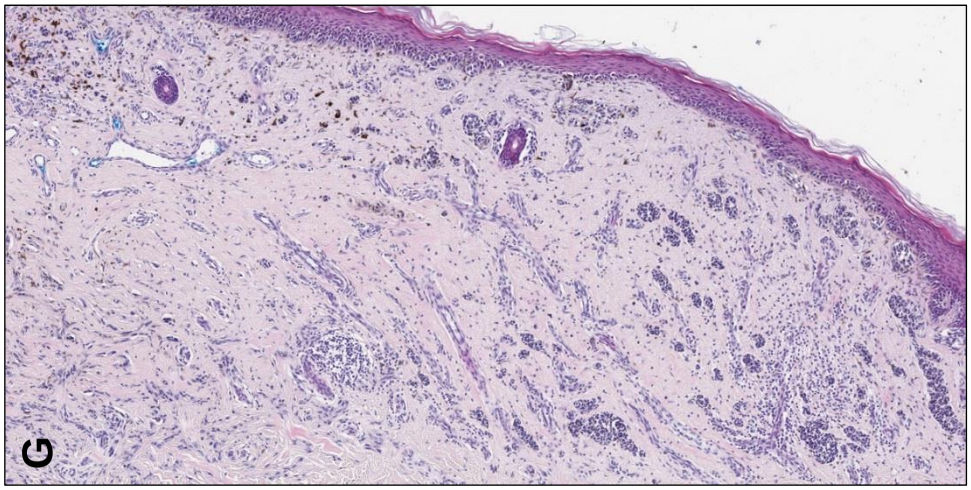
G

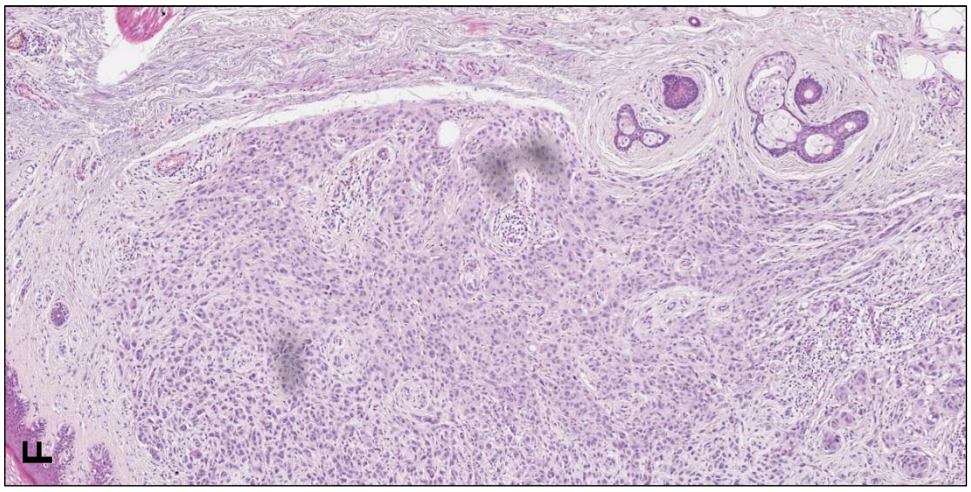
F

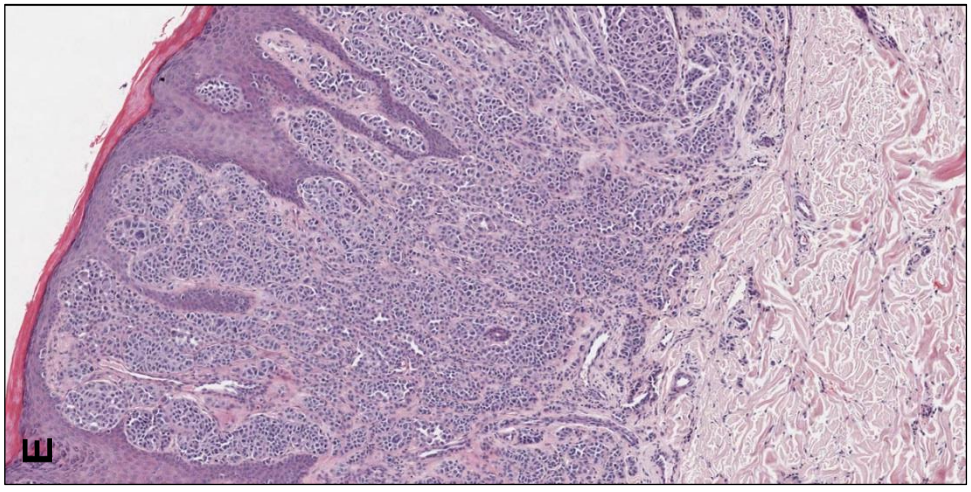
E

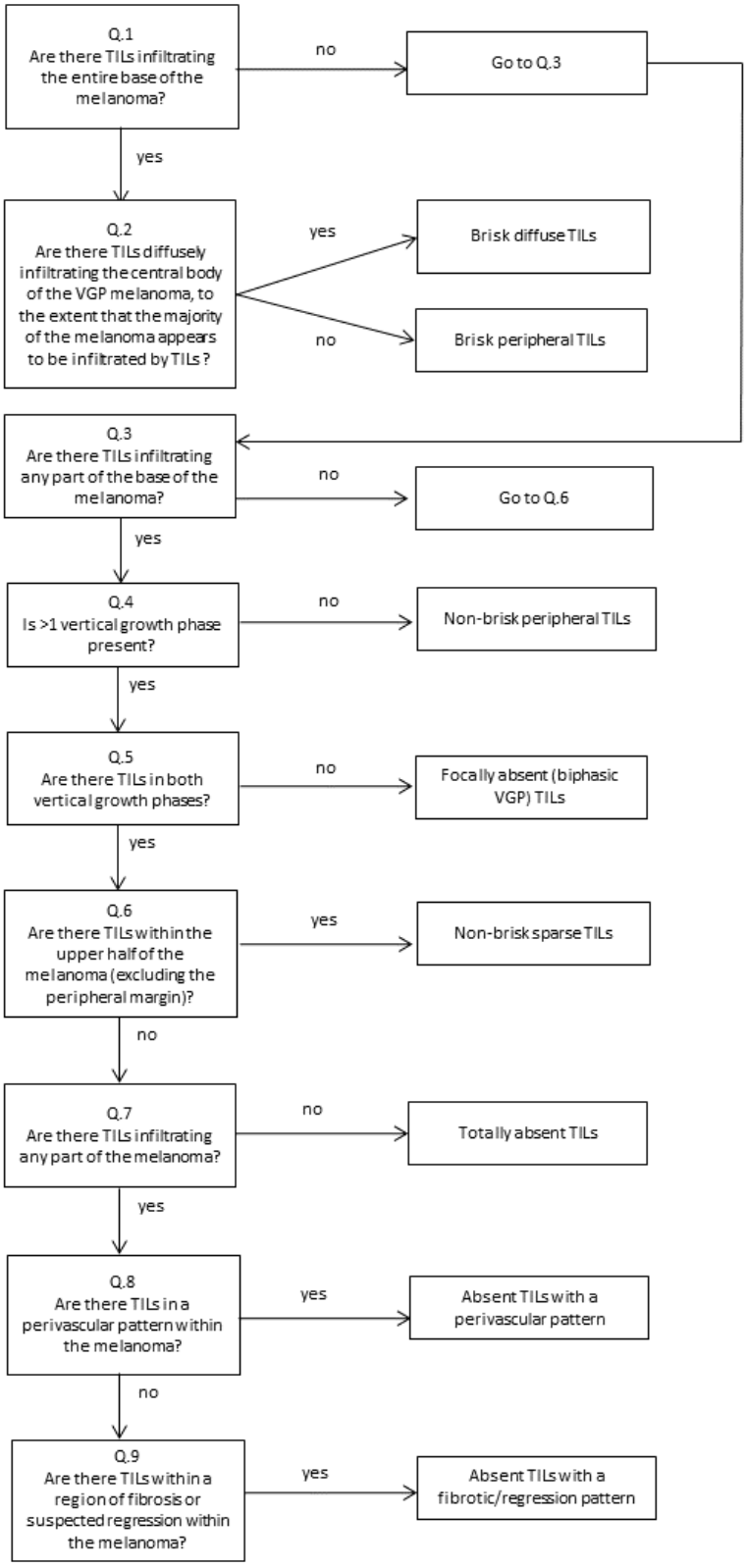

Figure 2.9: Flow chart for determining the category for tumour-infiltrating lymphocytes (TILs)

A series of questions was used to determine the pattern of TILs within the thickest section of melanoma. VGP=Vertical growth phase.

2.5.5 Regression and tumour loss

During interim analysis, it became clear that the regression variable was ill-defined and could have represented multiple, different features: an immune response consisting of lymphocytes or melanophages, in isolation or combined; a fibrous tissue reaction, a region of tumour destruction or even a skip lesion (i.e. a region lacking in melanoma due to architectural arrangement rather than destruction). An attempt was made to solidify this measure and to apply this both to melanomas already reviewed and to further cases. Different aspects of regression were recorded together and separately as follows: tumour loss, the maximum depth of tumour loss in millimetres, the presence of melanophages and their intensity and pattern within the thickest section of melanoma. Tumour loss was defined as a clear deficit within the silhouette of the melanoma at 4x magnification and composed of a variable presence of lymphocytes, melanophages and/or fibrous tissue. Verification of constituents was permissible at a higher magnification but the overall impression of tumour loss had to be gauged at 4x.

2.5.5.1 Type of tumour loss

Tumour loss was also categorised as superficial, deep or both (Figure 2.10). Superficial tumour loss was deemed to be present if there was a deficit within the melanoma underlying the dermo-epidermal junction and its immediately adjacent dermis, without overlying microscopic ulceration or melanoma *in situ*. This was to distinguish from a dyscohesive response that could be seen underlying a region of ulceration and from a lymphocytic response that could be seen in response to a region of *in situ* disease: not considered to represent tumour loss for the purpose of this study. Tumour loss was described as deep if the proximal aspect of the deficit began at a deeper level of the dermis or subcutis than that described in superficial. “Both” was assigned if there was a combination of superficial and deep types of tumour loss.

Figure 2.10 (on following page): Classification of tumour loss

Tumour loss was deemed to be present if there was a deficit within the melanoma, detectable at 4x magnification. The region of tumour loss could be composed of an infiltrate of melanophages alone, a mixture of fibrosis and an infiltrate of melanophages and/or lymphocytes, or fibrosis alone. Tumour loss was classified as superficial if the deficit was situated in the dermis, immediately underlying the dermo-epidermal junction, without overlying melanoma *in situ* or ulceration. Tumour loss was classified as deep if the deficit was within the dermis but without direct contact with the dermo-epidermal junction. Tumour loss was classified as both if both superficial and deep tumour loss were present.

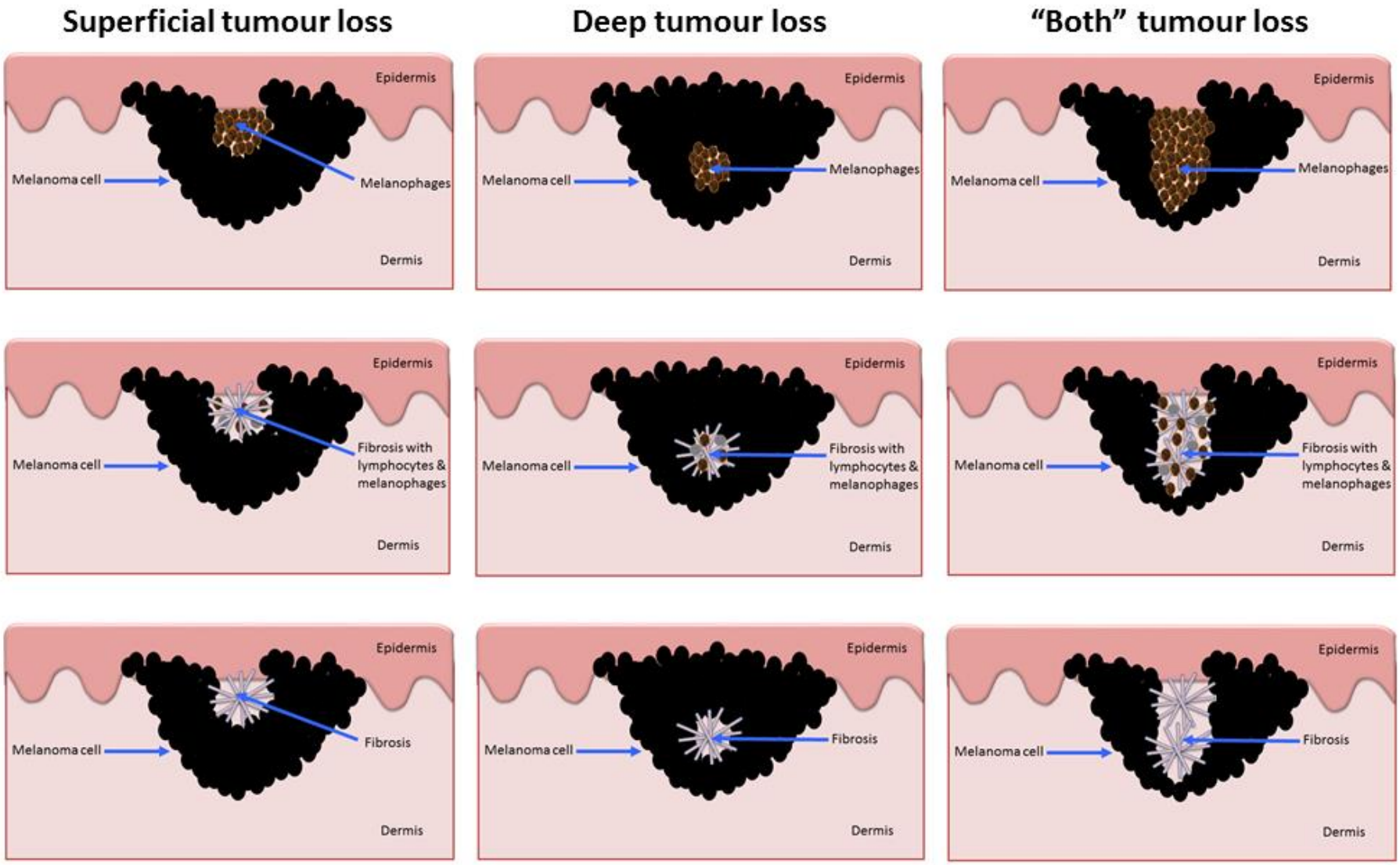
Superficial tumour loss
Deep tumour loss
"Both" tumour loss
Epidermis
Melanoma cell
Melanophages
Dermis
Fibrosis with lymphocytes & melanophages
Fibrosis

2.5.5.2 The maximum depth of tumour loss

The maximum depth was measured from the top of the granular cell layer to the lowest pole of the immune infiltrate within the region of loss, where present or the most inferior aspect of the perceived deficit.

2.5.6 Grading the intensity of melanophages

The intensity of melanophages was adjudged at 2x magnification on the thickest section of melanoma and was categorised as follows: none, very few, moderate or lots (Figure 2.12).

2.5.7 Grading the pattern of tumour-infiltrating melanophages

The pattern of infiltration by melanophages was summarised in a similar way to the method used to define TILs at 10x magnification on the thickest section, with a few exceptions (Figure 2.13 and Figure 2.14). Firstly, melanophages had to be in close proximity, but did not need to be in direct apposition, to melanoma cells. Secondly, if melanophages were present along part of the tumour base, the non-brisk peripheral category was assigned in preference to non-brisk sparse, regardless of whether or not some melanophages were present within the upper half of the melanoma.

Figure 2.11 (on following page): Virtual pathology images (A-C) showing melanomas with different types of tumour loss

Histopathological findings (x4 magnification) show (A) fibrosis and melanophages within a region of tumour loss in the superficial dermis, just inferior to the dermo-epidermal junction. This was classified as superficial tumour loss. (B) A dense infiltrate composed of melanophages at the deep aspect of the melanoma. The red line highlights the annotation for the depth of tumour loss. This was classified as deep tumour loss. Breslow thickness is annotated with green lines. (C) A focal, dense infiltrate of melanophages extends from the superficial dermis to the invasive margin of the melanoma. This was classified as “both” types of tumour loss.

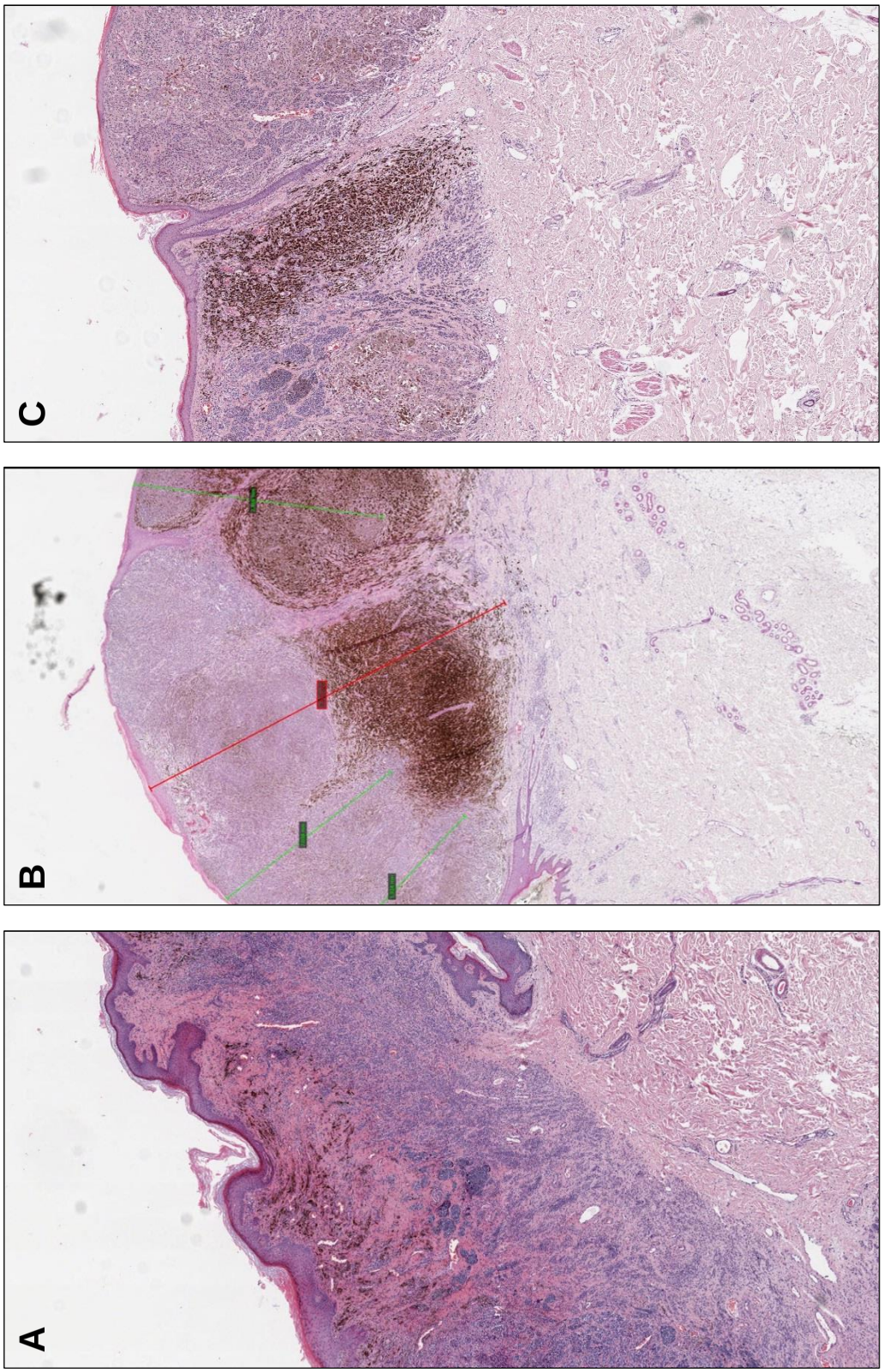
C
B
A

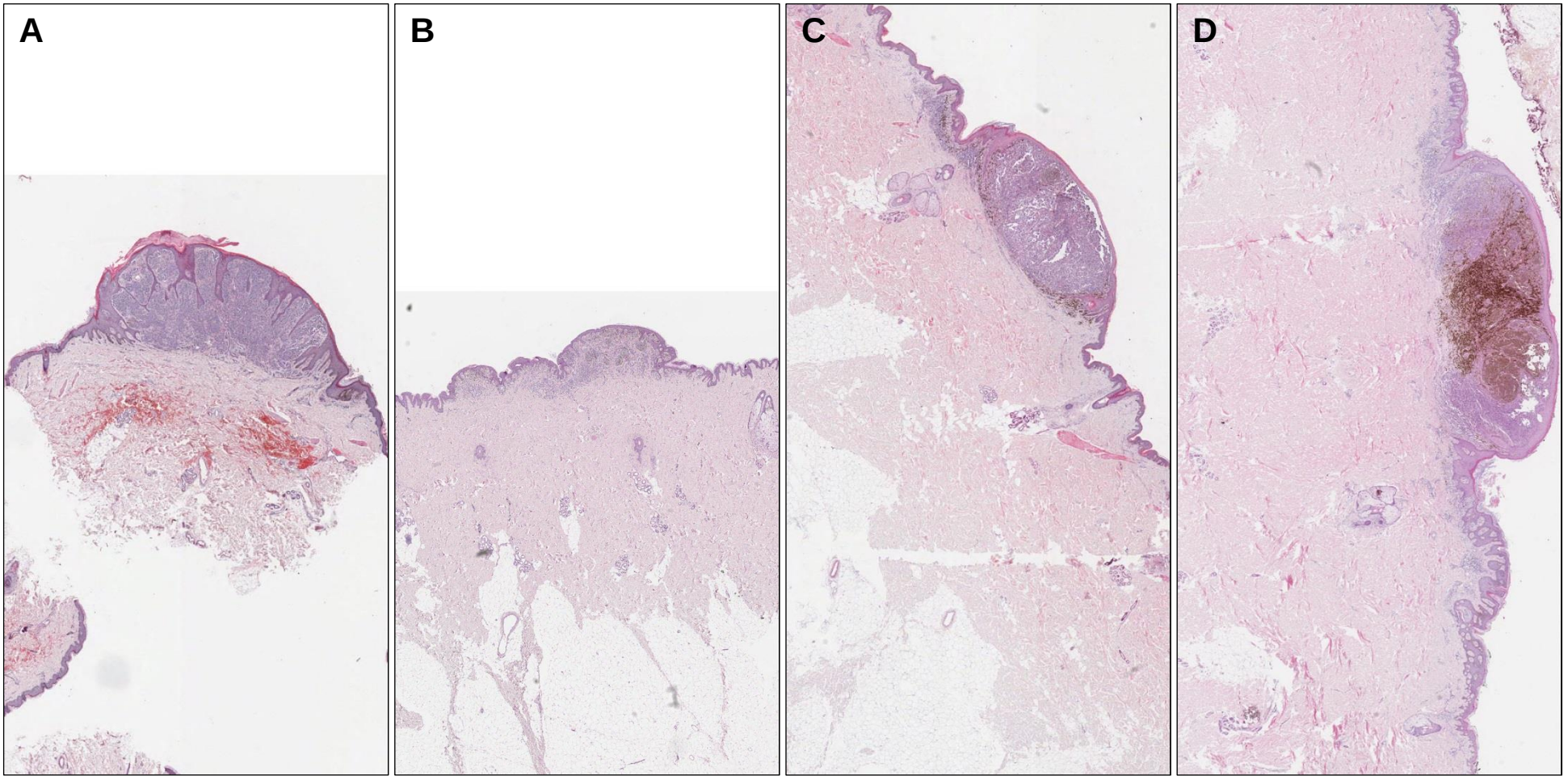

Figure 2.12: Virtual pathology images (A-D) varying intensities of melanophages

Histopathological findings (x2 magnification) show (A) none, (B) very few, (C) moderate and (D) lots of melanophages within the melanomas.

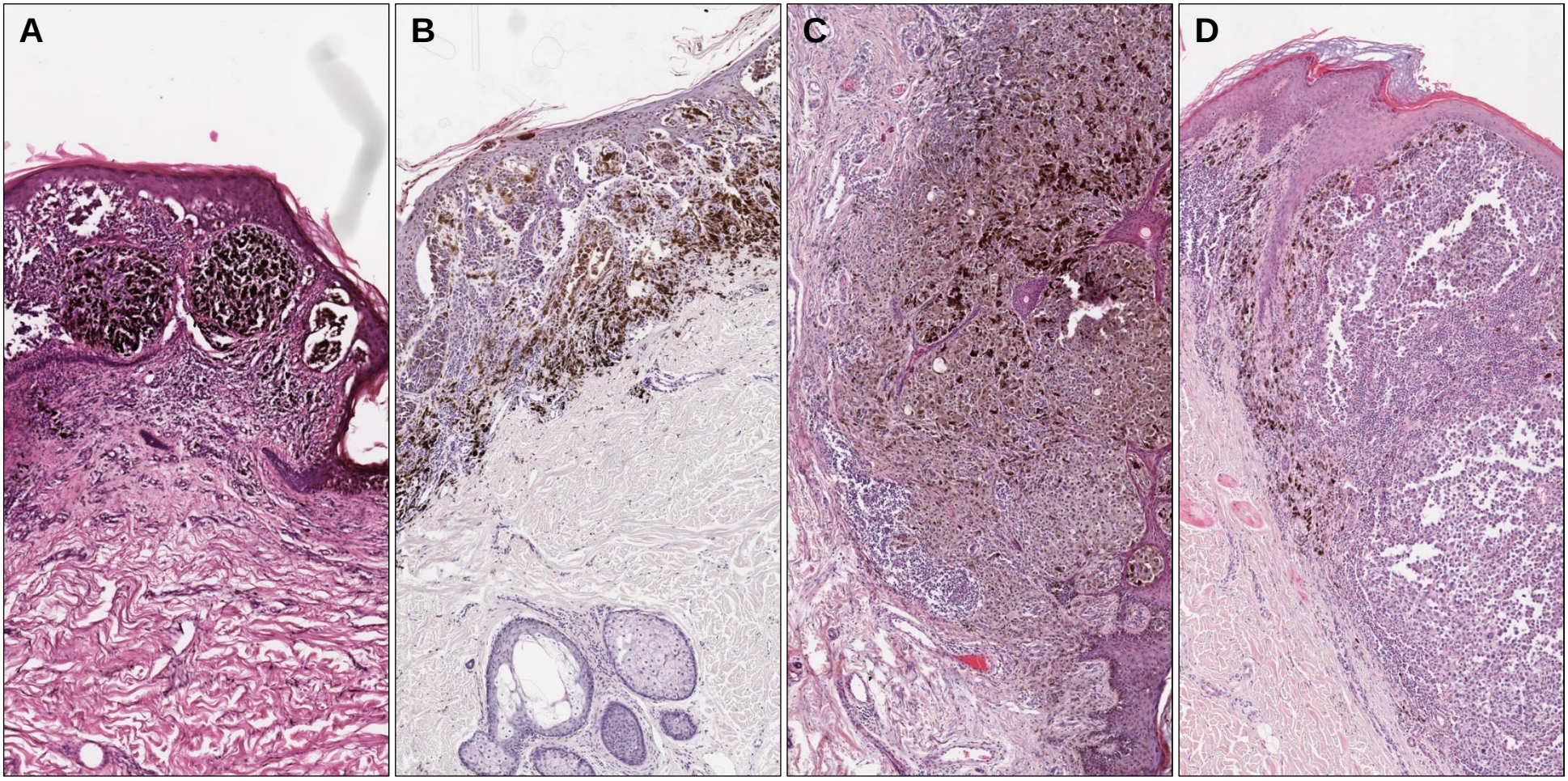

Figure 2.13: Virtual pathology images (A-D) of melanomas showing different patterns of tumour-infiltrating melanophages (TIMs)

Histopathological findings (x10 magnification) show (A) brisk diffuse TIMs, (B) brisk peripheral TIMs, (C) non-brisk sparse TIMs and (D) non-brisk peripheral TIMs.

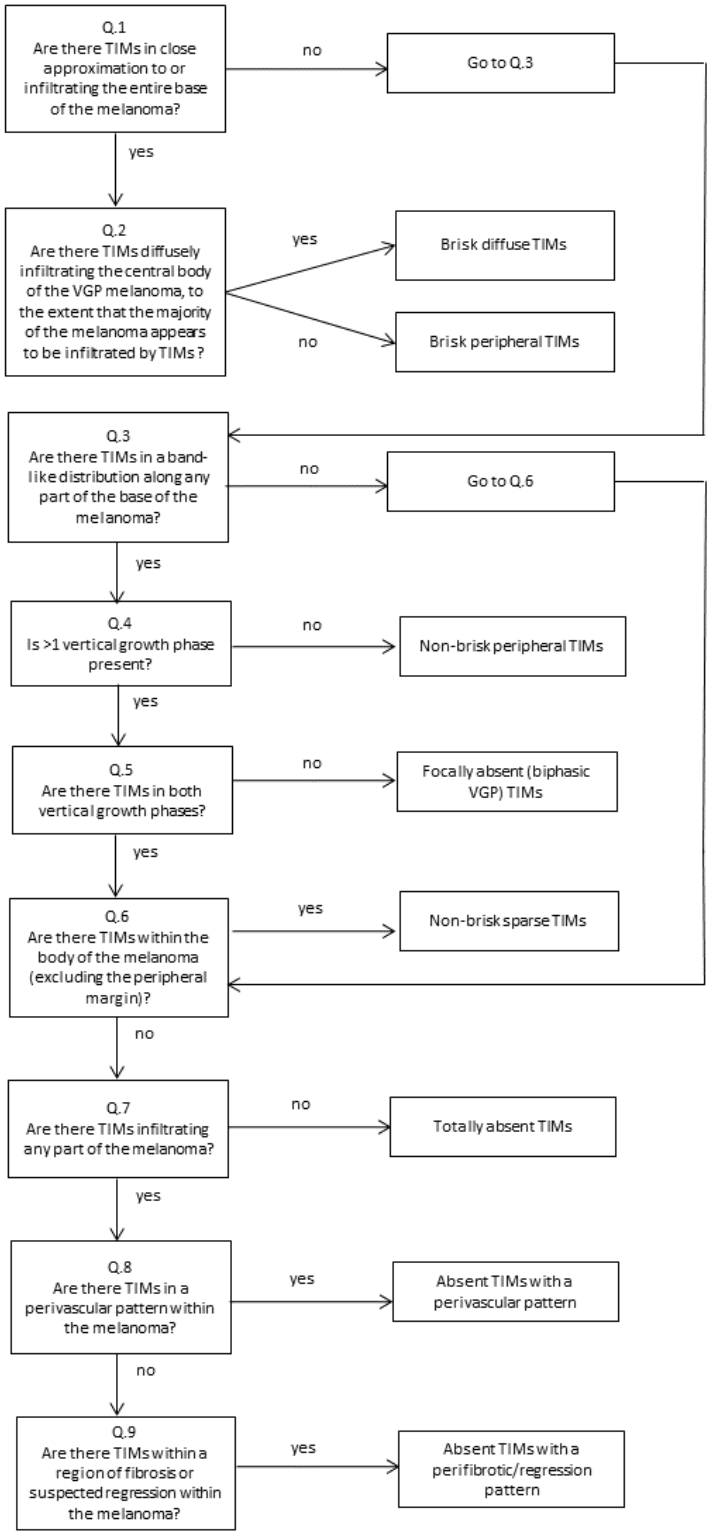

Figure 2.14: Flow chart for determining the category of tumour-infiltrating melanophages (TIMs)

A series of questions was used to determine the pattern of TIMs within the thickest section of melanoma. VGP=Vertical growth phase.

2.6 Virtual pathology protocol: cored region measures

Details of the scoring variables and schema for cored regions using the virtual pathology protocol are given in Table 2.3.

2.6.1 Calculating the proportion and the percentage of stroma

The cored regions were extracted in association with the flatbed-scanned image and the proportion of stroma was calculated using RandomSpot© as previously described in the “Pilot work using virtual pathology” section. On the basis of the pilot work, 50 spots were selected per core. The percentage of stroma (POS) was calculated by multiplying the proportion of stroma by 100. Several cut-off points were explored for the POS and the continuous measure was also divided into quintiles. The continuous measure for POS was used in multivariable survival analyses (Chapter 4), as it was the strongest prognostic factor.

2.6.2 The quality of the stroma

The quality of the stroma was used to describe the appearance of the connective tissue/collagen within the cored region (Figure 2.15). “Compact” was recorded if the connective tissue had a pink colour and adopted an organised, regular structure. “Loose” was recorded if the connective tissue appeared to be disorganised, with frequent gaps. “Mixed” was recorded if both compact and loose connective tissue was present within the cored region.

Table 2.3: Properties of the Histopathological Scoring Variables for Cored Region Measures using the Virtual Pathology Protocol

Details of variables recorded within the cored regions using the virtual pathology protocol.

Scoring variable	Detail of Scoring Schema
Absent pigmentation	The cytoplasm of melanoma cells lacking melanin.
Barely perceptible infiltrate	An immune cell infiltrate within the cored region that is very faint but just visible at 20x magnification.
Balloon cell shape	A melanoma cell shape that is round and contains abundant, nonstaining, vacuolated cytoplasm.
Blood vessel	A structure whose lumen contains red cells.
Compact stroma	Pink connective tissue that has a uniform structure and lacks significant gaps.
Dispersed	A type of melanoma structure characterised by individual melanoma cells separated from each other by strands of connective tissue.
Distribution of immune cell infiltrate	The location of the immune cell infiltrate within the cored regions.
Epithelioid cell shape	A melanoma cell shape consisting of a round nucleus, a prominent, pink nucleolus and variably eosinophilic and often abundant cytoplasm [97].
Location of the immune cell infiltrate	The location of the immune cell infiltrate within the cored regions: classified as follows: at the tumour/stroma interface, dispersed between tumour cells or both.
Faint pigmentation	Pigmentation of the melanoma cell cytoplasm that is slight, just detectable and significantly lighter than the melanoma cell nucleus.

Scoring variable	Detail of Scoring Schema
Fascicles	A melanoma cell structure consisting of elongated bundles of cells.
High pigmentation	Pigmentation of the melanoma cell cytoplasm such that it is darker than the melanoma cell nucleus.
Loose stroma	Connective tissue that has several gaps within it and does not form an orderly structure.
Lots of infiltrate	The most abundant amount of immune cell infiltrate within the cored region.
Melanoma cell structure	The way in which individual or small groups of melanoma cells tend to be arranged.
Mixed stroma	Connective tissue that has features of both compact and loose stroma.
Moderate infiltrate	An immune cell infiltrate within the cored region that is intermediate between some and lots.
Moderate pigmentation	Pigmentation of the melanoma cell cytoplasm that is intermediate between faint and high.
Naevoid cell shape	A melanoma cell shape that resembles a benign naevus cell and has prominent nuclear hyperchromasia and sparse cytoplasm.
Nests	A melanoma cell structure characterised by round/ovoid groups of melanoma cells.
Plasmacytoid cell shape	A melanoma cell shape that resembles a plasma cell and has an eccentric nucleus.
Round/ovoid cell shape	A melanoma cell shape consisting of a round to oval nucleus and lacking an eosinophilic nucleolus.
Sheets	A melanoma cell structure characterised by individual melanoma cells in close apposition to one another and relative absence of connective tissue between individual melanoma cells.

Scoring variable	Detail of Scoring Schema
Some infiltrate	An immune cell infiltrate within the cored region that is readily detectable at 20x magnification but the extent of which is mild.
Stroma	The part of the cored region that remains after subtracting the melanoma cells, i.e. the non-tumour compartment. This consists of collagen, vascular or lymphatic structures and immune cells. Squamous epithelium or rete ridges or non-informative regions are excluded.
Stroma quality	The appearance of the connective tissue within the cored region, i.e. loose, compact or mixed.
Spindle cell shape	A melanoma cell shape with an elongated or fusiform appearance and a long axis proportionally larger than the short axis.
Super spindle cell shape	A melanoma cell shape with a markedly elongated spindle cell shape and a narrow, long nucleus.
Very high pigmentation	Dark pigmentation of the melanoma cell cytoplasm, to the extent that the nucleus cannot be perceived.

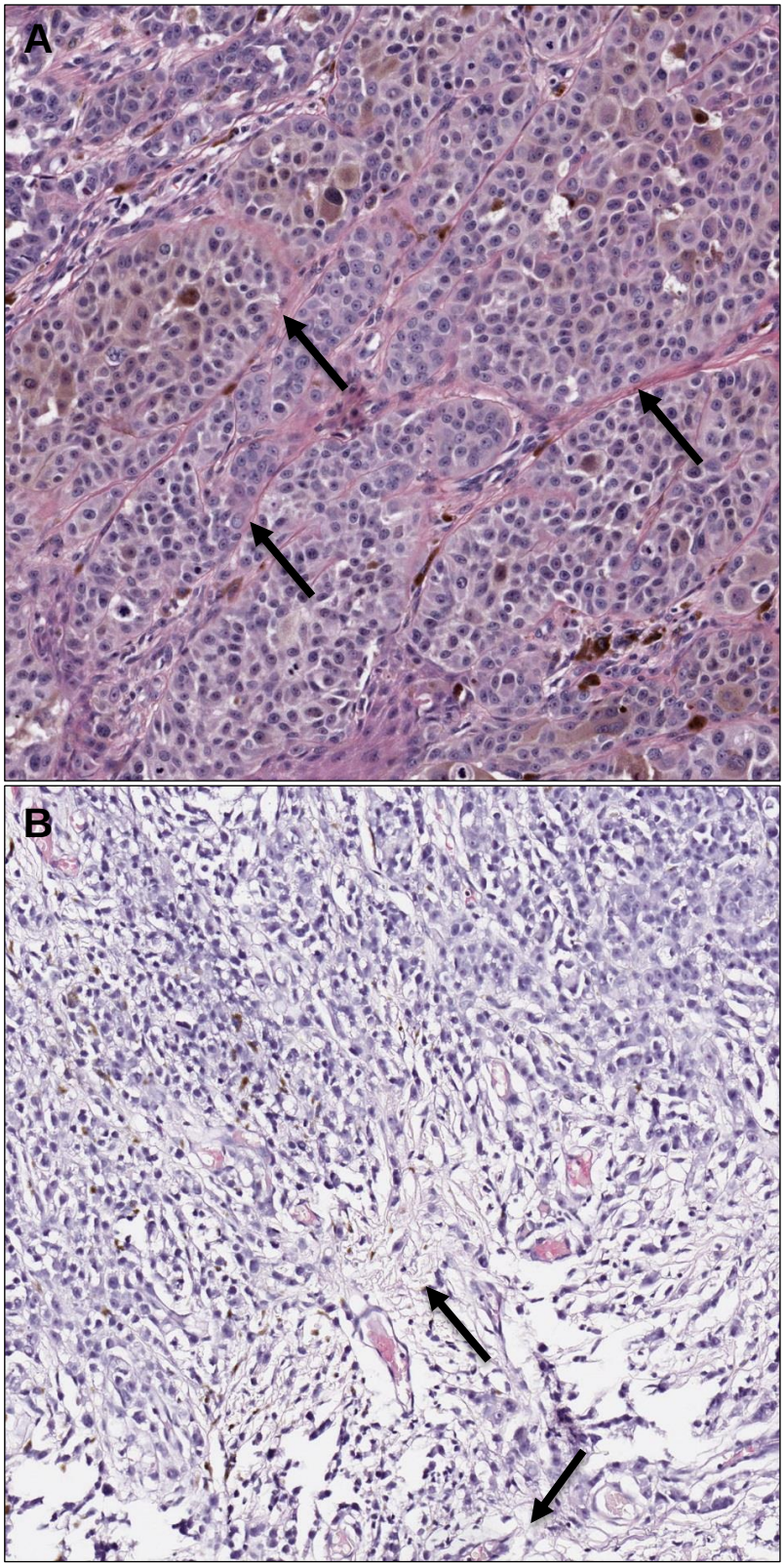

Figure 2.15: Virtual pathology images of cored regions from melanomas showing (A) compact and (B) loose stroma

Histopathological findings (x20 magnification) show digitally extracted cored regions containing (A) compact stroma (black arrows) with nests of epithelioid cells and (B) loose stroma (black arrows).

2.6.3 Melanoma cell shape

The digitally extracted cored regions were then opened as separated images in ImageScope© and each cored region was assessed separately (Figure 2.16). Melanoma cell shape categories were as follows: “epithelioid”, “round/ovoid”, “spindle”, “super spindle”, “naevoid”, “plasmacytoid” and “balloon”. Epithelioid cells were characterised by the presence of round nuclei containing prominent, eosinophilic nucleoli and often abundant eosinophilic cytoplasm. Round/ovoid cells were defined by the presence of round to oval nuclei and the absence of eosinophilic nucleoli. Spindle cells consisted of cells with cigar-shaped or fusiform nuclei. Super spindle cells were distinguished from spindle cells by their elongated, thinner nuclei. Naevoid cells contained nuclei with marked hyperchromasia and sparse amounts of cytoplasm and resembled benign melanocytes. Plasmacytoid cells had eccentric nuclei and resembled plasma cells. Balloon cells were round with abundant, nonstaining, vacuolated cytoplasm. The most abundant cell shape present (in approximately ≥80% melanoma cells by eyeball) within the cored region, was assigned to that core. If it was not possible to assign one of these choices, “other” was selected and further details were recorded. Where a mixture of melanoma cell shapes were present and no cell represented 80% of the cored region, up to two cell shapes were recorded: as “mixed-” followed by details of the most dominant cell shape and then the second most dominant cell shape. If two melanoma cell shapes accounted for approximately 50% of melanoma cells each, then “equal-” followed by the names of the categories was recorded.

Figure 2.16 (following page): Virtual pathology images (A-G) showing different melanoma cell shapes within the cored regions

Histopathological findings (x20 magnification) show digitally extracted cored regions containing (A) round/ovoid, (B) epithelioid, (C) spindle, (D) “super spindle”, (E) naevoid, (F) plasmacytoid and (G) balloon melanoma cell shapes.

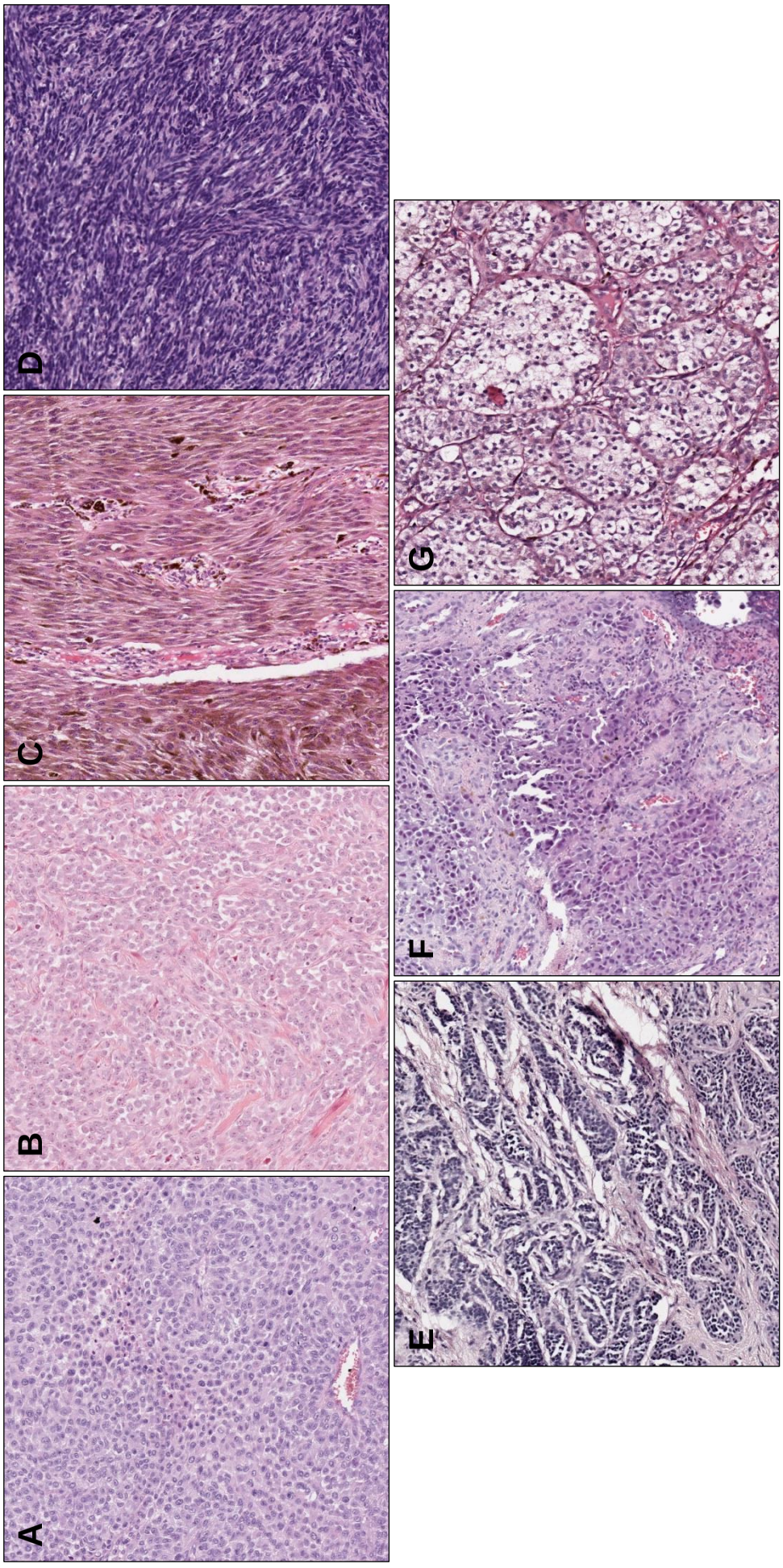
D
C
B
A
G
F
E

2.6.4 Melanoma cell structure

The structural arrangement of melanoma cells was termed “melanoma cell structure” and was defined by the following categories: nests, sheets, fascicles and dispersed (Figure 2.17). Nests defined the presence of melanoma cells in round/ovoid aggregates. Sheets referred to the presence of melanoma cells in close apposition to one another. Fascicles referred to the presence of melanoma cells in elongated bundles. Dispersed was used to define a sparse arrangement of melanoma cells, where individual cells were segregated by strands of collagen. The predominant structural arrangement was recorded and the option of “mixed-” followed by the two most dominant structural arrangements was allowed when no single type dominated. If two types of structural arrangement accounted for approximately 50% of melanoma cells each, then “equal-” followed by the names of the two structural arrangement categories was recorded.

2.6.5 Melanoma cell pigmentation

Melanoma cell pigmentation was graded according to a modified version of the Viros *et al*. method [108] (Figure 2.18). The level of pigmentation in at least 80% of melanoma cells (by eyeball) within the cored region was recorded. Melanophages were not included in the grading. “Absent” meant that the cytoplasm of the melanoma cells lacked any evidence of pigmentation. “Faint” meant that the cytoplasm was lightly pigmented, to the extent that it was just perceptible and was significantly lighter than the nucleus. “Moderate” meant that the melanoma cell cytoplasm was moderately pigmented, i.e. intermediate between faint and high. “High” meant that the melanoma cell cytoplasm was heavily pigmented, so that the cytoplasm was approximating or darker than the nucleus but the nucleus was still detectable. “Very high” was the highest grade of pigmentation, to the extent that the nucleus appeared to be obliterated and was not possible to distinguish from the surrounding cytoplasm. If one grade of pigmentation could not be ascribed to at least 80% of the melanoma cells, then “mixed” was recorded and the two most dominant pigmentation grades were assigned, with the most predominant grade listed first. If two grades of pigmentation accounted for approximately 50% of melanoma cells each, then “equal-” followed by the names of the two pigmentation grades was recorded.

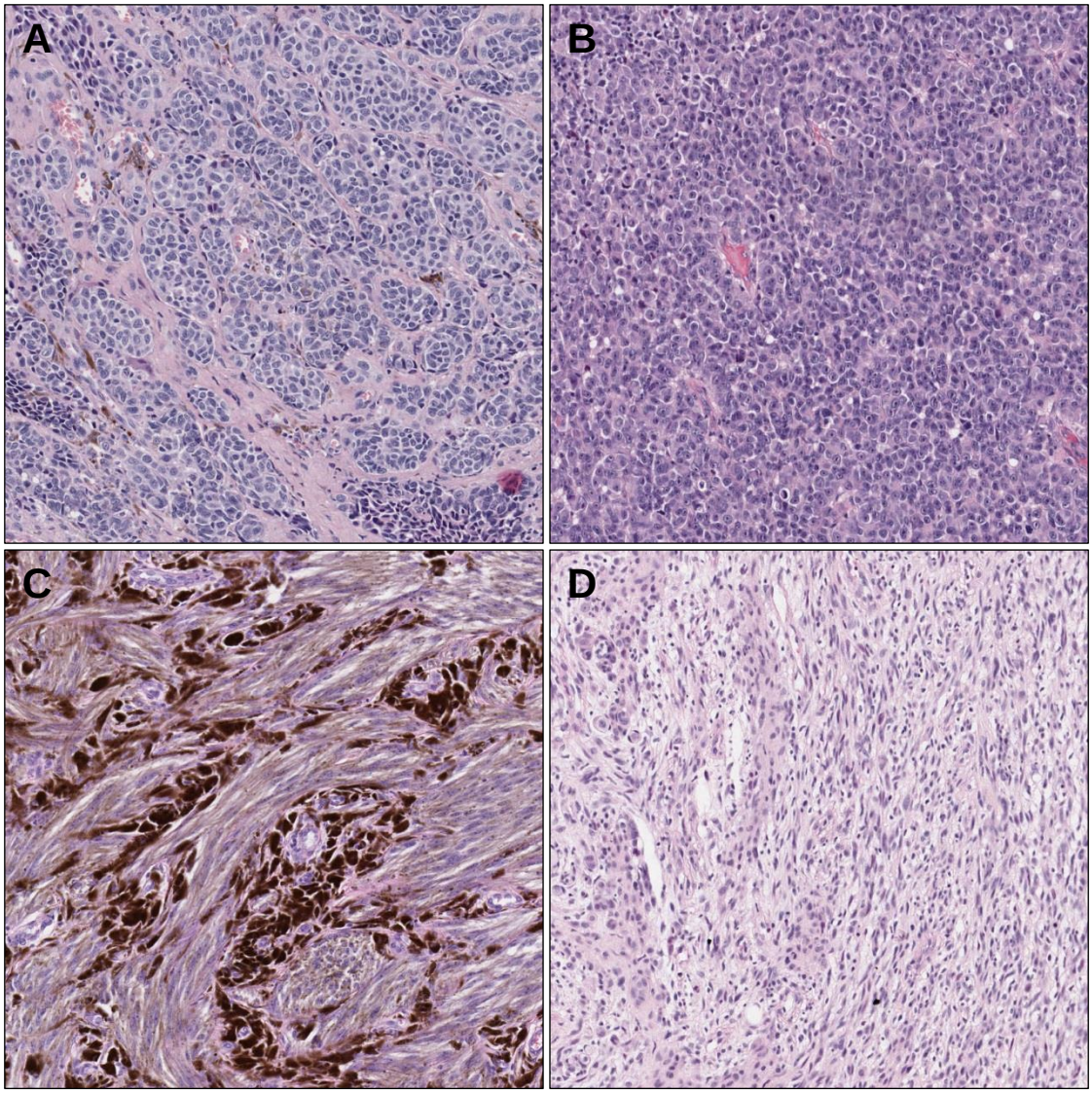

Figure 2.17: Virtual pathology images (A-D) showing different melanoma cell structures within the cored regions

Histopathological findings (x20 magnification) show digitally extracted cored regions with the following melanoma cell structures: (A) nests, (B) sheets, (C) fascicles and (D) dispersed.

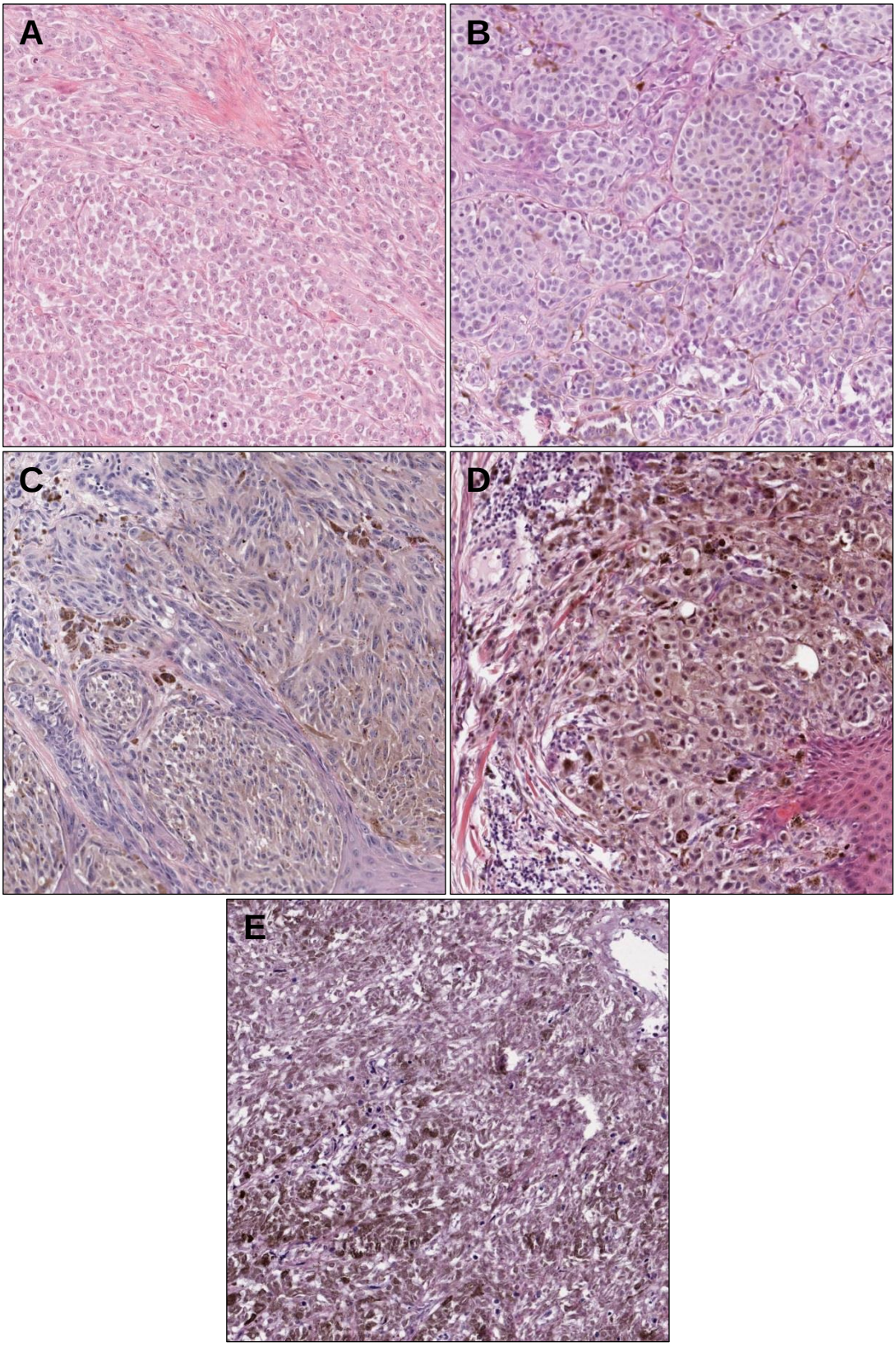

Figure 2.18: Virtual pathology images (A-E) of melanoma cored regions showing varying degrees of melanoma cell pigmentation

Histopathological findings (x20 magnification) show digitally extracted cored regions with (A) absent, (B) faint, (C) moderate, (D) high and (E) very high melanoma cell pigmentation.

2.6.6 The core immune cell infiltrate

The presence or absence of an immune cell infiltrate within each cored region was recorded as either “yes” or “no”. The immune cell infiltrate had to be readily seen at 20x magnification to be recorded as “yes”. If immune cells were too sparse to be visualised at 20x, the immune cell infiltrate was recorded as absent.

2.6.7 The extent of the core immune cell infiltrate

The extent of the core immune cell infiltrate was graded as follows: barely perceptible, some, moderate or lots (Figure 2.19). “Barely perceptible” was assigned if the immune cell infiltrate was just perceptible at 20x magnification. “Some” was recorded if the immune cell infiltrate was limited or minimal but easily visualised. “Lots” was recorded if there was a dense immune cell infiltrate. “Moderate” was recorded if the immune cell infiltrate was intermediate between some and lots. Where more than one type of immune cell was present, the overall abundance of immune cells, as a composite grade, was recorded.

2.6.8 The location of the core immune cell infiltrate

The location of the core immune cell infiltrate was recorded as follows: at the tumour/stroma interface, dispersed between tumour cells or both (Figure 2.20). If immune cells were mainly restricted to the boundary between the melanoma cells and the connective tissue/collagen, then “at the tumour/stroma interface” was selected. If the immune cells were predominantly lying between individual melanoma cells, “dispersed between tumour cells” was selected. “Both” was selected if the core immune cell infiltrate adopted both patterns.

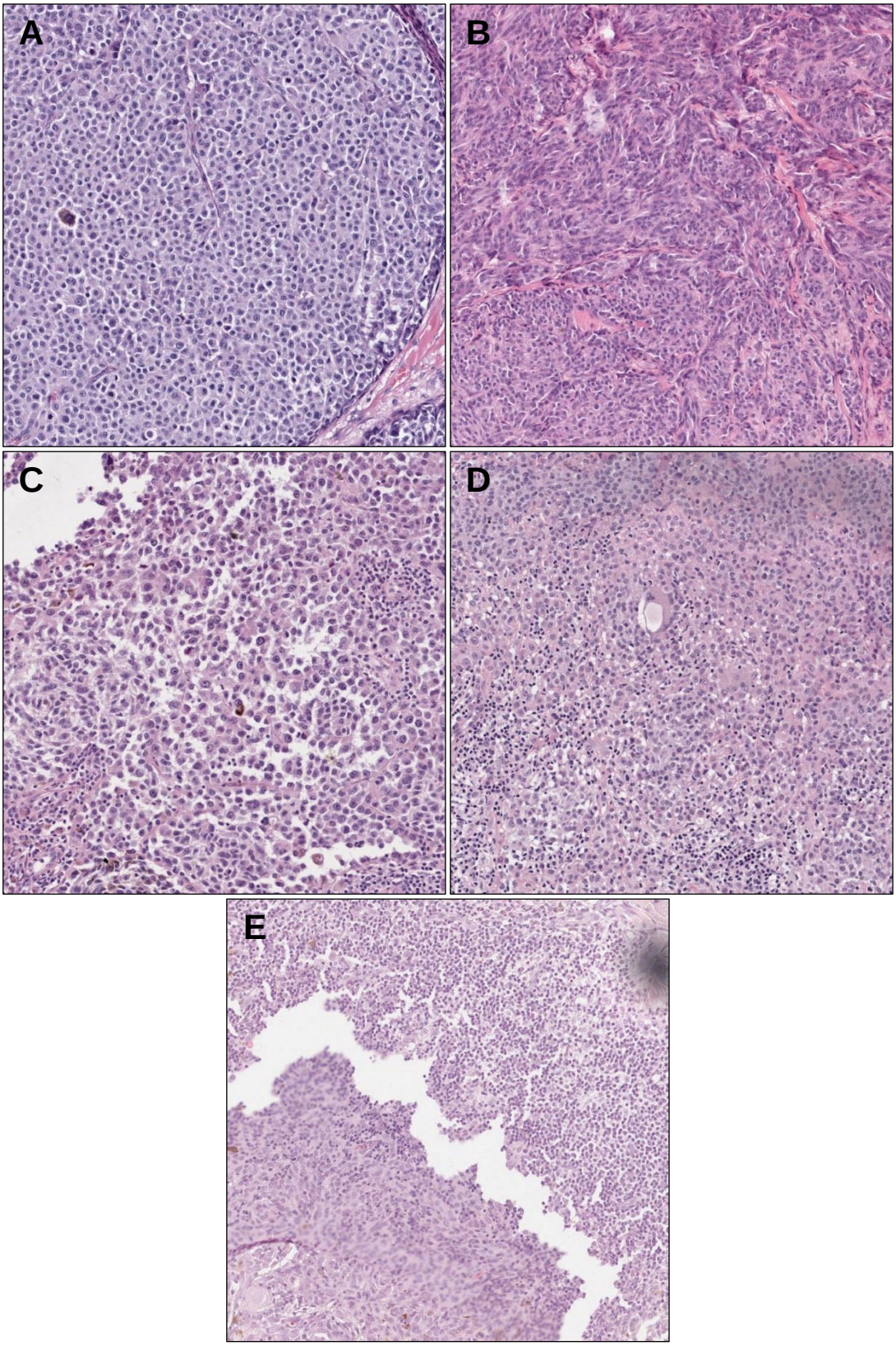

Figure 2.19 Virtual pathology images (A-E) showing melanoma cored regions with varying extents of immune cell infiltration

Histopathological findings (x20 magnification) show digitally extracted cored regions with (A) none, (B) barely perceptible, (C) some, (D) moderate and (E) lots of immune cell infiltrate within the core.

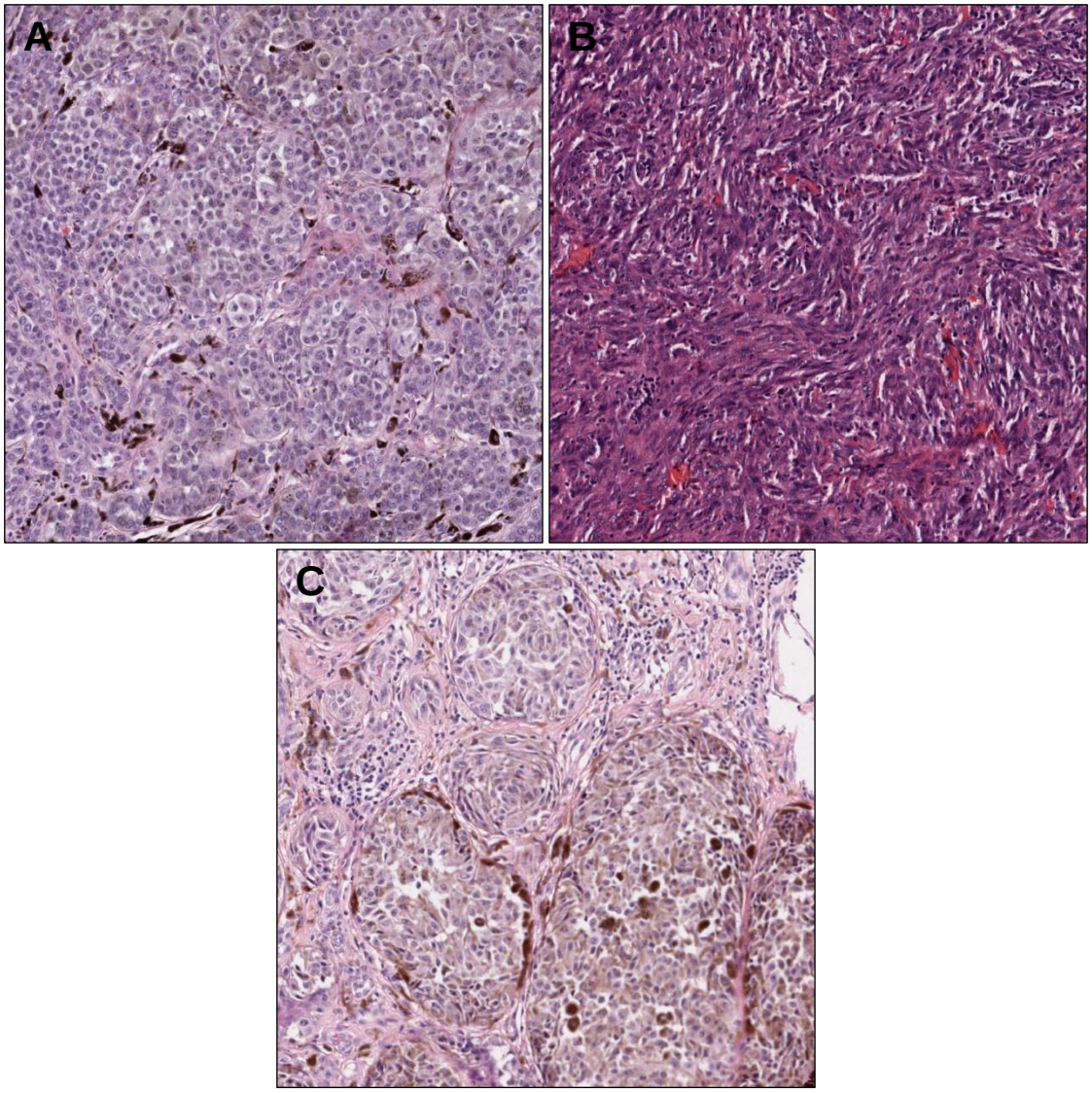

Figure 2.20: Virtual pathology images (A-C) of melanoma cored regions showing different locations of the core immune cell infiltrate

Histopathological findings (x20 magnification) show digitally extracted cored regions with immune cells (A) at the tumour/stroma interface, (B) dispersed between tumour cells and (C) both (at the tumour/stroma interface and dispersed between tumour cells).

2.6.9 The composition and extent of the constituents of the core immune cell infiltrate

The presence or absence of each of the following immune cells was recorded (if the extent of core immune cell infiltrate was graded as some, moderate or lots): lymphocytes, plasma cells, macrophages or melanophages, neutrophils and eosinophils (Figure 2.21). Where present, the extent of each of these immune cells was recorded as some, moderate or lots, using a similar approach to the grading of the overall immune cell infiltrate as previously discussed. The grading was adjudged at 20x magnification but it was permissible to view the immune cells briefly at 40x magnification if it was not possible to clearly distinguish between immune cell types at 20x. It is important to note that if the overall core immune cell infiltrate was recorded as either absent or barely perceptible, the presence or absence and the extent of the various immune cell subtypes was not further assessed.

2.6.10 The number of mitoses within the cored region

Each cored region was assessed at 40x magnification throughout, beginning at the top left corner of the extracted image, for the presence of nuclear mitoses. The arrow icon was selected in ImageScope© to annotate each mitosis separately, thus allowing the total number of mitoses to be accurately counted (Figure 2.22A).

2.6.11 The number of blood vessels within the cored region

The cored regions were assessed for the number of blood vessels using a similar method to that used to count mitoses (Figure 2.22B). As blood vessels were not always sectioned horizontally, it was not always possible to clearly visualise a lumen or to distinguish the boundaries of each blood vessel, where there appeared to be interconnecting vessels. Therefore, the decision was made to count a blood vessel only if there was a lumen containing red cells. If two lumina were in direct apposition and not separated by strands of connective tissue/collagen and interposing melanoma cells, then only one blood vessel was counted. Where the presence of red cells was clearly due to extravasation or artefactual haemorrhage, it was not counted.

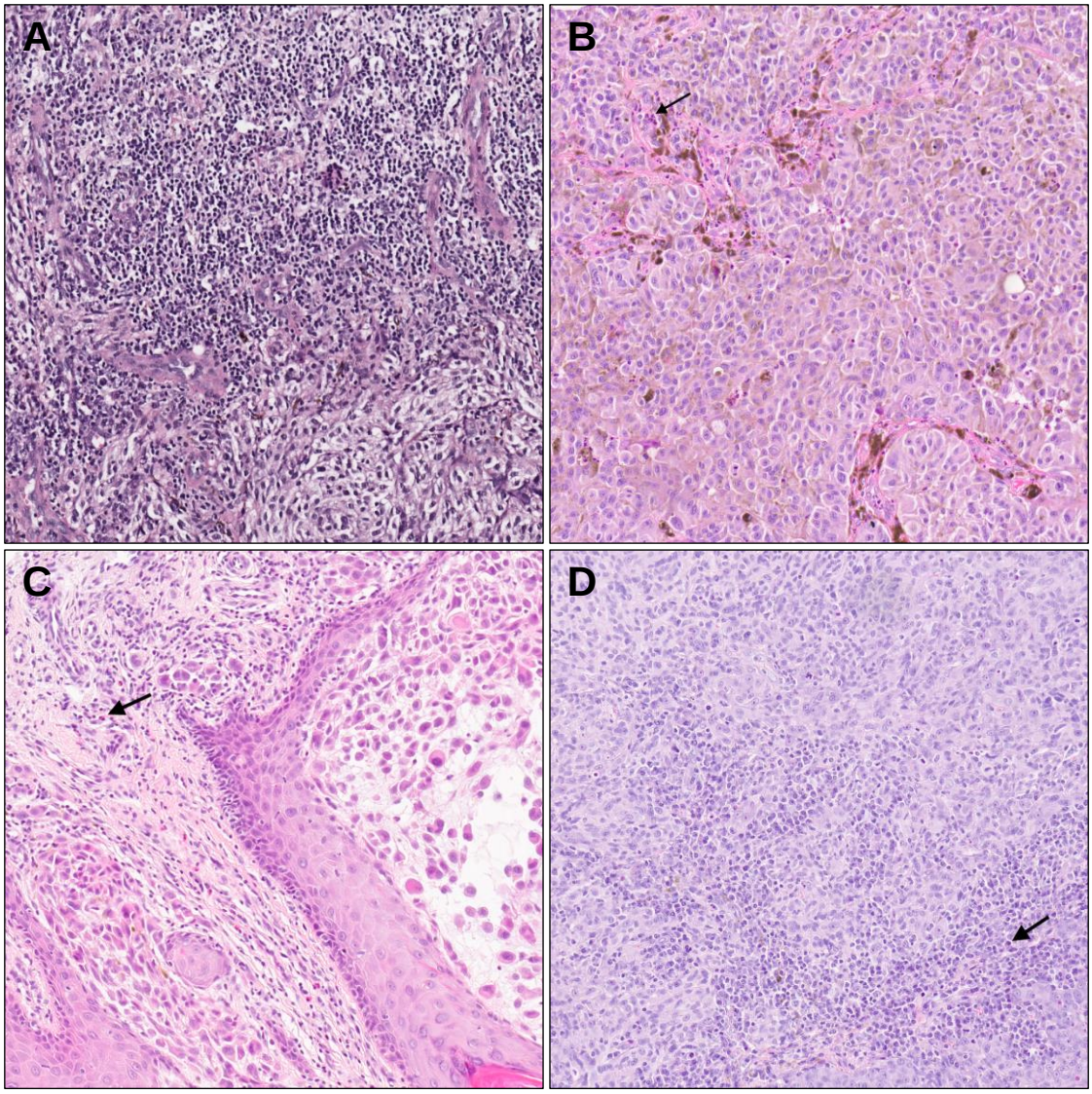

Figure 2.21 Virtual pathology images of melanoma cored regions (A-D) showing different types of immune cell infiltration

Histopathological findings (x20 magnification) show digitally extracted cored regions containing (A) lots of lymphocytes, (B) some neutrophils (highlighted by the black arrow) and some melanophages (dark brown), (C) some eosinophils (one of these is highlighted by the black arrow) and some lymphocytes and (D) lots of plasma cells (one of these is highlighted by the black arrow).

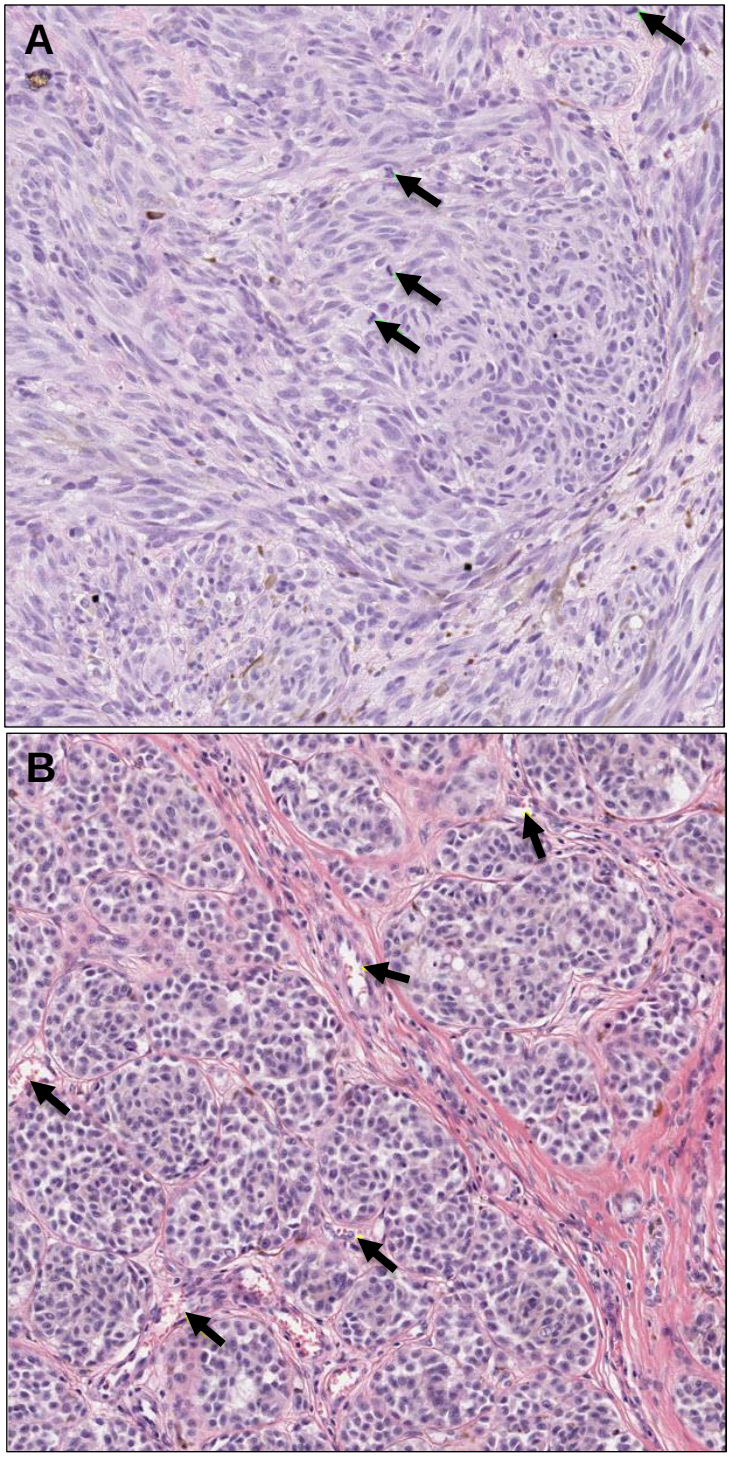

Figure 2.22 Virtual pathology images of cored regions showing (A) mitoses and (B) blood vessels

Histopathological findings (x20 magnification) show digitally extracted cored regions containing (A) 4 mitoses (annotated with black arrows) and (B) 5 blood vessels (annotated with black arrows). To be counted as a blood vessel, the lumen had to contain red cells. Although there are several lumina with red cells in this case, the definition necessitated that melanoma cells and collagen had to intervene between lumina to be counted as separate blood vessels.

2.7 Statistical methods

2.7.1 Categorical variables

The Pearson's chi-squared test for independence was used to test the association between two categorical variables. Fisher's exact test was used if the value in a single cell was less than 5.

2.7.2 Continuous variables

The mean and standard deviation were used to summarise continuous variables with a normally distributed frequency distribution. The median and range were used to summarise continuous variables with a non-normal frequency distribution. The Wilcoxon rank sum test was used to examine the association between a non-normally distributed continuous variable and a dichotomous variable. The Kruskal-Wallis test was used where there were ≥3 categories.

2.7.3 Clinical factors

STATA v12.1 (IC) was used for initial statistical analyses. STATA v14.2 (SE) was subsequently used to permit analyses of gene expression data, which involved a larger number of variables [188]. Age at diagnosis was analysed as a continuous variable. Sex (female versus male) was analysed as a binary variable. Site of primary melanoma was analysed as a categorical variable in broad (limbs, trunk, head and other) and site-specific categories (e.g. subungual). Although the majority of cases assessed were primary cutaneous melanomas, the "other" category consisted of melanomas located at the following sites: ear, nose and throat (ENT; n=6), acral (n=16), anal (n=5), cervix (n=1), clitoris (n=1), foot (n=16), hand (n=4), penis (n=3), perineal (n=1), subungual (n=12), vaginal (n=5) and vulval (n=13). The broad categories were generally used due to small numbers in the site-specific categories. AJCC stage was generated by incorporating the following whole tumour measures: Breslow thickness (using AJCC cut-off points), microscopic ulceration and the cored region mitotic count (as 0 versus ≥1) and information from histology reports and clinical notes regarding microsatellites, nodal and visceral metastases, which had been extracted by the Section of Epidemiology and Biostatistics staff.

2.7.4 Whole tumour measures

2.7.4.1 Breslow thickness

Breslow thickness was analysed as an ordinal variable, according to the AJCC cut-off groups, i.e. ≤1.0mm, 1.01mm-2.0mm, 2.01mm-4.0mm, >4.0mm [43].

2.7.4.2 Dominant nodule

The presence of a dominant nodule was analysed as a binary variable (yes versus no).

2.7.4.3 Microscopic ulceration

Ulceration was analysed as a binary variable, with no ulceration as the baseline (i.e. yes versus no). The extent of ulceration was analysed as an ordinal variable, with no ulceration as the baseline and then dividing measurements for the extent of ulceration into four equal groups as follows: (none), <0.87mm, 0.87-<2.4mm, 2.4-<5.15mm and ≥5.15mm. The cumulative extent of ulceration (for multiple, discontiguous ulcers on the same section) was analysed in a similar way, where available. The maximum extent of ulceration was used for analysis in preference to the cumulative extent of ulceration, as relatively few cases had multiple ulcers on the same section and therefore lacked measurements for the cumulative extent of ulceration.

2.7.4.4 Tumour-infiltrating lymphocytes

Eight categories of tumour-infiltrating lymphocytes were available for analysis (as previously described). However, some of the categories were merged for statistical analysis due to small numbers. Totally absent, absent with a perivascular pattern, absent with a perifibrotic or regression pattern and focally absent biphasic VGP TILs were merged and analysed as “absent”. Non-brisk sparse and non-brisk diffuse were analysed separately and merged as “non-brisk”. Brisk diffuse and brisk peripheral were summarised as “brisk”. TILs were analysed as an ordinal variable with absent as the baseline, followed by non-brisk and, finally, brisk.

2.7.4.5 Tumour loss

Tumour loss was analysed as a binary (yes versus no) and a categorical variable: none (reference category), deep, both and superficial. The maximum depth of tumour loss was analysed as an ordinal variable, with none as the baseline and then dividing the depth of tumour loss into four equal categories as follows: (none), <0.71mm, 0.71-<1.14mm, 1.14mm-<1.63mm and ≥1.63mm.

2.7.4.6 Relative tumour loss

To evaluate tumour loss in terms of the thickness of the melanoma, I generated a new variable called relative tumour loss. This was calculated by dividing the depth of tumour loss by the Breslow thickness in millimetres. This was then analysed as an ordinal variable because 81.8% (643/786) of cases had no relative tumour loss. Therefore, no relative tumour loss was the baseline category and the remaining measurements were divided into approximately four equal groups as follows: <0.26mm (4.4%, 35/786 cases), 0.26-<0.52mm (4.5%, 36/786), 0.52-<0.786mm (4.7%, 37/786) and ≥0.786mm (4.4%, 35/786).

2.7.4.7 Tumour-infiltrating melanophages

The intensity of tumour-infiltrating melanophages was analysed as an ordinal variable: none, very few, moderate and lots. Their pattern was also analysed as an ordinal variable, using a similar approach to that described for TILs, i.e. first as eight categories and then summarised as absent, non-brisk or brisk.

2.7.5 Cored region measures

2.7.5.1 The proportion and percentage of stroma

The proportion of stroma was converted to a percentage by multiplying each value by 100. The percentage of stroma was analysed as a continuous variable and as ordinal variables: by dividing into 2 categories by the median (i.e. high versus low as follows: ≥32.69% (50.1%, 352/702 cases) versus <32.69% (49.9%, 350/702 cases)), or quintiles (0-<17% (19.4%, 136/702 cases), 17<27% (20.9%, 147/702), 27-<38% (20.4%, 143/702), 38-<52% (20.5%, 144/702) and ≥52% (18.8%, 132/702)). Quintiles were chosen instead of tertiles or quartiles in order to retain as much information from the continuous measure as possible. Various binary cut-off points were also explored to assess if a particular cut-off point was more predictive than another (15%, 20%, 30%, 40% and 49%). The binary and quintile analyses were exploratory and were tested to assess whether or not using a categorical variable was more significantly predictive than using the continuous variable.

2.7.5.2 The quality of the stroma

The quality of the stroma was analysed as a categorical variable as follows: compact (baseline), loose and mixed.

2.7.5.3 Melanoma cell shape

Melanoma cell shape was analysed as a categorical variable in several combinations. Specific categories included round/ovoid, epithelioid, spindle, super spindle, naevoid, plasmacytoid and balloon. Round/ovoid was the most numerous cell shape and therefore was chosen as the reference category (baseline) in the statistical models. Cell shape was also explored using a composite variable for round/ovoid and epithelioid, while retaining the other categories. Round/ovoid was merged with epithelioid cell shape for survival analyses because intraobserver analysis showed that it was difficult to distinguish epithelioid cell shape from round/ovoid. Where a mixed cell shape was recorded, the dominant (first listed) cell shape was assigned and used for statistical analyses.

2.7.5.4 Melanoma cell structure

Melanoma cell structure was analysed as a categorical variable as follows: nests (baseline), sheets, fascicles and dispersed.

2.7.5.5 Melanoma cell pigmentation

Melanoma cell pigmentation was analysed as an ordinal variable: absent (baseline), faint, moderate, high and very high.

2.7.5.6 The core immune cell infiltrate

The core immune cell infiltrate was analysed as a binary variable (no versus yes). Yes was used as the baseline in the statistical models because the majority of cases had an immune cell infiltrate (and the baseline category was generally assigned to the largest category of discrete categorical variables for statistical modelling).

For survival analyses, the barely perceptible category for the extent of the core immune cell infiltrate was merged with “no” as there were very few cases with no immune cell infiltrate and the hazard ratios were similar. The extent of the immune cell infiltrate was then analysed as an ordinal variable: no/barely perceptible (baseline), some, moderate and lots.

The following factors were analysed as ordinal variables, with no/barely perceptible core immune cell infiltrate as the baseline: the lymphocytic, plasma cell, macrophage or melanophage, neutrophilic or eosinophilic infiltrate. No/barely perceptible core immune cell infiltrate was used as the baseline because the other immune cell constituents were not further assessed if the overall core immune cell infiltrate was regarded as absent or barely perceptible. Similarly, the location of the core immune cell infiltrate

was analysed as a categorical variable as follows: no/barely perceptible core immune cell infiltrate; at the tumour/stroma interface; dispersed between tumour cells; and both.

For the extent of the individual immune cell components (e.g. lymphocytes), the no/barely perceptible category (for the core immune cell infiltrate) was used as the baseline for the reasons described above and to increase the statistical power and then analysed as an ordinal variable in a similar way, i.e. no/barely perceptible, some, moderate and lots.

2.7.5.7 The number of mitoses

The number of mitoses was analysed as an ordinal variable by dividing the frequency distribution of mitoses into tertiles as follows: 0 (baseline), 1-2 and ≥3. The number of mitoses was also analysed as a binary variable for incorporation into AJCC stage (7^{th} edition) [43] as follows: 0 and ≥1.

2.7.5.8 The number of blood vessels

The number of blood vessels was analysed in a similar way to mitoses: as an ordinal variable as follows: 0 (baseline), 1-2 and ≥3.

2.8 Interobserver and intraobserver variation studies

Cross-tabulation of categorical variables was performed. The percentage agreement, kappa statistic, 95% confidence intervals and p-values were calculated. The Spearman correlation coefficient was calculated for non-normally distributed continuous variables. Scatter plots were used to illustrate the variation between two continuous measures.

2.9 Melanoma relapse and survival analyses

Cox proportional hazards models were used to generate hazard ratios, 95% confidence intervals and p-values for the likelihood of melanoma relapse or melanoma-specific death. Univariable and multivariable analyses were performed for each variable. Kaplan-Meier curves were used to graphically illustrate the time to melanoma relapse or melanoma-specific death. Box and whisker plots were used to illustrate how the frequency distribution of the continuous variables differed between categories of the categorical variables. Receiver Operator Characteristic (ROC) curves, based on logistic regression, were used to illustrate the area under the curve accounted for by AJCC

stage or the percentage of stroma alone and combined AJCC stage and the POS in predicting melanoma relapse and melanoma-specific death.

2.10 Analysis of the melanoma transcriptome

2.10.1 Analysis of the association between the transcriptome and the percentage of stroma

Linear regression models were performed to establish whether the percentage of stroma could predict the expression of each Illumina® probe. The mean expression, correlation coefficient, standard error and p-value for each probe was calculated. The p-values were corrected for multiple testing using the Bonferroni and false discovery rate (FDR) methods. The Bonferroni-corrected p-values were ranked in order of significance from high to low. I elected to utilise the Bonferroni-corrected p-value in order to restrict the analysis to the most significantly associated genes. Where more than one probe was available per gene, the probe with the highest level of detection was retained. Unsupervised hierarchical clustering was performed using probes with a Bonferroni-corrected p-value<0.05 in Cluster 3.0 [189]. Enrichment analyses were performed using MetaCore™ for gene probes within each cluster of the heat map in order to assess the pathways that were up- and downregulated in association with increasing POS. In MetaCore™, the threshold was set to 0 and the p-value to 1 and signals in both directions were selected (to show genes that were up- or down-regulated).

2.10.2 Analysis of the interaction between the transcriptome, the percentage of stroma and survival

I assessed the effect of the POS on survival in patients with low gene expression and then separately for patients with high gene expression. A likelihood ratio test was performed between a model including the interaction between the POS and gene expression and a model including only the main effects of the POS and gene expression. The p-value for the interaction was calculated from the likelihood ratio test. The p-values were corrected for multiple testing using the Bonferroni and FDR methods.

2.10.3 Analysis of the association between the transcriptome and the extent of either the core immune cell or lymphocytic infiltrates

Linear regression was performed to establish whether the extent of the core immune cell infiltrate, using a test for trend, could predict the expression of each Illumina® probe. The mean expression for each category of the core immune cell infiltrate and the correlation coefficient, standard error and p-value was calculated for each probe. The p-values were corrected for multiple testing using the Bonferroni and FDR methods. The Bonferroni-corrected p-values were ranked in order of significance from high to low. Where more than one probe was available per gene, the probe with the highest level of detection was retained. Unsupervised hierarchical clustering was performed using probes with a Bonferroni-corrected p-value<0.05 in Cluster 3.0 [189]. Enrichment analyses were performed using MetaCore™ for gene probes within each cluster of the heat map in order to assess the pathways that were up- and downregulated in association with the extent of the core immune cell infiltrate (the test for trend). In MetaCore™, the threshold was set to 0 and the p-value to 1 and signals in both directions were selected (to show genes that were up- or down-regulated). The same approach was used for the extent of the core lymphocytic infiltrate.

2.10.4 Analysis comparing the transcriptome and the percentage of stroma and the extent of the core immune cell and lymphocytic infiltrates

The POS was calculated using positive scoring for a range of stromal constituents, including collagen and various immune cells. Therefore, a comparative enrichment analysis was performed using MetaCore™ to assess the pathways that were similar and differentially expressed between the POS, the extent of the core immune cell infiltrate overall and the extent of the core lymphocytic infiltrate. In MetaCore™, the threshold was set to 0 and the p-value to 1. Upregulated signals were selected to see which pathways were most significantly positively associated with each factor.

2.10.5 Analysis of cancer history, *BAP1* variants and *BAP*-like histopathology

Cross-tabulation of cancer history and *BAP1* variants was performed to assess the association between each cancer type and the presence of a *BAP1* variant. Separate analyses were performed for the presence of a benign *BAP1* variant versus no variant and for the presence of a deleterious *BAP1* variant versus no variant. The Fisher's

exact test was used where a cell contained a value <5 and the Pearson's chi-squared test was used where each cell contained a value of ≥5. Similar cross-tabulations and calculations were performed to assess the association between each cancer type and the presence of *BAP*-like histopathological changes. Odds ratios and 95% confidence intervals were calculated.

2.10.6 Analysis of *BAP*-like histopathology or *ALK*-fusion like histopathology and the transcriptome

The T-test was performed to establish the association between either the presence or absence of *BAP*-like histopathology in the primary melanoma and each Illumina® probe. The mean expression for each category (no and yes) and the fold-change, standard error and p-value were calculated for each probe. The p-values were corrected for multiple testing using the Bonferroni and FDR methods. The Bonferroni-corrected p-values were ranked in order of significance from high to low. Where more than one probe was available per gene, the probe with the highest level of detection was retained. A similar approach was used to establish the association between or *ALK* fusion-like histopathology and each Illumina® probe.

Chapter 3 Inter- and intraobserver variation in the histopathological assessment of primary cutaneous melanomas

Melanoma pathology involves the examination of microscopic features of the tumour, using haematoxylin and eosin (H&E)-stained tissue sections. Visual clues, including the tumour shape, cellular components and physical dimensions, are used to categorise the melanoma. These features are observational and, consequently, open to interpretation.

In approaching this PhD, from a background of clinical dermatology, it was important to first learn the basics of melanoma pathology. I trained using textbooks and through one-to-one training with Dr Will Merchant, consultant dermatopathologist (Pathologist B). An initial learning period was anticipated, during which discrepancies between our pathology assessments could be identified and addressed. Indeed, the histopathology literature contains much evidence of interobserver variation between dermatopathologists, even among pathologists from the same institution, as described below.

This chapter examines both interobserver and intraobserver variation. The results are presented in separate stages, reflecting changes in the protocol. Early in the course of research, I utilised a light microscope and a protocol that had been developed by Prof. Martin Cook, consultant dermatopathologist, (Appendix B). I used these training set cases to learn melanoma pathology and to identify discrepancies between my pathology assessments and those of another consultant dermatopathologist (Pathologist A) who had previously assessed cases using the same protocol, a subset of which overlapped with my cases. The first part of the chapter examines the interobserver variation between my measures and those of Pathologist A. A database of Pathologist A's reviews was available. I used the data collected opportunistically to compare my skills with those of a consultant dermatopathologist using the same protocol. In practice, however, it also served as a learning opportunity. When differences occurred, I was subsequently able to resolve them by review with the Dr Merchant (Pathologist B), with whom I trained.

My understanding of the complexity of melanoma pathology increased over time. Therefore, as my knowledge increased through one-to-one training with Dr Merchant, I was conscious of the need to develop a new protocol that would be robust and reproducible. During this process, the factors that were retained were those for which

interobserver agreement was highest or which were regarded to be important. In addition, novel measures were developed, under the guidance of my supervisors. To determine the level of reproducibility of this new (virtual pathology) protocol, I examined both inter- and intraobserver agreement. This interobserver variation analysis was performed using data recorded by Dr Merchant (Pathologist B). Both whole-tumour and cored region (sampled using a TMA needle) measures were developed for the virtual pathology protocol, the results of which are reported separately.

Figure 3.1 provides an overview of the number of cases assessed for inter- and intraobserver variation, using each protocol.

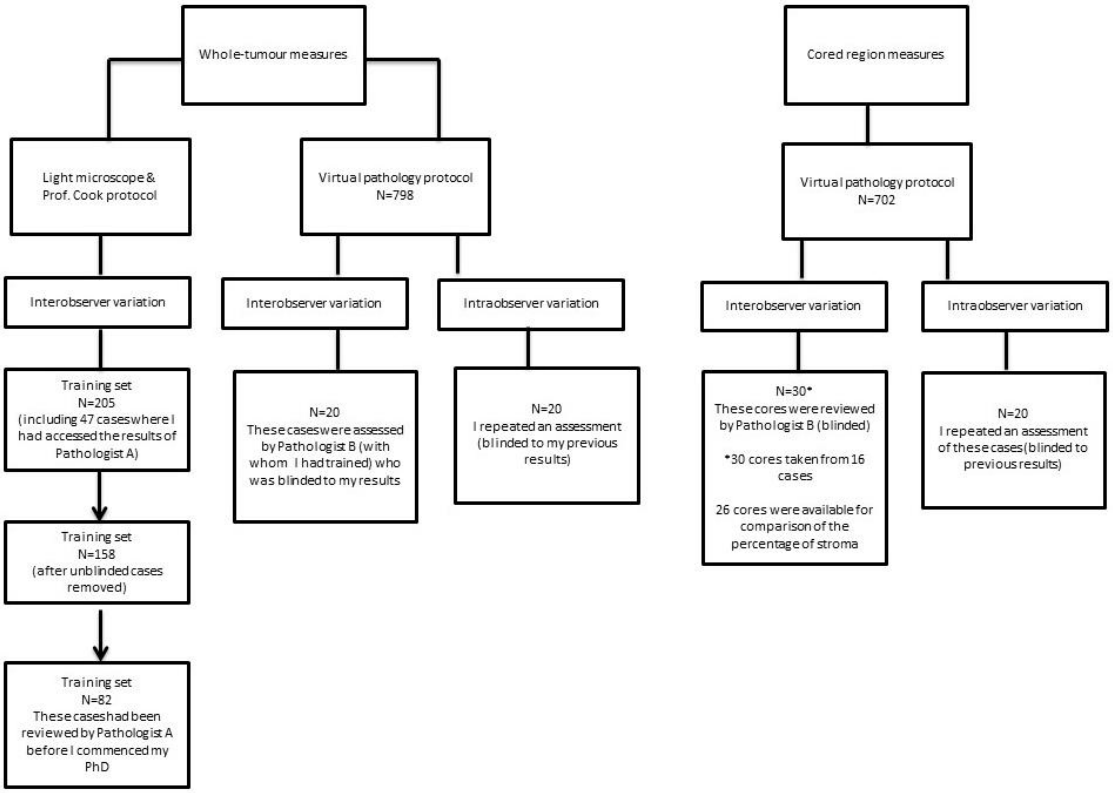

Figure 3.1: Flowchart for inter- and intraobserver variation analyses.

Whole tumour measures were available for the light microscope (training set) and virtual pathology protocols. Cored region measures were also recorded using the virtual pathology protocol.

This chapter will address the following aims:

- To examine interobserver variation in the histopathological assessment of primary cutaneous melanomas, using the Prof. Cook protocol, between my training set cases and the archived review of Pathologist A.

- To assess inter- and intraobserver variation in the histopathological review of primary cutaneous melanomas for both whole-tumour and cored region measures using a newly developed, virtual pathology protocol.

3.1 Reported interobserver agreement in the histopathological assessment of melanoma

The application of histopathological factors to prognostic estimation depends upon consistency between histopathologists, but as discussed below, many studies have shown considerable variation for some measures, indicating a degree of subjectivity. Breslow thickness is considered to be the most reproducible histopathological measure of primary cutaneous melanoma [190, 191]. Despite this, variation of up to 0.86mm has been noted among 3 pathologists from the same institution [192], while another study showed a mean interobserver variation of 0.76mm [193]. In a retrospective study of 588 cases, Patrawala *et al.* noted discordance in Breslow thickness 66% of the time, however the reviewing pathologist was unblinded to the initial clinical report [194]. These cases were reviewed at a tertiary referral centre and, therefore, the interobserver variation might reflect the complexity of the cases [194].

Good agreement has been found for microscopic ulceration status, with kappa statistics in the range of 0.69 [195] to 0.87 [196]. There was lower agreement for regression with a median kappa of 0.32 [197] and similar variability in histological subtype, with a kappa of 0.48 [198]. In an interobserver study of tumour-infiltrating lymphocytes (TILs) (n=74), agreement was slight (kappa=0.12), using a binary variable (i.e. present versus absent) [199]. Smaller studies report kappa statistics in the range 0.47 to 0.77 for TILs [27, 200, 201].

Interobserver agreement has been reported to be better, although somewhat variable, for mitotic count. In one study of thin (Breslow thickness <1mm) melanomas (n=92), the interclass correlation coefficient was 0.81 for 4 observers using H&E sections and improved further to 0.90 with the use of phosphohistone H3 (pHH3) immunostaining (which stains all phases of mitoses) [202]. A retrospective study (n=4924) showed a similar interclass correlation (0.83) for mitotic count; however, the second observer was not blinded [203]. The high level of agreement may reflect the fact that thinner melanomas were examined in these studies, thus the selection of the “hot spot” would be less likely to be open to interpretation than for thicker tumours. Monshizadeh *et al.* reported a kappa of 0.69 for mitotic count (n=35) [199]. In contrast to these findings, Garbe *et al.* reported a kappa statistic of 0.09 for mitotic count among 17 pathologists

who reviewed the same slide [204]. They noted that the number of mitoses often differed by between 0 and 4 mitoses between observers [204]. The kappa statistic improved to 0.35 when the number of mitoses was categorised as follows: 0-1, ≥2 [204].

In a study by Broekart *et al.* (n=20), interobserver weighted kappa scores among 11 pathologists ranged from 0.35 to 0.69 across a range of histopathological variables [155]. Melanoma cell pigmentation was among the most reproducible variables, whilst there was moderate agreement for melanoma cell shape and histological subtype and fair agreement for nesting [155]. In another study, the kappa for the predominant melanoma cell type (n=57) was 0.43 between observers [199].

Eriksson *et al.* reported about 20% overall variation among pathologists in the reporting of melanoma [195]. Distinction of *in situ* from early invasive melanoma and of true from artefactual ulceration contributed to discordant results [195]. Even slight changes in the reporting of early melanomas impact on decisions about surgical margins and the consideration of sentinel node biopsy [195]. Another study found that such discordance led to a change in stage in about a quarter of cases and recommendations for surgical margins and sentinel node biopsy were modified in 12% and 16% cases, respectively [205]. Patrawala *et al.* reported similar findings, with changes in stage occurring in 19% cases and corresponding recommendations for surgical margins and sentinel node biopsy in 10% and 8% cases, respectively [194]. Variability in the reporting of melanocytic lesions prompted the development of the “Melanocytic Pathology Assessment Tool and Hierarchy for Diagnosis” (MPATH-Dx) classification scheme, which defines 5 categories, ranging from a benign melanocytic nevus to melanoma, and corresponding recommendations, ranging from no intervention to wide excision [206]. The interrater kappa for the classification scheme among 3 pathologists was 0.58 [207] and similar results were reported for 16 pathologists, with a mean unweighted kappa of 0.57 [208].

Analysis of intraobserver concordance for the histopathological assessment of cutaneous melanoma is less frequently reported, however, variation tends to be less within than between observers [192, 197]. Colloby *et al.* reported the results of inter- and intraobserver variation for 3 observers, with intraobserver kappa values in the range of 0.54-0.78 for Breslow thickness and 0.23-0.55 for Clark’s level [192]. A median kappa of 0.51 has been reported for regression [197]. Garbe *et al.* reported slight to fair intraobserver agreement for mitotic count, with kappas in the range of 0.18-0.35 [204].

3.2 Methods

3.2.1 Assessment of the level of agreement for inter- and intraobserver variation studies

Cross-tabulation of categorical variables was performed. The percentage agreement, kappa statistic and corresponding 95% confidence intervals (95% CI) and p-values were calculated. The percentage agreement was calculated by adding the total number of cases that agreed in each category, dividing by the total number of cases and multiplying by 100. The percentage agreement includes missing values in the total, whereas the observed and expected agreement, which is calculated by the kappa statistic, does not include missing values. The kappa statistic was used to compare the observed agreement to the agreement that would be expected by chance and values were interpreted according to Table 3.1.

Table 3.1: Kappa statistic and the strength of agreement.

The strength of agreement for inter- and intraobserver variation analyses was interpreted using the kappa statistic cut-off points shown. (Adapted from Viera *et al.* [209]).

Kappa statistic	Strength of agreement
<0	Less than chance
0	Chance
0.01-0.20	Slight
0.21 -0.40	Fair
0.41-0.60	Moderate
0.61-0.80	Substantial
0.81-0.99	Almost perfect
1.0	Perfect

The Spearman correlation coefficient was calculated for continuous variables. Scatter plots were used to illustrate the variation between two continuous measures.

3.3 Interobserver variation in whole-tumour measures using a light microscope

I recorded a detailed histopathological review of 205 cases in this way using the Prof. Cook protocol. For 47 of these slides, I had access to the recorded measurements of a

consultant dermatopathologist (Pathologist A). For the purpose of interobserver studies, these 47 cases were dropped from the analysis because I had used Pathologist A's records to inform my measurements, leaving 158 cases. Of the 158 remaining cases, Pathologist A's review was unavailable for 76 cases. Therefore, 82 cases remained, which were used for interobserver variation studies.

3.3.1 Histological subtype

There was moderate interobserver agreement for histological subtype (Table 3.2). The majority of cases were superficial spreading melanomas. There was some overlap in the classification of superficial spreading and nodular subtypes. Each observer had classified one case as acral lentiginous melanoma, while the other observer had recorded superficial spreading melanoma for the same case.

3.3.2 The maximum macroscopic diameter

Measurements for the maximum macroscopic diameter were available for 82 cases in my data and just 2 cases in Pathologist A's data. In the first case, the measurements were similar, differing by 0.5mm. In the second case, the measurements differed by 2.3mm. It was not possible to ascertain whether or not the same slides/levels were used for the assessment. I used research H&E sections, whereas Pathologist A had access to clinical sections. However, the same number of slides were available for 56% of (46/82) cases.

3.3.3 Growth phase

There was fair agreement for growth phase (Table 3.3). The majority of cases were in vertical growth phase (VGP). I classified 9 cases as VGP when Pathologist A categorised them as radial growth phase (microinvasive).

3.3.4 Clark's level

Clark's level was poorly reproduced between observers (21%; 17/82; kappa=0.002 (95% CI -0.07-0.09), p=0.5, data not shown).

3.3.5 Breslow thickness

The median difference in Breslow thickness between my measures and those of Pathologist A was 0.2 (range=0-1.2) mm. The Spearman correlation coefficient was 0.94 ($p=3x10^{-37}$), indicating excellent agreement (Figure 3.2).

Table 3.2: Cross-tabulation of histological subtype for my measures (SOS) and those of Pathologist A (A).

There was 79% (65/82) agreement. Kappa=0.53 (95% CI 0.30-0.72), $p=7x10^{-11}$.

	Histological subtype (A)				
Histological subtype (SOS)	Superficial spreading	Nodular	Acral lentiginous	Other	Total
Superficial spreading	54	4	1	3	62
Nodular	1	8	0	0	9
Acral lentiginous	1	0	0	0	1
Other	4	0	0	3	7
Missing	1	0	0	2	3
Total	61	12	1	8	82

Table 3.3: Tabulation of growth phase for my measures (SOS) and those of Pathologist A (A).

There was 83% (68/82) agreement. Kappa=0.24 (95% CI -0.02-0.58), p=0.001.

	Growth phase (A)				
Growth phase (SOS)	Radial (*in situ*)	Radial (microinvasive)	Vertical	Missing	Total
Radial (*in situ*)	2	0	0	1	3
Radial (microinvasive)	1	0	2	1	4
Vertical	0	9	66	0	75
Total	3	9	68	2	82

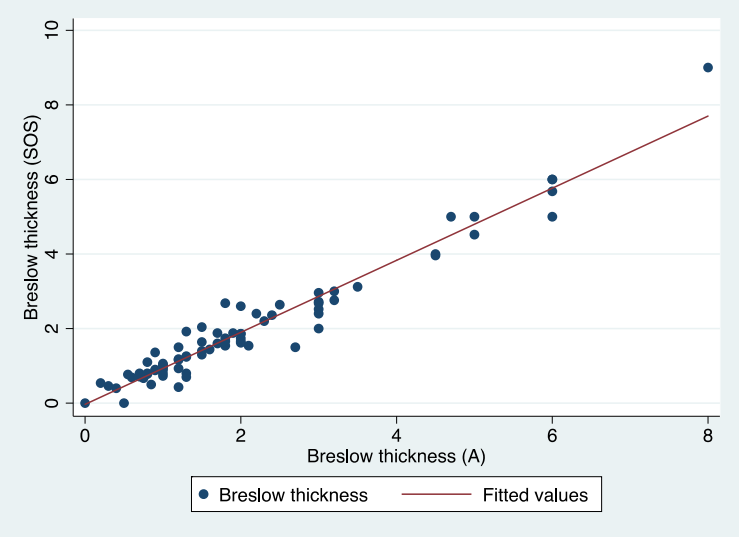

Figure 3.2: Scatter plot of Breslow thickness for my measures (on the y-axis) and for Pathologist A (on the x-axis).

There was substantial interobserver agreement for Breslow thickness (Table 3.4). Nonetheless, cases that had the greatest differences in Breslow thickness (and for which slides were still available) were reviewed with a second dermatopathologist (with whom I was training, Pathologist B) as learning points. Some of the differences in Breslow thickness could be accounted for as follows: a highly convoluted epidermis, which made the choice of site for the measurement difficult (and for which there is no formal guideline available); a difficult case where the base was heavily infiltrated by plasma cells. Immunohistochemically-stained sections had also been available to Pathologist A in the latter case.

Table 3.4: Breslow thickness (mm) for my measures (SOS) and those of Pathologist A (A), using the AJCC cut-off points [43].

There was 77% (63/82) agreement. Kappa=0.72 (95% CI 0.56-0.84), $p<1x10^{-16}$.

	Breslow thickness (A)					
Breslow thickness (SOS)	≤1.00mm	1.01 - 2.00mm	2.01 - 4.00mm	>4.00mm	Missing	Total
≤1.00mm	22	4	0	0	3	29
1.01-2.00mm	4	21	3	0	0	28
2.01-4.00mm	0	3	12	2	0	17
>4.00mm	0	0	0	8	0	8
Total	26	28	15	10	3	82

3.3.6 Dominant nodule

Interobserver concordance for the presence or absence of a dominant nodule was poor (Table 3.5). The kappa statistic was 0, suggesting that the observed agreement occurred by chance only. Also, the presence of a dominant nodule had not been recorded by Pathologist A and, therefore, the kappa statistic does not reflect the observed agreement.

3.3.7 Microscopic ulceration

There was almost perfect agreement for microscopic ulceration (Table 3.6). Ulceration width was available in 13 cases. The median difference in ulceration width was 0.6 (range 0-13) mm. The Spearman correlation coefficient for ulceration width was 0.77 (p=0.002).

Table 3.5: Cross-tabulation of the presence or absence of a dominant nodule (mm) for my measures (SOS) and those of Pathologist A (A).

There was 34% (28/82) agreement. Kappa=0 (95% CI not calculable).

	Dominant nodule (A)			
Dominant nodule (SOS)	No	Yes	Missing	Total
No	27	0	5	32
Yes	40	0	2	42
Missing	7	0	1	8
Total	74	0	8	82

Table 3.6: Cross-tabulation of microscopic ulceration status for my measures (SOS) and those of Pathologist A (A).

There was 93% (76/82) agreement for ulceration. Kappa=0.84 (95% CI 0.70-0.99), $p=2 \times 10^{-14}$.

	Ulceration status (A)			
Ulceration status (SOS)	No	Yes	Missing	Total
No	62	2	2	66
Yes	2	14	0	16
Total	64	16	2	82

3.3.8 Tumour-infiltrating lymphocytes (TILs)

There was slight interobserver agreement for TILs (Table 3.7).

Table 3.7: Cross-tabulation of tumour-infiltrating lymphocytes for my measures (SOS) and those of Pathologist A (A).

There was 43% (35/82) agreement for TILs. Kappa=0.14 (95% CI 0.02-0.30), p=0.02.

		TILs (A)				
TILs (SOS)	Absent	Non-brisk	Brisk	Non-evaluable	Missing	Total
Absent	1	1	1	0	1	4
Non-brisk	13	27	13	0	1	54
Brisk	1	5	7	0	0	13
Non-evaluable	6	2	1	0	1	10
Missing	0	0	1	0	0	1
Total	21	35	23	0	3	82

3.3.9 Regression

Although the percentage agreement for regression was high (89%, 73/82), the kappa statistic indicates slight agreement (0.2; Table 3.8). This reflects the rarity of the occurrence of regression, where there is good agreement in its absence but agreement for its presence is weaker.

Table 3.8: Cross-tabulation of regression for my measure (SOS) and those of Pathologist A (A).

There was 89% (73/82) agreement for regression. Kappa=0.2 (95% CI -0.03-0.60), p=0.003.

	Regression (A)				
Regression (SOS)	No	Yes	Uncertain	Missing	Total
No	72	0	1	2	75
Yes	3	1	0	0	4
Uncertain	3	0	0	0	3
Total	78	1	1	2	82

The stage of regression was recorded for 5 cases in my data and just 1 in Pathologist A's data. In the single case recorded by Pathologist A, it was recorded as stage 1 in my data and as stage 2 by Pathologist A. The thickness of regression was recorded by both observers for one case and the value differed by 0.5mm.

3.3.10 Mitotic count

Agreement was only fair for mitotic count (Table 3.9), possibly reflecting differences in selection of a "hot spot" for counting, or indeed, different H&E sections being used for assessment.

Table 3.9: Cross-tabulation of mitotic count for my measures (SOS) and those of Pathologist A (A).

There was 55% (45/82) agreement. Kappa=0.35 (95% CI 0.17-0.51), $p=3x10^{-6}$.

	Mitotic count (A)				
Mitotic count (SOS)	0	1-2	≥3	Missing	Total
0	13	7	0	3	23
1-2	11	12	8	0	31
≥3	2	6	20	0	28
Total	26	25	28	3	82

3.3.11 Microsatellites

There was 91% (75/82) agreement for microsatellite status. The kappa statistic was 0 because the expected agreement was the same as the observed, indicating that the agreement could have occurred by chance. Therefore, although the percentage agreement was high, the strength of the agreement was poor. This also reflects the rarity of the occurrence of microsatellites, where agreement between observers was high in its absence but low in its presence. Of the 82 cases, 4 were deemed to have microsatellites by Pathologist A. None of these were recorded as having microsatellites in my data. Therefore, these 4 cases were reviewed with Pathologist B (with whom I was training). Two of the four cases were considered to have microsatellites by Pathologist B. The other 2 cases were not deemed to have microsatellites: 1 showed artefactual adherence of cells at the edge of the section and the other fell short of the definition of microsatellites (as the tissue between the base of the melanoma and the underlying tumour was fibrotic and inflamed).

3.3.12 Vascular invasion

The strength of agreement for vascular invasion was fair (Table 3.10).

3.3.13 Perineural invasion

The negative kappa statistic indicated that there was less than chance agreement for perineural invasion (kappa -0.01, Table 3.11). This also reflects the rarity of the measure in this data set.

3.3.14 Distance to the peripheral and deep margins

Measurements to the peripheral and deep margins were available for 78/82 (95%) cases. The median difference between each observer for the peripheral margin was 0.5 (range 0-6.7). The median difference between each observer for the deep margin was 0.99 (range 0-10).

3.3.15 Melanoma cell shape

There was slight agreement for melanoma cell shape (Table 3.12). Pathologist A classified 24 cases as having a small cell/naevoid cell shape, which I had recorded as epithelioid. This occurred in the opposite direction to a smaller extent.

Table 3.10: Cross-tabulation of vascular invasion for my measures (SOS) and those of Pathologist A (A).

There was 87% (71/82) agreement. Kappa=0.23 (95% CI 0-0.56), p=0.0002.

	Vascular invasion (A)				
Vascular invasion (SOS)	No	Yes	Uncertain	Missing	Total
No	70	0	0	2	72
Yes	6	1	1	0	8
Uncertain	2	0	0	0	2
Total	78	1	1	2	82

Table 3.11: Cross-tabulation of perineural invasion for my measures (SOS) and those of Pathologist A (A).

There was 88% (72/82) agreement. Kappa=-0.01 (95% CI -0.04-0), p=0.6.

		Perineural invasion (A)			
Perineural invasion (SOS)	No	Yes	Uncertain	Missing	Total
No	72	0	1	6	79
Yes	2	0	0	0	2
Uncertain	1	0	0	0	1
Total	75	0	1	6	82

Table 3.12 Cross-tabulation of melanoma cell shape for my measures (SOS) and those of Pathologist A (A).

There was 46% (38/82) agreement. Kappa=0.19 (95% CI 0.06-0.34), p=0.003.

			Melanoma cell type (A)				
Melanoma cell type (SOS)	Epithelioid	Small cell/ naevoid	Spindle	Spitzoid	Balloon	Missing	Total
Epithelioid	26	24	4	0	0	2	56
Small cell/ naevoid	3	9	0	0	0	0	12
Spindle	0	5	3	0	0	0	8
Spitzoid	1	0	0	0	0	0	1
Balloon	0	1	0	0	0	0	1
Other	2	0	0	0	0	0	2
Missing	1	0	1	0	0	0	2
Total	33	39	8	0	0	2	82

3.3.16 Melanoma cell pigmentation

There was slight agreement for melanoma cell pigmentation (Table 3.13).

Table 3.13: Cross-tabulation of melanoma cell pigmentation for my measures (SOS) and those of Pathologist A (A).

There was 12% (10/82) agreement. Kappa=0.03 (95% CI -0.08-0.19), p=0.3.

		Melanoma cell pigmentation (A)				
Melanoma cell pigmentation (SOS)	No	Mild	Moderate	Severe	Missing	Total
No	3	0	0	0	0	3
Mild	13	2	0	0	0	15
Moderate	6	6	3	0	0	15
Severe	1	1	0	0	0	2
Missing	25	14	6	0	2	47
Total	48	23	9	0	2	82

I had recorded mild or moderate pigmentation for 19 cases where Pathologist A scored absent pigmentation. One case which I had graded as having severe pigmentation was recorded as absent pigmentation by Pathologist A. Data for melanoma cell pigmentation were missing for several cases, which limited the analysis of interobserver variation.

3.3.17 Interpretation of interobserver agreement using a light microscope and Prof. Cook's protocol

The results show that the best interobserver agreement was for Breslow thickness and microscopic ulceration. Variables for which the strength of agreement was weakest included microsatellites, TILs, perineural invasion, melanoma cell shape and melanoma cell pigmentation.

On the basis of these results, cases with discrepancies were reviewed with Pathologist B (with whom I trained), where possible. In the development of the subsequent virtual pathology protocol, a decision was made to drop several factors, including those for which interobserver agreement was weakest. These dropped measures included histological subtype, growth phase, Clark's level, microsatellites, vascular and perineural invasion. New measures and corresponding definitions were developed, in order to optimise reproducibility (Chapter 2), under the guidance of my supervisors, particularly, Dr Merchant. It was decided to enumerate mitoses and to classify melanoma cell shape within the cored regions, instead of the whole tumour. The

grading of melanoma cell pigmentation was changed, using a modified version of the approach reported by Viros *et al.* [108] and would be recorded within the cored region rather than for the whole tumour.

3.4 Interobserver variation in whole-tumour measures using virtual pathology

Twenty cases were selected to assess interobserver variation between my recorded measures and those of an experienced, consultant dermatopathologist (Pathologist B) using the new virtual pathology protocol. The selection of cases was random, except that cases were avoided if they had been flagged as being especially difficult or if the image quality was noted to be poor.

3.4.1 Breslow thickness

Perfect interobserver agreement was observed for the measurement of Breslow thickness (Table 3.14).

Table 3.14: Cross-tabulation of Breslow thickness for my measurements (SOS) and those of Pathologist B (B).

There was 100% (20/20) agreement using the AJCC cut-off points [43]. Kappa=1.0, $p=3x10^{-11}$.

	Breslow thickness (B)				
Breslow thickness (SOS)	≤1.00 mm	1.01-2.00 mm	2.01-4.00 mm	>4.00 mm	Total
≤1.00mm	1	0	0	0	1
1.01-2.00mm	0	6	0	0	6
2.01-4.00mm	0	0	10	0	10
>4.00mm	0	0	0	3	3
Total	1	6	10	3	20

The Spearman correlation coefficient was 0.99 ($p=7x10^{-18}$), indicating excellent agreement (Figure 3.3).

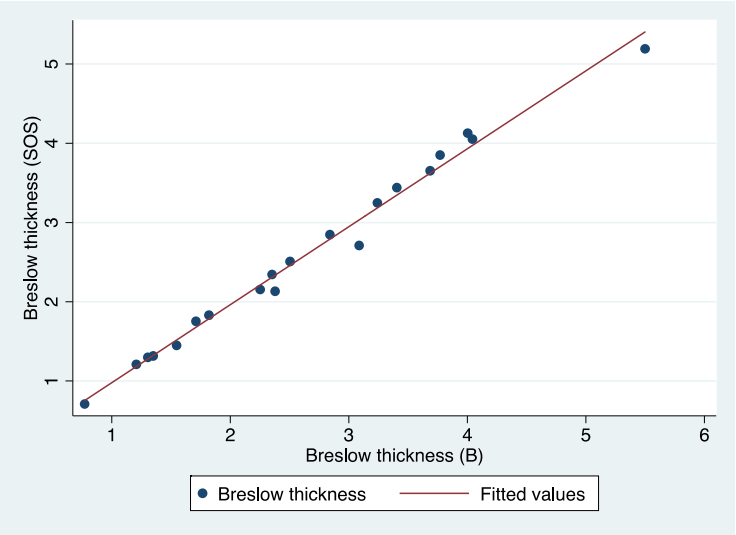

Figure 3.3: Scatter plot of Breslow thickness (as a continuous measure), as recorded by me (SOS, on the y-axis) and by Dr Merchant (B, on the x-axis).

3.4.2 Dominant nodule

Interobserver agreement was substantial for the presence or absence of a dominant nodule (Table 3.15).

Table 3.15: Cross-tabulation of the presence or absence of a dominant nodule for my measures (SOS) and those of Pathologist B (B).

There was 90% (18/20) agreement. Kappa=0.69 (95% CI 0.31-1.00), p=0.0006.

	Dominant nodule (B)		
Dominant nodule (SOS)	No	Yes	Total
No	15	0	15
Yes	2	3	5
Total	17	3	20

3.4.3 Microscopic ulceration

There was substantial agreement for microscopic ulceration (Table 3.16). The extent of ulceration could be compared between observers in 3 cases and the differences ranged from 0.4-1.1mm.

Table 3.16: Cross-tabulation of microscopic ulceration for my measures (SOS) and those of Pathologist B (B).

There was 90% (18/20) agreement for microscopic ulceration status. Kappa=0.69 (95% CI 0.29-1.00), p=0.001.

	Ulceration status (B)		
Ulceration status (SOS)	No	Yes	Total
No	15	1	16
Yes	1	3	4
Total	16	4	20

3.4.4 Tumour-infiltrating lymphocytes (TILs)

Interobserver agreement was moderate for TILs (Table 3.17).

Table 3.17: Cross-tabulation of the pattern of tumour-infiltrating lymphocytes for my measures (SOS) and those of Pathologist B (B).

There was 60% (12/20) agreement. Kappa=0.41 (95% CI 0.11-0.72), p=0.001.

	TILs (B)						
TILs (SOS)	Totally absent	Non-brisk sparse	Non-brisk peripheral	Brisk peripheral	Brisk diffuse	Not assessable	Total
Totally absent	1	0	0	0	0	0	1
Non-brisk sparse	2	6	0	0	1	0	9
Non-brisk peripheral	0	2	3	0	0	0	5
Brisk peripheral	0	2	0	1	0	0	3
Brisk diffuse	0	0	0	0	0	0	0
Not assessable	0	1	0	0	0	1	2
Total	3	11	3	1	1	1	20

3.4.5 The presence or absence of tumour loss

During the development of the virtual pathology protocol, the regression variable was dropped and tumour loss was recorded instead (Chapter 2). Interobserver agreement was fair for tumour loss (Table 3.18).

Table 3.18: Cross-tabulation of the presence or absence of tumour loss for my measures (SOS) and those of Pathologist B (B).

There was 85% (17/20) agreement. Kappa=0.32 (95% CI -0.27-0.90), p=0.07.

	Tumour loss (B)		
Tumour loss (SOS)	No	Yes	Total
No	16	1	17
Yes	2	1	3
Total	18	2	20

3.4.6 The type of tumour loss

Interobserver agreement was fair for the type of tumour loss (Table 3.19). Four cases were available for comparison for the depth of tumour loss. Differences ranged from 0.2mm to 1.4mm.

3.4.7 The intensity of tumour-infiltrating melanophages (TIMs)

There was almost perfect agreement for the intensity of tumour-infiltrating melanophages (TIMs, Table 3.20).

3.4.8 The pattern of tumour-infiltrating melanophages (TIMs)

There was perfect agreement for the pattern of TIMs (Table 3.21).

Table 3.19: Cross-tabulation of the type of tumour loss for my measures (SOS) and those of Pathologist B (B).

There was 85% (17/20) agreement. Kappa=0.33 (95% CI -0.07-1.0), p=0.04.

	Type of tumour loss (A)			
Type of tumour loss (SOS)	Absent	Deep	Superficial	Total
Absent	16	0	1	17
Deep	1	0	0	1
Superficial	1	0	1	2
Total	18	0	2	20

Table 3.20: Cross-tabulation of the intensity of tumour-infiltrating melanophages for my measures (SOS) and those of Pathologist B (B).

There was 90% (18/20) agreement. Kappa=0.85 (95% CI 0.65-1.0), $p=5x10^{-9}$.

	TIMs intensity (B)				
TIMs intensity (SOS)	None	Very few	Moderate	Lots	Total
None	8	0	0	0	8
Very few	1	6	1	0	8
Moderate	0	0	3	0	3
Lots	0	0	0	1	1
Total	9	6	4	1	20

Table 3.21: Cross-tabulation of the pattern of tumour-infiltrating melanophages for my measures (SOS) and those of Pathologist B (B).

There was 100% (20/20) agreement. Kappa=1.0, $p=1x10^{-8}$.

	TIMs (B)				
TIMs (SOS)	Totally absent	Non-brisk sparse	Non-brisk peripheral	Not assessable	Total
Totally absent	5	0	0	0	5
Non-brisk sparse	0	12	0	0	12
Non-brisk peripheral	0	0	2	0	2
Not assessable	0	0	0	1	1
Total	5	12	2	1	20

3.5 Intraobserver variation in whole-tumour measures using virtual pathology

In order to derive estimates of intraobserver agreement, I revisited 20 cases that I had reported in the preceding 12 months (median 6, range 5-6 months) using the virtual pathology protocol (Appendix C). I avoided cases that had been flagged as being especially difficult, requiring further assessment with Pathologist B. The first set of recordings was called set 1 and the second set was referred to as set 2.

3.5.1 Breslow thickness

There was almost perfect intraobserver agreement for Breslow thickness (Table 3.22; Figure 3.4).

Table 3.22 Breslow thickness measurements in the first (Breslow thickness 1) and second (Breslow thickness 2) sets, using the AJCC cut-off points [43].

There was 95% (19/20) agreement for Breslow thickness category. Kappa=0.92 (95% CI 0.69-1.0), $p=6x10^{-10}$.

	Breslow thickness 2				
Breslow thickness 1	≤1.00mm	1.01-2.00mm	2.01-4.00mm	>4.00 mm	Total
≤1.00mm	3	0	0	0	3
1.01-2.00mm	0	10	1	0	11
2.01-4.00mm	0	0	5	0	5
>4.00mm	0	0	0	1	1
Total	3	10	6	1	20

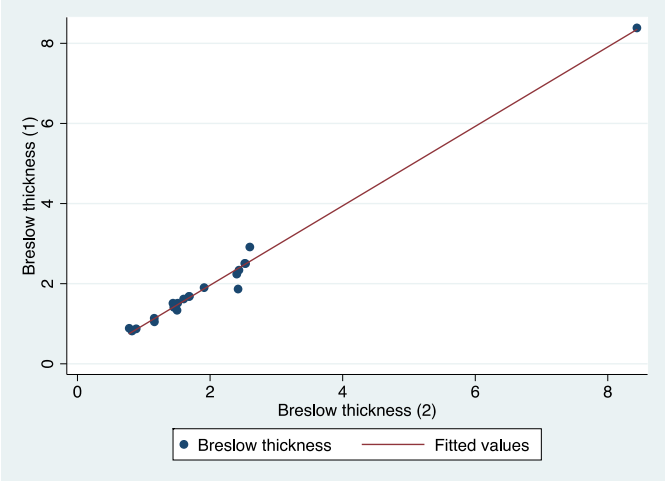

Figure 3.4: Scatter plot of Breslow thickness (as a continuous measure), which I recorded in the first (1, on the x-axis) and second (2, on the y-axis) sets.

Spearman correlation coefficient=0.98, $p=4x10^{-14}$.

3.5.2 Dominant nodule

There was 95% (19/20) agreement for the presence or absence of a dominant nodule (kappa=0 because the observed and expected agreement were the same, indicating chance agreement only, Table 3.23). The presence of a dominant nodule was rare in the cases studied and, therefore, the results may not be reflective of the true level of agreement.

Table 3.23: Cross-tabulation of the presence or absence of a dominant nodule.

95% (19/20) cases were categorised the same way in both sets. Kappa=0 (95% CI not calculable).

	Dominant nodule 2		
Dominant nodule 1	No	Yes	Total
No	19	0	19
Yes	1	0	1
Total	20	0	20

3.5.3 Microscopic ulceration

There was perfect intraobserver agreement for microscopic ulceration (Table 3.24). The extent of ulceration was measured in the single case with ulceration and was similar for each set (1.3mm for set 1 and 1.1mm for set 2).

Table 3.24: Cross-tabulation of microscopic ulceration status for set 1 and set 2.

There was 100% (20/20) agreement for microscopic ulceration status. Kappa=1.0, $p=4x10^{-6}$.

	Ulceration status 2		
Ulceration status 1	No	Yes	Total
No	19	0	19
Yes	0	1	1
Total	19	1	20

3.5.4 Tumour-infiltrating lymphocytes (TILs)

There was 75% (15/20) agreement (kappa=0.63, indicating substantial agreement), using a protocol adapted from Clemente *et al.* (Table 3.25) [61].

3.5.5 The presence or absence of tumour loss

There was substantial agreement for the presence or absence of tumour loss (Table 3.26).

Table 3.25: Cross-tabulation of tumour-infiltrating lymphocytes in the first (TILs 1) and second (TILs 2) sets, using a protocol adapted from Clemente *et al.* [61].

There was 75% (15/20) agreement using this classification. Kappa=0.63 (95% CI 0.29-0.85), $p=2x10^{-6}$.

	TILs 2						
TILs 1	Totally absent	Focally absent (biphasic VGP)	Non-brisk sparse	Non-brisk peripheral	Brisk peripheral	Not assessable	Total
Totally absent	2	0	0	0	0	0	2
Focally absent (biphasic VGP)	0	0	1	0	0	0	1
Non-brisk sparse	0	0	4	2	0	0	6
Non-brisk peripheral	0	0	2	5	0	0	7
Brisk peripheral	0	0	0	0	3	0	3
Not assessable	0	0	0	0	0	1	1
Total	2	0	7	7	3	1	20

Table 3.26: Cross-tabulation of the presence or absence of tumour loss in set 1 and set 2.

There was 90% (18/20) agreement for tumour loss. Kappa=0.62 (95% CI 0.15-1.0), p=0.001.

	Tumour loss 2		
Tumour loss 1	No	Yes	Total
No	16	2	18
Yes	0	2	2
Total	16	4	20

3.5.6 The type of tumour loss

There was substantial agreement for the type of tumour loss (Table 3.27). Two cases were available for comparison of the depth of tumour loss and the differences were as follows: 0.05mm and 0.2mm.

3.5.7 The intensity of tumour-infiltrating melanophages (TIMs)

There was moderate agreement for the intensity of TIMs between the first and second sets (Table 3.28).

Table 3.27: Cross-tabulation of the type of tumour loss in set 1 and set 2.

There was 90% (18/20) agreement for the type of tumour loss. Kappa=0.62 (95% CI 0.15-1.0), p=0.001.

	Type of tumour loss 2		
Type of tumour loss 1	Absent	Deep	Total
Absent	16	2	18
Deep	0	2	2
Total	16	4	20

Table 3.28: Cross-tabulation of the intensity of melanophages in set 1 and set 2.

There was 70% (14/20) agreement. Kappa=0.58 (95% CI 0.31-0.80), p=0.00001.

	TIMs intensity 2				
TIMs intensity 1	None	Very few	Moderate	Lots	Total
None	3	2	0	0	5
Very few	0	5	2	0	7
Moderate	0	0	5	1	6
Lots	0	1	0	1	2
Total	3	8	7	2	20

3.5.8 The pattern of tumour-infiltrating melanophages (TIMs)

Intraobserver agreement was also moderate for the pattern of TIMs (Table 3.29).

3.5.9 Interpretation of inter- and intraobserver agreement for whole-tumour measures

Both inter- and intra-observer agreement were highest for Breslow thickness and microscopic ulceration, using the virtual pathology protocol. These findings were consistent with initial interobserver results using a light microscope. There was better agreement for TILs and tumour loss (rather than regression) using the new virtual pathology protocol. Yet, interobserver agreement for tumour loss was fair. Intraobserver agreement was even better for TILs and tumour loss. Overall, there was moderate to substantial intraobserver agreement for whole-tumour measures, using the virtual pathology protocol. Table 3.30 summarises the findings for inter- and intraobserver variation analyses of whole tumour measures.

Table 3.29: Cross-tabulation of the pattern of tumour-infiltrating melanophages (TIMs) in set 1 and set 2, using the 8 categories, adapted from a protocol by Clemente *et al.* [61].

There was 75% (15/20) agreement for the pattern of TIMs. Kappa= 0.56 (95% CI 0.27-0.91), p=0.0006.

	TIMs 2					
TIMs 1	Totally absent	Focally absent (biphasic VGP)	Non-brisk sparse	Non-brisk peripheral	Not assessable	Total
Totally absent	1	0	0	0	0	1
Focally absent (biphasic VGP)	0	0	0	1	0	1
Non-brisk sparse	1	0	7	2	0	10
Non-brisk peripheral	0	0	1	6	0	7
Not assessable	0	0	0	0	1	1
Total	2	0	8	9	1	20

Table 3.30 (following page): Summary table of the results for inter- and intraobserver analyses of whole-tumour measures.

The percentage agreement, kappa statistic, 95% confidence intervals (95%CI), p-value and strength of agreement are shown for factors recorded using a light microscope and/or virtual pathology protocol. For the virtual pathology protocol, melanoma cell shape and melanoma cell pigmentation were recorded in the cored region rather than in the whole tumour. NA=not applicable. NC=not calculable.

Note that the variable used for tumour-infiltrating lymphocytes (TILs) differed between the initial assessment using a light microscope and the virtual pathology protocol. The TILs variable in the light microscope study had 3 categories (absent, non-brisk and brisk), whilst the TILs variable for the virtual pathology protocol consisted of 8 categories (please see Chapter 2 for more details).

Whole-tumour measures												
	Interobserver agreement (light microscope, training set)				Interobserver agreement (virtual pathology)				Intraobserver agreement (virtual pathology)			
Factor	**% Agreement**	**Kappa (95%CI)**	**p-value**	**Strength of agreement**	**% Agreement**	**Kappa (95%CI)**	**p-value**	**Strength of agreement**	**% Agreement**	**Kappa (95%CI)**	**p-value**	**Strength of agreement**
Histological subtype	79	0.53 (0.30-0.72)	$7x10^{-11}$	Moderate	NA	NA	NA	NA	NA	NA	NA	NA
Growth phase	83	0.24 (-0.02-0.58)	0.001	Fair	NA	NA	NA	NA	NA	NA	NA	NA
Clark's level	21	0.002 (-0.07-0.09)	0.5	Chance	NA	NA	NA	NA	NA	NA	NA	NA
Breslow thickness	77	0.72 (0.56-0.84)	$<1x10^{-16}$	Substantial	100	1.0	$3x10^{-11}$	Perfect	95	0.92 (0.69-1.0)	$6x10^{-10}$	Almost perfect
Dominant nodule	34	0 (NC)	NC	Chance	90	0.69 (0.31-1.0)	0.0006	Substantial	95	0 (NC)	NC	Chance
Microscopic ulceration	93	0.84 (0.70-0.99)	$2x10^{-14}$	Almost perfect	90	0.69 (0.29-1.0)	0.001	Substantial	100	1.0 (1.0-1.0)	$4x10^{-6}$	Perfect
Tumour-infiltrating lymphocytes	43	0.14 (0.02-0.30)	0.02	Slight	60	0.41 (0.11-0.72)	0.001	Moderate	75	0.63 (0.29-0.85)	$2x10^{-6}$	Substantial
Regression	89	0.20 (-0.03-0.6)	0.003	Slight	NA	NA	NA	NA	NA	NA	NA	NA
Presence or absence of tumour loss	NA	NA	NA	NA	85	0.32 (-0.27-0.9)	0.07	Fair	90	0.62 (0.15-1.0)	0.001	Substantial
Type of tumour loss	NA	NA	NA	NA	85	0.33 (-0.07-1.0)	0.04	Fair	90	0.62 (0.15-1.0)	0.001	Substantial

Whole-tumour measures												
	Interobserver agreement (light microscope, training set)				Interobserver agreement (virtual pathology)				Intraobserver agreement (virtual pathology)			
Factor	**% Agreement**	**Kappa (95%CI)**	**p-value**	**Strength of agreement**	**% Agreement**	**Kappa (95%CI)**	**p-value**	**Strength of agreement**	**% Agreement**	**Kappa (95%CI)**	**p-value**	**Strength of agreement**
Intensity of tumour-infiltrating melanophages	NA	NA	NA	NA	90	0.85 (0.65-1.0)	$5x10^{-9}$	Almost perfect	70	0.58 (0.31-0.80)	0.00001	Moderate
Pattern of tumour-infiltrating melanophages	NA	NA	NA	NA	100	1.0	$1x10^{-8}$	Perfect	75	0.56 (0.27-0.91)	0.0006	Moderate
Mitotic count	55	0.35 (0.17-0.51)	$3x10^{-6}$	Fair	NA	NA	NA	NA	NA	NA	NA	NA
Microsatellites	91	0 (NC)	NC	Chance	NA	NA	NA	NA	NA	NA	NA	NA
Vascular invasion	87	0.23 (0-0.56)	0.0002	Fair	NA	NA	NA	NA	NA	NA	NA	NA
Perineural invasion	88	-0.01 (-0.04-0)	0.6	Less than chance	NA	NA	NA	NA	NA	NA	NA	NA
Melanoma cell shape	46	0.19 (0.06-0.34)	0.003	Slight	NA	NA	NA	NA	NA	NA	NA	NA
Melanoma cell pigmentation	12	0.03 (-0.08-0.19)	0.3	Slight	NA	NA	NA	NA	NA	NA	NA	NA

3.6 Interobserver variation in cored region measures using virtual pathology

The transition to virtual pathology brought about the prospect of developing a new approach, including the use of bespoke software and annotating a particular region of interest. When I commenced my PhD, staff in the Section of Epidemiology and Biostatistics had already begun to generate whole-genome transcriptomic data (from tissue microarray (TMA) core biopsies of primary melanomas), which ultimately culminated in 703 transcriptomes. This presented the opportunity to describe the estimated cored regions in detail, which would facilitate subsequent comparisons of the histopathological appearances with gene expression data. Therefore, I annotated and digitally extracted a 600-micron region of tumour, which was estimated to correspond to the site that had been sampled using a 0.6mm TMA needle. The following inter- and intraobserver analyses refer to measures recorded on this cored region.

The selection of cases for interobserver variation of the cored region was randomly selected, except that cases with poor image quality were avoided. Dr Merchant and I had each reviewed the same thirty cores (in 16 cases), and the resulting data were used for interobserver variation analyses of the cored region (except for the percentage of stroma, for which 26 cores were available for analysis). Four cases had one core, 10 cases had 2 cores and 2 cases had 3 cores available for analysis.

3.6.1 The percentage of stroma

Twenty-six cases were available for comparison of the percentage of stroma between observers (Figure 3.5). The Spearman correlation coefficient for the percentage of stroma for my recorded measures and those of Pathologist B was 0.7 (p=0.0001), indicating a strong association.

3.6.2 Stroma quality

Interobserver agreement was slight for the quality of the stroma (Table 3.31).

3.6.3 Melanoma cell shape

There were thirty cases available for comparison of melanoma cell shape. There was moderate interobserver agreement for melanoma cell shape (Table 3.32).

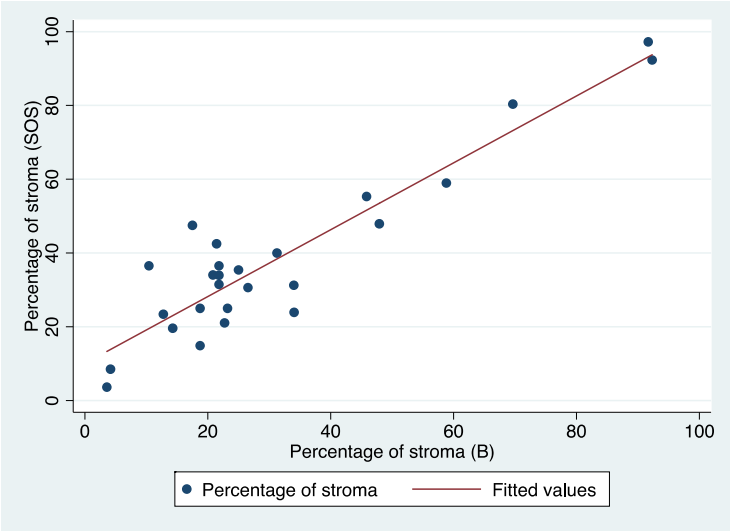

Figure 3.5: Scatter plot of the percentage of stroma, recorded by me (SOS, on the y-axis) and by Pathologist B (x-axis).

Table 3.31: Cross-tabulation of stroma quality for my measures (SOS) and those of Pathologist B (B).

There was 60% (18/30) agreement. Kappa=0.21 (95% CI -0.11-0.49), p=0.03.

	Stroma quality (B)				
Stroma quality (SOS)	Compact	Loose	Mixed	Not assessable	Total
Compact	15	0	1	6	22
Loose	1	2	0	0	3
Mixed	2	0	0	1	3
Not assessable	1	0	0	1	2
Total	19	2	1	8	30

Table 3.32: Cross-tabulation of melanoma cell shape for my measures (SOS) and those of Pathologist B (B).

There was 73% (22/30) agreement. Kappa 0.49 (95% CI 0.24-0.77), $p=8x10^{-8}$.

	Melanoma cell shape (B)				
Melanoma cell shape (SOS)	Round/ovoid	Epithelioid	Spindle	Naevoid	Total
Round/ovoid	17	0	0	0	17
Epithelioid	7	0	0	0	7
Spindle	0	0	2	1	3
Naevoid	0	0	0	3	3
Total	24	0	2	4	30

3.6.4 Melanoma cell structure

Interobserver agreement was slight for melanoma cell structure (Table 3.33).

Table 3.33: Cross-tabulation of melanoma cell structure for my measures (SOS) and those of Pathologist B (B).

There was 40% (12/30) agreement. Kappa=0.08 (95% CI -0.11-0.32), p=0.3.

	Melanoma cell structure (B)				
Melanoma cell structure (SOS)	Nests	Sheets	Fascicles	Dispersed	Total
Nests	4	7	0	0	11
Sheets	1	8	1	1	11
Fascicles	6	2	0	0	8
Dispersed	0	0	0	0	0
Total	11	17	1	1	30

3.6.5 Melanoma cell pigmentation

There was almost perfect agreement for melanoma cell pigmentation (Table 3.34).

Table 3.34: Cross-tabulation of melanoma cell pigmentation for my measures (SOS) and those of Pathologist B (B).

There was 93% (28/30) agreement. Kappa=0.82 (95% CI 0.52-1.0), $p=9x10^{-10}$.

	Melanoma cell pigmentation (B)			
Melanoma cell pigmentation (SOS)	Absent	Faint	Moderate	Total
Absent	23	0	0	23
Faint	0	3	0	3
Moderate	1	1	2	4
Total	24	4	2	30

3.6.6 The presence or absence of a core immune cell infiltrate

There was moderate agreement between observers for the presence or absence of an immune cell infiltrate within the cored region (Table 3.35).

Table 3.35: Cross-tabulation of the presence or absence of the core immune cell infiltrate for my measures (SOS) and those of Pathologist B (B).

There was 83% (25/30) agreement. Kappa=0.57 (95% CI 0.26-0.88), p=0.0003.

	Core immune cell infiltrate (B)		
Core immune cell infiltrate (SOS)	No	Yes	Total
No	5	0	5
Yes	5	20	25
Total	10	20	30

3.6.7 The extent of the core immune cell infiltrate

Similarly, there was moderate agreement for the extent of the core immune cell infiltrate (Table 3.36).

Table 3.36: Cross-tabulation of the extent of the core immune cell infiltrate for my measures (SOS) and those of Pathologist B (B).

There was 70% (21/30) agreement. Kappa=0.59 (95% CI 0.37-0.78), $p=4x10^{-9}$.

	Extent of core immune cell infiltrate (B)				
Extent of core immune cell infiltrate (SOS)	None	Barely perceptible	Some	Moderate	Total
None	5	0	0	0	5
Barely perceptible	5	6	2	0	13
Some	0	0	8	1	9
Moderate	0	0	1	2	3
Total	10	6	11	3	30

The none/barely perceptible categories were merged (as “no/barely perceptible”) and used as the reference group for analyses of the core immune cell subsets. This is because further details about the core immune cell subsets were not recorded unless the core immune cell infiltrate was classified as some, moderate or lots (i.e. not recorded if the core immune cell infiltrate was deemed to be absent or barely perceptible).

3.6.8 The location of the core immune cell infiltrate

There was moderate agreement for the location of the core immune cell infiltrate (Table 3.37).

Table 3.37: Cross-tabulation of the location of the core immune cell infiltrate for my measures (SOS) and those of Pathologist B (B).

There was 77% (23/30) agreement. Kappa=0.62 (95% CI 0.42-0.83), $p=1x10^{-8}$.

	Location of core immune cell infiltrate (B)				
Location of core immune cell infiltrate (SOS)	No/barely perceptible	At the tumour/ stroma interface	Dispersed	Both	Total
No/barely perceptible	16	1	0	1	18
At the tumour/ stroma interface	0	1	0	0	1
Dispersed	0	1	2	1	4
Both	0	3	0	4	7
Total	16	6	2	6	30

3.6.9 The presence or absence of a core lymphocytic infiltrate

There was substantial agreement for the presence or absence of a core lymphocytic infiltrate (Table 3.38).

Table 3.38: Cross-tabulation of the presence or absence of a core lymphocytic infiltrate for my measures (SOS) and those of Pathologist B (B).

There was 90% (27/30) agreement. Kappa=0.80 (95% CI not calculable), $p=2x10^{-6}$.

	Core lymphocytic infiltrate (B)			
Core lymphocytic infiltrate (SOS)	No/barely perceptible	No	Yes	Total
No/barely perceptible	16	0	2	18
No	0	0	0	0
Yes	0	1	11	12
Total	16	1	13	30

3.6.10 The extent of the core lymphocytic infiltrate

Interobserver agreement was substantial for the extent of the core lymphocytic infiltrate (Table 3.39).

Table 3.39: Cross-tabulation of the extent of the core lymphocytic infiltrate for my measures (SOS) and those of Pathologist B (B).

There was 87% (26/30) agreement. Kappa=0.76 (95% CI 0.53-0.94), $p=3x10^{-8}$.

	Extent of core lymphocytic infiltrate (B)				
Extent of core lymphocytic infiltrate (SOS)	No/barely perceptible	None	Some	Moderate	Total
No/barely perceptible	16	0	2	0	18
None	0	0	0	0	0
Some	0	1	8	0	9
Moderate	0	0	1	2	3
Total	16	1	11	2	30

3.6.11 The presence or absence of a core plasma cell infiltrate

Agreement was almost perfect for the presence or absence of a core plasma cell infiltrate, although it was infrequently present (Table 3.40).

Table 3.40: Cross-tabulation of the presence or absence of a core plasma cell infiltrate for my measures (SOS) and those of Pathologist B (B).

There was 90% (27/30) agreement. Kappa=0.82 (95% CI 0.61-1.0), $p=1x10^{-8}$.

	Core plasma cell infiltrate (B)			
Core plasma cell infiltrate (SOS)	No/barely perceptible	No	Yes	Total
No/barely perceptible	16	2	0	18
No	0	9	0	9
Yes	0	1	2	3
Total	16	12	2	30

3.6.12 The extent of the core plasma cell infiltrate

Similarly, agreement was almost perfect for the extent of the core plasma cell infiltrate (Table 3.41).

Table 3.41: Cross-tabulation of the extent of the core plasma cell infiltrate for my measures (SOS) and those of Pathologist B (B).

There was 90% (27/30) agreement. Kappa=0.82 (95% CI 0.61-1.0), $p=1x10^{-8}$.

	Extent of core plasma cell infiltrate (B)			
Extent of core plasma cell infiltrate (SOS)	No/barely perceptible	None	Some	Total
No/barely perceptible	16	2	0	18
None	0	9	0	9
Some	0	1	2	3
Total	16	12	2	30

3.6.13 The presence or absence of a core melanophage infiltrate

Interobserver agreement was substantial for the presence or absence of melanophages within the core (Table 3.42).

Table 3.42: Cross-tabulation of the presence or absence of a core melanophage infiltrate for my measures (SOS) and those of Pathologist B (B).

There was 90% (27/30) agreement. Kappa=0.83 (95% CI 0.61-1.0), $p=1x10^{-10}$.

	Core melanophage infiltrate (B)			
Core melanophage infiltrate (SOS)	No/barely perceptible	No	Yes	Total
No/barely perceptible	16	2	0	18
No	0	5	0	5
Yes	0	1	6	7
Total	16	8	6	30

3.6.14 The extent of the core melanophage infiltrate

Agreement was substantial for the extent of melanophages infiltrating the cored region (Table 3.43).

Table 3.43: Cross-tabulation of the extent of the core melanophage infiltrate for my measures (SOS) and those of Pathologist B (B).

There was 87% (26/30) agreement. Kappa=0.78 (95% CI 0.60-0.95), $p=4x10^{-11}$.

	Extent of core melanophage infiltrate (B)				
Extent of core melanophage infiltrate (SOS)	No/barely perceptible	None	Some	Moderate	Total
No/barely perceptible	16	2	0	0	18
None	0	5	0	0	5
Some	0	1	4	0	5
Moderate	0	0	1	1	2
Total	16	8	5	1	30

3.6.15 The presence or absence of a core neutrophilic infiltrate

Agreement was almost perfect for the presence or absence of a neutrophilic infiltrate within the core (Table 3.44).

Table 3.44: Cross-tabulation of the presence or absence of a core neutrophilic infiltrate for my measures (SOS) and those of Pathologist B (B).

There was 93% (28/30) agreement. Kappa=0.87 (95% CI 0.67-1.0), $p=6x10^{-8}$.

	Core neutrophilic infiltrate (B)			
Core neutrophilic infiltrate (SOS)	No/barely perceptible	No	Yes	Total
No/barely perceptible	16	2	0	18
No	0	11	0	11
Yes	0	0	1	1
Total	16	13	1	30

3.6.16 The extent of the core neutrophilic infiltrate

A core neutrophilic infiltrate was noted in one case, the extent of which was recorded as “some” by both observers (Table 3.45). The extent of the core neutrophilic infiltrate was infrequently recorded. Interobserver agreement was almost perfect.

Table 3.45: Cross-tabulation of the extent of the core neutrophilic infiltrate for my measures (SOS) and those of Pathologist B (B).

There was 93% (28/30) agreement. Kappa=0.87 (95% CI 0.67-1.0), $p=6x10^{-8}$.

	Core neutrophilic infiltrate (B)			
Core neutrophilic infiltrate (SOS)	No/barely perceptible	None	Some	Total
No/barely perceptible	16	2	0	18
None	0	11	0	11
Some	0	0	1	1
Total	16	13	1	30

3.6.17 The presence or absence of a core eosinophilic infiltrate

There was substantial interobserver agreement for the presence or absence of a core eosinophilic infiltrate (Table 3.46).

Table 3.46: Cross-tabulation of the presence or absence of a core eosinophilic infiltrate for my measures (SOS) and those of Pathologist B (B).

There was 87% (26/30) agreement. Kappa=0.74 (95% CI 0.51-0.93), $p=3x10^{-6}$.

	Core eosinophilic infiltrate (B)			
Core eosinophilic infiltrate (SOS)	No/barely perceptible	No	Yes	Total
No/barely perceptible	16	2	0	18
No	0	10	1	11
Yes	0	1	0	1
Total	16	13	1	30

3.6.18 The extent of the core eosinophilic infiltrate

There was a similar level of agreement for the extent of the core eosinophilic infiltrate, although this was infrequently reported (Table 3.47).

Table 3.47 Cross-tabulation of the extent of the core eosinophilic infiltrate for my measures (SOS) and those of Pathologist B (B).

There was 87% (26/30) agreement. Kappa=0.74 (95% CI 0.51-0.93), $p=3x10^{-6}$.

	Extent of core eosinophilic infiltrate (B)			
Extent of core eosinophilic infiltrate (SOS)	No/barely perceptible	None	Some	Total
No/barely perceptible	16	2	0	18
None	0	10	1	11
Some	0	1	0	1
Total	16	13	1	30

3.6.19 The number of mitoses within the cored region

The Spearman correlation coefficient for the number of mitoses within the cored region was 0.9 ($p=4x10^{-12}$). Interobserver agreement was almost perfect for the number of core mitoses (Table 3.48).

Table 3.48: Cross-tabulation of the number of core mitoses for my measures (SOS) and those of Pathologist B (B).

There was 87% (26/30) agreement. Kappa=0.80 (95% CI 0.57-0.95), $p=2x10^{-10}$.

	Number of core mitoses (B)			
Number of core mitoses (SOS)	0	1-2	≥3	Total
0	9	0	0	9
1-2	2	9	1	12
≥3	0	1	8	9
Total	11	10	9	30

3.6.20 The number of blood vessels within the cored region

The Spearman correlation coefficient for the number of blood vessels within the cored region was 0.8 ($p=2x10^{-7}$). Interobserver agreement was fair for the enumeration of blood vessels within the cored region (Table 3.49).

Table 3.49: Cross-tabulation of the number of core blood vessels for my measures (SOS) and those of Pathologist B (B).

There was 60% (18/30) agreement. Kappa=0.40 (95% CI 0.14-0.66), p=0.001.

	Number of core blood vessels (B)			
Number of core blood vessels (SOS)	0	1-2	≥3	Total
0	5	2	0	7
1-2	5	6	2	13
≥3	0	3	7	10
Total	10	11	9	30

3.7 Intraobserver variation in cored region measures using virtual pathology

In order to assess intraobserver variation for the cored region measures, I repeated an assessment of the cored regions for twenty cases that had been reviewed in the previous 12 months (median 6, range 5-6 months). These were the same cases referred to previously, in which intraobserver variation of whole tumour measures using virtual pathology was assessed. The first set of recordings was called set 1 and the second set was referred to as set 2.

3.7.1 Percentage of stroma within the cored regions

The Spearman correlation coefficient for the percentage of stroma between set 1 and set 2 was 0.9 ($p=6x10^{-8}$), indicating a strong association (Figure 3.6).

3.7.2 Stroma quality

The kappa statistic suggests slight agreement because neither of the cores with a mixed infiltrate agrees. However, compact stroma was frequently recorded and there was very good agreement for this stroma quality overall (Table 3.50).

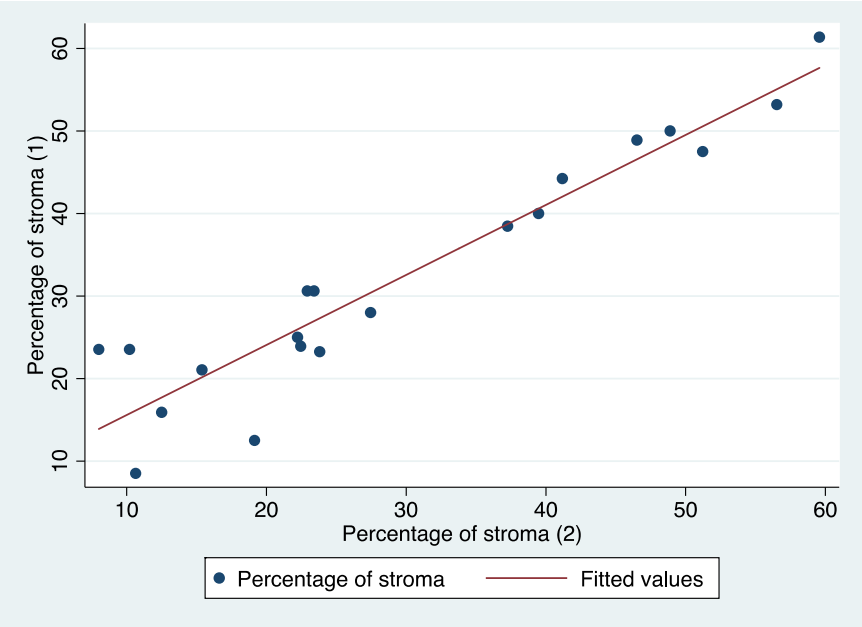

Figure 3.6 Scatter plot of the percentage of stroma in set 1 and set 2.

Table 3.50: Cross-tabulation of the stroma quality in set 1 and set 2.

There was 70% (14/20) agreement. Kappa=0.05 (95% CI -0.11-0.36), p=0.4.

	Stroma quality 2			
Stroma quality 1	Compact	Loose	Mixed	Total
Compact	14	0	1	15
Loose	1	0	1	2
Mixed	2	0	0	2
Not assessable	1	0	0	1
Total	18	0	2	20

3.7.3 Melanoma cell shape

Intraobserver agreement was substantial for melanoma cell shape (Table 3.51). The analysis highlights limitations in the distinction of round/ovoid and epithelioid cell shapes from one another.

Table 3.51 Cross-tabulation of melanoma cell shape for set 1 and set 2.

There was 80% (16/20) agreement for cell shape. Kappa=0.69 (95% CI 0.42-0.92), $p=6x10^{-6}$).

	Melanoma cell shape 2			
Melanoma cell shape 1	Round/ovoid	Epithelioid	Spindle	Total
Round/ovoid	6	4	0	10
Epithelioid	0	7	0	7
Spindle	0	0	3	3
Total	6	11	3	20

3.7.4 Melanoma cell structure

Intraobserver agreement was moderate for melanoma cell structure (Table 3.52).

Table 3.52: Cross-tabulation of melanoma cell structure in set 1 and set 2.

There was 75% (15/20) agreement. Kappa 0.58 (95% CI 0.28-0.90), p=0.0001.

	Melanoma cell structure 2			
Melanoma cell structure 1	Nests	Sheets	Fascicles	Total
Nests	9	0	1	10
Sheets	2	2	1	5
Fascicles	1	0	4	5
Total	12	2	6	20

3.7.5 Melanoma cell pigmentation

There was almost perfect agreement for melanoma cell pigmentation (Table 3.53). Absent pigmentation was the most commonly recorded grade of pigmentation.

Table 3.53 Cross-tabulation of melanoma cell pigmentation in set 1 and set 2.

There was 85% (17/20) agreement. Kappa=0.82 (95% CI 0.57-1.0), $p=7x10^{-9}$.

	Melanoma cell pigmentation 2				
Melanoma cell pigmentation 1	Absent	Faint	Moderate	High	Total
Absent	12	0	0	0	12
Faint	1	2	0	0	3
Moderate	0	0	3	0	3
High	0	0	1	1	2
Total	13	2	4	1	20

3.7.6 The presence or absence of a core immune cell infiltrate

There was fair agreement for the presence or absence of an immune cell infiltrate within the cored region (Table 3.54).

Table 3.54 Cross-tabulation of the core immune cell infiltrate in set 1 and set 2.

There was 85% (17/20) agreement. Kappa=0.35 (95% CI -0.17-0.86), p=0.02.

	Core immune cell infiltrate 2		
Core immune cell infiltrate 1	No	Yes	Total
No	1	3	4
Yes	0	16	16
Total	1	19	20

3.7.7 The extent of the core immune cell infiltrate

Intraobserver agreement was higher for the extent of the core immune cell infiltrate (Table 3.55).

Table 3.55: Cross-tabulation of the extent of the core immune cell infiltrate in set 1 and set 2.

There was 65% (13/20) agreement. Kappa=0.53 (95% CI 0.25-0.78), $p=6x10^{-6}$.

	Extent of core immune cell infiltrate 2					
Extent of core immune cell infiltrate 1	None	Barely perceptible	Some	Moderate	Lots	Total
None	1	3	0	0	0	4
Barely perceptible	0	2	1	0	0	3
Some	0	0	6	2	0	8
Moderate	0	0	1	3	0	4
Lots	0	0	0	0	1	1
Total	1	5	8	5	1	20

3.7.8 The location of the core immune cell infiltrate

There was moderate agreement for the location of the core immune cell infiltrate (Table 3.56).

Table 3.56: Cross-tabulation of the location of the core immune cell infiltrate in the cored regions for set 1 and set 2.

There was 70% (14/20) agreement. Kappa=0.59 (95% CI 0.35-0.85), $p=1x10^{-6}$.

	Location of core immune cell infiltrate 2				
Location of core immune cell infiltrate 1	No/barely perceptible	At the tumour/ stroma interface	Dispersed	Both	Total
No/barely perceptible	6	0	0	1	7
At the tumour/ stroma interface	0	2	1	3	6
Dispersed	0	0	1	1	2
Both	0	0	0	5	5
Total	6	2	2	10	20

3.7.9 The presence or absence of a core lymphocytic infiltrate

There was almost perfect agreement for the presence or absence of a core lymphocytic infiltrate (Table 3.57).

Table 3.57: Cross-tabulation of the presence or absence of a core lymphocytic infiltrate in set 1 and set 2.

There was 95% (19/20) agreement. Kappa=0.92 (95% CI 0.78-1.0), $p=3x10^{-9}$.

	Core lymphocytic infiltrate 2			
Core lymphocytic infiltrate 1	No/barely perceptible	No	Yes	Total
No/barely perceptible	6	1	0	7
No	0	5	0	5
Yes	0	0	8	8
Total	6	6	8	20

3.7.10 The extent of the core lymphocytic infiltrate

Intraobserver agreement was substantial for the extent of the lymphocytic infiltrate within the cored region (Table 3.58).

Table 3.58: Cross-tabulation of the extent of the core lymphocytic infiltrate for set 1 and set 2.

There was 85% (17/20) agreement. Kappa=0.79 (95% CI 0.61-1.0), $p=5x10^{-10}$.

	Extent of core lymphocytic infiltrate 2					
Extent of core lymphocytic infiltrate 1	No/barely perceptible	None	Some	Moderate	Lots	Total
No/barely perceptible	6	1	0	0	0	7
None	0	5	0	0	0	5
Some	0	0	5	2	0	7
Moderate	0	0	0	0	0	0
Lots	0	0	0	0	1	1
Total	6	6	5	2	1	20

3.7.11 The presence or absence of a core plasma cell infiltrate

Intraobserver agreement was almost perfect, however, none of the cores assessed had a plasma cell infiltrate, which limits the interpretation of these results (Table 3.59).

Table 3.59: Cross-tabulation of the presence or absence of a core plasma cell infiltrate for set 1 and set 2.

There was 95% (19/20) agreement. Kappa=0.89 (95% CI 0.67-1.00), p=0.00003.

	Core plasma cell infiltrate 2		
Core plasma cell infiltrate 1	No/barely perceptible	No	Total
No/barely perceptible	6	1	7
No	0	13	13
Total	6	14	20

3.7.12 The presence or absence of a core melanophage infiltrate

There was almost perfect intraobserver agreement for the presence or absence of melanophages within the cored region (Table 3.60).

Table 3.60: Cross-tabulation of the presence of an infiltrate of core melanophages for set 1 and set 2.

There was 95% (19/20) agreement. Kappa=0.91 (95% CI 0.67-1.0), $p=1x10^{-7}$.

	Core melanophage infiltrate 2			
Core melanophage infiltrate 1	No/barely perceptible	No	Yes	Total
No/barely perceptible	6	0	1	7
No	0	2	0	2
Yes	0	0	11	11
Total	6	2	12	20

3.7.13 The extent of the core melanophage infiltrate

There was moderate agreement for the extent of melanophages within the cored region (Table 3.61).

Table 3.61: Cross-tabulation of the extent of the core melanophage infiltrate for set 1 and set 2.

There was 65% (13/20) agreement. Kappa=0.54 (95% CI 0.32-0.86), $p=9x10^{-7}$.

	Extent of core melanophage infiltrate 2					
Extent of core melanophage infiltrate 1	No/barely perceptible	None	Some	Moderate	Lots	Total
No/barely perceptible	6	0	1	0	0	7
None	0	2	0	0	0	2
Some	0	0	2	2	0	4
Moderate	0	0	0	3	4	7
Lots	0	0	0	0	0	0
Total	6	2	3	5	4	20

3.7.14 The presence or absence of a core neutrophilic infiltrate

Similarly, intraobserver agreement was almost perfect for the core neutrophilic infiltrate, however, it appears that only one of the cores analysed contained neutrophils (Table 3.62).

3.7.15 The extent of the core neutrophilic infiltrate

Substantial agreement is indicated by the kappa statistic, however, the extent of the core neutrophilic infiltrate was recorded as some in set 1 and moderate in set 2. The

rarity of neutrophils within the core limits conclusions about intraobserver agreement (Table 3.63.)

Table 3.62: Cross-tabulation of the presence of a core neutrophilic infiltrate for set 1 and set 2.

There was 95% (19/20) agreement. Kappa=0.9 (95% CI 0.67-1.0), $p=2x10^{-6}$.

	Core neutrophilic infiltrate 2			
Core neutrophilic infiltrate 1	No/barely perceptible	No	Yes	Total
No/barely perceptible	6	1	0	7
No	0	12	0	12
Yes	0	0	1	1
Total	6	13	1	20

Table 3.63: Cross-tabulation of the extent of the core neutrophilic infiltrate for set 1 and set 2.

There was 90% (18/20) agreement. Kappa=0.8 (95% CI 0.57-1.0), p=0.00001.

	Core neutrophilic infiltrate 2				
Core neutrophilic infiltrate 1	No/barely perceptible	None	Some	Moderate	Total
No/barely perceptible	6	1	0	0	7
None	0	12	0	0	12
Some	0	0	0	1	1
Moderate	0	0	0	0	0
Total	6	13	0	1	20

3.7.16 The presence or absence of a core eosinophilic infiltrate

It appears that none of the cores had an eosinophilic infiltrate, therefore, it is not possible to make inferences about its reproducibility as a recorded measure (Table 3.64).

Table 3.64: Cross-tabulation of the presence of a core eosinophilic infiltrate for set 1 and set 2.

There was 95% (19/20) agreement. Kappa=0.89 (95% CI 0.67-1.0), p=0.00003.

	Core eosinophilic infiltrate 2		
Core eosinophilic infiltrate 1	No/barely perceptible	No	Total
No/barely perceptible	6	1	7
No	0	13	13
Total	6	14	20

3.7.17 The number of mitoses within the cored region

The Spearman correlation coefficient for the number of mitoses, as a continuous variable, in set 1 and set 2 was 0.57 (p=0.01). There was substantial agreement for the number of mitoses within the core (Table 3.65).

Table 3.65: Cross-tabulation of the number of core mitoses for set 1 and set 2.

There was 75% (15/20) agreement. Kappa=0.63 (95% CI 0.35-0.91), p=0.00001.

	Number of mitoses within the cored region 2			
Number of mitoses within the cored region 1	0	1-2	≥3	Total
0	3	0	0	3
1-2	2	7	0	9
≥3	2	1	5	8
Total	7	8	5	20

3.7.18 The number of blood vessels within the cored region

The Spearman correlation coefficient for the number of blood vessels within the cored regions for set 1 and set 2 was 0.84 ($p=3x10^{-6}$). There was moderate agreement for the number of blood vessels within the core (Table 3.66).

Table 3.66: Cross-tabulation of the number of core blood vessels for set 1 and set 2.

There was 75% (15/20) agreement. Kappa=0.56 (95% CI 0.15-0.84), p=0.001.

	Number of blood vessels within the cored region 2			
Number of blood vessels within the cored region 1	0	1-2	≥3	Total
0	1	1	0	2
1-2	0	7	3	10
≥3	0	1	7	8
Total	1	9	10	20

3.7.19 Interpretation of inter- and intraobserver agreement for cored region measures

Interobserver agreement was weakest for the quality of the stroma and melanoma cell structure within the cored region. There was higher interobserver agreement for melanoma cell shape in the cored region than within the whole tumour using a light microscope. There was substantial interobserver agreement for melanoma cell pigmentation and the core immune cell infiltrates. These findings suggest that interobserver agreement could be improved by performing a focused assessment of such measures within smaller regions of the melanoma.

There was high intraobserver concordance for cored region measures overall, particularly for the presence or absence of lymphocytes or melanophages within the core. The grading of the extent of the core immune cell infiltrate was more variable and there was only slight agreement for the quality of the stroma, although the kappa statistic may be misleading due to the rarity of loose and mixed types of stroma.

There was a strong association for the percentage of stroma recorded for both observers and within the same observer. Table 3.67 provides a summary of the findings for inter- and intraobserver variation analyses of cored region measures.

Table 3.67 (on following page): Summary table of the results for inter- and intraobserver analyses of cored region measures.

The Spearman correlation coefficient (rho), percentage agreement, kappa statistic, 95% confidence intervals (95%CI), p-value and strength of agreement are shown for factors recorded using the virtual pathology protocol. The extent of the plasma cell infiltrate and melanophages within the cored region were not available for intraobserver variation analysis because the cores that were assessed did not contain either of these cells. NA = not applicable. NC = not calculable.

Cored region measures										
	Interobserver agreement (virtual pathology)					Intraobserver agreement (virtual pathology)				
Factor	**Spearman rho**	**% Agreement**	**Kappa (95%CI)**	**p-value**	**Strength of agreement**	**Spearman rho**	**% Agreement**	**Kappa (95%CI)**	**p-value**	**Strength of agreement**
Percentage of stroma	0.7			0.0001		0.9			$6x10^{-8}$	
Quality of the stroma		60	0.21 (-0.11-0.49)	0.03	Fair		70	0.05 (-0.11-0.36)	0.4	Slight
Melanoma cell shape		73	0.49 (0.24-0.77)	$8x10^{-8}$	Moderate		80	0.69 (0.42-0.92)	$6x10^{-6}$	Substantial
Melanoma cell structure		40	0.08 (-0.11-0.32)	0.3	Slight		75	0.58 (0.28-0.9)	0.0001	Moderate
Melanoma cell pigmentation		93	0.82 (0.52-1.0)	$9x10^{-10}$	Almost perfect		85	0.82 (0.57-1.0)	$7x10^{-9}$	Almost perfect
Presence or absence of core immune cell infiltrate		83	0.57 (0.26-0.88)	0.0003	Moderate		85	0.35 (-0.17-0.86)	0.02	Fair
Extent of core immune cell infiltrate		70	0.59 (0.37-0.78)	$4x10^{-9}$	Moderate		65	0.53 (0.25-0.78)	$6x10^{-6}$	Moderate
Location of core immune cell infiltrate		77	0.62 (0.42-0.83)	$1x10^{-8}$	Substantial		70	0.59 (0.35-0.85)	$1x10^{-6}$	Moderate
Presence or absence of core lymphocytic infiltrate		90	0.80 (NC)	$2x10^{-6}$	Substantial		95	0.92 (0.78-1.0)	$3x10^{-9}$	Almost perfect
Extent of core lymphocytic infiltrate		87	0.76 (0.53-0.94)	$3x10^{-8}$	Substantial		85	0.79 (0.61-1.0)	$5x10^{-10}$	Substantial
Presence or absence of core plasma cell infiltrate		90	0.82 (0.61-1.0)	$1x10^{-8}$	Almost perfect		95	0.89 (0.67-1.0)	0.00003	Almost perfect
Extent of core plasma cell infiltrate		90	0.82 (0.61-1.0)	$1x10^{-8}$	Almost perfect		NA	NA	NA	NA

Cored region measures										
	Interobserver agreement (virtual pathology)					Intraobserver agreement (virtual pathology)				
Factor	**Spearman rho**	**% Agreement**	**Kappa (95%CI)**	**p-value**	**Strength of agreement**	**Spearman rho**	**% Agreement**	**Kappa (95%CI)**	**p-value**	**Strength of agreement**
Presence or absence of core macrophage/melanophage infiltrate		90	0.83 (0.61-1.0)	$1x10^{-10}$	Almost perfect		95	0.91 (0.69-1.0)	$1x10^{-7}$	Almost perfect
Extent of core macrophage/melanophage infiltrate		87	0.78 (0.6-0.95)	$4x10^{-11}$	Substantial		65	0.54 (0.32-0.86)	9x10-7	Moderate
Presence or absence of core neutrophilic infiltrate		93	0.87 (0.67-1.0)	$6x10^{-8}$	Almost perfect		95	0.90 (0.67-1.0)	$2x10^{-6}$	Almost perfect
Extent of core neutrophilic infiltrate		93	0.87 (0.67-1.0)	$6x10^{-8}$	Almost perfect		90	0.80 (0.57-1.0)	0.00001	Substantial
Presence or absence of core eosinophilic infiltrate		87	0.74 (0.51-0.93)	$3x10^{-6}$	Substantial		95	0.89 (0.67-1.0)	0.00003	Almost perfect
Extent of core eosinophilic infiltrate		87	0.74 (0.51-0.93)	$3x10^{-6}$	Substantial		NA	NA	NA	NA
Core mitoses (tertiles)		87	0.80 (0.57-0.95)	$2x10^{-10}$	Substantial		75	0.63 (0.35-0.91)	0.00001	Substantial
Core blood vessels		60	0.40 (0.14-0.66)	0.001	Fair		75	0.56 (0.15-0.84)	0.001	Moderate

3.8 Summary

- Breslow thickness, microscopic ulceration, the POS, melanoma cell pigmentation, the presence or absence of a core lymphocytic infiltrate and its extent and the number of core mitoses (categorised as tertiles) were factors for which reproducibility was highest.
- Growth phase, Clark's level, the presence or absence of a dominant nodule, regression, microsatellites, vascular and perineural invasion, the quality of the stroma, melanoma cell structure and the number of blood vessels were poorly reproduced.
- Interobserver agreement improved for the grading of TILs when a modified version of Clemente *et al*.'s [61] protocol was utilised.
- Tumour loss was variably reported between observers, however, it was highly reproducible within the same observer.
- The presence of a plasma cell, neutrophilic or eosinophilic infiltrate within the core was seldom recorded.

3.9 Discussion

Consistency in the histopathological assessment of melanoma is crucial for the estimation of prognosis. Interobserver agreement was highest for Breslow thickness and microscopic ulceration, irrespective of the protocol used. Initial histopathology training with a light microscope highlighted several discrepancies, which are likely to reflect the training nature of the cases analysed and the complexity of melanoma pathology. Reassessment of measures was performed to seek factors that would have the best reproducibility. Several factors were dropped prior to commencing the histopathological review using virtual pathology. These included measures for which the weakest interobserver agreement was observed, i.e. microsatellites and perineural invasion. Interobserver agreement was also slight for regression, TILs, melanoma cell shape and pigmentation. These measures were modified and retained for assessment using the virtual pathology protocol because they were of particular interest.

The first study of interobserver variation using a light microscope was complicated by a number of factors. Firstly, it is likely that the consultant pathologist had reviewed clinical sections, whilst I had used research sections in the majority of cases. Consequently, additional sections that had been stained for immunohistochemistry were not included in my analysis. Some of the differences seen could be accounted for by the use of

different sections. Patrick *et al.* found a mean increase of 0.12mm for Breslow thickness in half of cases, comparing serial sections of thin melanomas [210]. In addition, it was my first time reviewing melanoma pathology slides independently, in tandem with the gradual accumulation of knowledge, having had limited clinical exposure to histopathology. For this protocol, training was provided by a different consultant pathologist (Dr Merchant, Pathologist B) to the one who acted as the observer (Pathologist A). Potential differences in the approach of each pathologist might have contributed further to variability. The protocol which I used had been developed by Prof. Cook, however, the approach to the parameters within the protocol were interpreted by the training consultant pathologist and I. Our approach might have differed from what had been intended by Prof. Cook and Pathologist A.

Studies of interobserver variation in the reporting of melanoma pathology have been recorded in different contexts in the literature. Some describe retrospective studies, where the second observer was privy to the report of the first and the reporting pathologists had different levels of specialisation [199, 203]. This unblinding could have resulted in more favourable reproducibility scores.

The subsequent interobserver variation analysis for whole tumour measures was based on a different protocol, using different technology and was recorded for different observers (Dr Merchant and I, as opposed to Pathologist A and I). Interobserver studies using this virtual pathology protocol showed a high degree of concordance. This might reflect the fact that the training dermatopathologist was the second observer for this analysis. Additionally, some of the measures were relatively novel and had been developed in collaboration with the training pathologist. Furthermore, it was possible to record images of annotated measurements using virtual pathology, which might have increased reproducibility for these factors. Better interobserver agreement was observed for TILs using the virtual pathology protocol, in which a modified version of the approach by Clemente *et al.* was employed (discussed in more detail in Chapter 2) [61]. However, agreement was still moderate, highlighting the subjective nature of the measure. The results of the initial interobserver analysis (using Prof. Cook's protocol) had indicated difficulties in recognising regression. Therefore, the regression variable was re-defined as tumour loss and the extent of melanophages within the tumour was also recorded separately (discussed in more detail in Chapter 2). There was substantial to almost perfect interobserver agreement for the intensity and pattern of melanophages, respectively, which suggests that these cells were easily recognised, perhaps due to the presence of pigment. However, there was only a modest improvement in concordance for the presence of tumour loss using the new approach, which might reflect the subjective nature of this measure. Intraobserver agreement for

the whole-tumour measures was moderate to substantial for most factors, being highest for Breslow thickness and microscopic ulceration. There was moderate to substantial agreement for the presence of tumour loss and the intensity and pattern of melanophages within the whole tumour. Limitations of the virtual pathology study include the relatively small number of cases available for comparison for interobserver variation analysis and intraobserver concordance was not examined in the second observer (Pathologist B).

The use of virtual pathology enabled me to develop new measures and to focus on a precise region of tumour. By digitally extracting the cored region, it was possible to be certain that both observers assessed the exact same part of the tumour. The cored region measures, including the percentage of stroma, were highly reproducible. The poorest interobserver agreement was recorded for melanoma cell structure, the quality of the stroma and for the number of blood vessels within the cored region, indicating that these measures could be more subjective. Broekart *et al.* previously reported moderate interobserver agreement for nesting, which was one element recorded in the melanoma cell structure variable (kappa ~0.4) [155]. Interobserver agreement was only slight in this regard, however, intraobserver agreement was better. This might imply that although there were some differences in its interpretation, my data were recorded consistently. It was not surprising that there was limited reproducibility for the number of blood vessels within the core, as it was difficult to define the boundary, where one blood vessel began and ended, relative to its tributaries. Artefactual haemorrhage could also have led to discrepancies in the enumeration of blood vessels, as the definition I used to record their presence was of red cells within a lumen.

Overall, there was moderate to almost perfect intraobserver agreement using the virtual pathology protocol, suggesting that consistent entries were made during the period of data recording. The poorest agreement was for the quality of the stroma, however, compact stroma predominated which limited the number of cases available for comparison with other types of stroma. Intraobserver agreement was fair for the presence of a core immune cell infiltrate but was higher for other core immune cell variables. Lymphocytes and melanophages predominated within the cored regions, indicating that these immune cells could underlie some of the biological variation in melanoma.

The factors that were most consistently reproduced were Breslow thickness and microscopic ulceration. These histopathological features have been incorporated into AJCC stage and are therefore used to predict outcome from cutaneous melanoma [43]. Their high degree of reproducibility is likely to contribute to their prognostic power in large data sets, such as those used to determine stage. Microsatellites also contribute

to AJCC stage [43] but interobserver agreement was poor for this factor using the Prof. Cook protocol, which might reflect the training nature of the data set. The apparent rarity of the occurrence of microsatellites within the data set limits the conclusions that could be drawn, however, it appeared that this measure was subjective, despite its definition. The results for the percentage of stroma, measured using RandomSpot© [185], were concordant within and between observers. This highlights a novel factor that could be incorporated into the histopathological assessment of primary melanomas, were it to be of diagnostic or prognostic significance. The application of the software being limited by the need for digitised pathology images, which could restrict its clinical use.

In the future, if I were designing a study to examine interobserver variation among pathologists, I would include 3 or more observers and a larger number of cases. A variable for which a high level of concordance was achieved between the three observers, would be considered highly reproducible. For measures where results were more variable, a process of discussion and review would be needed in order to reach a consensus about the approach, similar to that reported by Carney *et al.* [207]. If reproducibility continued to be low, the measure would be regarded as subjective and unlikely to be reproducible. During my PhD, interobserver variation was studied between different observers, using different protocols, therefore, it was not possible to achieve consensus between 3 or more observers but it may be feasible to evaluate in the future.

In summary, measures that would have been predicted to be highly reproducible, such as Breslow thickness and ulceration were consistently reported. The recording of other factors, used in the histopathological reporting of melanoma pathology, was more variable. Highly reproducible results were achieved using a newly developed, virtual pathology protocol. A unique data set was made available to me at the beginning of my PhD, which I hope to have further enriched through this research. Several novel measures were developed, the potential prognostic implications of which will be explored in Chapter 4**.**

Chapter 4 Melanoma-specific relapse and survival

4.1 Introduction

A detailed overview of the factors known to be associated with melanoma prognosis is provided in Chapter 1. Briefly, clinical, histopathological and molecular profiles have been reported to play a role. Adverse clinical factors include advancing age [6, 7] and male sex [16, 19, 211]. The AJCC staging system (7th edition) incorporates several histopathological measures, which have been established to be predictors of outcome in melanoma, e.g. Breslow thickness, microscopic ulceration and, for stage IB melanomas, mitotic count/mm^2 [43]. The AJCC 8th edition will be effective from 1st January 2017 but in my thesis, I will refer only to the 7th edition, which I used in my research.

The width of ulceration has also been reported to be an important prognostic factor. Day *et al.* proposed that an ulceration width >3mm was hazardous [55]. Grande Sarpa *et al.* calculated the ulceration width as a percentage of the maximum diameter and noted that the presence of >2% and >5% ulceration was associated with an increased risk of sentinel lymph node positivity and melanoma-specific death, respectively [54]. Another study showed that an ulceration width >5mm or a percentage ulceration >70% was associated with a significantly increased risk of melanoma-specific death [53].

Although the biological basis of ulceration has not been fully elucidated, it has been reported to be an established predictor of a better response to interferon therapy [167], suggesting that understanding the biological determinants of ulceration is important. Activation of pro-inflammatory cytokines and biological pathways associated with wound healing have been identified in ulcerated primary melanomas [49], suggesting that these tumours harbour a pro-tumourigenic, inflammatory milieu. Consistent with this hypothesis, ulcerated melanomas display increased microvessel density, lymphovascular invasion and macrophage infiltration [50]. Therefore, I was interested to quantify the extent of microscopic ulceration, to assess whether or not this might prove to be an independent predictor of outcome in participants recruited to the Leeds Melanoma Cohort Study.

As discussed in Chapter 1, there are conflicting results regarding the significance of other histopathological measures, e.g. tumour-infiltrating lymphocytes (TILs) [24, 27, 60-62, 64, 65, 67, 212] and regression [72, 74, 80, 81, 213-215]. Several studies have reported TILs to be an independent predictor of outcome in melanoma, with brisk TILs

having the best prognosis [27, 60-63]. However, in others, TILs have no independent prognostic value [25, 64-67]. This could reflect the subjective nature of the classification of TILs or variation in the cohorts studied (consisting of melanomas with different thicknesses). In view of these findings and the revolutionary advances in immunotherapy for the treatment of melanoma [216], I was interested to classify TILs using a protocol adapted from Clemente *et al.* [61], which was developed to better capture the variation in the distribution of TILs within primary melanomas.

The prognostic significance of regression is more controversial. It has been reported to occur more frequently in patients with adverse clinical characteristics, e.g. older age and male sex [74] but more favourable histopathological features, e.g. a lower mitotic count and absence of ulceration [75]. Some studies have established a protective role for regression in primary melanoma [74, 76, 79]. However, Rubenstein *et al.* reported an association with false-negative sentinel node biopsies and hypothesised that a similar mechanism could have led to regression in the lymph node [71]. Other studies have demonstrated a worse outcome, with an increased risk of metastasis, particularly among thin melanomas [82-84, 86]. This suggests the possibility that the true Breslow depth could have been underestimated, due to the erosion of the invasive edge of the tumour. Regression of 50% or more of the melanoma has been reported to increase the risk of death [78].

Regression has been postulated to result from host-mediated, immunologic tumour destruction [71], however, Bastian *et al.* cited telomere “crisis” as a putative mechanism [73]. Telomeres are repetitive nucleotide sequences at the ends of chromosomes, which are designed to maintain their integrity and to prevent inadvertent fusion with other chromosomes [217]. Telomeres shorten with successive cell divisions and on exposure to carcinogens and are known to decrease with age [217]. It is this shortening that determines the number of divisions that a cell will undergo in its lifetime [73]. Mutations can lead to telomere dysfunction, which permits cancer cells to continue to divide unchecked, exposing the DNA and increasing the chances of fusion with other chromosomes [73]. A critical point is reached, known as “crisis”, which is induced by these chromosomal abnormalities and this initiates cell death (“apoptosis”) [73]. This process might trigger some of the cancer cells to activate telomerase and to become immortal and can be viewed as an evolutionary process [73], suggesting that regions of tumour cell death may be associated with the concomitant generation of clonal populations which would be linked to a worse prognosis. The alternative hypothesis, therefore, is that regression in some tumours might reflect tumour cell death related to intrinsic events within the tumour rather than an immune event, and that this process might result in the selection of more aggressive cancer cells.

Due to the lack of clarity about the prognostic role of regression in melanoma, I elected to record a detailed assessment of factors that are considered to represent regression, namely, a region of tumour that has vanished ("tumour loss"). I was also interested to measure its depth and location with respect to the tumour, in light of the fact that ≥50% regression had previously been shown to predict an increased risk of death [78]. Furthermore, I calculated the "relative tumour loss" by dividing the depth of tumour loss by the Breslow thickness, to assess whether this might more accurately reflect the degree of tumour loss and whether or not it might be a better predictor of outcome. Moreover, I graded the intensity and pattern of macrophages/melanophages (TIMs), which could be seen in association with regression [73] and because of their possible association with a particularly aggressive tumour biology, e.g. microscopic ulceration [49].

The AJCC staging system is a powerful tool in predicting melanoma prognosis, yet, it is estimated that unexplained variation in the predicted survival of up to 32% remains [151]. Moreover, there are several features of primary cutaneous melanomas, which have long been described by pathologists but are of undetermined significance, e.g. melanoma cell pigmentation. Viros *et al.* performed a detailed morphological analysis of 302 primary cutaneous melanomas and found that *BRAF*-mutated melanomas tended to have rounder, larger and more heavily pigmented melanoma cells [108], thereby implying genomic variation is impacting on pigmentation. Melanoma cell pigmentation can also be viewed as a marker of differentiation [111], with amelanotic melanomas likely to represent a less differentiated state. An inverse relationship between pigmentation and cell elasticity has been demonstrated in melanoma cells and this appears to inhibit their capacity to migrate *in vitro* [114]. However, some studies have suggested a potentially hazardous role for pigmentation [111, 115].

Furthermore, two distinct patterns of cancer cell migration have been reported, based upon *in vitro* and murine models, a faster, rounded, "amoeboid" type and an elongated, "mesenchymal" type [105]. There is some evidence that these patterns of cell movement might correspond with morphological characteristics in formalin-fixed, paraffin-embedded (FFPE) sections of primary cutaneous melanoma [107] and I decided, therefore, to assess the association between melanoma cell shape and melanoma-specific survival. The virtual pathology protocol, which I developed under the supervision of Prof. Newton-Bishop and Drs Will Merchant and Darren Treanor, incorporated some of these descriptors of uncertain significance.

Apart from histopathological factors, molecular profiles can help to delineate subgroups that are distinct in terms of survival [149-151]. To date, many of these profiles have been generated predominantly using metastatic melanoma samples, due to the limited

availability of cryopreserved primary melanoma tissue [149, 153]. The Leeds group has succeeded in amassing H&E-stained, archival sections from primary melanoma tumours with matched transcriptomic data for 703 cases, over several years. The transcriptomic data were generated from RNA extracted from a 0.6mm diameter core taken horizontally through the deepest part of the tumour and were generated using the Illumina® DASL assay, designed to produce high quality data from formalin-fixed (degraded) RNA. Using primary melanomas, the group has replicated the molecular profiles reported by Harbst *et al.* [150, 151], named by them as pigmentation, proliferative, high-immune and normal-like. More recently, the Leeds group has utilised a bioinformatics approach, developed by the group of Jerome Galon and known as the "immunome" [174] to study the role of immune cell subsets within primary melanoma tumours, at a gene expression level. The Galon group derived lists of genes that data had suggested are exclusively expressed by specific immune cell subsets and then used the expression of those genes to infer the presence of 28 immune cell subsets in tumour tissue [174]. Galon's group worked predominantly on colon cancer.

The basis of the statistical analysis reported herein refers to 798 cases from the Leeds Melanoma Cohort Study for which I recorded a detailed histopathological review of the primary, using a virtual pathology protocol. A detailed assessment was recorded for the whole tumour and the cored regions. The latter could be identified in 702 cases (the remaining cases lacking black markings on the glass slides, which corresponded to regions of the block that had been sampled using a tissue microarray (TMA) biopsy needle). Transcriptomic data were available for 703 cases but only 676 of these had been studied using the virtual pathology protocol (H&E sections were unavailable for assessment in the remainder). Therefore, of the 798 cases assessed using the virtual pathology protocol, 676 had gene expression data, including 596 cases with data for both gene expression and cored region measures.

The aims that this chapter will address are as follows:

- To summarise the clinical and histopathological characteristics of the 798 cases that were reviewed using the virtual pathology protocol
- To assess which clinical and histopathological factors (scored within the whole tumour and cored regions) were statistically significant predictors of melanoma relapse and melanoma-specific survival in univariable and multivariable analyses, using Cox proportional hazards models

4.2 Methods

Relapse and survival (based on melanoma-specific death) times were censored at 10 years. Cox proportional hazards models were used to generate hazard ratios (HR), 95% confidence intervals (95% CI) and p-values for the likelihood of melanoma relapse or melanoma-specific death. Univariable and multivariable analyses were performed for clinical factors, including age at diagnosis and sex; and histopathological factors in the whole tumour and within the cored regions. Tests for trend were performed for ordered categorical variables where there appeared to be increasing hazard ratios when testing with individual categories. Kaplan-Meier curves were used to graphically represent the time to melanoma relapse or melanoma-specific death.

The AJCC stage variable was generated using a mixture of clinical and histopathological data for the whole tumour and cored region measures as follows: Breslow thickness and microscopic ulceration (whole tumour) and the presence or absence of mitoses in core 1. Although more than one cored region was examined for 423 cases, the first core was used for this analysis, to increase the statistical power (as all cases for which cored region measures were available had a least one core) and because comparisons of measures between the first and second cores showed similar results (Appendix D).

Data on microsatellite status, micro- and macrometastases and metastatic disease had previously been recorded for each case by Section staff from the histology reports and clinical notes. These data were incorporated into the stage variable. In 8 patients, where stage could not be computed due to missing Breslow thickness and/or mitoses, the stage recorded from the histology reports and clinical notes was used instead.

Relapse and survival data were generated by departmental staff by extraction from the clinical notes, contact with the patient annually, data requests to the GP and cancer registry data.

For relapse and survival analyses, the round/ovoid melanoma cell shape category was merged with the epithelioid cell shape category because the results of intraobserver studies showed that the distinction between these subtypes was poorly reproducible (Chapter 3).

4.3 Results

4.3.1 Descriptive statistics and univariable analysis

Descriptive statistics, unadjusted HRs, 95% CI and p-values are reported for clinical factors in Table 4.1, for whole tumour measures in Table 4.2 and for cored region measures in Table 4.3.

4.3.1.1 Clinical factors

Table 4.1 shows unadjusted HRs for melanoma relapse and melanoma-specific death and the corresponding 95% CI and p-values for clinical factors. The mean age at diagnosis was 56 years; 54% (430/798) cases were female. The most common site of primary melanoma was the limbs (44%, 349/798). Approximately 86% (683/798) cases had AJCC stage I or II disease.

The median relapse survival time was 4.8 years (range 0-10 years; censored at 10 years) and the median melanoma-specific survival time was 5.8 years (range 0.5-10 years; censored at 10 years) (data not shown). In univariable analysis, an older age at diagnosis was a poor prognostic factor, contributing to a 2% increased risk of relapse (HR 1.02, 95% CI 1.01-1.03, Cox proportional hazards model, p=0.00001) and a 3% increased risk of death from melanoma (HR 1.03, 95% CI 1.02-1.04, Cox proportional hazards model, $p=3x10^{-7}$) for every year older.

Table 4.1 (on following page): Unadjusted hazard ratios for relapse and melanoma-specific death for clinical factors.

The unadjusted hazard ratios (HR), 95% confidence intervals (95% CI) and p-values were estimated from Cox proportional hazards models. The second column refers to descriptive statistics for the factor in the first column. N = number of cases. S.D. = standard deviation. 'N' in 3rd and 7th columns refers to the number of cases in the statistical model(s). "Other" refers to sun-protected sites, including acral, subungual, genital, anal, and ear, nose and throat (ENT). The test for trend was performed for AJCC stage [43] because this was an ordered variable and there was an increasing trend in the hazard ratios for individual AJCC stage categories. Events refers to the number of cases that had either relapsed or died due to melanoma. Exact p-values are provided where possible. STATA (the statistical package) could not provide exact p-values for some variables because they were so significant (e.g. AJCC stage III/IV) and the estimated p-values are provided instead. The reference category (baseline) is the first category listed for each of the categorical variables.

		Melanoma relapse (N=797, 253 events)				Melanoma-specific death (N=798, 207 events)			
Factor	**Mean (S.D.) or Median (range) or N (%)**	**N**	**HR**	**95% CI**	**p-value**	**N**	**HR**	**95% CI**	**p-value**
Age at diagnosis (years)	56.3 (12.8)	797	1.02	1.01-1.03	0.00001	798	1.03	1.02-1.04	$3x10^{-7}$
Sex		797				798			
Male	368 (46.1)		1.0				1.0		
Female	430 (53.9)		0.7	0.5-0.9	0.003		0.7	0.5-0.9	0.007
Site of primary melanoma		797				798			
Limbs	349 (43.7)		1.0				1.0		
Trunk	269 (33.7)		1.4	1.1-1.9	0.02		1.7	1.2-2.4	0.001
Head	88 (11.0)		1.4	0.9-2.1	0.1		1.2	0.7-2.0	0.5
Other	92 (11.6)		2.3	1.6-3.3	$6x10^{-6}$		2.9	2.0-4.3	$9x10^{-8}$
AJCC stage		796				797			
I	339 (42.5)		1.0				1.0		
II	344 (43.1)		2.8	2.1-3.8	$6x10^{-11}$		2.6	1.8-3.6	$7x10^{-8}$
III/IV	114 (14.3)		4.8	3.4-6.9	$<1x10^{-16}$		5.6	3.8-8.3	$<1x10^{-16}$
Missing	1 (0.1)								
Test for trend			2.2	1.8-2.6	$<1x10^{-16}$		2.4	1.9-2.9	$<1x10^{-16}$

Female sex was significantly protective for both melanoma relapse and death (HR for relapse 0.7, 95% CI 0.5-0.9, Cox proportional hazards model, p=0.003 and HR for melanoma-specific death 0.7, 95% CI 0.5-0.9, Cox proportional hazards model, p=0.007). Cases whose melanomas were located on the trunk or "other" sites (sun-protected sites, including acral, subungual, genital, anal, and ear, nose and throat (ENT)) had a significantly increased risk of relapse (HR for "other" site 2.3, 95% CI 1.6-3.3, Cox proportional hazards model, $p=6x10^{-6}$) and melanoma-specific death (HR for "other" site 2.9, 95% CI 2.0-4.3, Cox proportional hazards model, $p=9x10^{-8}$) compared to the limbs. AJCC stage was significantly predictive of a poorer outcome. There was a significant trend in the HRs for advancing AJCC stage, both for melanoma relapse and death.

4.3.1.2 Whole-tumour measures

Data for whole-tumour measures are presented in Table 4.2.

Table 4.2 (on following page): Unadjusted hazard ratios for melanoma relapse and melanoma-specific death for whole-tumour measures

Unadjusted hazard ratios (HR), 95% confidence intervals (95% CI) and p-values were estimated from Cox proportional hazards models. The second column refers to descriptive statistics for the factor. N=number of cases. S.D.=standard deviation. 'N' in 3rd and 7th columns refers to the number of cases in the statistical model. Events refers to the number of cases that either relapsed or died due to melanoma. * AJCC cut-off points [43] were used to define Breslow thickness categories. ** For one patient, tumour loss was present but the type of tumour loss could not be assessed. Exact p-values are provided where possible. STATA could not provide exact p-values for some variables because they were so significant and the estimated p-values are provided instead (e.g. the test for trend for Breslow thickness). The reference category (baseline) is the first category listed for each of the categorical variables.

		Melanoma relapse (N=797, 253 events)				Melanoma-specific death (N= 798, 207 events)			
Factor	**Mean (S.D.) or Median (range) or N (%)**	**N**	**HR**	**95%CI**	**p-value**	**N**	**HR**	**95% CI**	**p-value**
*Breslow thickness (mm)**	2 (0.5-19.5)	788				789			
≤1.00	83 (10.4)		1.0				1.0		
1.01-2.00	312 (39.1)		2.3	1.2-4.7	0.02		2.2	1.04-4.6	0.04
2.01-4.00	272 (34.1)		4.3	2.2-8.5	0.00003		3.9	1.9-8.2	0.0002
>4.00	122 (15.3)		9.6	4.8-19.1	$2x10^{-10}$		7.6	3.7-16.0	$7x10^{-8}$
Missing	9 (1.1)								
Test for trend			2.0	1.8-2.4	$<1x10^{-16}$		1.9	1.6-2.2	$3x10^{-15}$
Dominant nodule		797				798			
No	721 (90.4)		1.0				1.0		
Yes	77 (9.6)		2.6	1.9-3.7	$3x10^{-9}$		2.1	1.5-3.0	0.00007
Microscopic ulceration		797				798			
No	621 (77.8)		1.0				1.0		
Yes	177 (22.2)		2.6	2.0-3.3	$6X10^{-13}$		2.3	1.7-3.1	$9x10^{-9}$
Extent of microscopic ulceration (mm)	2.5 (0.1-17.4)	795				796			
None	621 (77.8)		1.0				1.0		
<0.87	43 (5.4)		2.4	1.5-3.8	0.0002		2.1	1.2-3.5	0.006
0.87-<2.4	44 (5.5)		2.0	1.2-3.2	0.004		1.5	0.9-2.7	0.1
2.4-<5.15	44 (5.5)		2.8	1.8-4.3	$4x10^{-6}$		2.8	1.8-4.5	0.00002
≥5.15	44 (5.5)		3.2	2.1-4.9	$3x10^{-8}$		3.0	1.9-4.7	$4x10^{-6}$
Missing	2 (0.3)								
Test for trend			1.4	1.3-1.5	$5x10^{-13}$		1.3	1.2-1.5	$2x10^{-9}$

		Melanoma relapse (N=797, 253 events)				Melanoma-specific death (N= 798, 207 events)			
Factor	**Mean (S.D.) or Median (range) or N (%)**	**N**	**HR**	**95%CI**	**p-value**	**N**	**HR**	**95% CI**	**p-value**
Tumour-infiltrating lymphocytes		706				706			
Absent	52 (6.5)		1.0				1.0		
Non-brisk	581 (72.8)		0.6	0.4-1.02	0.06		0.7	0.4-1.1	0.09
Brisk	73 (9.2)		0.7	0.4-1.3	0.3		0.5	0.2-1.01	0.05
Missing	92 (11.5)								
Test for trend			0.9	0.6-1.2	0.4		0.7	0.5-1.0	0.05
Tumour loss		793				793			
No	649 (81.3)		1.0				1.0		
Yes	144 (18.1)		1.5	1.1-2.0	0.007		1.5	1.1-2.1	0.008
Missing	5 (0.6)								
*Type of tumour loss ***		792				792			
None	649 (81.3)		1.0				1.0		
Deep	72 (9.0)		1.1	0.7-1.8	0.6		1.2	0.7-1.9	0.5
Both	22 (2.8)		3.0	1.7-5.2	0.0002		2.3	1.2-4.4	0.01
Superficial	49 (6.1)		1.5	0.97-2.4	0.07		1.8	1.1-2.9	0.02
Missing	6 (0.8)								
Depth of tumour loss (mm)	1.1 (0.2-7.2)	793				793			
None	649 (81.3)		1.0				1.0		
<0.71	41 (5.2)		1.1	0.7-1.9	0.7		1.4	0.8-2.5	0.2
0.71-<1.14	36 (4.5)		0.9	0.5-1.8	0.8		0.9	0.4-1.8	0.7
1.14-<1.63	31 (3.9)		1.8	1.02-3.0	0.04		1.9	1.1-3.4	0.03

		Melanoma relapse (N=797, 253 events)				Melanoma-specific death (N= 798, 207 events)			
Factor	**Mean (S.D.) or Median (range) or N (%)**	**N**	**HR**	**95%CI**	**p-value**	**N**	**HR**	**95% CI**	**p-value**
≥1.63	36 (4.5)		2.6	1.7-4.2	0.00004		2.2	1.3-3.7	0.003
Missing	5 (0.6)								
Test for trend			1.2	1.1-1.4	0.00009		1.2	1.1-1.3	0.001
Relative tumour loss (mm)	0.5 (0.04-1.6)	786				786			
None	643 (80.6)		1.0				1.0		
<0.26	35 (4.4)		2.0	1.3-3.3	0.004		2.4	1.5-4.1	0.001
0.26-<0.52	36 (4.5)		2.0	1.3-3.3	0.003		2.0	1.2-3.4	0.01
0.52-<0.786	37 (4.6)		1.4	0.8-2.4	0.2		1.2	0.6-2.3	0.6
≥0.786	35 (4.4)		0.7	0.3-1.4	0.3		0.8	0.4-1.8	0.6
Missing	12 (1.5)								
Test for trend			1.1	0.96-1.2	0.3		1.1	0.9-1.2	0.3
Intensity of tumour-infiltrating macrophages/melanophages		789				790			
None	256 (32.1)		1.0				1.0		
Very few	286 (35.8)		0.9	0.7-1.2	0.4		0.9	0.7-1.3	0.7
Moderate	175 (21.9)		0.96	0.7-1.4	0.8		0.8	0.6-1.2	0.3
Lots	73 (9.2)		1.0	0.6-1.6	1.0		0.8	0.5-1.4	0.4
Missing	8 (1.0)								
Test for trend			1.0	0.9-1.1	0.9		0.9	0.8-1.1	0.2

		Melanoma relapse (N=797, 253 events)				Melanoma-specific death (N= 798, 207 events)			
Factor	**Mean (S.D.) or Median (range) or N (%)**	**N**	**HR**	**95%CI**	**p-value**	**N**	**HR**	**95% CI**	**p-value**
Pattern of tumour-infiltrating macrophages/melanophages		708				708			
Absent	140 (17.5)		1.0				1.0		
Non-brisk	560 (70.2)		0.8	0.6-1.2	0.3		0.9	0.6-1.3	0.7
Brisk	8 (1.0)		0.3	0.04-2.3	0.3		0.9	0.2-3.6	0.8
Missing	90 (11.3)								
Test for trend			0.8	0.6-1.1	0.2		0.9	0.7-1.3	0.6

Breslow thickness was available for 789 cases (Table 4.2). The median Breslow thickness was 2mm (range 0.5-19.5mm). Figure 4.1 shows a histogram of the frequency distribution of the Breslow thickness.

Microscopic ulceration was present in 22% (177/798) cases (Table 4.2). Figure 4.2 shows the frequency distribution for the extent (width) of ulceration.

Data on tumour loss (where this means a clear deficit within the silhouette of the melanoma at 4x magnification; being composed of a variable presence of lymphocytes, melanophages and/or fibrous tissue) were available for 793 cases. Tumour loss was present in 18% (144/798) of cases. Figure 4.3 shows the frequency distribution of the depth of tumour loss. Due to the skewed frequency distributions, the extent of ulceration and the depth of tumour loss were grouped into approximate quartiles for the time-to-event analyses. The reference categories were “no ulceration” and “no tumour loss”, respectively.

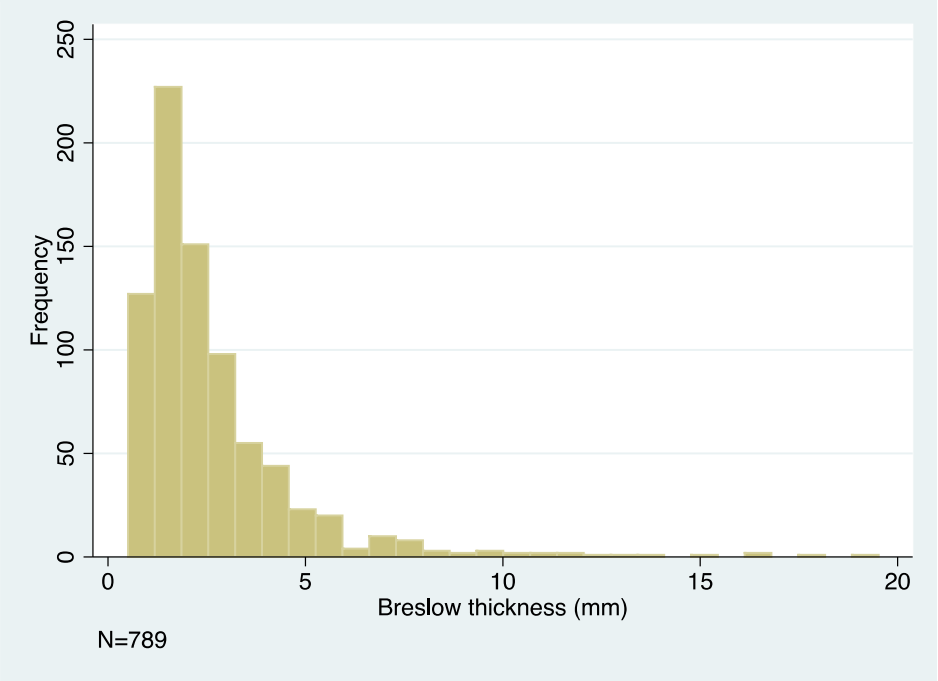

Figure 4.1: Histogram of the frequency distribution of the Breslow thickness

The histogram shows the frequency distribution in 789 cases reviewed using the virtual pathology protocol.

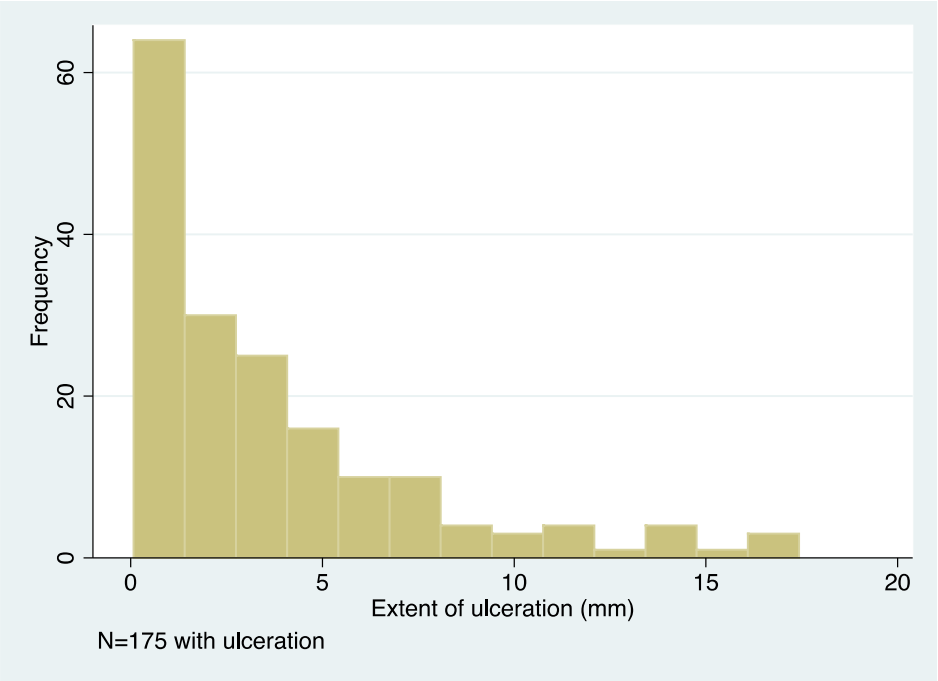

Figure 4.2: Histogram of the frequency distribution of the measurements of the extent of ulceration.

The median extent of ulceration was 2.5mm (range 0.1-17.4mm).

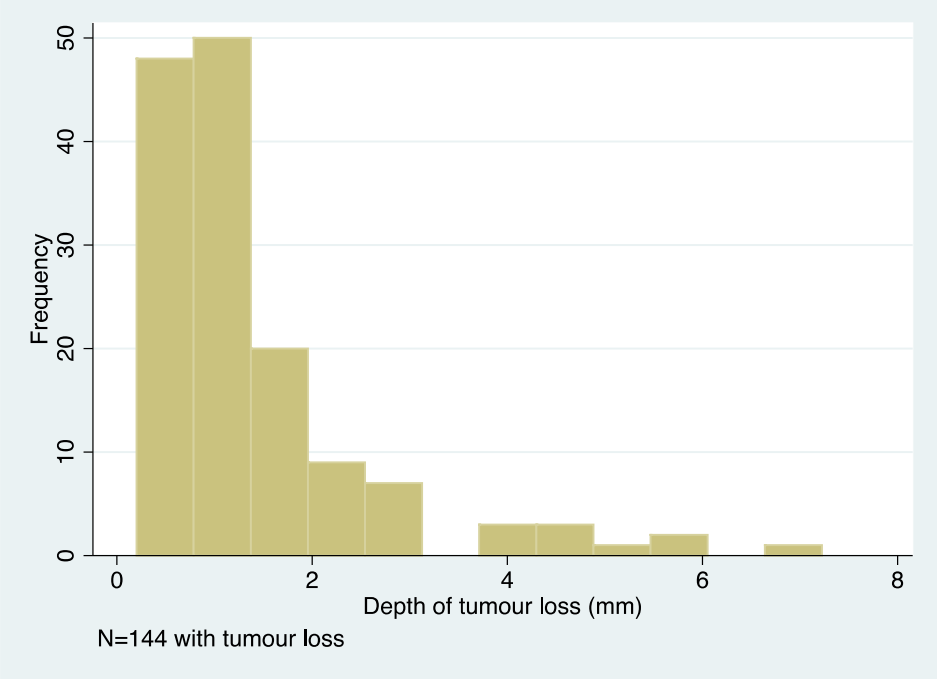

Figure 4.3: Histogram of the frequency distribution of the measurements of the depth of tumour loss.

The median depth of tumour loss was 1.1mm (range 0.2-7.2mm).

The results of the univariable analysis of all whole-tumour measures are summarised in Table 4.2. As expected, increasing Breslow thickness was associated with an increased risk of relapse and melanoma-specific death. Hazard ratios increased for each Breslow thickness cut-off point (derived from AJCC stage [43]) and tests for trend were highly significant (e.g. HR 1.9, 95% CI 1.6-2.2, Cox proportional hazards model, $p=3x10^{-15}$ for melanoma-specific death). The presence of a dominant nodule and the presence of microscopic ulceration were each significantly associated with a poor prognosis. The HRs for the presence of brisk or non-brisk tumour-infiltrating lymphocytes (TILs) were less than 1, suggesting a protective effect compared to absent TILs but the tests did not reach statistical significance. The presence of tumour loss was associated with a poor prognosis and this result was statistically significant, particularly if both deep and superficial types were present (referred to as “both” in Table 4.2). Increasing depth of tumour loss (measured in mm) was associated with an increased risk of melanoma relapse and death, especially when the thickness reached >1.63mm, compared to none. The corresponding tests for trend were highly statistically significant. Neither the intensity nor the pattern of tumour-infiltrating melanophages significantly influenced relapse or melanoma-specific death.

4.3.1.3 Cored region measures

Cored region variables were recorded on 702 cases for which black markings were still present on the histology slides (corresponding to the sites that had been cored using a TMA biopsy needle) prior to the slides being cleaned with ethanol and scanned, to create the virtual pathology repository of primary melanoma images. Table 4.3 summarises the frequency distribution of each cored region factor and the corresponding unadjusted HR, 95% CI and p-value for both melanoma relapse and death.

The median estimated percentage of stromal content was 32.7% (range 0-98.1%) (Table 4.3, page 151). Figure 4.4 shows the histogram of the frequency distribution of the percentage of stroma (POS).

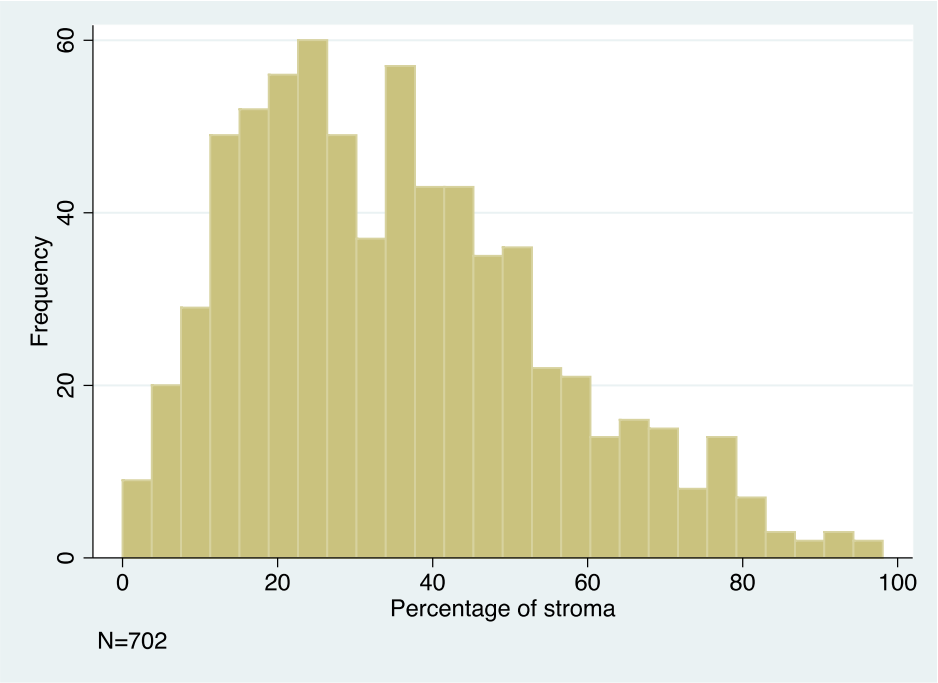

Figure 4.4: Histogram of the frequency distribution of the percentage of stroma

The median POS was 32.69%.

Table 4.3 (on following page): Unadjusted hazard ratios for melanoma relapse and melanoma-specific death for cored region measures

Unadjusted hazard ratios (HR), 95% confidence intervals (95% CI) and p-values were estimated from Cox proportional hazards models. The second column refers to descriptive statistics for the factor in the first column. N=number of cases. S.D.=standard deviation. 'N' in 3rd and 7th columns refers to the number of cases in the statistical model. Events refers to the number of cases that had either relapsed or died due to melanoma. No/barely perceptible* refers to the absence of a core immune cell infiltrate or its presence to a barely perceptible extent. These were grouped together as the reference category (baseline) for analyses of other core immune cell variables, e.g. lymphocytes. Yes* for the presence of a core immune cell infiltrate in this table means that the extent of the core immune cell infiltrate was either some, moderate or lots. Exact p-values are provided where possible. STATA could not provide exact p-values for some variables because they were so significant and the estimated p-values are provided instead (e.g. the test for trend for core mitoses). The reference category (baseline) is the first category listed for each of the categorical variables. Some of the hazard ratios, 95% CIs and/or p-values could not be calculated because there were no events for that category (e.g. plasmacytoid cell shape), i.e. none of these cases had relapsed or died due to melanoma. NC = not calculable.

		Melanoma relapse (N=701, 223 events)				Melanoma-specific death (N= 702, 181 events)			
Factor	**Mean (S.D.) or Median (range) or N (%)**	**N**	**HR**	**95% CI**	**p-value**	**N**	**HR**	**95% CI**	**p-value**
Percentage of stroma (continuous)	32.69 (0-98.08)	701	0.98	0.97-0.99	$8X10^{-9}$	702	0.97	0.97-0.98	$6x10^{-9}$
Percentage of stroma (quintiles)		701				702			
0-<17	136 (17.0)		1.0				1.0		
17-<27	147 (18.4)		0.7	0.5-0.97	0.03		0.8	0.6-1.2	0.4
27-<38	143 (17.9)		0.6	0.4-0.8	0.004		0.5	0.3-0.8	0.004
38-<52	144 (18.1)		0.4	0.2-0.6	$3x10^{-6}$		0.3	0.2-0.5	$4x10^{-6}$
≥52	132 (16.6)		0.3	0.2-0.4	$1x10^{-7}$		0.3	0.2-0.5	$7x10^{-6}$
Missing	96 (12.0)								
Test for trend			0.7	0.7-0.8	$4x10^{-10}$		0.7	0.6-0.8	$1x10^{-9}$
Percentage of stroma (15% cut-off)		701				702			
0-15	107 (13.4)		1.0				1.0		
>15	595 (74.6)		0.5	0.3-0.6	$9X10^{-7}$		0.5	0.4-0.7	0.00005
Missing	96 (12.0)								
Percentage of stroma (20% cut-off)		701				702			
0-20	172 (21.6)		1.0				1.0		
>20	530 (66.4)		0.5	0.4-0.6	$2x10^{-7}$		0.5	0.3-0.6	$1x10^{-6}$
Missing	96 (12.0)								
Percentage of stroma (30% cut-off)		701				702			
0-30	321 (40.2)		1.0				1.0		
>30	381 (47.7)		0.5	0.4-0.7	$1x10^{-6}$		0.5	0.3-0.6	$5x10^{-7}$
Missing	96 (12.0)								

		Melanoma relapse (N=701, 223 events)				Melanoma-specific death (N= 702, 181 events)			
Factor	**Mean (S.D.) or Median (range) or N (%)**	**N**	**HR**	**95% CI**	**p-value**	**N**	**HR**	**95% CI**	**p-value**
Percentage of stroma (40% cut-off)		701				702			
0-40	438 (54.9)		1.0				1.0		
>40	264 (33.1)		0.4	0.3-0.6	$2x10^{-7}$		0.4	0.3-0.6	$2x10^{-7}$
Missing	96 (12.0)								
Percentage of stroma (49% cut-off)		701				702			
0-49	536 (67.2)		1.0				1.0		
>49	166 (20.8)		0.5	0.3-0.7	0.00004		0.4	0.3-0.6	0.00009
Missing	96 (12.0)								
Percentage of stroma (median cut-off)		701				702			
0-<32.69	350 (43.9)		1.0				1.0		
≥32.69	352 (44.1)		0.5	0.3-0.6	$2x10^{-8}$		0.4	0.3-0.6	$2x10^{-8}$
Missing	96 (12.0)								
Quality of the stroma		651				651			
Compact	595 (74.6)		1.0				1.0		
Loose	22 (2.8)		0.8	0.4-1.6	0.5		0.8	0.3-1.8	0.6
Mixed	34 (4.2)		0.5	0.2-1.05	0.07		0.5	0.2-1.2	0.1
Missing	147 (18.4)								
Melanoma cell shape		699				700			
Round/ovoid/epithelioid	602 (75.4)		1.0				1.0		
Spindle	60 (7.5)		0.8	0.5-1.3	0.3		0.8	0.4-1.4	0.4
Super spindle	14 (1.8)		0.4	0.1-1.7	0.2		0.6	0.2-2.5	0.5

		Melanoma relapse (N=701, 223 events)				Melanoma-specific death (N= 702, 181 events)			
Factor	**Mean (S.D.) or Median (range) or N (%)**	**N**	**HR**	**95% CI**	**p-value**	**N**	**HR**	**95% CI**	**p-value**
Naevoid	16 (2.0)		0.9	0.4-2.1	0.8		1.3	0.6-2.9	0.6
Plasmacytoid	6 (0.8)		NC	NC	NC		NC	NC	NC
Balloon	2 (0.2)		5.7	1.4-23.2	0.01		2.0	0.3-14.3	0.5
Missing	98 (12.3)								
Melanoma cell structure		694				695			
Nests	413 (51.8)		1.0				1.0		
Sheets	134 (16.8)		1.7	1.2-2.3	0.001		1.8	1.3-2.6	0.001
Fascicles	127 (15.9)		1.2	0.8-1.7	0.3		1.2	0.8-1.8	0.3
Dispersed	21 (2.6)		1.9	0.98-3.6	0.06		2.0	0.9-4.0	0.07
Missing	103 (12.9)								
Melanoma cell pigmentation		699				700			
Absent	522 (65.4)		1.0				1.0		
Faint	45 (5.6)		0.99	0.6-1.7	1.0		0.9	0.5-1.7	0.8
Moderate	82 (10.3)		0.8	0.5-1.2	0.2		0.6	0.3-1.05	0.07
High	46 (5.8)		1.2	0.7-1.9	0.5		0.9	0.5-1.7	0.7
Very high	5 (0.6)		0.9	0.1-6.3	0.9		2.7	0.7-11.0	0.2
Missing	98 (12.3)								
Test for trend			0.98	0.9-1.1	0.8		0.9	0.8-1.1	0.3
Core immune cell infiltrate (categorised)		698				699			
Yes (immune cells, excluding barely perceptible)	400 (50.1)		1.0				1.0		

		Melanoma relapse (N=701, 223 events)				Melanoma-specific death (N= 702, 181 events)			
Factor	**Mean (S.D.) or Median (range) or N (%)**	**N**	**HR**	**95% CI**	**p-value**	**N**	**HR**	**95% CI**	**p-value**
No (immune cells)	33 (4.2)		2.0	1.2-3.4	0.01		2.4	1.3-4.3	0.004
Barely perceptible (immune cells)	266 (33.3)		1.8	1.4-2.4	0.00003		2.3	1.7-3.1	$2x10^{-7}$
Missing	99 (12.4)								
Extent of the core immune cell infiltrate		698				699			
*No/barely perceptible**	299 (37.5)		1.0				1.0		
Some (immune cells)	252 (31.6)		0.7	0.5-0.9	0.005		0.5	0.3-0.7	0.00002
Moderate (immune cells)	100 (12.5)		0.4	0.2-0.7	0.0002		0.4	0.2-0.6	0.0002
Lots (immune cells)	48 (6.0)		0.3	0.2-0.7	0.003		0.4	0.2-0.8	0.01
Missing	99 (12.4)								
Test for trend			0.7	0.6-0.8	$2x10^{-6}$		0.6	0.5-0.8	$2x10^{-6}$
Location of the core immune cell infiltrate		696				697			
*No/barely perceptible**	299 (37.5)		1.0				1.0		
At the tumour/stroma interface	126 (15.8)		0.6	0.4-0.9	0.005		0.5	0.3-0.7	0.001
Dispersed between tumour cells	150 (18.8)		0.6	0.4-0.8	0.003		0.4	0.3-0.7	0.0001
Both	122 (15.3)		0.5	0.3-0.7	0.001		0.4	0.3-0.7	0.0002
Missing	101 (12.6)								
Core lymphocytic infiltrate		697				698			
*No/barely perceptible**	299 (37.5)		1.0				1.0		
No (lymphocytes)	132 (16.5)		0.8	0.6-1.1	0.2		0.7	0.5-0.97	0.04
Yes (lymphocytes)	267 (33.5)		0.4	0.3-0.6	$5x10^{-7}$		0.3	0.2-0.5	$5x10^{-9}$
Missing	100 (12.5)								

		Melanoma relapse (N=701, 223 events)				Melanoma-specific death (N= 702, 181 events)			
Factor	**Mean (S.D.) or Median (range) or N (%)**	**N**	**HR**	**95% CI**	**p-value**	**N**	**HR**	**95% CI**	**p-value**
Test for trend			0.7	0.6-0.8	$5x10^{-7}$		0.6	0.5-0.7	$3x10^{-9}$
Extent of the core lymphocytic infiltrate		697				698			
*No/barely perceptible**	299 (37.5)		1.0				1.0		
No (lymphocytes)	132 (16.6)		0.8	0.6-1.1	0.2		0.7	0.5-0.97	0.04
Some (lymphocytes)	179 (22.4)		0.5	0.4-0.8	0.0004		0.4	0.3-0.6	$6x10^{-6}$
Moderate (lymphocytes)	47 (5.9)		0.3	0.1-0.7	0.002		0.2	0.05-0.5	0.001
Lots (lymphocytes)	41 (5.1)		0.2	0.1-0.6	0.002		0.3	0.1-0.7	0.006
Missing	100 (12.5)								
Test for trend			0.7	0.6-0.8	$1x10^{-7}$		0.6	0.5-0.7	$8x10^{-9}$
Core plasma cell infiltrate		696				697			
*No/barely perceptible**	299 (37.5)		1.0				1.0		
No (plasma cells)	384 (48.1)		0.6	0.4-0.7	0.00001		0.4	0.3-0.6	$5x10^{-8}$
Yes (plasma cells)	14 (1.8)		0.4	0.1-1.4	0.2		0.6	0.2-1.8	0.3
Missing	101 (12.6)								
Test for trend			0.6	0.4-0.7	0.00001		0.5	0.3-0.6	$2x10^{-7}$
Extent of the core plasma cell infiltrate		696				697			
*No/barely perceptible**	299 (37.5)		1.0				1.0		
No (plasma cells)	384 (48.1)		0.6	0.4-0.7	0.00001		0.4	0.3-0.6	$5x10^{-8}$
Some (plasma cells)	12 (1.5)		0.5	0.2-1.7	0.3		0.7	0.2-2.1	0.5
Moderate (plasma cells)	0 (0)		NC	NC	NC		NC	NC	NC
Lots (plasma cells)	2 (0.3)		NC	NC	NC		NC	NC	NC

Factor	Mean (S.D.) or Median (range) or N (%)	Melanoma relapse (N=701, 223 events)				Melanoma-specific death (N= 702, 181 events)			
		N	HR	95% CI	p-value	N	HR	95% CI	p-value
Missing	101 (12.6)								
Test for trend			0.6	0.4-0.7	0.00001		0.5	0.3-0.6	$2x10^{-7}$
Core macrophage/melanophage infiltrate		697				698			
*No/barely perceptible**	299 (37.5)		1.0				1.0		
No (macrophages/melanophages)	121 (15.2)		0.6	0.4-0.8	0.003		0.4	0.3-0.7	0.0002
Yes (macrophages/melanophages)	278 (34.8)		0.6	0.4-0.7	0.00009		0.4	0.3-0.6	$3x10^{-6}$
Missing	100 (12.5)								
Test for trend			0.7	0.6-0.9	0.00005		0.7	0.5-0.8	$1x10^{-6}$
Extent of the core macrophage/melanophage infiltrate		697				698			
*No/barely perceptible**	299 (37.5)		1.0				1.0		
No (macrophages/melanophages)	121 (15.2)		0.6	0.4-0.8	0.003		0.4	0.3-0.7	0.0002
Some (macrophages/melanophages)	118 (14.8)		0.5	0.4-0.8	0.002		0.4	0.2-0.7	0.0002
Moderate (macrophages/melanophages)	112 (14.0)		0.7	0.4-0.96	0.03		0.5	0.3-0.8	0.004
Lots (macrophages/melanophages)	48 (6.0)		0.4	0.2-0.8	0.008		0.4	0.2-0.8	0.02
Missing	100 (12.5)								
Test for trend			0.8	0.7-0.9	0.0002		0.8	0.7-0.9	0.00003
Core neutrophilic infiltrate		696				697			
*No/barely perceptible**	299 (37.5)		1.0				1.0		
No (neutrophils)	386 (48.4)		0.5	0.4-0.7	$5x10^{-6}$		0.4	0.3-0.6	$6x10^{-8}$
Yes (neutrophils)	12 (1.5)		1.2	0.5-2.8	0.7		0.5	0.1-1.9	0.3

		Melanoma relapse (N=701, 223 events)				Melanoma-specific death (N= 702, 181 events)			
Factor	**Mean (S.D.) or Median (range) or N (%)**	**N**	**HR**	**95% CI**	**p-value**	**N**	**HR**	**95% CI**	**p-value**
Missing	101 (12.6)								
Test for trend			0.6	0.5-0.8	0.00006		0.5	0.3-0.6	$1x10^{-7}$
Extent of the core neutrophilic infiltrate		696				697			
*No/barely perceptible**	299 (37.5)		1.0				1.0		
No (neutrophils)	386 (48.4)		0.5	0.4-0.7	$5x10^{-6}$		0.4	0.3-0.6	$6x10^{-8}$
Some (neutrophils)	12 (1.5)		1.2	0.5-2.8	0.7		0.5	0.1-1.9	0.3
Moderate (neutrophils)	0 (0)		NC	NC	NC		NC	NC	NC
Lots (neutrophils)	0 (0)		NC	NC	NC		NC	NC	NC
Missing	101 (12.6)								
Test for trend			0.6	0.5-0.8	0.00006		0.5	0.3-0.6	$1x10^{-7}$
Core eosinophilic infiltrate		696				697			
*No/barely perceptible**	299 (37.5)		1.0				1.0		
No (eosinophils)	396 (49.6)		0.6	0.4-0.7	0.00001		0.4	0.3-0.6	$7x10^{-8}$
Yes (eosinophils)	2 (0.3)		NC	NC	NC		NC	NC	NC
Missing	101 (12.6)								
Test for trend			0.5	0.4-0.7	$7x10^{-6}$		0.4	0.3-0.6	$4x10^{-8}$
Extent of the core eosinophilic infiltrate		696				697			
*No/barely perceptible**	299 (37.5)		1.0				1.0		
No (eosinophils)	396 (49.6)		0.6	0.4-0.7	0.00001		0.4	0.3-0.6	$7x10^{-8}$
Some (eosinophils)	2 (0.3)		NC	NC	NC		NC	NC	NC
Moderate (eosinophils)	0 (0)		NC	NC	NC		NC	NC	NC

		Melanoma relapse (N=701, 223 events)				Melanoma-specific death (N= 702, 181 events)			
Factor	**Mean (S.D.) or Median (range) or N (%)**	**N**	**HR**	**95% CI**	**p-value**	**N**	**HR**	**95% CI**	**p-value**
Lots (eosinophils)	0 (0)		NC	NC	NC	NC	NC	NC	NC
Missing	101 (12.6)								
Test for trend			0.5	0.4-0.7	$7x10^{-6}$		0.4	0.3-0.6	$4x10^{-8}$
Core mitoses (tertiles)	1 (0-31)	694				695			
0	206 (25.8)		1.0				1.0		
1-2	257 (32.2)		1.9	1.2-2.8	0.004		1.9	1.2-3.0	0.008
≥3	232 (29.1)		4.5	3.1-6.7	$3x10^{-14}$		4.2	2.7-6.5	$2x10^{-10}$
Missing	103 (12.9)								
Test for trend			2.2	1.8-2.7	$<1x10^{-16}$		2.1	1.7-2.6	$3x10^{-12}$
Core blood vessels	2 (0-64)	699				700			
0	122 (15.3)		1.0				1.0		
1-2	264 (33.1)		1.04	0.7-1.5	0.8		0.9	0.6-1.3	0.6
≥3	314 (39.4)		0.9	0.6-1.2	0.4		0.9	0.6-1.3	0.5
Missing	98 (12.3)								
Test for trend			0.9	0.8-1.1	0.3		0.9	0.8-1.1	0.6

The majority (75%, 595/798) of cases had a compact stroma (Table 4.3). Melanoma cells with a round/ovoid/epithelioid appearance were the most common type to be identified within the cored region. In more than half of cases, melanoma cells were arranged in nests. Interestingly, absent pigmentation was recorded in 65% (522/798) of cored regions. Most (83%, 666/798) cored regions contained an immune cell infiltrate, although this was barely perceptible in one third of cases overall. The most commonly reported immune cell infiltrates within the cored region were lymphocytes and melanophages, whilst plasma cells, neutrophils and eosinophils were infrequently recorded. The presence of ≥3 mitoses or ≥3 blood vessels was recorded in 29% (232/798) and 39% (314/798) of cored regions, respectively. Figure 4.5 shows the frequency distribution of mitoses within the core. Due to the skewed frequency distribution, this measure was grouped into approximate tertiles for the time-to-event analyses (categories 0, 1-2 and ≥3). Similarly, the number of blood vessels within the core was grouped as 0, 1-2 and ≥3 (histogram not shown).

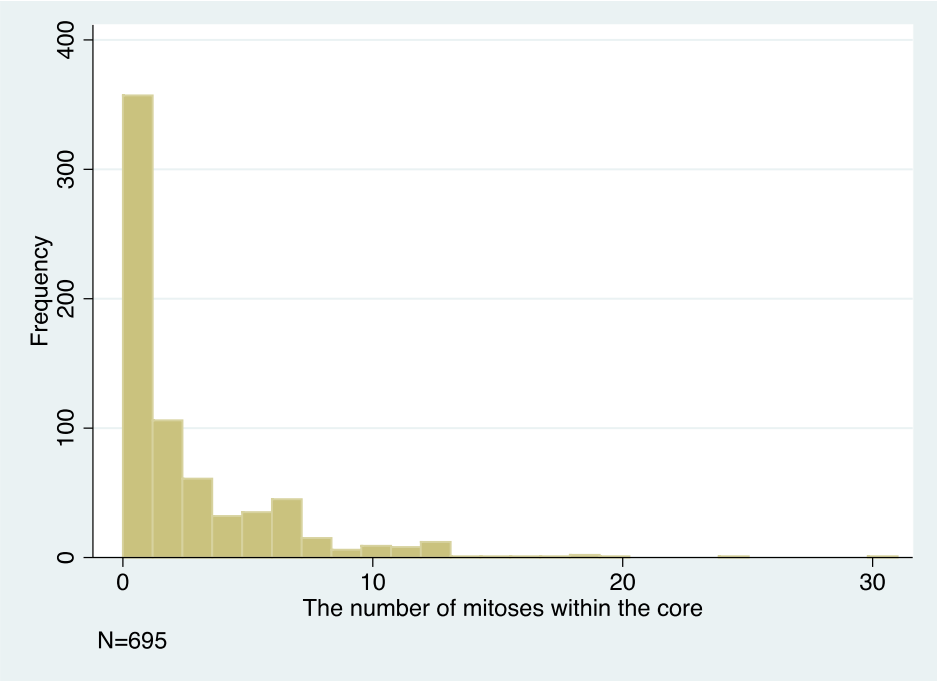

Figure 4.5 Histogram of the frequency distribution of the number of mitoses within the core

The median number of core mitoses was 1 (range 0-31). The number of mitoses was grouped into approximately three equal groups (tertiles).

In the univariable analysis, the POS was significantly associated with a decreased risk of relapse (HR 0.98, 95% CI 0.97-0.99, Cox proportional hazards model, $p=8x10^{-9}$) and melanoma-specific death (HR 0.97, 95% CI 0.97-0.98, Cox proportional hazards model, $p=6x10^{-9}$) (Table 4.3). For every percentage increase in the POS, there was a

2% decreased risk of melanoma relapse and a 3% decreased risk of death and this was highly statistically significant. The POS was also divided into quintiles to see whether there was a decreasing risk per quintile. There was a clear trend to decreasing risk of relapse and death with increasing quintiles of the POS. A definitive cut-off point for the POS, to help to stratify cases according to prognosis, could not be identified. Balloon cells appeared to increase the risk of relapse, compared to round/ovoid/epithelioid cells (HR 5.7, 95% CI 1.4-23.2, Cox proportional hazards model, p=0.01), however they were recorded in just 2 (0.2%) cases. The presence of melanoma cells arranged in sheets within the cored region was significantly hazardous for both melanoma relapse and death when compared with nests (HR for relapse 1.7, 95% CI 1.2-2.3, Cox proportional hazards model, p=0.001 and HR for melanoma-specific death 1.8, 95% CI 1.3-2.6, Cox proportional hazards model, p=0.001). The degree of melanoma cell pigmentation did not influence outcome. The increasing abundance of immune cells within the cored region (referred to as the “extent of core immune cell infiltrate”), particularly of lymphocytes (referred to as the “extent of core lymphocytic infiltrate”), was associated with a decreased risk of melanoma relapse and death. In total, 4% (33/798) cases lacked a core immune cell infiltrate. One third of cases (266/798) had a barely perceptible core immune cell infiltrate, whilst half of cases (400/798) had a core immune cell infiltrate graded as some, moderate or lots. As there were only 33 cases that lacked a core immune cell infiltrate and the HRs for “no” and “barely perceptible” were similar, these were grouped together for statistical analyses. This was utilised as the reference category (baseline) for analyses of the location of the core immune cell infiltrate and of the core immune cell subtypes (e.g. the extent of the core lymphocytic infiltrate) to increase the statistical power. The corresponding tests for trend were highly statistically significant. The presence of mitoses within the cored region was significantly hazardous for melanoma relapse (HR 1.9, 95% CI 1.2-2.8, Cox proportional hazards model, p=0.004 for 1-2 versus 0 mitoses and HR 4.5, 95% CI 3.1-6.7, Cox proportional hazards model, $p=3x10^{-14}$ for ≥3 versus 0 mitoses) and death (HR 1.9, 95% CI 1.2-3.0, Cox proportional hazards model, p=0.008 for 1-2 versus 0 mitoses and HR 4.2, 95% CI 2.7-6.5, Cox proportional hazards model, $p=2x10^{-10}$ for ≥3 versus 0 mitoses) and there was a significant trend with increasing numbers of mitoses. Neither the presence nor the number of blood vessels within the cored region were significantly associated with melanoma relapse or death.

4.3.2 Multivariable relapse analysis

4.3.2.1 Selection of variables from the univariable analysis for the multivariable relapse analyses

In multivariable analyses of melanoma relapse, I elected to adjust for AJCC stage rather than the Breslow thickness, microscopic ulceration and the number of core mitoses because AJCC stage is utilised clinically to predict outcome. The test for trend was used for AJCC stage in multivariable analyses because there was a trend for HRs and it was highly statistically significant in unadjusted analysis (Table 4.1).

In univariable analyses of the whole tumour measures, the presence of a dominant nodule and the depth of tumour loss were significant predictors of melanoma relapse (Table 4.2). The depth of tumour loss was selected for multivariable analyses, in preference to the type of tumour loss (or to the relative tumour loss), because it was a stronger predictor of relapse (Table 4.2). The test for trend was used in multivariable analyses in preference to analysing individual categories for the depth of tumour loss because the test for trend was highly significant (Table 4.2) and using this reduced the degrees of freedom, thereby increasing the statistical power and hence, the ability to detect significant effects. Therefore, a multivariable model was constructed including the presence of a dominant nodule and the depth of tumour loss plus age, sex, AJCC stage and the site of primary melanoma (data not shown). In this model, age, sex, “other” body site, AJCC stage, the presence of a dominant nodule and the depth of tumour loss remained independent predictors of melanoma relapse (data not shown).

Of the cored region variables, the POS, melanoma cell shape, melanoma cell structure and all of the core immune cell infiltrate variables were significant predictors of melanoma relapse (Table 4.3). In pairwise analyses, the core immune cell infiltrate variables were shown to be highly associated with each other (data not shown). For example, the Spearman correlation coefficient between the extent of the core immune cell infiltrate and the extent of the core lymphocytic infiltrate was 0.9 ($p=2x10^{-245}$) (Table 4.4). Also, the reference category (baseline) for each of the core immune cell subtypes was the same, i.e. “no/barely perceptible” immune cell infiltrate, which was recorded in 299 cases. The extent of the core immune cell infiltrate and the extent of the core lymphocytic infiltrate were chosen to be used in separate multivariable models (Table 4.5 and Table 4.6) as these were the most significant predictors of melanoma relapse in univariable analyses out of the core immune cell subtypes (Table 4.3).

Table 4.4: Cross-tabulation of the extent of the core immune cell and lymphocytic infiltrates.

The reference category (no/barely perceptible for the core immune cell infiltrate) is the same for each of these factors. As previously discussed, this was because the presence of a barely perceptible core immune cell infiltrate conferred a similar hazard ratio to an absent core immune cell infiltrate. This merged no/barely perceptible category was then used as the reference category (baseline) for specific types of immune cells (lymphocytes in this case) to increase the statistical power.

	Extent of the core lymphocytic infiltrate					
Extent of the core immune cell infiltrate N (%)	No/barely perceptible (immune cells)	None	Some	Moderate	Lots	Total
No/barely perceptible (immune cells)	299 (100)	0 (0)	0 (0)	0 (0)	0 (0)	299 (100)
Some (immune cells)	0 (0)	87 (65.9)	156 (87.2)	8 (17)	0 (0)	251 (36)
Moderate (immune cells)	0 (0)	35 (26.5)	19 (10.6)	37 (78.7)	9 (22)	100 (14.3)
Lots (of immune cells)	0 (0)	10 (7.6)	4 (2.2)	2 (4.3)	32 (78)	48 (6.9)
Total	299 (100)	132 (100)	179 (100)	47 (100)	41 (100)	698 (100)

4.3.2.2 The multivariable model for melanoma relapse

A multivariable model, combining clinical, whole tumour and cored region measures included the following factors: age, sex, site of primary melanoma, AJCC stage, the presence of a dominant nodule, the depth of tumour loss, the POS, melanoma cell shape, melanoma cell structure and the extent of the core immune cell infiltrate (Table 4.5). The results show that age, “other” site, AJCC stage, the presence of a dominant nodule, the depth of tumour loss, the POS, balloon cells, dispersed structure and the extent of the core immune cell infiltrate remained independent predictors of relapse. The HR for “other” body site versus limbs was 1.6 (95% CI 1.1-2.4, Cox proportional hazards model, p=0.02). Balloon cell shape conferred a HR of 6.1 (95% CI 1.5-26.0, Cox proportional hazards model, p=0.01) when compared with the reference category (baseline) of round/ovoid/epithelioid, however, there were only 2 patients with balloon cell shape and the confidence interval was very wide. Both cases with balloon cell shape relapsed by 4 years.

Dispersed cell structure conferred a HR of 2.7 (95% CI 1.3-5.8, Cox proportional hazards model, p=0.01) when compared with nests (Table 4.1). Again, there were small numbers of patients with dispersed cell structure and, therefore, the estimates may be unstable. Therefore, the multivariable analysis was repeated for the same factors, excluding melanoma cell shape.

The second statistical model in Table 4.5 (on the right) shows the results of the multivariable analysis for the same factors, excluding melanoma cell shape. In this model, age, AJCC stage, the presence of a dominant nodule, the depth of tumour loss, the POS and the extent of the core immune cell infiltrate remained independent predictors of relapse.

A similar analysis was then performed using the extent of the core lymphocytic infiltrate, instead of the extent of the core immune cell infiltrate. Table 4.6 shows the results of the multivariable model, including age, sex, site of primary melanoma, AJCC stage, the presence of a dominant nodule, the depth of tumour loss, the POS, melanoma cell shape, melanoma cell structure and the extent of the core lymphocytic infiltrate. Age, “other” site, AJCC stage, the presence of a dominant nodule, the depth of tumour loss, the POS, balloon cells, dispersed structure and the extent of the core lymphocytic infiltrate remained independent predictors of relapse.

The second statistical model in Table 4.6 (on the right) shows the results of the multivariable model, including age, sex, site of primary melanoma, AJCC stage, the presence of a dominant nodule, the depth of tumour loss, the POS, melanoma cell structure and the extent of the core lymphocytic infiltrate. Melanoma cell shape was excluded from this model, for the reasons previously discussed. Age, AJCC stage, the presence of a dominant nodule, the depth of tumour loss and the POS remained independent predictors of relapse. The extent of the core lymphocytic infiltrate was marginally significant.

Multivariable models were performed for the other immune cell types (e.g. macrophages, plasma cells, etc.), however, none of these immune cell subtypes were independently predictive of melanoma relapse (data not shown).

Table 4.5: Hazard ratios for melanoma relapse for clinical, whole-tumour and cored region measures (including the extent of the core immune cell infiltrate, with and without melanoma cell shape)

Adjusted hazard ratios (HR), 95% confidence intervals (95% CI) and p-values were estimated from multivariable Cox proportional hazards models. N refers to the number of cases. There were 687 cases in the statistical model. The number of cases analysed per category is provided. Events refers to the number of cases that had relapsed. The reference category (baseline) is the first category listed for each of the categorical variables. The first column provides the name and, where relevant, the categories for the variable. The first multivariable analysis includes melanoma cell shape (2^{nd}-5^{th} columns). The HR and 95% CI for plasmacytoid cell shape could not be calculated because there were no events in this category, i.e. none of these cases had relapsed. The multivariable analysis was repeated excluding melanoma cell shape (last 4 columns). NC = not calculable. NA = not applicable.

	Multivariable analysis *including* melanoma cell shape				**Multivariable analysis *excluding* melanoma cell shape**			
	Melanoma relapse (N=687, 216 events)				**Melanoma relapse (N=687, 216 events)**			
Factor	**N**	**Adjusted HR**	**95% CI**	**p-value**	**N**	**Adjusted HR**	**95% CI**	**p-value**
Age at diagnosis (years)	687	1.02	1.01-1.03	0.003	687	1.02	1.01-1.03	0.006
Sex								
Male	318	1.0			318	1.0		
Female	369	0.8	0.6-1.03	0.08	369	0.8	0.6-1.05	0.1
Site of primary melanoma								
Limbs	296	1.0			296	1.0		
Trunk	231	1.1	0.8-1.6	0.5	231	1.1	0.8-1.5	0.7
Head	81	1.1	0.7-1.7	0.7	81	1.1	0.7-1.7	0.8
Other	79	1.6	1.1-2.4	0.02	79	1.5	0.98-2.2	0.06
AJCC stage - Test for trend	687	1.9	1.6-2.4	$8x10^{-10}$	687	1.9	1.6-2.4	$4x10^{-10}$

	Multivariable analysis *including* melanoma cell shape				Multivariable analysis *excluding* melanoma cell shape			
	Melanoma relapse (N=687, 216 events)				Melanoma relapse (N=687, 216 events)			
Factor	**N**	**Adjusted HR**	**95% CI**	**p-value**	**N**	**Adjusted HR**	**95% CI**	**p-value**
Dominant nodule								
No	614	1.0			614	1.0		
Yes	73	1.6	1.1-2.3	0.02	73	1.7	1.2-2.5	0.007
Depth of tumour loss (mm)								
Test for trend	687	1.1	1.01-1.3	0.03	687	1.1	1.02-1.3	0.03
Percentage of stroma (continuous)	687	0.99	0.98-0.99	0.04	687	0.99	0.98-0.99	0.01
Melanoma cell shape								
Round/ovoid/epithelioid	590	1.0			NA	NA		
Spindle	60	0.8	0.4-1.3	0.3	NA	NA	NA	NA
Super spindle	14	0.2	0.1-1.1	0.06	NA	NA	NA	NA
Naevoid	15	0.8	0.3-2.2	0.7	NA	NA	NA	NA
Plasmacytoid	6	NC	NC	NC	NA	NA	NA	NA
Balloon	2	6.1	1.5-26.0	0.01	NA	NA	NA	NA
Melanoma cell structure								
Nests	410	1.0			410	1.0		
Sheets	130	0.9	0.6-1.3	0.7	130	0.9	0.6-1.2	0.4
Fascicles	127	1.1	0.7-1.6	0.8	127	0.9	0.6-1.4	0.7
Dispersed	20	2.7	1.3-5.8	0.01	20	1.9	0.9-4.1	0.09
Extent of the core immune cell infiltrate								
Test for trend	687	0.8	0.7-0.97	0.03	687	0.8	0.7-0.99	0.04

Table 4.6: Hazard ratios for melanoma relapse for clinical, whole-tumour and cored region measures (including the extent of the core lymphocytic infiltrate, with and without melanoma cell shape)

Adjusted hazard ratios (HR), 95% confidence intervals (95% CI) and p-values were estimated from multivariable Cox proportional hazards models. N = number of cases in the statistical model. Events = number of relapsed cases. The reference category (baseline) is the first category listed for each categorical variable. The first column provides the name and, where relevant, the categories for the variable. The first multivariable analysis includes melanoma cell shape, the second excludes melanoma cell shape. The HR and 95% CI for plasmacytoid cell shape could not be calculated because there were no relapse events in this category. NC = not calculable. NA = not applicable.

	Multivariable analysis *including* melanoma cell shape				**Multivariable analysis *excluding* melanoma cell shape**			
	Melanoma relapse (N= 687, 216 events)				**Melanoma relapse (N= 687, 216 events)**			
Factor	**N**	**Adjusted HR**	**95% CI**	**p-value**	**N**	**Adjusted HR**	**95% CI**	**p-value**
Age at diagnosis (years)		1.02	1.01-1.03	0.003		1.02	1.005-1.03	0.006
Sex					318			
Male	318	1.0			369	1.0		
Female	369	0.8	0.6-1.04	0.09		0.8	0.6-1.05	0.1
Site of primary melanoma								
Limbs	296	1.0			296	1.0		
Trunk	231	1.1	0.8-1.6	0.6	231	1.1	0.8-1.5	0.7
Head	81	1.1	0.7-1.7	0.7	81	1.04	0.7-1.6	0.9
Other	79	1.6	1.1-2.4	0.02	79	1.5	0.97-2.2	0.07
AJCC stage								
Test for trend	687	1.9	1.5-2.3	$3x10^{-9}$	687	1.9	1.5-2.4	$1x10^{-9}$

	Multivariable analysis *including* melanoma cell shape				Multivariable analysis *excluding* melanoma cell shape			
	Melanoma relapse (N= 687, 216 events)				Melanoma relapse (N= 687, 216 events)			
Factor	**N**	**Adjusted HR**	**95% CI**	**p-value**	**N**	**Adjusted HR**	**95% CI**	**p-value**
Dominant nodule								
No	614	1.0			614	1.0		
Yes	73	1.6	1.1-2.3	0.02	73	1.7	1.2-2.5	0.007
Depth of tumour loss (mm)								
Test for trend	687	1.1	1.01-1.3	0.04	687	1.1	1.01-1.3	0.03
Percentage of stroma (continuous)	687	0.99	0.98-0.99	0.03	687	0.99	0.98-0.99	0.009
Melanoma cell shape								
Round/ovoid/epithelioid	590	1.0			NA	NA		
Spindle	60	0.8	0.4-1.3	0.3	NA	NA	NA	NA
Super spindle	14	0.2	0.1-1.04	0.06	NA	NA	NA	NA
Naevoid	15	0.8	0.3-2.2	0.7	NA	NA	NA	NA
Plasmacytoid	6	NC	NC	NC	NA	NA	NA	NA
Balloon	2	6.3	1.5-26.5	0.01	NA	NA	NA	NA
Melanoma cell structure								
Nests	410	1.0			410	1.0		
Sheets	130	0.9	0.6-1.3	0.7	130	0.9	0.6-1.2	0.4
Fascicles	127	1.05	0.7-1.5	0.8	127	0.9	0.6-1.3	0.7
Dispersed	20	2.8	1.3-6.0	0.008	20	2.0	0.9-4.1	0.08
Extent of the core lymphocytic infiltrate								
Test for trend	687	0.8	0.7-0.98	0.03	687	0.9	0.7-1.0	0.05

4.3.3 Multivariable melanoma-specific survival analysis

In multivariable melanoma-specific survival analyses, AJCC stage was used in preference to Breslow thickness, microscopic ulceration and the core mitotic count, for the same reasons as previously discussed (Section 4.3.2.1). In terms of other whole-tumour measures, the presence of a dominant nodule and the type and depth of tumour loss were predictors of melanoma-specific death in univariable analyses (Table 4.2). The test for trend for the depth of tumour loss was used in multivariable analyses, as this was a more powerful predictor than the categorised variable or the type of tumour loss (or the relative tumour loss) (Table 4.2). A multivariable model was constructed consisting of age, sex, site of primary melanoma, AJCC stage, the presence of a dominant nodule and the depth of tumour loss (data not shown). In this model, age, “other” body site and AJCC stage remained independent predictors of melanoma-specific death (data not shown). The presence of a dominant nodule and the test for trend for the depth of tumour loss were not independent predictors of death and, therefore, were not carried forward to subsequent multivariable analyses containing the cored region measures (data not shown).

Of the cored region factors, the POS, melanoma cell structure and all of the core immune cell infiltrate variables were predictive for melanoma-specific death in univariable analyses (Table 4.3). Figure 4.6 shows the Kaplan-Meier survival estimates for melanoma-specific death for high and low POS (based on the median cut-off point).

The extent of the core immune cell infiltrate and the extent of the core lymphocytic infiltrate were the most significant predictors of melanoma-specific death in univariable analyses of cored immune infiltrate measures (Table 4.3). Therefore, a multivariable model was constructed, containing age, sex, site of primary melanoma, AJCC stage, the POS, melanoma cell structure and each of the following factors separately: the extent of the core immune cell infiltrate and the extent of the core lymphocytic infiltrate (Table 4.7). The results show that age, “other” site, AJCC stage, the POS and dispersed structure remained independent predictors of melanoma-specific death. The extent of the core immune cell infiltrate was marginally significant. The HR for “other” body site versus limbs was 1.8 (95% CI 1.2-2.8, Cox proportional hazards model, p=0.007). Dispersed structure conferred a HR of 2.4 (95% CI 1.1-5.5, Cox proportional hazards model, p=0.03) when compared with nests. There were small numbers of patients with dispersed structure and, therefore, the estimates may be unstable.

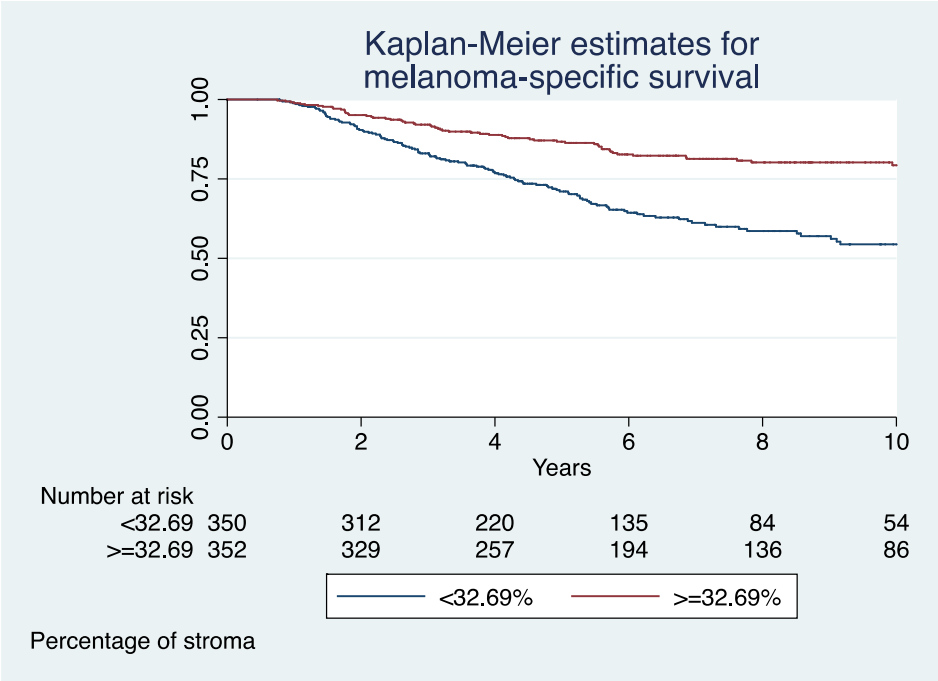

Figure 4.6: Kaplan-Meier curves and risk table for melanoma-specific survival for cases with high and low percentage of stroma

The median (32.69%) was used as the cut-off point to define cases with a high (≥32.69%) or low (<32.69) POS. Cases with a high POS tended to survive longer (HR 0.4, 95% CI 0.3-0.6, Cox proportional hazards model, $p=2x10^{-8}$).

The second statistical model in Table 4.7 shows the results of the multivariable analysis containing age, sex, site of primary melanoma, AJCC stage, the POS, melanoma cell structure and the extent of the core lymphocytic infiltrate. Age, “other” body site, AJCC stage, the POS, dispersed structure and the extent of the core lymphocytic infiltrate remained independent predictors of survival.

Table 4.7 (on following page): Hazard ratios for melanoma-specific death for clinical, whole-tumour and cored region measures (including either the extent of the core immune cell or lymphocytic infiltrate)

Adjusted hazard ratios (HR), 95% confidence intervals (95% CI) and p-values were estimated from multivariable Cox proportional hazards models. N refers to the number of cases in the statistical model. Events refers to the number of cases that had died due to melanoma. The reference category (baseline) is the first category listed for each of the categorical variables.

	Multivariable analysis with the extent of the core *immune cell* infiltrate				Multivariable analysis with the extent of the core *lymphocytic* infiltrate			
	Melanoma-specific death (N=692, 177 events)				Melanoma-specific death (N= 692, 177 events)			
Factor	**N**	**Adjusted HR**	**95% CI**	**p-value**	**N**	**Adjusted HR**	**95% CI**	**p-value**
Age at diagnosis (years)		1.03	1.02-1.04	0.00004		1.03	1.02-1.04	0.00005
Sex								
Male	320	1.0			320	1.0		
Female	372	0.8	0.6-1.1	0.3	372	0.8	0.6-1.2	0.3
Site of primary melanoma								
Limbs	297	1.0			297	1.0		
Trunk	232	1.4	0.97-2.1	0.07	232	1.4	0.9-2.0	0.1
Head	81	0.9	0.5-1.6	0.8	81	0.9	0.5-1.6	0.7
Other	82	1.8	1.2-2.8	0.007	82	1.7	1.1-2.6	0.02
AJCC stage								
Test for trend	692	2.3	1.8-2.9	$9x10^{-12}$	692	2.2	1.7-2.8	$6x10^{-11}$
Percentage of stroma (continuous)	692	0.99	0.98-0.99	0.005	692	0.99	0.98-0.99	0.009
Melanoma cell structure								
Nests	411	1.0			411	1.0		
Sheets	133	1.1	0.7-1.6	0.7	133	1.1	0.7-1.6	0.7
Fascicles	127	1.02	0.7-1.5	0.9	127	1.0	0.7-1.5	1.0
Dispersed	21	2.4	1.1-5.5	0.03	21	2.4	1.1-5.5	0.03
Extent of the core immune cell infiltrate or extent of the core lymphocytic infiltrate								
Test for trend	692	0.8	0.7-0.99	0.05	692	0.8	0.7-0.9	0.01

Figure 4.7 shows the Kaplan-Meier curves for the time-to-event analysis for melanoma-specific death by the type of melanoma cell structure.

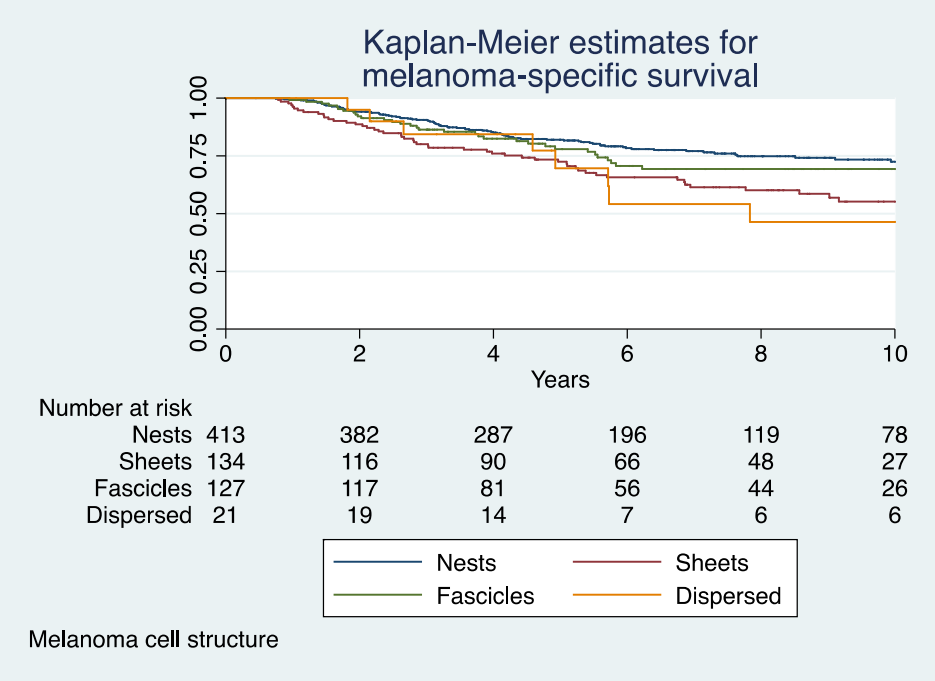

Figure 4.7: Kaplan-Meier curves and risk table for melanoma-specific survival for each melanoma cell structure.

The curve for dispersed cell structure appeared to be more unstable than the curves for other cell structures, which might reflect the small numbers in this group. “Nests” was the reference category. Table 4.3 shows the HRs, 95% CI and p-values for melanoma-specific death according to melanoma cell structure. Dispersed cell structure was not statistically significant in univariable survival analysis but was an independent predictor in multivariable analyses (Table 4.7).

Figure 4.8 shows the Kaplan-Meier curves for melanoma-specific survival by the extent of the core immune cell infiltrate.

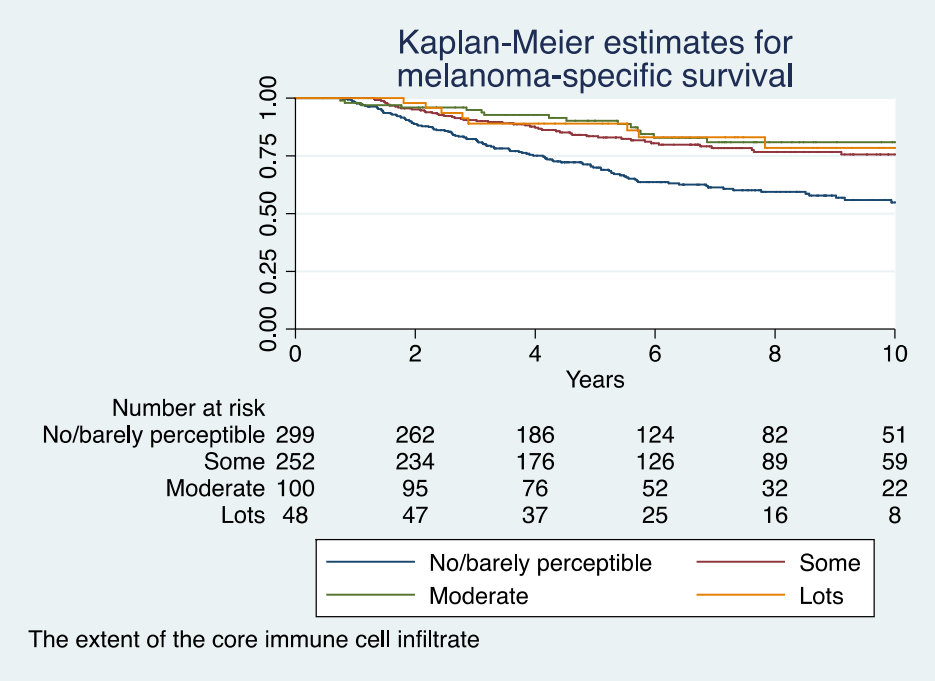

Figure 4.8: Kaplan-Meier curves and risk table for melanoma-specific survival by the extent of the core immune cell infiltrate

Cases with a core immune cell infiltrate categorised as no/barely perceptible tended to have a worse outcome, compared to some, moderate or lots (test for trend, Cox proportional hazards model, $p=2x10^{-6}$).

Figure 4.9 shows the Kaplan-Meier curves for melanoma-specific survival by the extent of the core lymphocytic infiltrate.

Multivariable models were performed for the other core immune cell subset variables and the results were similar for the presence of plasma cells, neutrophils and eosinophils, however, the presence of macrophages was not significant in multivariable analysis (data not shown).

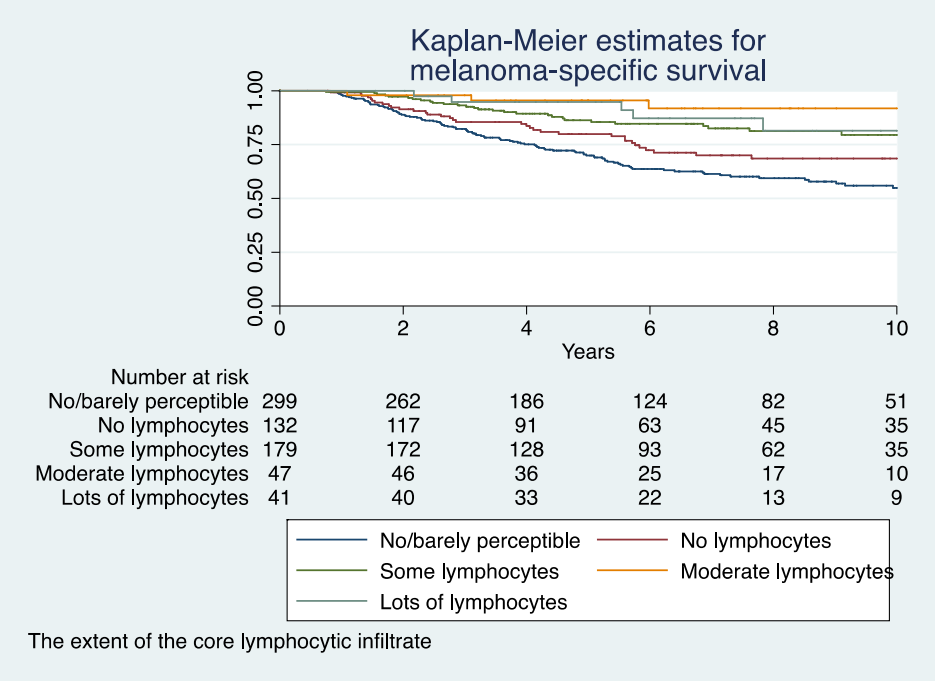

Figure 4.9: Kaplan-Meier curves and risk table for melanoma-specific survival by the extent of the core lymphocytic infiltrate

No/barely perceptible refers to the extent of the core immune cell infiltrate, which was the reference category (baseline) for the analyses of the core immune cell subtypes. Cases with a core immune cell infiltrate categorised as no/barely perceptible tended to have the shortest interval to melanoma-specific death, followed by cases without a core lymphocytic infiltrate. If the core immune cell infiltrate was classified as no or barely perceptible, no further assessment was done for the type of immune cells present, e.g. lymphocytes or macrophages. Although cases in the “no lymphocytes” category lacked lymphocytes, other types of immune cells within the core could have contributed to the benefit seen compared to cases within the no/barely perceptible category. Of the 132 cases in the “no lymphocytes” category, the following immune cells were present within the core: macrophages/melanophages (n=132), plasma cells (n=1), neutrophils (n=6). Cases with a core lymphocytic infiltrate tended to survive longer (test for trend, Cox proportional hazards model, $p=8x10^{-9}$).

4.4 Summary

In terms of clinical factors, older age at diagnosis, male sex, trunk, “other” site of primary melanoma and advancing AJCC stage were significantly predictive of an increased risk of both melanoma relapse and death in univariable analyses (Table 4.1). Age, “other” site and stage remained independent prognostic factors in multivariable analyses, both for relapse and melanoma-specific death (Table 4.5, Table 4.6 and Table 4.7).

Regarding whole-tumour measures, increasing Breslow thickness, the presence of a dominant nodule, microscopic ulceration, and its increasing extent, the presence of tumour loss, “both” or superficial types of tumour loss, an increasing depth of tumour loss and a relative tumour loss of <0.26mm or 0.26-<0.52mm were significantly associated with an increased risk of both melanoma relapse and death in univariable analyses (Table 4.2). The pattern of TILs was not significantly associated with relapse and it was of borderline statistical significance in predicting melanoma-specific death (Table 4.2). Neither the intensity nor the pattern of TIMs was significantly predictive of either melanoma relapse or death in univariable analyses (Table 4.2). AJCC stage was used in multivariable analyses instead of Breslow thickness, microscopic ulceration and the number of mitoses because stage incorporates all of these factors and is what is used clinically to predict outcome. The presence of a dominant nodule and the test for trend for the increasing depth of tumour loss were independently hazardous for melanoma relapse (Table 4.2 and Table 4.2) but not melanoma-specific death (data not shown). This could reflect a lack of statistical power in the survival analysis, i.e. fewer cases had died than had relapsed.

Several of the new histopathological variables, which were recorded within the cored region, were significant prognostic factors (Table 4.3). The POS was significantly protective for both melanoma relapse and death in univariable analyses and remained an independent predictor in multivariable analyses (Table 4.5, Table 4.6 and Table 4.7) but the quality of the stroma had no significant effect (Table 4.3). In univariable and multivariable analyses, balloon cell shape was significantly hazardous for melanoma relapse (Table 4.3**,** Table 4.5 and Table 4.6) but not death. The multivariable analyses for relapse were repeated without melanoma cell shape (Table 4.5 and Table 4.6) because only balloon cell shape showed significance in the model, however, only 2 cases had a balloon cell shape. A melanoma cell structure composed of sheets was significantly hazardous for both melanoma relapse and death in univariable analyses (Table 4.3) but the dispersed cell structure was an independent prognostic factor in multivariable analyses for relapse (Table 4.5 and Table 4.6) and death (Table 4.7). The

degree of melanoma cell pigmentation was not predictive of either relapse or death (Table 4.3).

A detailed analysis of the immune cell infiltrates within the cored region was performed. An increasing extent of immune cells within the core, particularly lymphocytes, was significantly protective for both relapse and melanoma-specific death in univariable analyses (Table 4.3). The test for trend for the extent of the core immune cell infiltrate was an independent prognostic factor for relapse (Table 4.5) but was of borderline statistical significance for melanoma-specific death (Table 4.7). The test for trend for the core lymphocytic infiltrate was of borderline statistical significance for relapse in multivariable analyses (Table 4.6) and was independently protective for melanoma-specific death (Table 4.7). All categories for the locations of immune cells within the core (at the tumour-stroma interface, etc.) were protective for both relapse and death, in univariable analyses (Table 4.3). Both the presence and absence of core macrophages/melanophages were protective for melanoma relapse and death, in univariable analyses (Table 4.3). This may be because out of the 121 patients with absent macrophages/melanophages within the core, 118 had a core lymphocytic infiltrate (data not shown). Plasma cells, neutrophils and eosinophils were infrequently recorded within the core (Table 4.3).

Mitoses were enumerated within the core and their increasing number was significantly hazardous for both melanoma relapse and death, in univariable analyses (Table 4.3). The presence or absence of core mitoses was incorporated into the generated AJCC stage IB variable, instead of the reported mitotic count (data not shown).

Overall, age and AJCC stage were consistently predictive of a poor prognosis in multivariable analyses for both melanoma relapse (Table 4.5 and Table 4.6) and death (Table 4.7). The dispersed melanoma cell structure was significantly hazardous in multivariable analyses (Table 4.5, Table 4.6 and Table 4.7). The POS and the extent of either the core immune cell or lymphocytic infiltrate were predictive of a better outcome for both relapse (Table 4.5 and Table 4.6) and melanoma-specific death (Table 4.7) in multivariable analyses (although the immune cell infiltrates were of borderline statistical significance in some of the multivariable models; Table 4.6 and Table 4.7). The consistency of the results for independent prognostic factors between multivariable Cox proportional hazards models for relapse and melanoma-specific death, suggests that these measures are robust.

Although similar results were obtained for multivariable relapse and survival analyses, there were some exceptions. The presence of a dominant nodule and the depth of tumour loss were predictive of melanoma relapse (Table 4.5 and Table 4.6) but not death (data not shown). Many of the core immune cell variables remained significant in

multivariable survival analyses but were not significantly associated with relapse, including the presence of immune cells dispersed between tumour cells and the test for trend for the following core immune cell subtypes: plasma cells, neutrophils and eosinophils (data not shown).

4.5 Discussion

This was a unique study of a large primary melanoma cohort in the UK, which assessed the effect of both recognised and novel histopathological factors on survival. The cohort was representative of the sex distribution for melanoma [218], although participants were slightly younger than the UK average [2]. Older age at diagnosis has previously been shown to be an independent prognostic factor in cutaneous melanoma [6-8] and this was replicated in my project, with a 3% increased risk of death for every year older (Table 4.7). This not inconsiderable effect is the focus of intense research currently in other centres. Decreased self-detection [11], more aggressive tumour characteristics [7, 8] and immunosenescence [12] have previously been cited in the literature as possible causes for this effect and I plan to explore this in future research. Sex has also been reported to be an independent predictor of melanoma-specific death, with females tending to survive longer [17, 219]. Similarly, in this study, female sex was protective in univariable analysis (Table 4.1) but lost statistical significance in multivariable analyses (Table 4.7). This could reflect the relatively small numbers studied. “Other” site of primary (including acral, subungual and genital melanomas) was significantly hazardous in multivariable analyses for both melanoma relapse and death (Table 4.1). Melanomas at these sites are difficult to detect, however, the effect persisted after adjusting for stage, suggesting that such melanomas possess a distinct biology. A poor outcome has previously been demonstrated for melanomas at vulval, vaginal and acral sites [38-40] and *c-KIT* mutations occur more frequently in acral and mucosal melanomas, supporting the hypothesis that the biology of these melanomas might be different.

As expected, AJCC stage was a highly significant predictor of both melanoma relapse and death (Table 4.1), consistent with findings in larger data sets [43, 44]. Moreover, established prognostic factors, including Breslow thickness [22, 43, 45] and microscopic ulceration [43] were significantly hazardous (Table 4.2) and were incorporated into the AJCC stage variable for multivariable analyses. There was a convincing trend in the hazard ratios for an increasing extent (width) of ulceration and the test for trend was highly significant (Table 4.2), indicating that no particular cut-off point was more prognostic than another and suggesting that the extent of ulceration

should be measured on a continuous scale. Previous studies have reported different prognostic cut-off points for the extent of ulceration [53-56]. The extent of ulceration could be an indicator of the duration of ulceration or it might be a marker of a more profound, pro-tumourigenic inflammatory response within the melanoma. Jewell *et al.* showed that genes involved in wound healing were upregulated in ulcerated compared to non-ulcerated melanomas [49].

The presence of a dominant nodule was an independent predictor of melanoma relapse (Table 4.5 and Table 4.6) but not death (data not shown), consistent with another study, although the authors' definition of a dominant nodule differed to mine [70]. The explanation for the independent effect of a dominant nodule for relapse but not for survival could be a reflection of the lack of statistical power, in that there were fewer events in the multivariable survival analysis, i.e. fewer patients had died than had relapsed. Therefore, this might prove to be an independent predictor of survival in a larger data set. Furthermore, melanomas that had a dominant nodule were significantly thicker, more likely to be ulcerated and to have a higher core mitotic count and a lesser extent of immune cell infiltration within the core (data not shown). The literature on the topic of a dominant nodule is sparse but the hypothesis is that it represents a clonal expansion of a population of tumour cells [70]. The nodular melanoma subtype is regarded as an indicator of a more aggressive tumour, being associated with a higher mitotic count [220] and an increased risk of death [221]. Superficial spreading melanomas tend to have a nested pattern [187], however, some contain a nodular component. Lateral epidermal involvement, of up to 3 rete ridges beyond the vertical growth phase melanoma [187], may be present in nodular melanomas. These somewhat arbitrary limits make subtype distinctions less precise. I recorded the presence of a dominant nodule, hypothesising that this feature could reflect a more aggressive tumour. My study provided some support for this hypothesis.

Surprisingly, TILs within the whole tumour were not a significant predictor of relapse and were of borderline statistical significance in predicting melanoma-specific death (Table 4.2). Brisk TILs are reported to have the best prognosis and tend to occur more frequently in thin melanomas [61]. Therefore, the lack of statistical significance in my study could be a reflection of the thicker melanomas reviewed. Although TILs are part of the minimum data set recorded by pathologists [51] in the reporting of primary cutaneous melanoma, they have not been incorporated into AJCC stage [43]. This might reflect the subjective nature of the measure [199]. I utilised a modified version of the approach adopted by Clemente *et al.,* however, the number of cases allocated to some of the subgroups was small and, ultimately, had to be merged into 3 categories (absent, non-brisk and brisk) for statistical analyses. Apparently, this method did not

improve the predictive power of TILs, although replication in a larger data set might show a significant effect. As previously discussed, some studies have demonstrated TILs to be an independent prognostic factor [24, 27, 69], while others have not corroborated these findings [25, 65, 67]. It was remarkable that the extent of the core lymphocytic infiltrate was independently protective for melanoma-specific death (Table 4.7). There was a weak, positive correlation between TILs within the whole tumour and the extent of the core lymphocytic infiltrate (Spearman rho=0.2, $p=3x10^{-7}$, data not shown), which is not entirely surprising, given that the TMA core biopsy was obtained from the region of tumour that had the least immune cell infiltration. The extent of the core lymphocytic infiltrate was moderately correlated with the ESTIMATE immune score (Spearman rho=0.5, $p=3x10^{-31}$, data not shown). Similarly, the Cancer Genome Atlas Network reported that cases with enrichment for the expression of immune cell genes had a higher lymphocyte score (a score of the extent and distribution of lymphocytes) and a better survival, although they analysed a mixture of primary and metastatic melanoma cases [153]. The significant predictive power of the extent of the core lymphocytic infiltrate suggests the possibility that pathologists could focus on a specific region within the advancing edge of the melanoma for the assessment of TILs, which might increase the reproducibility of this measure and might be more informative of outcome. Although heterogeneity is a feature of cutaneous melanoma [117, 222], the findings suggest the possibility that a cored sample of the advancing tumour edge might represent an informative snapshot of the melanoma, however, future research could clarify whether or not this is the case.

There are conflicting reports in the literature regarding the prognostic significance of regression. Some studies have proposed a protective role [72, 74, 77, 79], while others have reported a worse prognosis in association with regression [82, 84, 86]. In this study, the presence, type and depth of tumour loss were significantly hazardous for melanoma relapse and death in univariable analyses (Table 4.2). This was particularly significant when the tumour loss reached a depth >1.63mm (Table 4.2). In contrast, the "deep" subtype of tumour loss did not reach statistical significance in univariable analysis. "Deep" tumour loss was defined as tumour loss within the dermis, in the absence of direct contact with the dermo-epidermal junction. Therefore, its depth in millimetres is likely to have varied between tumours. I also calculated the "relative tumour loss" by dividing the depth of tumour loss by the Breslow thickness, considering that this might more accurately reflect the effect of regression in the context of the size of the melanoma, however, the depth of tumour loss was a more significant predictor (Table 4.2). Moreover, the depth of tumour loss was an independent predictor of melanoma relapse (Table 4.5 and Table 4.6) but not death (data not shown). The latter could reflect a lack of statistical power. It is dermatological dogma that regression

represents a host immune response to the tumour, however, the findings of this study do not support this premise. An alternative hypothesis is that regression represents “crisis”, a stage in the evolution of a potentially more aggressive melanoma, and that the accompanying tumour cell apoptosis is the antigenic stimulus that drives immune cells into the region of tumour destruction [73]. In addition, an association between tumour loss and necrosis, an adverse prognostic factor [223], cannot be ruled out. Macrophages are often used to define areas of regression [74] and tumour-associated macrophages have been reported to be associated with angiogenesis [50], invasion and metastasis in cancer [224].

Furthermore, I graded the intensity and pattern of TIMs across the whole tumour but there was no significant association with either relapse or melanoma-specific death (Table 4.2). An increasing extent of melanophages within the core was significantly protective, however their absence was also protective in univariable analysis, suggesting that the beneficial effects noted might have been accounted for by other immune cells within the core (Table 4.3). Moreover, the extent of melanophages within the core was not an independent prognostic factor (data not shown). It was not possible to determine the polarisation of the macrophages identified, i.e. whether they were “M1” type macrophages, associated with anti-tumour immunity or alternatively activated “M2” type macrophages, which have a role in tumour remodelling and are associated with pro-tumourigenic inflammation [170, 224].

In terms of other core immune cell variables, the presence of a core immune cell infiltrate (of any type) was protective, irrespective of its proximity to the tumour cells (at the tumour/stroma interface, dispersed between tumour cells or both) (Table 4.3). Plasma cells, neutrophils and eosinophils were infrequently recorded within the core (Table 4.3), indicating that these types of immune cells appear to be rarely encountered within the thickest part of the melanoma. The lack of specific immune cell populations within the deep tumour suggests an incomplete immune response. An increasing extent of lymphocytes within the core was protective, suggesting no evidence of T cell exhaustion [225].

It is increasingly recognised that tumour stroma is effectively part of the cancer “organ” and that the environment may be either pro-tumourigenic or protective [226]. I was therefore interested in exploring the relationship between the POS and outcome. The cores were consistently taken from the deepest part of the tumour, which had the least amount of inflammation/stroma so that the data could be compared between tumours. I found that the POS within the cored region was a powerful prognostic factor in multivariable analyses, independent of age, AJCC stage, the site of primary melanoma and other combinations of factors (Table 4.5, Table 4.6 and Table 4.7). The POS was

calculated by the positive scoring of immune cells and non-immune stromal components, including collagen. Therefore, the protective effect conferred by the POS could be a reflection of the degree of lymphocytic infiltration within the core or, alternatively, might be due to non-immune stromal constituents. This finding will be explored further in Chapter 5.

There was a striking abundance of round/ovoid/epithelioid melanoma cells within the core, thus, limiting comparisons with rarer cell types (Table 4.3). The hazard ratios for balloon cells suggest a hazardous effect on melanoma relapse but not death, however, the number of cases in this category was very small. Balloon cells are known to be a rare finding [227] and their biological significance has not been fully elucidated [228]. Hypotheses proffered include defective melanosome formation and adipocytic degeneration [228]. Balloon cells can also occur within melanocytic naevi [229]. Although balloon cell melanomas have been reported to metastasise, their metastatic behaviour is thought to be similar to other melanoma subtypes [228, 230]. The suggestion that balloon cells are hazardous in this study, therefore, may simply reflect the small numbers.

Nests were the most common type of melanoma cell structure to be recorded and a dispersed cell structure was independently hazardous in some multivariable analyses for relapse (Table 4.5 and Table 4.6) and death (Table 4.7). The biological significance of this finding is uncertain and, again, might reflect the small numbers in this category.

Neither the degree of melanoma cell pigmentation nor the number of core blood vessels had an impact on melanoma relapse or death (Table 4.3). Pigmentation is considered to be a marker of melanocyte differentiation [111] and amelanotic melanomas tend to be more advanced at the time of presentation [231], therefore, it is surprising that pigmentation had no effect on outcome. However, melanoma cells are capable of “switching” between states of high and low pigmentation [116], so it is possible that the H&E section, taken at one point within the lifetime of the melanoma was not representative of its plasticity, evolution and, hence, its metastatic potential. Moreover, it is possible that the pigmentation recorded within the core was not representative of pigmentation within the whole tumour. The TMA core biopsy was taken from the advancing edge of the tumour and it is possible that these melanocytes were less well differentiated, which is suggested by the overwhelming majority of cases having an amelanotic appearance within the core. Unfortunately, I did not record pigmentation in other regions of the tumour, which means it is not possible to verify this hypothesis. Furthermore, analysing pigmentation as a binary variable, i.e. present versus absent, might be more informative and this could be explored in future research. I enumerated blood vessels within the core because I was interested to

establish whether or not they might be predictive of outcome. Ulcerated tumours have previously been shown to be associated with an increased microvessel density and hence a more aggressive tumour [50]. However, the number of core blood vessels was not predictive of outcome. This could reflect the relatively poor reproducibility of the variable (Chapter 3). The definition I used to assert the presence of a blood vessel was that red cells were present within a lumen. This was used in an effort to overcome difficulties in deciphering individual blood vessels from its tributaries. Nonetheless, it was problematic and enumeration of the core blood vessels proved difficult. This might explain the lack of prognostic effect and one could argue that the use of immunohistochemistry to stain vessels might have been more productive.

Previous studies have reported a strong prognostic role for mitotic count [26, 43, 59]. The presence of ≥1 mitosis is used to define AJCC stage IB (7^{th} edition) [43] but has not been retained in the 8^{th} edition (in press). In this study, there was a significantly increased risk of both melanoma relapse and death in association with an increasing number of core mitoses (Table 4.3). This suggests that, in the future, pathologists could enumerate mitoses within one 600 micron region within the thickest part of the primary melanoma, containing the least amount of immune and non-immune stroma. This could be beneficial in clinical practice, particularly in view of the time required to apply the “hotspot” method for calculating mitotic count [232]. However, interobserver studies regarding the selection of the appropriate 600 micron region between pathologists would be needed, in order to establish reproducibility in this regard.

One of the limitations of the study was the sample size: much larger numbers of cases were analysed to determine the factors that were selected for the AJCC stage [43]. I did not record the histological subtype and microsatellites using the virtual pathology protocol. These measures were dropped following the results of interobserver studies in my earlier histological review using a light microscope (Chapter 3). I relied upon information about microsatellite status, nodal and visceral metastatic disease, which I incorporated into the AJCC stage variable [43], based upon data that had previously been extracted from clinical notes and histology reports by Section staff. The histopathological review was based on a biased set of primary melanomas, being inherently thicker and more likely to be ulcerated and possibly mitotically active: these tumours had to have a minimum thickness of 0.75mm. In this study, there was a bias towards sampling thicker tumours and some of the histopathological characteristics might reflect this bias. Nonetheless, the data are uniquely based on a population-ascertained cohort. A further limitation of the study was that mitoses were enumerated within the cored region and not within the whole-tumour. Despite this, the core mitotic count appeared to be a significant prognostic factor. Some of the recorded factors were

based on “eyeball” measures, e.g. the extent of the core immune cell infiltrate and immune cell subtypes, which could be subject to interobserver variation and might limit reproducibility. Yet, their high statistical significance in this study suggests that these measures were recorded in a consistent manner.

In summary, this study reports an analysis of clinical factors and of a detailed histopathological assessment of >700 primary melanomas. The study was original in many ways, being based on a large cohort of population-ascertained melanoma cases with detailed clinical and survival data. The median follow-up for these cases was 5.8 years, providing a reasonably strong basis upon which to draw conclusions about melanoma-specific survival. Furthermore, the histopathological review was carried out by a single observer, with good intra- and interobserver agreement (Chapter 3). Several novel histopathological factors were developed and analysed, some of which showed significant prognostic power, e.g. the extent of the core immune cell and lymphocytic infiltrates and the POS. As expected, established predictors of survival, e.g. age and AJCC stage remained independent prognostic factors, replicating the findings of previous studies [8, 43]. Moreover, an increasing number of core mitoses was significantly hazardous for both relapse and death. Surprisingly, sex and TILs, which have been shown to be independent predictors of outcome in some previous studies [22, 27], were not independently or significantly predictive of relapse or death, respectively. This might be due to the relatively small numbers studied or the bias towards sampling thicker primary melanomas.

In the future, I would like to verify my findings in an independent data set. Furthermore, the curious finding of the POS being independently protective for melanoma-specific death was exciting, as it could represent a potential biomarker in melanoma. Therefore, I decided to explore whether or not this effect was additive to AJCC stage. This work will be presented in Chapter 5.

Chapter 5 Stroma

5.1 Introduction

In this chapter, I will explore the role of the stromal content within primary melanomas. The stroma, or “non-tumour” component, comprises a diverse array of structures and cell types, including connective and adipose tissue, endothelial cells, fibroblasts and an assortment of immune cells, including lymphocytes, neutrophils, macrophages, eosinophils and plasma cells [138, 233]. In my study, I have defined and measured all non-tumour cell structures as stroma, so that I have included fibroblasts, immune cells and structural components, e.g. collagen, as “stroma”.

I chose to evaluate the stroma as a potential prognostic biomarker because of the evidence to suggest that the stroma plays an active role in tumour development. The nature of the melanoma microenvironment has been explored in previous studies [132, 234-241]. The stroma, although clearly a multicomponent factor, is largely made up of connective tissue and thus, the role of stromal fibroblasts in cancer progression has received much attention [238, 240, 242-244]. Fibroblasts have been reported to play a role in the chemoresistance of melanoma cells to doxorubicin [238] and vemurafenib [245]. In addition, the nature of “normal”, resident fibroblasts is postulated to differ from cancer-associated fibroblasts (CAFs) [246], with the latter adopting features of myofibroblasts and demonstrating increased expression of alpha-smooth muscle actin [247]. Stromal mesenchymal cells and fibrocytes, expressing fibroblast-activation protein alpha (FAP), can evoke an immunosuppressive microenvironment [248] and senescent fibroblasts are thought to play a role in melanoma progression [249]. Fibroblasts, situated in disparate regions of the melanoma are thought to have different characteristics, i.e. resident fibroblasts in pre-existent adjacent tissue versus myofibroblasts at the advancing peritumoural zone [132]. Zhou *et al.* reported that melanomas grew more rapidly in a mouse model in the presence of fibroblasts in which beta-catenin had been deactivated [250]. In contrast, there was increased apoptosis, cell cycle arrest and a decrease in markers of epithelial-mesenchymal transition in melanomas occurring in the presence of normal dermal fibroblasts [250]. This suggests that CAFs and native fibroblasts may have divergent roles in cutaneous melanoma and that the distinction of CAFs from untransformed fibroblasts may be important.

An interplay exists between melanoma cells and their neighbouring stroma, communicating via the release of growth factors, cytokines and through cell-to-cell contact [132]. In the process of invasion, melanoma cells interact with the stroma.

Remodelling of the extracellular matrix (ECM) occurs in the presence of proteolytic enzymes called matrix metalloproteinases (MMPs) [251]. This transition is carefully balanced by the secretion of MMPs and their inhibitors, so-called “tissue inhibitors of metalloproteinases” [251] and appears to be important in terms of melanoma progression. For example, MMP-1, 2 and 9 have been reported to be associated with melanoma cell invasion [252] and a worse prognosis [251, 253].

Attachment to the extracellular matrix (ECM) is an attribute of normal cells and dysregulation of adhesion molecules permits the detachment and migration of cancer cells in the process of invasion and metastasis [254]. Loss of E-cadherin expression is characteristic of this phenomenon, referred to as “epithelial-to-mesenchymal transition” [254] and the stroma has been implicated in promoting its evolution. Izar *et al.* derived melanoma cell cultures from 50 patients with stage III/IV melanoma and identified *BRAF* and *NRAS* mutations in 19 and 11 cases, respectively [255]. By performing a series of *in vitro* experiments on the 30 cases with *BRAF/NRAS* mutations, they identified a subpopulation of cells that lacked these driver mutations [255]. They surmised that these cells were CAFs, based on their lack of *BRAF/NRAS* mutations and their expression of FAP, among other markers [255]. In order to gather more evidence in support of this supposition, they performed a transcriptomic analysis, which revealed 200 genes that were significantly enriched among the “CAFs” and the expression of these genes had also previously been reported to be highly variable among leukocytes, endothelial cells and FAP+ fibroblasts in colorectal cancer [255]. A significant overlap in the gene expression signature was identified between these “CAFs” and that reported for FAP+ fibroblasts [255]. The top biological pathway associated with these “CAFs” revealed enrichment of genes involved in the epithelial-mesenchymal transition [255]. Furthermore, the “CAFs” were reported to grow more rapidly in a melanoma cell-conditioned medium, compared with media conditioned with either “CAFs” or normal dermal fibroblasts [255]. Moreover, for 2 of the 3 cases presented, the melanoma cells were reported to grow more efficiently in the presence of CAF-conditioned medium, compared with a medium conditioned with normal dermal fibroblasts [255]. The results support the hypothesis that a two-way communication could exist between melanoma cells and their stromal neighbours, and that CAFs might promote melanoma cell proliferation.

In order to assess whether or not melanoma cell invasion might be influenced by CAFs, Izar *et al.* performed cell invasion assays using melanoma cell lines [255]. All 6 cell lines that had been co-cultured with their matched CAFs, allowing for direct cell-to-cell contact, were reported to show enhanced invasion [255]. Conversely, only half (3/6) of the cases that had been grown in matched CAF-conditioned media were reported to

show similar invasion [255]. These findings suggest that CAFs might promote melanoma cell invasion and that direct cell-to-cell contact between melanoma cells and CAFs could enhance this process.

Contrary to reports of a hazardous role for the microenvironment, the “non-immune” component of the stroma might promote the delivery of immune cells to the tumour, thereby assisting in the mounting of an appropriate host immune response in reprisal against the tumour [235, 256]. Whether this non-immune compartment is a passive bystander or an instigator of immune cell infiltration remains to be seen. Melanoma is regarded to be a highly immunogenic tumour [257]. I recorded a measure of the non-tumour compartment (the percentage of stroma (POS)), which comprised a melange of immune and non-immune, stromal cells. Therefore, the quantification of the immune cell fraction may well have played an important role in the protective effects of the POS in my study. Melanoma is capable of eliciting a variable immune response, the nature and extent of which may contribute to survival [129, 212]. Tumour-infiltrating lymphocytes have been shown to be of prognostic significance in some studies [60-63, 212], while others have failed to show an independent survival advantage [64, 65, 67]. The durability of response to immunotherapy in metastatic melanoma supports the view that the immune system is critical in combatting melanoma and improving survival [126, 129, 258, 259]. In a study of 333 melanomas from the Cancer Genome Atlas, composed of a mixture of primary and metastatic samples, the lymphocyte score was shown to be a protective factor [153]. This score was generated based on the “distribution” (the fraction of tumour infiltrated by lymphocytes; 0, <25%, 25-50%, >50%) and the “density” (absent, mild, moderate or severe) of lymphocytes within the tumour sample [153]. *Lymphocyte-specific protein tyrosine kinase* (*LCK*), which is involved in T-lymphocyte signalling, was enriched in samples with a high immune gene expression signature and its protein expression was significantly associated with the lymphocyte score and a more favourable outcome [153]. *Spleen-associated tyrosine kinase* (*SYK*), which is linked to B-lymphocyte signalling, was also upregulated in the immune gene signature but its protein expression was not significantly associated with outcome [153].

The melanoma microenvironment may also be affected by ageing [260]. A recent study reported that melanomas grew at a slower rate but were associated with increased angiogenesis and lung metastases in older versus younger mice [260]. Decreased proliferation and increased melanoma cell invasion were recorded for melanoma cells grown in a medium conditioned with aged rather than young fibroblasts (obtained from donors >55 and <35 years of age, respectively) [260].

The POS was identified as an independent prognostic factor in survival analyses (Chapter 4) in my study. For every percentage increase in stroma, there was a corresponding 1% decreased risk of melanoma-specific death, adjusting for age, sex, the site of primary melanoma, AJCC stage, melanoma cell structure and the extent of the core immune cell infiltrate (adjusted HR for the POS 0.99, 95% CI 0.98-0.99, Cox proportional hazards model, p=0.005). As a novel histopathological biomarker for primary cutaneous melanoma, this observation appeared to be worth exploring further. The prognostic effect of stromal content has previously been reported for several cancers. In the majority of studies, a high proportion of stroma is associated with a poor prognosis, while in a minority, it is protective. Cancers in which a higher quantity of stroma has been reported to be associated with a worse prognosis include colorectal cancer [137, 139, 141, 261], oesophageal squamous cell carcinoma [140], gastric [142], ovarian [138, 262], non-small cell lung cancer [134], hepatocellular carcinoma [135] and triple-negative breast cancer [131]. Stromal cells have also been reported to have a pro-tumoural effect in follicular lymphoma [263]. Conversely, a higher stromal content is associated with a better outcome in oestrogen receptor-positive breast cancer [136] and lung adenocarcinoma [264], while it is of no proven prognostic value in inflammatory breast cancer [265] and laryngeal squamous cell carcinoma [266]. A worse outcome has been observed in early stage cervical adenocarcinoma for cases with a higher proportion of stroma but the latter was not an independent predictor, although the sample size was small [267].

These findings suggest that the contribution of the stromal compartment might be tissue/tumour-specific. There is some evidence, albeit limited, that the composition and nature of the stroma may vary by location, for example, renal, colon and prostate cell lines have been reported to be more responsive to immunotherapy and less vascularised when inoculated into a subcutaneous rather than a visceral site [268].

The diverse observed effects of stromal content may be attributable to experimental variation. The reported studies utilised different methods to quantify the stromal content (e.g. systematic random sampling using a microscope with an eyepiece graticule containing a grid or digital methods, e.g. RandomSpot©) [185]. The lack of a consistent approach in the estimation of the relative proportions of stroma and tumour has led to controversy regarding the best method to use [265, 269]. Furthermore, Webster *et al.* used automated image analysis to quantify the amount of stroma within biobank specimens, which included 70 melanomas [145]. However, the automated technique failed to analyse 10/70 (14%) cases [145]. They found that the median percentage of stroma was about 26% (range 0.2%-93.2%) in melanoma [145]. Recently, Rashed *et al.* reported that the density of melanoma cells, estimated at the site of the Breslow

thickness measurement, was an independent predictor of melanoma-specific death in a series of 100 cases of primary cutaneous melanoma [270]. Cases with a higher melanoma cell density had an increased risk of melanoma-specific death [270]. Using a light microscope, they recorded an “eyeball” measure of melanoma cell density to the nearest 5% [270].

Moreover, there are reported differences in how stroma is described qualitatively, i.e. there are variable definitions for stroma. Some studies have considered the cellular and structural components, while others have largely addressed the latter. Where the structural component was considered important, there was variation in how different “types” of collagen were reported. Smolle *et al.* studied the density and calibre of collagen fibres in 12 melanomas and 12 melanocytic naevi, using automated image analysis of azan trichrome-stained sections (which stains collagen fibres blue) [143]. They found that collagen was more abundant towards the periphery of both melanomas and benign melanocytic naevi and that the calibre of collagen fibres was greater at the periphery than at the centre of melanomas, although there was no significant difference in the collagen fibre diameter within naevi between the centre and the periphery [143]. Collagen of the surrounding reticular dermis was thicker still [143]. Moreover, benign melanocytic naevi contained more collagen than the melanomas and the collagen had a more delicate appearance in the former [143]. The study size was small and failed to account for the thickness of the melanomas (which were >1mm thick) and of the naevi [143]. It is possible that the observed differences were due to naevi occupying the papillary dermis, compared to melanomas, which most likely invaded the reticular dermis [143]. Nonetheless, the observations are interesting and suggest the possibility that intrinsic differences in the quantity of stroma may exist between naevi and melanomas. Melanomas with a greater quantity (as opposed to diameter) of collagen might more closely resemble benign naevi biologically and thus, have a better prognosis. However, the way in which the POS was estimated using RandomSpot© did not account for the collagen fibre diameter and, therefore, it is also possible that a higher POS reflects thicker rather than more abundant collagen fibres within melanoma.

Although I reported that the POS was protective for melanoma death in my study, Smolle *et al.* reported that the presence of an increased area of “pre-existing” collagen (>0.13mm^2) within primary melanomas (n=267), as measured by automated image analysis of H&E sections, was significantly hazardous for survival, however, it lost statistical significance after adjusting for Breslow thickness in a multivariable survival analysis [144]. They identified the tumour stroma as being “wavy” in consistency, having abundant fibroblasts and inflammatory cells, and forming septa between tumour

nests, whereas they considered pre-existing collagen to be thicker, more compact and acellular [144]. The authors noted a weak, positive correlation between the area of the collagen and Breslow thickness [144]. The algorithm used by Smolle *et al.* did not measure the “fine collagenous structures of the stroma itself” [144] but instead, was based on the automated recognition of a previously digitally annotated collagen fibre, to retain only “pre-existing collagen fibres from the reticular dermis” in the measurement [144]. This might account for the incongruity between their results and mine. In addition, I would suspect that the distinction of pre-existing collagen from the tumour stroma is likely to be subjective, although they report >95% concordance between observers [144]. My measurement of the POS included both immune cells, and collagen that was located between tumour cells. It is therefore likely that the measures Smolle *et al.* refer to are not directly comparable to mine because of the aforementioned differences and because it appears that they did not include immune cells in their score. Indeed, the same authors studied 344 cutaneous/subcutaneous melanoma metastases and found that the presence of a peripheral fibrous capsule, or fibrous septa and fibroblasts within the tumour were associated with a better outcome [271]. Conversely, the incorporation of pre-existing collagen from the reticular dermis or adipocytes within the metastases were indicative of an increased risk of death [271]. Bioinformatics techniques can also be employed to gauge the relative proportions of tumour and stroma within samples. A recent pan-cancer analysis of tumour purity, applied a series of bioinformatics algorithms to analyse the transcriptomes of 21 cancers within the Cancer Genome Atlas (TCGA) data set [272]. A tumour purity of >90% was found in only 12% cutaneous melanomas, while a tumour purity <60% was present in 20% of cases [272]. Sampling from disparate regions of the same tumour generated similar results for tumour purity [272]. These findings must be interpreted in the context of the data set, however, which was largely composed of metastatic melanoma samples. One of the programmes utilised in the TCGA study was ESTIMATE, i.e. Estimation of STromal and Immune cells in MAlignant Tumour tissues using Expression data [169]. This is an algorithm that generates immune and stromal scores based on gene expression signatures, derived through a process of gene filtering [169]. These scores are then combined as the ESTIMATE score, from which the tumour purity score is derived [169]. The TCGA and public databases were used to identify >10,000 commonly expressed genes [169]. The immune score was determined as follows: genes that were enriched (2-fold higher expression) in haematopoietic cells compared to other normal cells were retained [169]; leukocyte methylation scores (in ovarian carcinoma) were used to identify genes that were differentially expressed between samples containing high versus low immune cell infiltration [169]; overlapping genes between the two gene lists were ranked to isolate 141 genes, upon which the

immune score is based [169]. The stromal score was generated as follows: genes that were present in normal, non-haematopoietic cells were compared to genes that were expressed in tumour or stromal samples that had been extracted by laser capture microdissection of breast, colorectal and ovarian cancers [169]; genes that displayed low variation in cancer cell lines or had reduced expression in glioma-like stem cells were then removed from the list, leaving 141 genes to form the basis of the stromal score [169]. The evaluation of the immune and stromal scores across a range of cancers suggested that these signatures were each measuring different components [169]. Furthermore, leukocyte methylation scores were highly correlated with the immune score but not the stromal score [169]. The predicted tumour purity calculated using ESTIMATE was comparable to that obtained using an alternative, DNA copy number based-algorithmic approach, called ABSOLUTE [169, 273]. Disappointingly, there was a weak correlation between the immune, stromal and ESTIMATE scores and the histopathologically-estimated percentage of tumour, stroma and lymphocytes (using H&E sections) [169]. Comparatively poorer correlations were noted between ABSOLUTE and the histopathological estimation of tumour purity [169].

Immune cell subsets within the tumour microenvironment can also be explored using gene expression data. Bindea *et al*. developed a compilation of transcriptomic profiles, based on the existing literature, which were considered to be specific for 28 distinct immune cell subsets and by means of a bioinformatics approach, examined the immune microenvironment of colorectal cancer [174]. They reported that the nature and location of the infiltrating immune cell subsets or the “immunome” was dynamic with respect to cancer progression, indicating a complex relationship between the tumour and its host immune response [174]. This approach has been modified by the Leeds Melanoma Group to better understand the role of the immune response in primary cutaneous melanoma. Dr Jeremie Nsengimana tailored this approach for use in melanoma by filtering out genes that had been reported to be highly expressed by normal melanocytes (as per a publically available database [274]), or genes that had been shown to be highly expressed by melanoma cell lines by previous PhD students within the group. By performing unsupervised clustering of this modified gene list for cases in the Leeds Melanoma Cohort Study, he was able to identify 6 clusters that showed distinctive differences in the expression of genes associated with these immune cell subsets (paper submitted).

In this chapter, I have elected to employ some of these techniques to elucidate the transcriptomic correlates of the stromal compartment. The following aims will be addressed:

- To assess the association between the POS and clinical and histopathological factors for cases in the Leeds Melanoma Cohort Study.
- To establish whether or not combining the POS with AJCC stage (7th edition) [43] could improve the accuracy of the prediction of melanoma-specific death in these primary melanoma cases, by performing ROC curve analyses.
- To investigate the association between the POS and the "immunome", to better understand the contribution of the immune cell component of the POS.
- To examine the association between the histopathological estimate of the POS and ESTIMATE [169], which utilises gene expression signatures to calculate immune, stromal and tumour purity scores.
- To explore the association between the POS and the corresponding primary melanoma transcriptome, derived from TMA core biopsies of formalin-fixed, paraffin-embedded (FFPE) tumour, using an agnostic approach.
- To assess whether or not there is a statistical interaction between the POS, the transcriptome and melanoma-specific death.
- To employ an agnostic approach to assess the association between the extent of both the core immune cell and lymphocytic infiltrates, independently, and the transcriptome.
- To delineate the top biological pathways that are up- and/or downregulated in association with each of the following: the POS, the extent of the core immune cell and lymphocytic infiltrates, separately, and as a comparative experiment, by performing enrichment analyses using MetaCore™ (version 6.28, © 2016 Thomson Reuters).

5.2 Methods

As previously discussed in Chapter 2, I annotated a 600 micron square onto the virtual pathology image, corresponding to the cored region. Fifty arrowheads were overlaid onto the square, using RandomSpot©. Each arrow was scored as 't' if the arrowhead landed on tumour and 's' if it landed on stroma. Therefore, all tissue that was not tumour was scored as stroma, except for non-informative regions, which were scored as '▪'. Similarly, when an arrowhead landed on squamous epithelium or a hair follicle, it was scored as "▪". As a result, the stromal score consisted of a mixture of different stromal components, including collagen, blood vessels and a variety of immune cells, i.e. lymphocytes, macrophages/melanophages, plasma cells, neutrophils, and eosinophils.

The median and range for the POS was calculated for each of the clinical and histopathological categorical factors. Box and whisker plots were used to graphically illustrate the frequency distribution for the POS by the categorical variable of interest. The Spearman correlation coefficient was calculated to assess the association between the POS and continuous variables, e.g. age at diagnosis. The Wilcoxon rank-sum test was performed to assess the association between the POS and binary variables. The Kruskal-Wallis test was performed to assess the association between the POS and unordered categorical variables with >2 categories. Non-parametric tests for trend were performed to assess the association between the POS and ordered categorical variables.

Receiver operator characteristic (ROC) curves were plotted to estimate the area under the curve for melanoma-specific relapse or death accounted for by the AJCC stage and the POS, alone and combined. This statistical calculation does not take the time to event into account.

Cox proportional hazards models were used to estimate hazard ratios (HR), 95% confidence intervals (95% CI) and p-values for the likelihood of melanoma-specific death. Multivariable survival analyses were performed for the POS, the ESTIMATE score, tumour purity, immune and stromal scores (five multivariable models).

Univariable linear regression models were performed to test whether POS could predict the expression of each Illumina® probe. The mean expression, correlation coefficient, standard error and p-value were calculated. Bonferroni and false discovery rate (FDR) correction methods were applied to correct the p-values for multiple testing. A sensitivity analysis was also performed, excluding outliers for the POS (>87% POS; calculated as being more than 1.5 x interquartile range (IQR) higher than the 75^{th} percentile of the POS).

Similarly, univariable linear regression models were performed firstly to test whether the extent of the core immune cell infiltrate could predict the expression of each Illumina® probe and then to assess whether or not the extent of the core lymphocytic infiltrate could predict the expression of each Illumina® probe, to generate corresponding correlation coefficients, standard errors and p-values. Bonferroni and FDR correction methods were applied to correct the p-values for multiple testing.

The Bonferroni-corrected p-values were used to rank genes that were most significantly associated with each of the following variables: the POS, the test for trend for both the extent of the core immune cell infiltrate and the extent of the core lymphocytic infiltrate. This was selected in preference to the FDR-corrected p-value

because it is a more stringent test and would rationalise the number of genes, thereby identifying the genes that were most significantly associated with the factor of interest.

To establish whether or not there was a statistical interaction between the POS and the transcriptome on melanoma-specific survival, I performed an interaction analysis as follows: I assessed the effect of the POS on melanoma-specific survival in cases with low gene expression and then separately in cases with high gene expression for each of the Illumina® probes. A likelihood ratio test was performed between a statistical model including the interaction between the POS and the gene expression and a model including only the main effects of the POS and the gene expression. The p-value for the interaction was calculated using a likelihood ratio test. Bonferroni and FDR correction methods were applied to correct the p-values for multiple testing.

Unsupervised hierarchical clustering was performed using Cluster 3.0 for the genes that were most significantly associated with the POS or the test for trend for the extent of each of the core immune cell and lymphocytic infiltrates. A Bonferroni-corrected p-value of <0.05 was used as a cut-off point to identify the most highly ranked probes and, where more than one probe was available for a gene, the probe with the highest level of detection was retained. Heat maps were viewed using Java TreeView (v1.1.6r4). Separate enrichment analyses were performed using MetaCore™ (version 6.28, © 2016 Thomson Reuters) for the genes within each cluster for each heat map, in order to identify the pathways that were up- or downregulated in the corresponding cluster.

A comparative enrichment analysis was performed using MetaCore™ (version 6.28, © 2016 Thomson Reuters), to evaluate the pathways associated with the top ranked 1000 genes (with a Bonferroni-corrected p-value of <0.05) for the POS and the test for trend for the extent of the core immune cell and lymphocytic infiltrates.

The ESTIMATE score, tumour purity, immune and stromal scores [169] were generated by Dr Jeremie Nsengimana, using R (version 2.15.3), which I subsequently used for analyses of their association with the POS (by calculating Spearman correlation coefficients) and the effect of the ESTIMATE scores on melanoma-specific survival (using Cox proportional hazards models). Dr Jeremie Nsengimana also performed unsupervised clustering for a gene list modified from Bindea *et al.* [174] to generate the “immunome” clusters, which I then used to analyse for the association with the POS (by performing the Kruskal-Wallis test).

5.3 Results

5.3.1 The percentage of stroma in 702 cases from the Leeds Melanoma Cohort Study

Figure 5.1 shows the frequency distribution for the POS within the cored region. It was notable that the median POS was 32.69%, although values ranged from 0% to 98.1%.

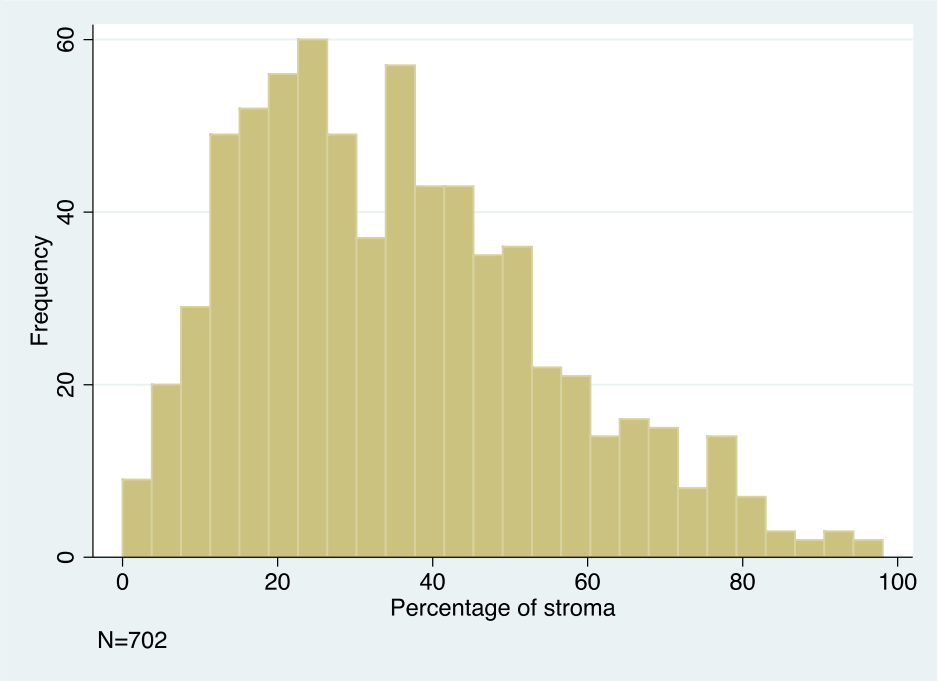

Figure 5.1: Histogram of the percentage of stroma

The frequency distribution of the POS is shown for 702 cases in which the POS was recorded.

Figure 5.2 shows examples of different amounts of stroma within the cored regions.

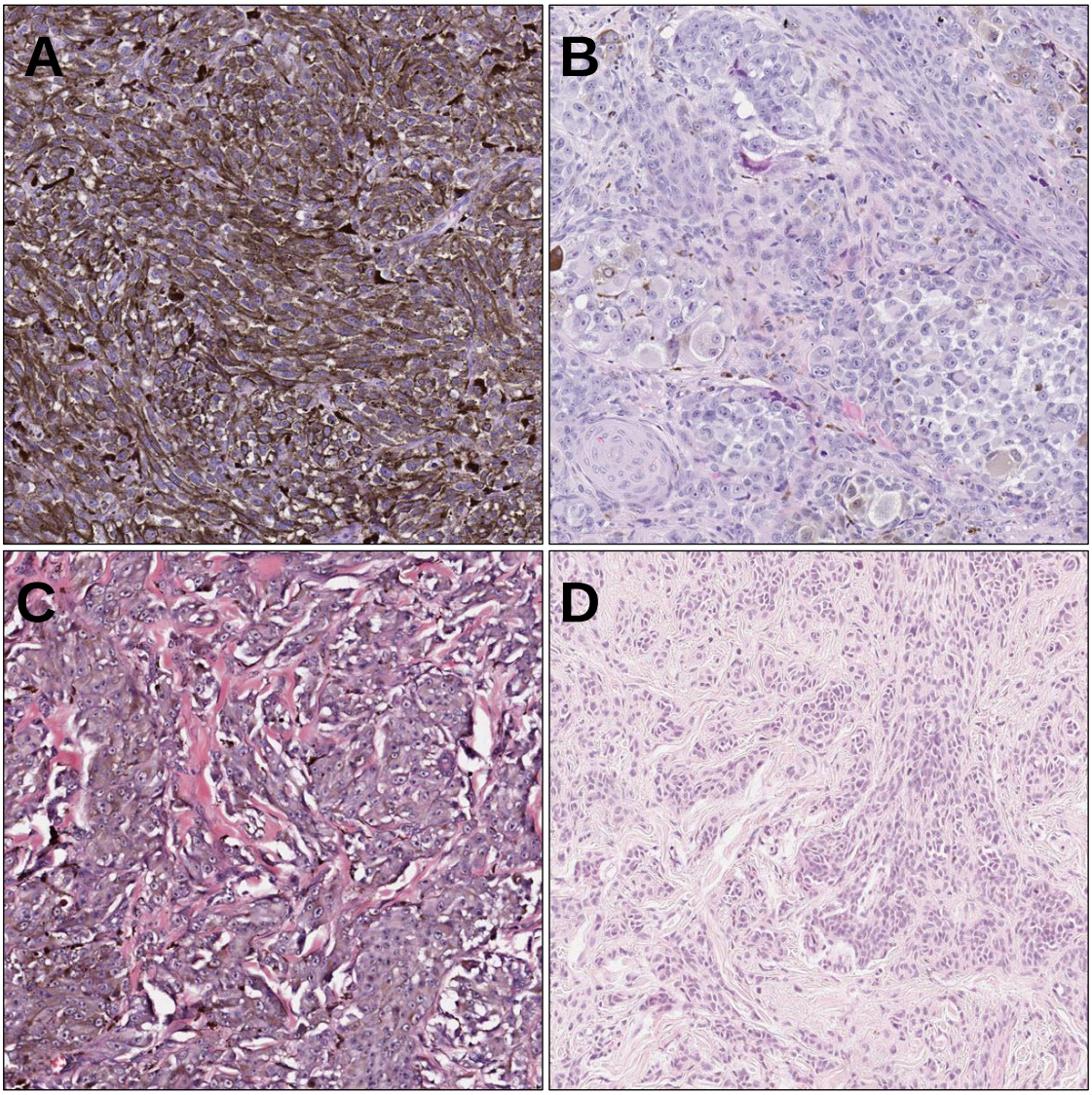

Figure 5.2: Virtual pathology images of digitally-extracted cored regions showing variation in the stromal content of primary melanomas

A) A cored region with a low stromal content (x20 magnification). The POS was 12%. B) A cored region with a moderate stromal content (x20 magnification). The POS was 32%. C) A cored region with abundant stroma (x20 magnification). The POS was 50%. D) A cored region with 68% stroma (x20 magnification).

5.3.2 The percentage of stroma and clinical factors

The POS was associated with several clinical factors (Table 5.1). There was an inverse correlation between the POS and age at diagnosis. Females tended to have a higher POS within their primary melanoma (median POS in females 35.3% and median POS in males 29.7%, Wilcoxon rank-sum, p=0.04). The POS tended to be lower within primary melanomas located on the trunk compared to other sites, although this was not statistically significant. Cases presenting with AJCC stage I melanoma, tended to have a higher POS (stage I, II, III/IV medians 40.4%, 25.5% and 28.8% respectively, non-parametric test for trend, $p<1x10^{-16}$, Figure 5.3**)**. Cases whose primary melanomas harboured a *NRAS* mutation tended to have a lower POS than the *BRAF*-mutated melanomas (median 25.5% and 33.3%, respectively) and this difference was statistically significant (Kruskal-Wallis, p=0.004). Figure 5.4 shows the frequency distribution for the POS for cases with a *BRAF* or *NRAS* mutation or cases that were wild type for both *BRAF* and *NRAS*.

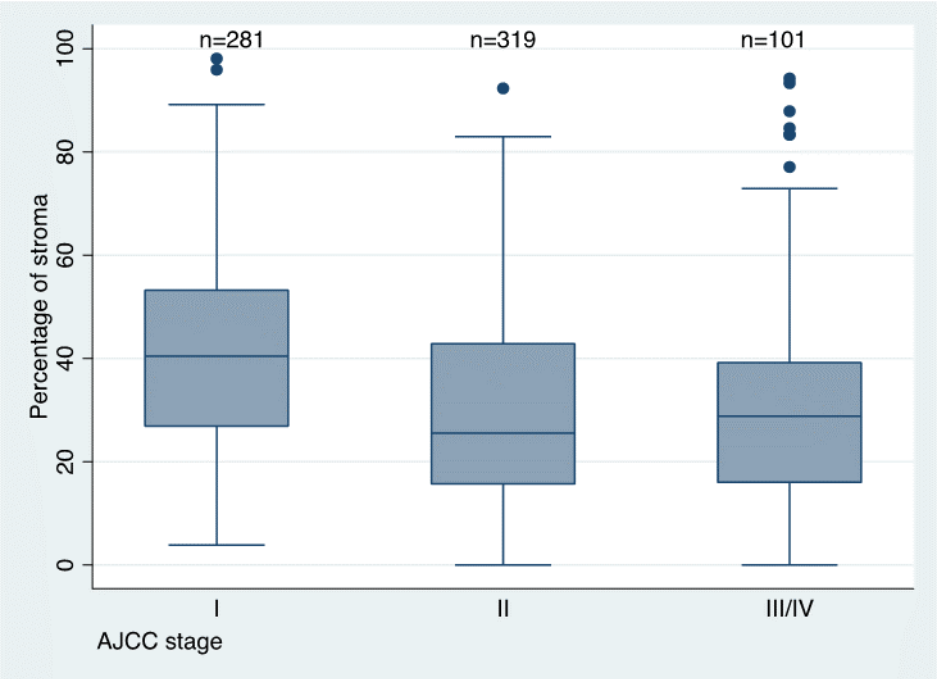

Figure 5.3: Box and whisker plots for the percentage of stroma by AJCC stage

The POS was highest in AJCC stage I melanomas (Table 5.1).

Table 5.1: The median (range) for the percentage of stroma and statistical tests (and corresponding p-values) for the pairwise associations between the percentage of stroma and clinical factors, including *BRAF* and *NRAS* mutation status.

The median percentage of stroma (POS) is not shown for age at diagnosis, which was tested as a continuous variable, for each year at diagnosis. AJCC stage was missing for 1 case and *BRAF*/*NRAS* mutation status was available for 565 cases. The statistic indicates the statistical test performed. Spearman's rho=the Spearman correlation coefficient.

Factor	Number	Median (range)	Statistic	P-value
Age at diagnosis (years)			Spearman's rho = -0.16	0.00002
Sex				
Male	326	29.7 (1.9-95.9)	Wilcoxon rank-sum	0.04
Female	376	35.3 (0-98.1)		
Total	702			
Site of primary melanoma				
Limbs	300	35.3 (0-94.2)	Kruskal-Wallis	0.27
Trunk	237	28.8 (2.0-98.1)		
Head	82	30.8 (3.9-83.0)		
Other	83	32.0 (0-92.3)		
Total	702			
AJCC stage				
I	281	40.4 (3.8-98.1)	Non-parametric test for trend	$<1x10^{-16}$
II	319	25.5 (0-92.3)		
III/IV	101	28.8 (0-94.2)		
Total	701			
Mutation status				
BRAF positive	260	33.3 (1.9-93.3)	Kruskal-Wallis	0.004
NRAS positive	146	25.5 (0-84.6)		
Wild type	159	34.6 (0-98.1)		
Total	565			

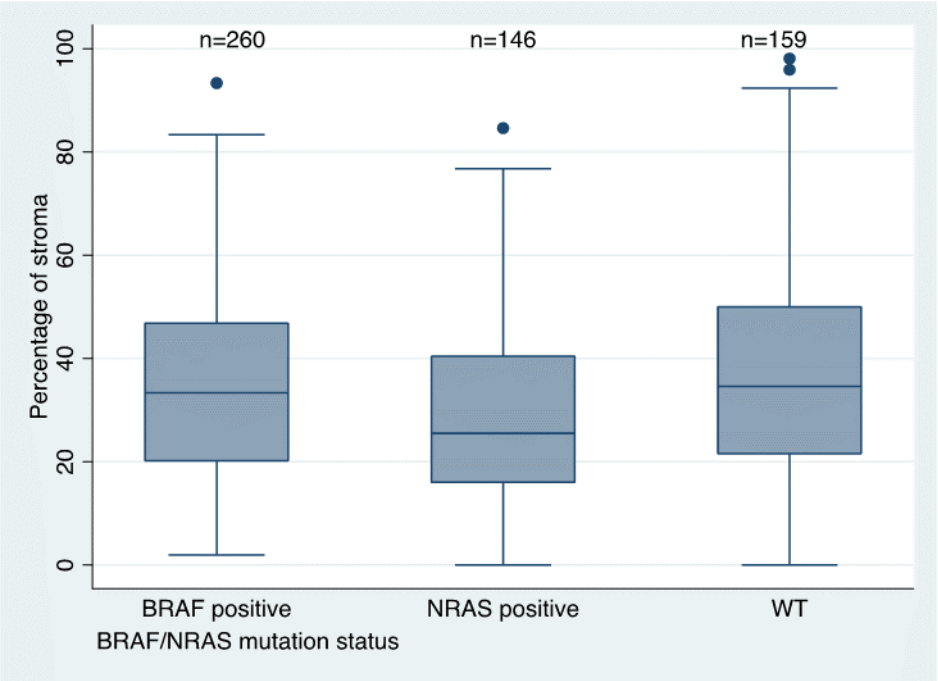

Figure 5.4 Box and whisker plots for the percentage of stroma by *BRAF/NRAS* mutation status

NRAS-mutated melanomas had a lower POS (Table 5.1).

5.3.3 The percentage of stroma and whole-tumour histopathological measures

Table 5.2 shows the median (range) POS in relation to whole-tumour measures and the results of statistical tests for the pairwise associations. There was an inverse relationship between the POS and Breslow thickness, with melanomas ≤1mm thick having the highest amount of stroma and this was highly statistically significant (non-parametric test for trend, $p<1x10^{-16}$). The median POS was 53.1% in cases with a Breslow thickness ≤1mm, compared with 36% for cases 1.01-2mm thick, 25.5% for cases 2.01-4mm thick and 22.9% for melanomas >4mm in thickness (non-parametric test for trend, $p<1x10^{-16}$). Figure 5.5 shows the frequency distribution for the POS by Breslow thickness (using the AJCC 7th edition cut-off points) [43].

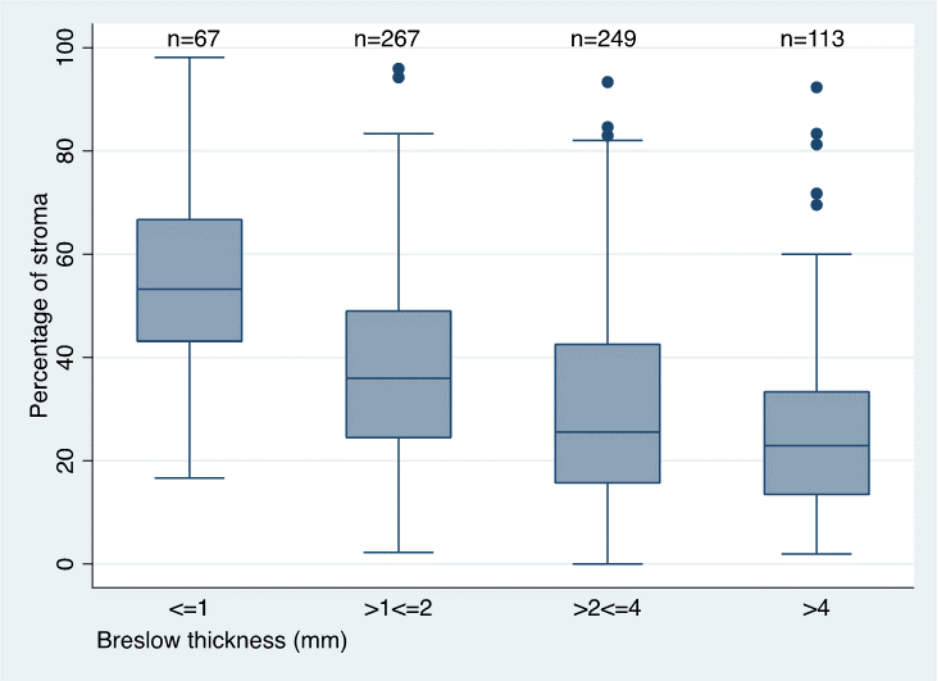

Figure 5.5: Box and whisker plots for the percentage of stroma by Breslow thickness category (using AJCC cut-off points) [43]

There was a significant inverse association between the POS and Breslow thickness (Table 5.2).

Similarly, ulcerated melanomas or melanomas containing a dominant nodule tended to have significantly less stroma (median for ulcerated 24.5% and non-ulcerated 34.7%; median with a dominant nodule 17.3% and without a dominant nodule 34.6%, Table 5.2). It follows that cases with a lesser extent (width) of ulceration (<0.87mm) tended to have more stroma than cases with more extensive ulceration. Interestingly, there was no significant difference in the POS according to the pattern of tumour-infiltrating lymphocytes (TILs; Kruskal-Wallis, p=0.87) or by the presence or absence of tumour loss (Wilcoxon rank-sum, p=0.18). There was a borderline significant association between the POS and the intensity of tumour-infiltrating macrophages/melanophages (TIMs), with melanomas that had lots of TIMs tending to have more stroma compared to cases with none, very few or moderate TIMs (non-parametric test for trend, p=0.05). Melanomas with a brisk pattern of TIMs tended to have more abundant stroma, however, this was not statistically significant (non-parametric test for trend, p=0.16).

Table 5.2: The median (range) for the percentage of stroma and statistical tests (and corresponding p-values) for the association between the percentage of stroma and whole-tumour factors

The Breslow thickness categories were defined using the AJCC cut-off points (7th edition) [43]. The extent of microscopic ulceration was categorised as none and the remaining values were divided into 4 approximately equal categories. The depth of tumour loss and relative tumour loss were categorised in a similar way. The statistic indicates the statistical test performed. The footnote provides the number of cases in which tumour-infiltrating lymphocytes (TILs) and macrophages/melanophages (TIMs) were non-evaluable. This occurred when the entire base of the tumour could not be visualised, e.g. due to shave excision.

Factor	Number	Median (range)	Statistic	p-value
Breslow thickness (mm)				
≤1.00	67	53.1 (16.7-98.1)	Non-parametric test for trend	$<1x10^{-16}$
1.01-2.00	267	36.0 (2.2-95.9)		
2.01-4.00	249	25.5 (0-93.3)		
>4.00	113	22.9 (1.9-92.3)		
Total	696			
Dominant nodule				
No	627	34.6 (0-98.1)	Wilcoxon rank-sum	$5x10^{-11}$
Yes	75	17.3 (1.9-69.6)		
Total	702			
Microscopic ulceration				
No	538	34.7 (1.9-98.1)	Wilcoxon rank-sum	$4x10^{-8}$
Yes	164	24.5 (0-82.0)		
Total	702			
Extent of microscopic ulceration (mm)				
None	538	34.7 (1.9-98.1)	Non-parametric test for trend	$3x10^{-8}$
<0.87	39	28.0 (2.1-82.0)		
0.87-<2.4	40	19.4 (2.2-70.0)		
2.4-<5.15	42	24.3 (0-81.3)		
≥5.15	41	24.0 (0-51.1)		
Total	700			
Tumour-infiltrating lymphocytes				
Absent	49	34.0 (0-80.0)	Kruskal-Wallis	0.87
Non-brisk	501	33.3 (0-94.2)		
Brisk	72	32.4 (3.8-98.1)		
Total	622*			

Factor	Number	Median (range)	Statistic	p-value
Tumour loss				
No	573	33.3 (0-92.3)	Wilcoxon rank-sum	0.18
Yes	124	29.0 (3.8-98.1)		
Total	697			
Type of tumour loss				
None	573	33.3 (0-92.3)	Kruskal-Wallis	0.15
Deep	56	34.0 (3.8-98.1)		
Both	21	22.9 (9.8-94.2)		
Superficial	46	27.6 (4.4-95.9)		
Total	696			
Depth of tumour loss (mm)				
None	573	33.3 (0-92.3)	Non-parametric test for trend	0.07
<0.71	38	32.1 (4.4-89.2)		
0.71-<1.14	30	38.4 (6.3-98.1)		
1.14-<1.63	24	30.7 (8.5-60.0)		
≥1.63	32	28.8 (3.8-84.6)		
Total	697			
Relative tumour loss (mm)				
None	570	33.3 (0-92.3)	Non-parametric test for trend	0.5
<0.26	35	19.2 (4.4-65.0)		
0.26-<0.52	29	25.0 (7.7-93.3)		
0.52-<0.786	33	36.0 (3.8-95.9)		
≥0.786	26	37.1 (5.8-98.1)		
Total	693			
Tumour-infiltrating macrophages/melanophages				
None	236	32.2 (0-92.3)	Non-parametric test for trend	0.05
Very few	245	31.7 (1.9-95.9)		
Moderate	148	32.0 (0-98.1)		
Lots	67	37.3 (2.6-94.2)		
Total	696			
Pattern of tumour-infiltrating macrophages/melanophages				
Absent	133	32.0 (3.8-83.3)	Non-parametric test for trend	0.16
Non-brisk	485	33.3 (0-98.1)		
Brisk	5	54.5 (19.6-76.7)		
Total	623**			

* Tumour-infiltrating lymphocytes could not be assessed in 76 patients

** Pattern of tumour-infiltrating macrophages/melanophages could not be assessed in 75 patients

5.3.4 The percentage of stroma and cored region histopathological measures

Table 5.3 shows the median (range) POS and its pairwise associations with the cored region measures. Cases with a "mixed" quality of stroma tended to have a higher POS (Kruskal-Wallis, p=0.01). Cores with balloon cells tended to have a sparse amount of stroma but there were only 2 cases in this category (Kruskal-Wallis, p=0.01). As expected, cores with a structure classified as "sheets" tended to have the least amount of stroma (Kruskal-Wallis, p=0.0001). An increasing degree of melanoma cell pigmentation within the core was associated with a higher POS (non-parametric test for trend, p=0.00005). The presence of a core immune cell infiltrate and its increasing extent were each significantly associated with a higher POS (The median POS was 62.6% for cases with lots of immune cells within the cored region, compared to 24% for none, 34.7% for some and 41.6% for moderate, non-parametric test for trend, $p<1x10^{-16}$). Figure 5.6 shows the frequency distribution for the POS by the extent of the core immune cell infiltrate.

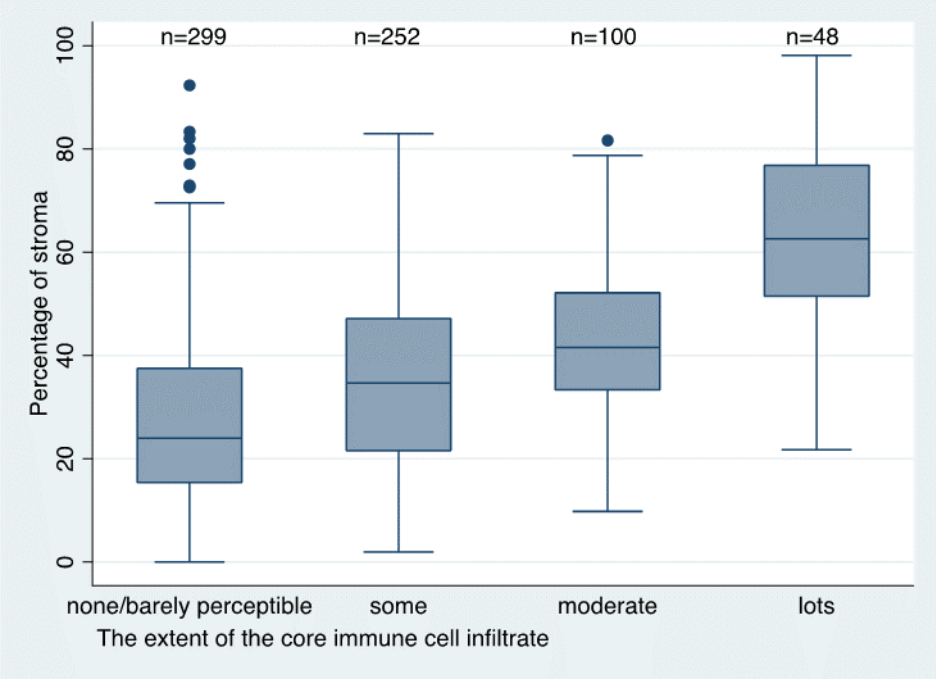

Figure 5.6: Box and whisker plots for the percentage of stroma by the extent of the core immune cell infiltrate

There was a significant association between the POS and the increasing extent of the core immune cell infiltrate (Table 5.3).

Table 5.3: The median (range) for the percentage of stroma and statistical tests (and corresponding p-values) for the association between the percentage of stroma and cored region factors

The core immune cell infiltrate was recorded as absent (no) or present (yes). If the core immune cell infiltrate was considered to be barely perceptible, further assessment of the presence and extent of the core immune cell subsets (e.g. lymphocytes) was not performed. Therefore, the "yes" category for the core immune cell infiltrate contained cases for which the extent was barely perceptible, some, moderate or lots. The core immune cell infiltrate is divided into no, barely perceptible and yes in order to provide more detail. The POS was similar for cores with an absent or barely perceptible immune cell infiltrate and therefore, the no/barely perceptible categories were merged. Similar hazard ratios had also been shown for these two categories in univariable survival analyses (Chapter 4). This no/barely perceptible core immune cell infiltrate was then used as the baseline for subsequent immune cell categories, e.g. the location of the immune cell infiltrate, the core lymphocytic infiltrate. Categories for core mitoses and core blood vessels were assigned on the basis of 3 approximately equal groups (tertiles). The statistic indicates the statistical test performed.

Factor	Number	Median (range)	Statistic	p-value
Quality of the stroma				
Compact (Figure 2.15)	595	33.3 (0-98.1)	Kruskal-Wallis	0.01
Loose	22	37.2 (12.5-87.9)		
Mixed	34	49.4 (4.4-89.2)		
Total	651			
Melanoma cell shape				
Round/ovoid/epithelioid	602	32.6 (0-98.1)	Kruskal-Wallis	0.01
Spindle	60	27.5 (0-94.2)		
Super spindle	14	38.6 (22.0-92.3)		
Naevoid	16	39.6 (14.6-81.0)		
Plasmacytoid	6	53.8 (29.2-65.3)		
Balloon	2	17.2 (11.5-22.9)		
Total	700			
Melanoma cell structure				
Nests	413	36.5 (3.8-98.1)	Kruskal-Wallis	0.0001
Sheets	134	19.4 (0-84.6)		
Fascicles	127	28.8 (3.8-94.2)		
Dispersed	21	69.6 (28.1-95.9)		
Total	695			

Factor	Number	Median (range)	Statistic	p-value
Melanoma cell pigmentation				
Absent	522	30.6 (0-95.9)	Non-parametric test for trend	0.00005
Faint	45	29.8 (5.8-80.0)		
Moderate	82	37.2 (10.6-93.3)		
High	46	42.0 (1.9-98.1)		
Very high	5	36.0 (28.3-94.2)		
Total	700			
Immune cell infiltrate (categorised)				
No	33	21.6 (5.8-68.1)	Non-parametric test for trend	$<1x10^{-16}$
Barely perceptible	266	24.5 (0-92.3)		
Yes	400	38.5 (1.9-98.1)		
Total	699			
Extent of immune cell infiltrate				
No/barely perceptible immune cell infiltrate	299	24.0 (0-92.3)	Non-parametric test for trend	$<1x10^{-16}$
Some	252	34.7 (1.9-83.0)		
Moderate	100	41.6 (9.8-81.6)		
Lots	48	62.6 (21.7-98.1)		
Total	699			
Location of immune cell infiltrate				
No/barely perceptible immune cell infiltrate	299	24.0 (0-92.3)	Kruskal-Wallis	0.0001
At the tumour/stroma interface	126	35.3 (1.9-83.0)		
Dispersed between tumour cells	150	40.6 (2.2-98.1)		
Both	122	42.7 (4.4-81.0)		
Total	697			
Lymphocytic infiltrate				
No/barely perceptible immune cell infiltrate	299	24.0 (0-92.3)	Non-parametric test for trend	$<1x10^{-16}$
No	132	30.7 (1.9-84.6)		
Yes	267	44.0 (4.4-98.1)		
Total	698			
Extent of lymphocytic infiltrate				
No/barely perceptible immune cell infiltrate	299	24.0 (0-92.3)	Non-parametric test for trend	$<1x10^{-16}$
No	132	30.7 (1.9-84.6)		
Some	179	38.5 (4.4-94.2)		
Moderate	47	44.2 (12.5-81.6)		
Lots	41	60.8 (26.9-98.1)		
Total	698			

Factor	Number	Median (range)	Statistic	p-value
Plasma cell infiltrate				
No/barely perceptible immune cell infiltrate	299	24 (0-92.3)	Non-parametric test for trend	$<1x10^{-16}$
No	384	38.5 (1.9-98.1)		
Yes	14	44.3 (7.7-78.7)		
Total	697			
Extent of plasma cell infiltrate				
No/barely perceptible immune cell infiltrate	299	24.0 (0-92.3)	Non-parametric test for trend	$<1x10^{-16}$
None	384	38.5 (1.9-98.1)		
Some	12	44.3 (7.7-78.7)		
Moderate	0	-		
Lots	2	39.5 (28.0-51.0)		
Total	697			
Macrophage/melanophage infiltrate				
No/barely perceptible immune cell infiltrate	299	24.0 (0-92.3)	Non-parametric test for trend	$4x10^{-16}$
No	121	40.0 (4.4-95.9)		
Yes	278	38.0 (1.9-98.1)		
Total	698			
Extent of macrophage/melanophage infiltrate				
No/barely perceptible immune cell infiltrate	299	24.0 (0-92.3)	Non-parametric test for trend	$2x10^{-16}$
None	121	40.0 (4.4-95.9)		
Some	118	36.8 (2.2-98.1)		
Moderate	112	37.3 (1.9-81.6)		
Lots	48	51.0 (14.3-94.2)		
Total	698			
Neutrophilic infiltrate				
No/barely perceptible immune cell infiltrate	299	24.0 (0-92.3)	Non-parametric test for trend	$<1x10^{-16}$
No	386	38.8 (1.9-98.1)		
Yes	12	37.5 (15.7-81.3)		
Total	697			
Extent of neutrophilic infiltrate				
No/barely perceptible immune cell infiltrate	299	24.0 (0-92.3)	Non-parametric test for trend	$<1x10^{-16}$
None	386	38.8 (1.9-98.1)		
Some	12	37.5 (15.7-81.3)		
Moderate	0	-		
Lots	0	-		
Total	697			

Factor	Number	Median (range)	Statistic	p-value
Eosinophilic infiltrate				
No/barely perceptible immune cell infiltrate	299	24.0 (0-92.3)	Non-parametric test for trend	$<1x10^{-16}$
No	396	38.5 (1.9-98.1)		
Yes	2	41.4 (23.9-59.0)		
Total	697			
Extent of eosinophilic infiltrate				
No/barely perceptible immune cell infiltrate	299	24.0 (0-92.3)	Non-parametric test for trend	$<1x10^{-16}$
None	396	38.5 (1.9-98.1)		
Some	2	41.4 (23.9-59.0)		
Moderate	0			
Lots	0			
Total	697			
Core mitoses (tertiles)				
0	206	45.0 (10.4-98.1)	Non-parametric test for trend	$<1x10^{-16}$
1-2	257	33.3 (0-84.6)		
≥3	232	20.9 (0-76.9)		
Total	695			
Core blood vessels				
0	122	33.0 (0-93.3)	Non-parametric test for trend	0.91
1-2	264	34.0 (1.9-98.0)		
≥3	314	31.3 (0-95.9)		
Total	700			

Cores that had immune cells which were both dispersed between tumour cells and at the tumour/stroma interface tended to have more stroma (Kruskal-Wallis, p=0.0001). Cases with a lymphocytic infiltrate within the cored region had a higher POS compared to cases without a lymphocytic infiltrate or to cases with an absent or minimal (no/barely perceptible) immune cell infiltrate within the core (non-parametric test for trend, $p<1x10^{-16}$). Similarly, an increasing abundance (extent) of lymphocytes within the core was associated with a higher POS (non-parametric test for trend, $p<1x10^{-16}$). Figure 5.7 shows the frequency distribution for POS by the extent of the lymphocytic infiltrate within the cored region.

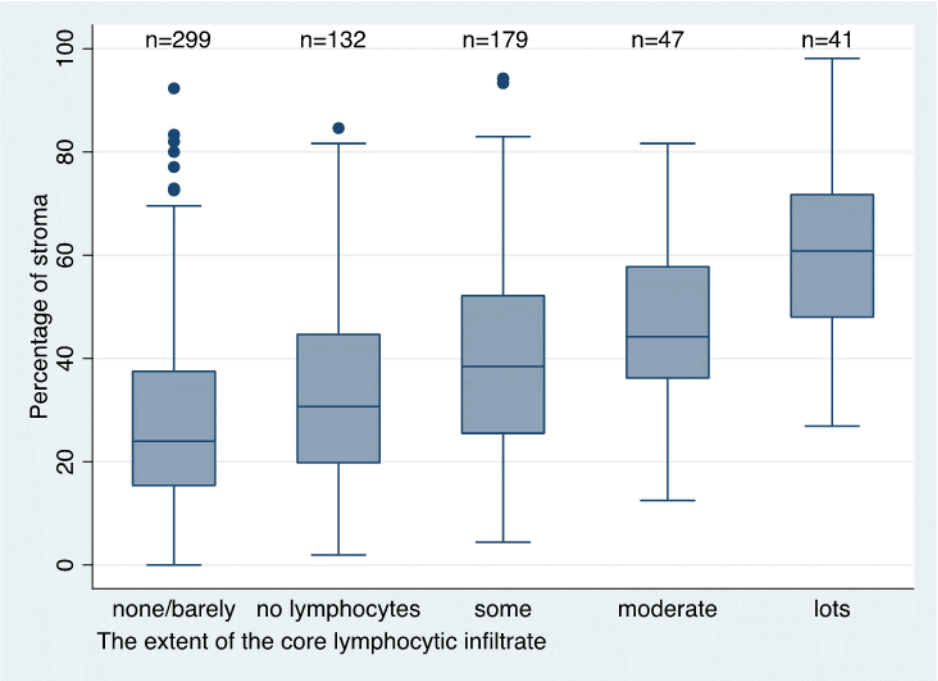

Figure 5.7: Box and whisker plots for the percentage of stroma by the extent of the core lymphocytic infiltrate

There was a significant trend for an increasing POS in association with an increasing extent of lymphocytes within the core (non-parametric test for trend, $p<1x10^{-16}$, Table 5.3).

Few cases had plasma cells, neutrophils or eosinophils within the cored region, indicating that these immune cells were infrequently encountered in the advancing part of the melanoma, which had been selected for TMA sampling and, therefore, by definition had the least amount of immune cells/stroma. There was a trend for an increasing extent of core macrophages/melanophages to have a higher POS (non-parametric test for trend, $p=2x10^{-16}$). There was a highly significant inverse relationship between the POS and the number of core mitoses. The POS was lowest in cores with ≥3 mitoses (20.9%), compared to 33.3% for cores with 1-2 mitoses and 45% where no mitoses were recorded within the core (non-parametric test for trend, $p<1x10^{-16}$) but no significant difference was seen for the number of blood vessels within the core (non-parametric test for trend, p=0.91). Figure 5.8 shows the frequency distribution of the POS by the number of core mitoses (tertiles).

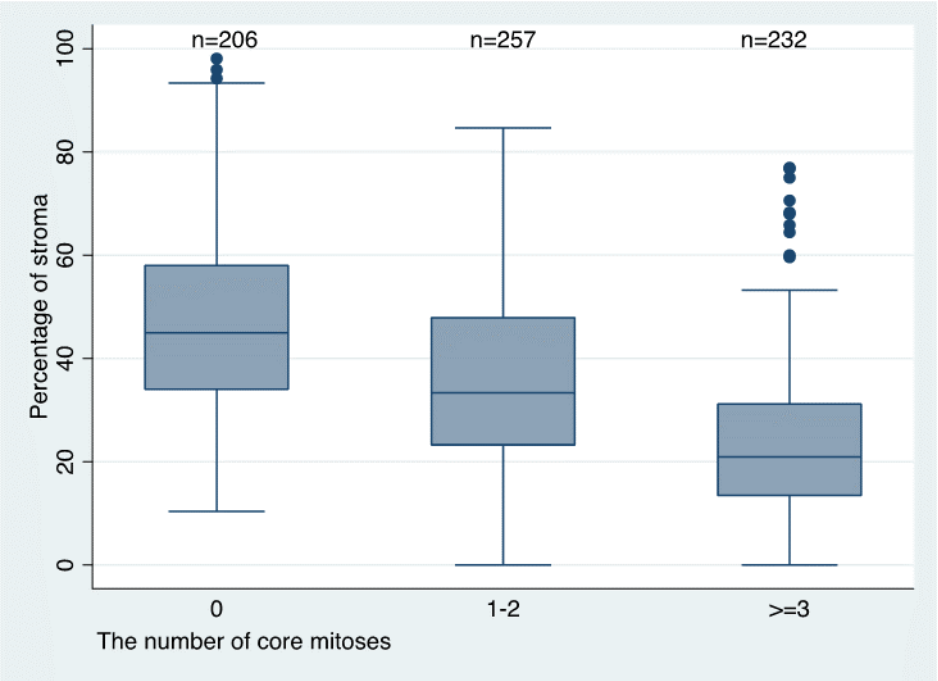

Figure 5.8: Box and whisker plots for the percentage of stroma by the number of core mitoses (tertiles)

A significant inverse association with the number of mitoses within the cored region was noted (Table 5.3).

5.3.5 The percentage of stroma and melanoma relapse

ROC curves for melanoma relapse showed that AJCC stage alone accounted for 67% of the area under the curve, whilst the POS alone contributed to 63%. When combined, the prognostic effect was increased, such that AJCC stage and the POS predicted melanoma relapse accurately 70% of the time (Figure 5.9).

5.3.6 The percentage of stroma and melanoma-specific survival

Similarly, ROC curves showed that AJCC stage accounted for 67% of the area under the curve for melanoma-specific death, whilst POS alone accounted for 64%. The effect of AJCC stage and the POS was additive, predicting melanoma-specific death accurately 70% of the time (Figure 5.10).

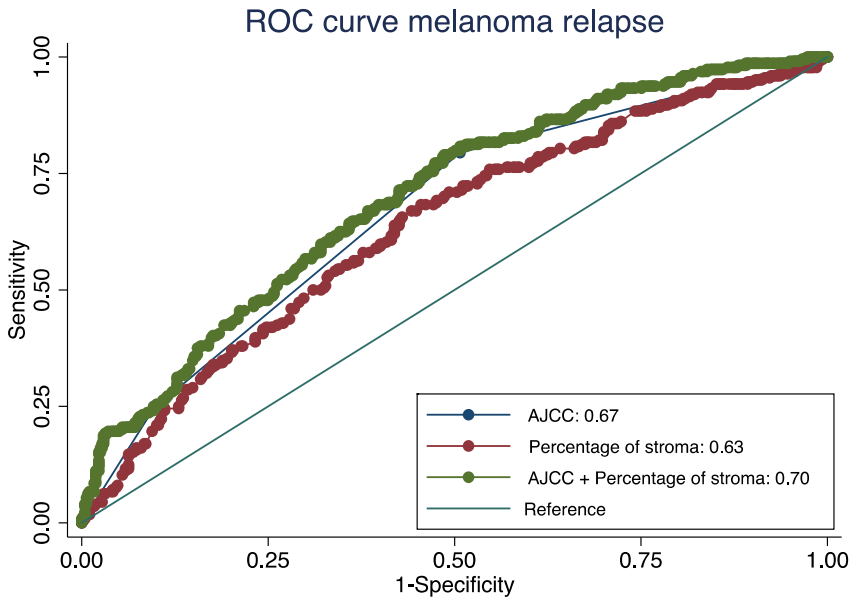

Figure 5.9: Receiver operator characteristic curves for the effect of AJCC stage alone, the percentage of stroma alone and AJCC stage and the percentage of stroma combined on melanoma relapse

The predictive power was improved by the addition of the POS to AJCC stage (increasing by 3%) compared to AJCC stage alone.

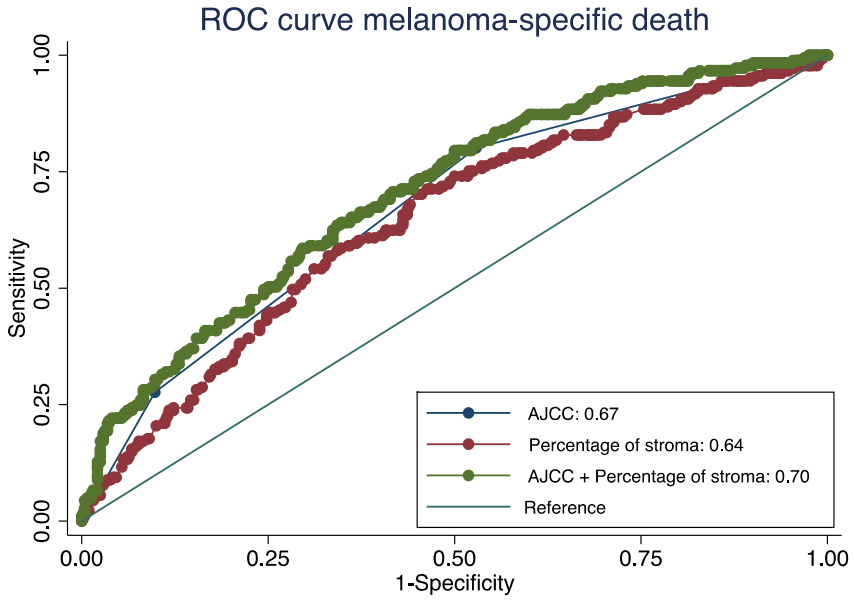

Figure 5.10: Receiver operator characteristic curves for the effect of AJCC stage alone, the percentage of stroma alone and AJCC stage and the percentage of stroma combined on melanoma-specific death

The predictive power was improved by the addition of the POS to AJCC stage (increasing by 3%) compared to AJCC stage alone.

5.3.7 The percentage of stroma and the "immunome"

In order to better understand the relationship between the POS and the immune cell components, I assessed the association between the POS and the six "immunome" clusters. These clusters were derived by Dr Jeremie Nsengimana (Section 5.2). Cluster 4 had the worst outcome and the lowest gene expression for immune cells relative to the other clusters (data not shown). Figure 5.11 shows the heat map for the unsupervised clustering analysis of the modified immunome gene list in 703 cases from the Leeds Melanoma Cohort Study.

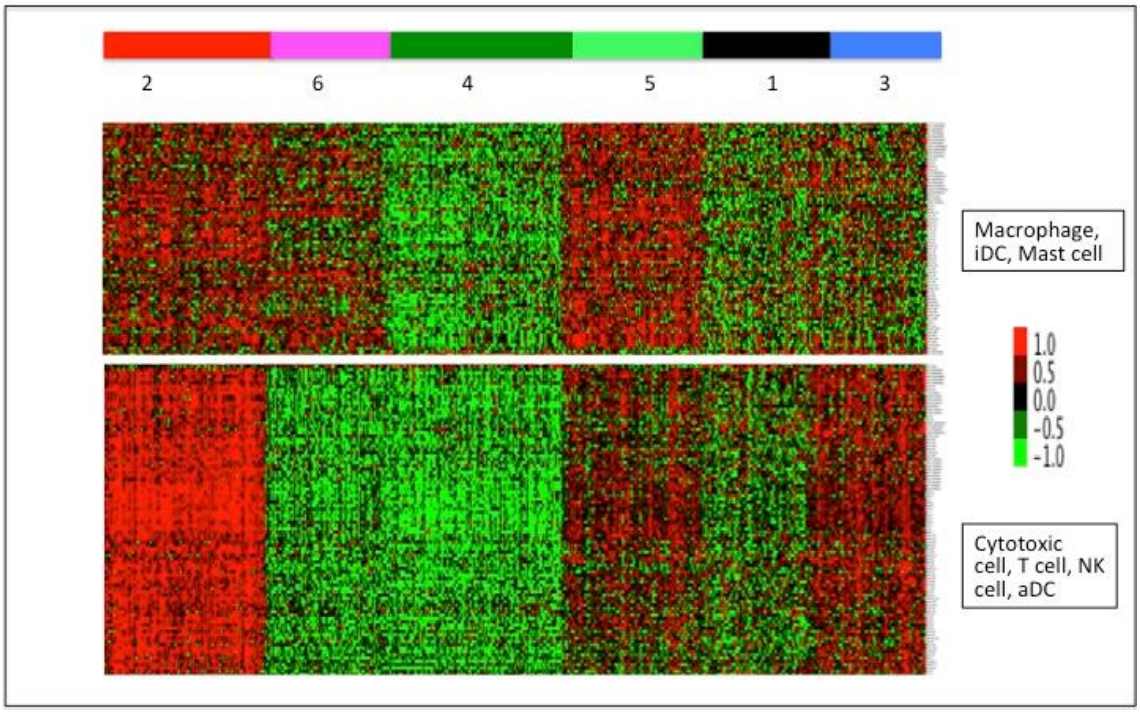

Figure 5.11: Heat map for unsupervised clustering of the modified immunome gene list

Two gene clusters (from top to bottom) and 6 distinct tumour clusters are shown (from left to right). The tumour clusters are represented by the labels at the top, numbered 1-6. The uppermost of the two gene clusters is dominated by genes expressed by macrophages, immature dendritic cells (iDCs) and mast cells. The lowermost gene cluster is dominated by genes expressed by cytotoxic cells, T cells, natural killer cells (NK) and activated dendritic cells (aDCs). Red=gene upregulation. Green=gene downregulation.

Figure 5.12 shows the frequency distribution of the POS by the six immunome clusters. Interestingly, cluster 4 also had the lowest median value for the POS and there was a significant association between the POS and the immunome clusters (Figure 5.12).

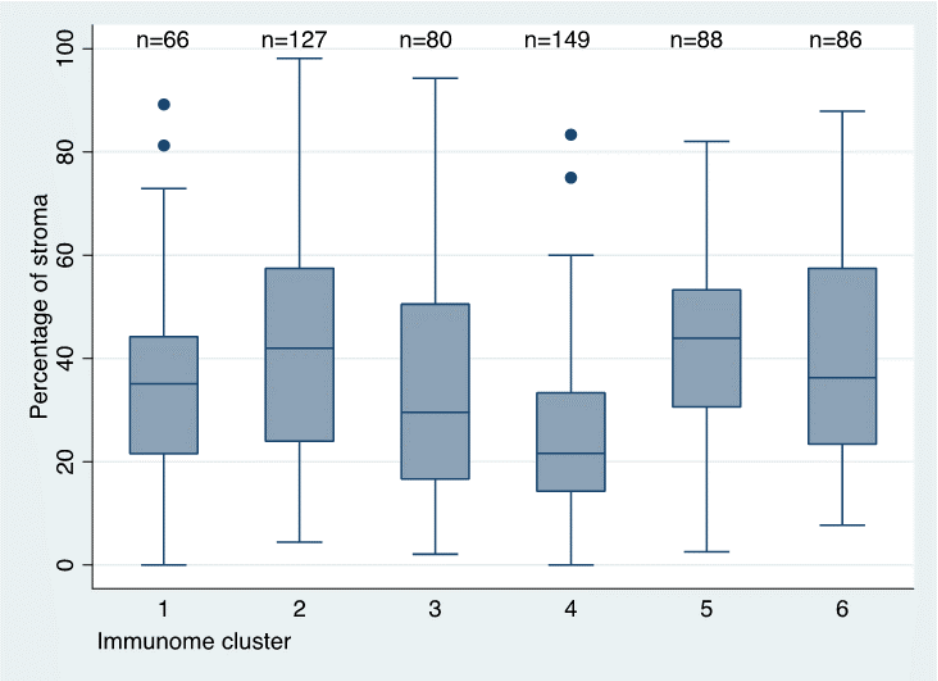

Figure 5.12: Box and whisker plots for the percentage of stroma by the "immunome" clusters

The median POS for the immunome clusters were as follows: 35.1%, 42%, 29.6%, 21.6%, 43.9% and 36.3% for clusters 1, 2, 3, 4, 5 and 6, respectively. There was a significant association between the POS and the immunome clusters (Kruskal-Wallis, p=0.0001).

5.3.8 The percentage of stroma and ESTIMATE

As previously discussed, ESTIMATE produces an ESTIMATE score, which represents the combined immune and stromal scores, and a separate tumour purity score [169]. The frequency distribution for each of these scores is shown in Figure 5.13 - Figure 5.16. The ESTIMATE scores were generated by Dr Jeremie Nsengimana, using R (version 2.15.3).

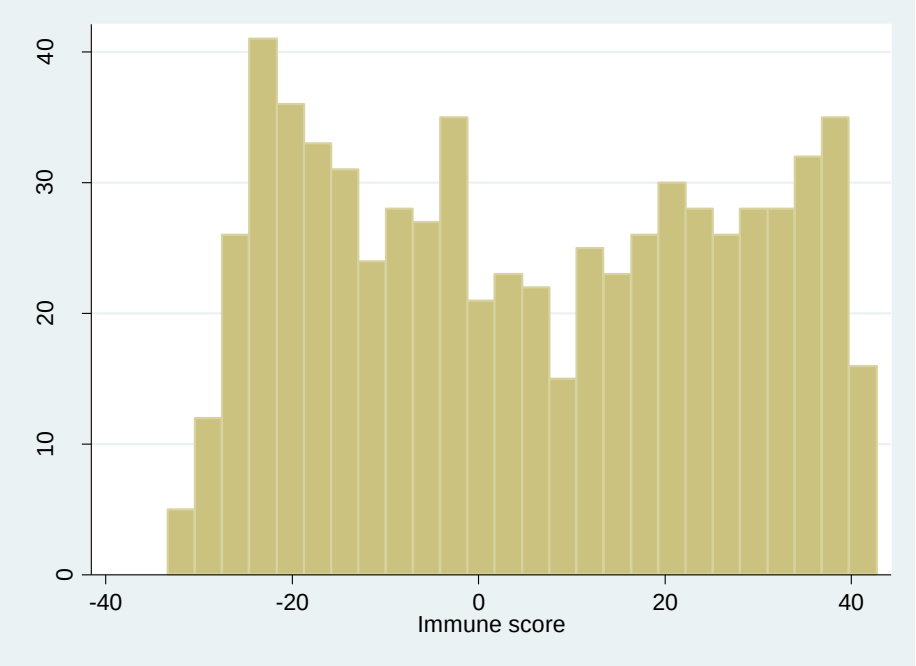

Figure 5.13: Histogram of the immune score

The histogram shows the frequency distribution of the immune score (n=676) produced by ESTIMATE, which has a bimodal appearance. The score was generated based on the expression of 141 immune genes.

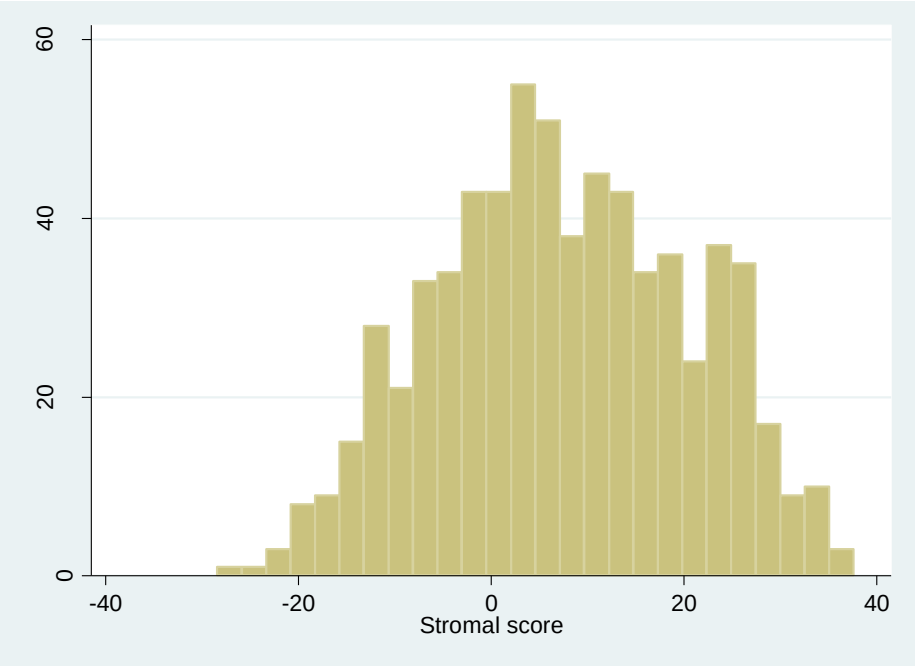

Figure 5.14: Histogram of the stromal score

The histogram shows the frequency distribution of the stromal score (n=676), which follows a normal distribution. This score was produced by ESTIMATE and was based on the expression of 141 stromal genes.

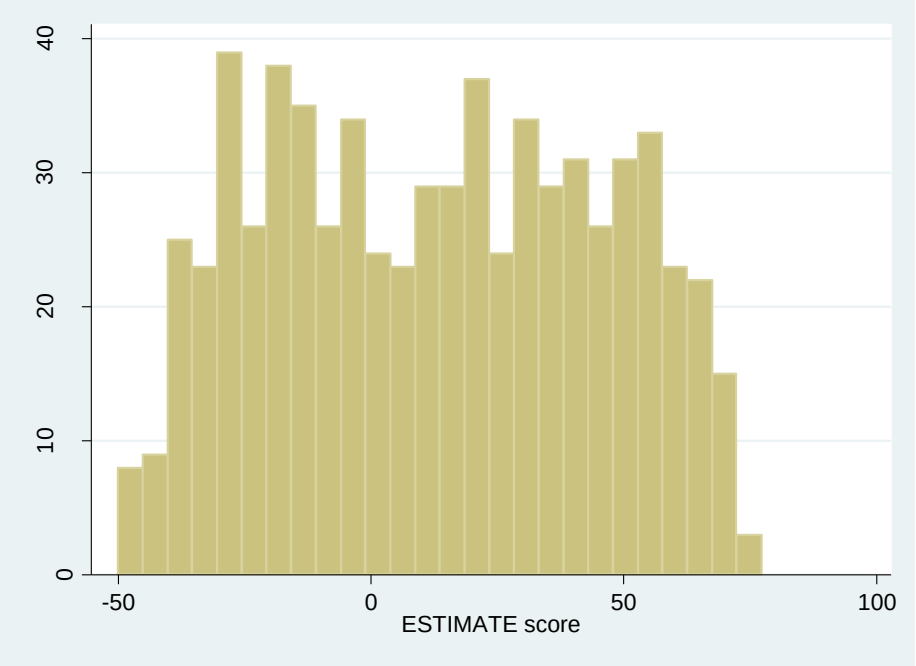

Figure 5.15 Histogram of the ESTIMATE score

The histogram shows the frequency distribution for the ESTIMATE score (n=676), which represents the addition of the immune and stromal scores.

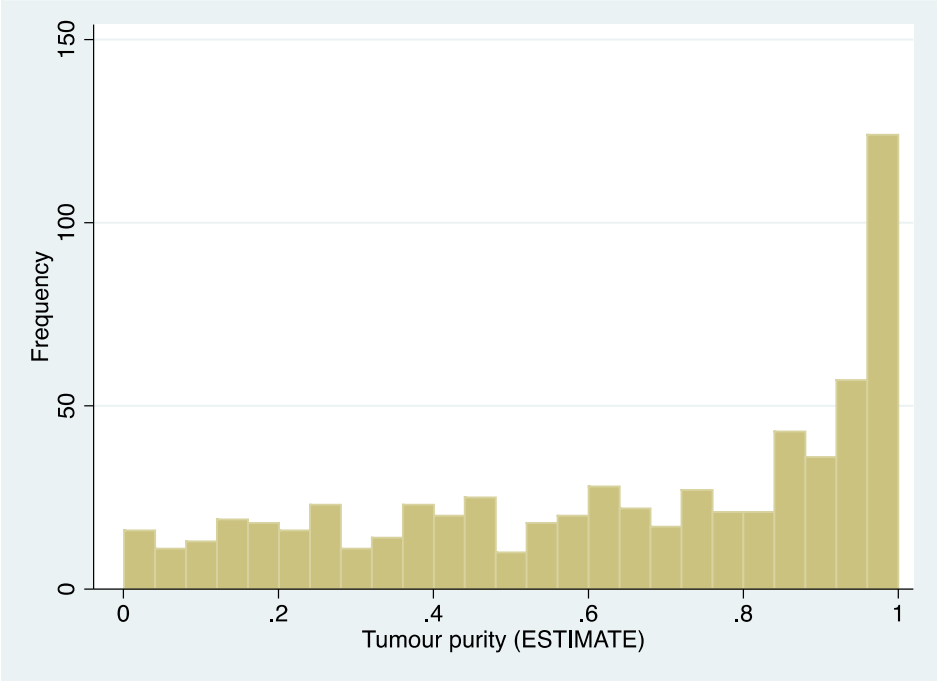

Figure 5.16 Histogram of the tumour purity

The histogram shows the frequency distribution for the tumour purity score (n=653), which is derived from the ESTIMATE score. 1 represents pure tumour (equivalent to 100%) and 0.1 represents only 10% tumour. The median tumour purity was 0.72 (72%).

There was a positive correlation between the POS and several of the ESTIMATE-derived scores, including the immune score (Spearman rho=0.29, $p=5x10^{-13}$), the stromal score (Spearman rho=0.36, $p=8x10^{-20}$) and the ESTIMATE score (Spearman rho=0.34, $p=3x10^{-17}$). Conversely there was a negative correlation between the POS and the tumour purity score (Spearman rho=-0.32, $p=5x10^{-15}$).

5.3.9 The percentage of stroma (POS), ESTIMATE score, tumour purity, immune and stromal scores as predictors of melanoma-specific death

I have shown, using simple pairwise analyses, that the POS was associated with each of the ESTIMATE scores. Next, I will explore whether or not each of the ESTIMATE scores was independently prognostic of melanoma-specific death, in multivariable survival analyses. Table 5.4 shows the results of five multivariable survival models, each adjusted for age, sex, site of primary, AJCC stage, melanoma cell structure and the extent of the core immune cell infiltrate, for each of the following variables: the POS, ESTIMATE score, tumour purity, immune and stromal scores. The POS, ESTIMATE score, tumour purity, immune and stromal scores were each independent prognostic factors in these models, all being protective except for the tumour purity score, which appeared to be hazardous (HR for the tumour purity score 1.01, 95% CI 1.0-1.02, Cox proportional hazards model, p=0.002). The p-values in Table 5.4 suggest that ESTIMATE's stromal score is the strongest predictor of melanoma-specific death (Cox proportional hazards model, p=0.0002).

Table 5.4: Adjusted hazard ratios (HRs) and 95% confidence intervals (95% CI) for the effects of the POS, ESTIMATE score, tumour purity score, immune score and stromal score on melanoma-specific death, adjusted for age, sex, site of primary, AJCC stage, melanoma cell structure and the extent of the core immune cell infiltrate

The percentage of stroma (POS), ESTIMATE score, immune and stromal scores were independently protective for melanoma-specific death (as indicated by hazard ratios <1.0 and p-values <0.05). The tumour purity score was hazardous. N=the number of cases. The number of events refers to the number of melanoma-specific deaths. 95% CI=95% confidence interval.

	Melanoma Death									
	POS N=692 (177 events)		ESTIMATE score N=589 (153 events)		Tumour purity score N=568 (149 events)		Immune score N=589 (153 events)		Stromal score N=589 (153 events)	
Factor	**Adjusted HR (95% CI)**	**p-value**	**Adjusted HR (95% CI)**	**p-value**	**Adjusted HR (95% CI)**	**p-value**	**Adjusted HR (95% CI)**	**p-value**	**Adjusted HR (95% CI)**	**p-value**
Age at diagnosis (years)	1.03 (1.02-1.04)	0.00004	1.03 (1.02-1.05)	0.00004	1.03 (1.02-1.05)	0.00008	1.03 (1.02-1.05)	0.00004	1.03 (1.02-1.05)	0.00003
Sex										
Male	1		1		1		1		1	
Female	0.84 (0.61-1.15)	0.27	0.85 (0.61-1.20)	0.36	0.86 (0.61-1.21)	0.38	0.85 (0.61-1.19)	0.35	0.84 (0.60-1.17)	0.31
Site of primary melanoma										
Limbs	1		1		1		1		1	
Trunk	1.41 (0.97-2.05)	0.07	1.70 (1.13-2.56)	0.01	1.61 (1.06-2.43)	0.02	1.70 (1.13-2.57)	0.01	1.66 (1.10-2.51)	0.02
Head	0.93 (0.55-1.59)	0.80	0.92 (0.51-1.65)	0.77	0.85 (0.47-1.54)	0.59	0.93 (0.52-1.66)	0.80	0.89 (0.50-1.60)	0.71

	Melanoma Death									
	POS N=692 (177 events)		ESTIMATE score N=589 (153 events)		Tumour purity score N=568 (149 events)		Immune score N=589 (153 events)		Stromal score N=589 (153 events)	
Factor	**Adjusted HR (95% CI)**	**p-value**	**Adjusted HR (95% CI)**	**p-value**	**Adjusted HR (95% CI)**	**p-value**	**Adjusted HR (95% CI)**	**p-value**	**Adjusted HR (95% CI)**	**p-value**
Other	1.81 (1.18-2.79)	0.007	1.70 (1.07-2.70)	0.02	1.63 (1.02-2.60)	0.04	1.71 (1.07-2.71)	0.02	1.73 (1.09-2.74)	0.02
AJCC stage										
Test for trend	2.26 (1.79-2.85)	$9x10^{-12}$	2.33 (1.81-3.00)	$7x10^{-11}$	2.34 (1.81-3.03)	$1x10^{-10}$	2.31 (1.79-2.99)	$1x10^{-10}$	2.39 (1.85-3.08)	$2x10^{-11}$
POS or ESTIMATE score or Tumour purity score or Immune score or Stromal score	0.99 (0.98-0.99)	0.005	0.99 (0.98-0.99)	0.0003	1.01 (1.00-1.02)	0.002	0.99 (0.98-0.99)	0.001	0.97 (0.96-0.99)	0.0002
Melanoma cell structure										
Nests	1		1		1		1		1	
Sheets	1.08 (0.74-1.58)	0.67	1.45 (0.98-2.14)	0.06	1.48 (1.00-2.19)	0.05	1.49 (1.01-2.21)	0.05	1.35 (0.92-1.99)	0.13
Fascicles	1.02 (0.68-1.54)	0.92	1.15 (0.74-1.80)	0.54	1.13 (0.72-1.78)	0.59	1.16 (0.74-1.82)	0.51	1.12 (0.72-1.75)	0.63
Dispersed	2.44 (1.09-5.48)	0.03	2.09 (0.98-4.47)	0.06	1.75 (0.75-4.11)	0.20	1.90 (0.89-4.05)	0.10	2.28 (1.06-4.90)	0.03
Extent of immune cell infiltrate										
Test for trend	0.81 (0.66-0.99)	0.05	0.82 (0.67-1.01)	0.06	0.80 (0.65-0.99)	0.05	0.82 (0.67-1.01)	0.06	0.80 (0.65-0.98)	0.03

Table 5.5 shows the results of multivariable survival analyses, adjusted for age, sex, site of primary, AJCC stage, melanoma cell structure and the extent of the core lymphocytic infiltrate, for each of the following variables: the POS, ESTIMATE score, tumour purity, immune and stromal scores. The POS and each of the ESTIMATE scores were independent predictors of melanoma-specific death. As before, the POS, ESTIMATE score, immune and stromal scores were protective, whilst ESTIMATE's tumour purity score was hazardous (Table 5.5).

5.3.10 The percentage of stroma and the transcriptome

I performed 29354 univariable linear regression models, regressing the POS on all 29354 probes in the Illumina® DASL assay in order to establish the transcriptomic correlates of the POS (please see Chapter 2). Similar results were obtained using a sensitivity analysis (to exclude outliers with a POS >87%; data not shown). Unsupervised hierarchical clustering was performed using the top ranked gene probes found to be most significantly associated with the POS, by selecting genes that had a Bonferroni-corrected p-value <0.05 (and the best detected probe where >1 probe was available for a gene). Figure 5.17 shows the resultant heat map, ranked from low to high POS. Two distinct clusters can be discerned. Of the top 2180 genes identified to be significantly associated with increasing POS, 1064 genes were downregulated. The top 10 pathways identified by MetaCore™ enrichment analyses for the probes in each cluster are shown. Cell cycle pathways were enriched in cases with low stroma, whilst T-cell signalling and chemotaxis were among the top ranked pathways in cases with high stroma.

Table 5.5 (on following page): Adjusted hazard ratios (HRs) and 95% confidence intervals (95% CI) for the effects of the POS, ESTIMATE score, tumour purity, immune and stromal scores on melanoma-specific death, adjusted for age, sex, site of primary, AJCC stage, melanoma cell structure and the extent of the core lymphocytic infiltrate

The percentage of stroma (POS), ESTIMATE score, immune and stromal scores were independently protective of melanoma-specific death (as indicated by hazard ratios <1.0 and p-values <0.05). The tumour purity score was hazardous. One of the lines in the table reads as follows: "*POS or ESTIMATE score or Tumour purity score or Immune score or Stromal score*". This line refers to which of the 5 statistical models the HRs, 95% CI and p-values correspond. N=the number of cases. The number of events refers to the number of melanoma-specific deaths. 95% CI=95% confidence interval.

	Melanoma Death									
	POS N=692 (177 events)		ESTIMATE score N=589 (153 events)		Tumour purity score N=568 (149 events)		Immune score N=589 (153 events)		Stromal score N=589 (153 events)	
Factor	**Adjusted HR (95% CI)**	**p-value**	**Adjusted HR (95% CI)**	**p-value**	**Adjusted HR (95% CI)**	**p-value**	**Adjusted HR (95% CI)**	**p-value**	**Adjusted HR (95% CI)**	**p-value**
Age at diagnosis (years)	1.03 (1.02-1.04)	0.00005	1.03 (1.02-1.05)	0.00005	1.03 (1.02-1.05)	0.0001	1.03 (1.02-1.05)	0.00005	1.03 (1.02-1.05)	0.00004
Sex										
Male	1		1		1		1		1	
Female	0.84 (0.62-1.15)	0.28	0.85 (0.60-1.19)	0.34	0.85 (0.61-1.20)	0.36	0.85 (0.60-1.19)	0.33	0.83 (0.59-1.17)	0.29
Site of primary melanoma										
Limbs	1		1		1		1		1	
Trunk	1.38 (0.95-2.00)	0.10	1.65 (1.09-2.49)	0.02	1.55 (1.03-2.35)	0.04	1.66 (1.10-2.50)	0.02	1.61 (1.07-2.43)	0.02
Head	0.92 (0.54-1.56)	0.75	0.90 (0.50-1.62)	0.72	0.83 (0.46-1.51)	0.54	0.91 (0.51-1.63)	0.75	0.87 (0.49-1.56)	0.65
Other	1.71 (1.11-2.65)	0.02	1.63 (1.02-2.60)	0.04	1.56 (0.97-2.50)	0.07	1.64 (1.03-2.61)	0.04	1.64 (1.03-2.62)	0.04
AJCC stage										
Test for trend	2.20 (1.74-2.78)	$6x10^{-11}$	2.26 (1.75-2.93)	$5x10^{-10}$	2.27 (1.74-2.95)	$1x10^{-9}$	2.25 (1.74-2.92)	$6x10^{-10}$	2.31 (1.78-2.99)	$2x10^{-10}$
POS or ESTIMATE score or Tumour purity score or Immune score or Stromal score	0.99 (0.98-0.99)	0.009	0.99 (0.98-0.99)	0.001	1.01 (1.00-1.02)	0.004	0.99 (0.98-0.99)	0.004	0.98 (0.96-0.99)	0.0003

	Melanoma Death									
	POS N=692 (177 events)		ESTIMATE score N=589 (153 events)		Tumour purity score N=568 (149 events)		Immune score N=589 (153 events)		Stromal score N=589 (153 events)	
Factor	**Adjusted HR (95% CI)**	**p-value**	**Adjusted HR (95% CI)**	**p-value**	**Adjusted HR (95% CI)**	**p-value**	**Adjusted HR (95% CI)**	**p-value**	**Adjusted HR (95% CI)**	**p-value**
Melanoma cell structure										
Nests	1		1		1		1		1	
Sheets	1.09 (0.75-1.59)	0.65	1.45 (0.98-2.14)	0.06	1.48 (1.00-2.19)	0.05	1.49 (1.01-2.20)	0.05	1.36 (0.92-2.00)	0.13
Fascicles	1.00 (0.66-1.51)	1.0	1.13 (0.72-1.76)	0.60	1.11 (0.71-1.75)	0.65	1.14 (0.73-1.78)	0.57	1.09 (0.70-1.71)	0.69
Dispersed	2.45 (1.09-5.50)	0.03	2.14 (1.00-4.60)	0.05	1.81 (0.77-4.25)	0.17	1.96 (0.92-4.18)	0.08	2.35 (1.09-5.04)	0.03
Extent of lymphocytic infiltrate										
Test for trend	0.80 (0.68-0.95)	0.01	0.83 (0.69-0.99)	0.04	0.81 (0.67-0.97)	0.03	0.82 (0.69-0.99)	0.03	0.81 (0.68-0.96)	0.02

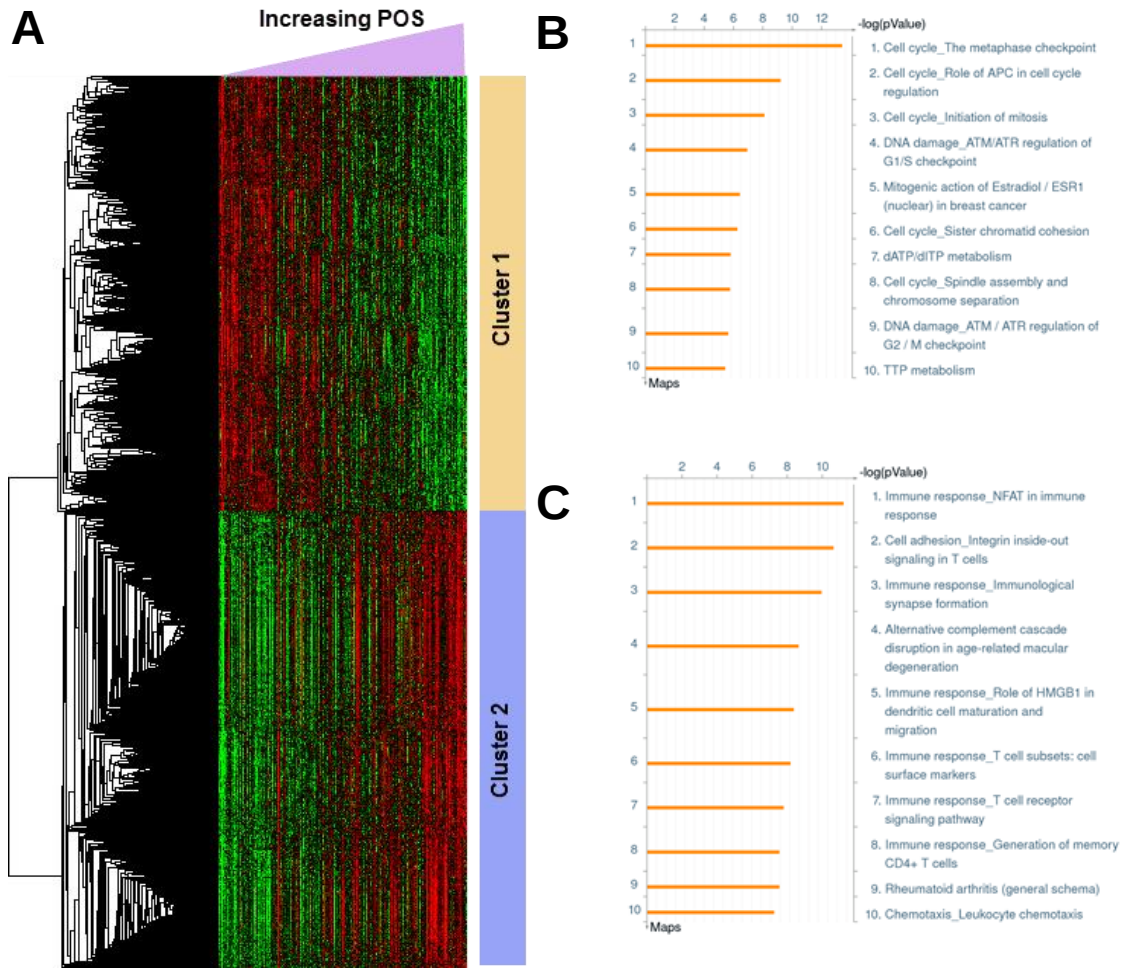

Figure 5.17: Heat map and functional annotation for stroma-associated genes

A) The gene dendrogram and heat map for stroma-associated genes are shown. Going from left to right across the heat map, the tumours are ordered from low to high POS (using the continuous values for POS). The genes in Cluster 1 were upregulated in melanomas with low POS, while genes in Cluster 2 were upregulated in melanomas with high POS. Red=gene upregulation. Green=gene downregulation.

Separate enrichment analyses were performed for genes within each of the two gene clusters, using MetaCore™. The top ten pathways for each gene cluster are shown (B and C). The first gene cluster (low POS) was enriched in cell cycle and the second (high POS) was enriched in immune pathways.

5.3.11 Interaction analysis between the percentage of stroma (POS), the transcriptome and melanoma-specific death

There was no significant statistical interaction between the POS and the transcriptome on melanoma-specific death (data not shown).

5.3.12 The extent of the core immune cell infiltrate and the transcriptome

The POS was composed of a mixture of immune and non-immune stromal cells. The extent of the core immune cell infiltrate was also predictive of melanoma-specific survival (Chapter 4). Therefore, I next explored the association between the core immune cell infiltrate and the transcriptome. This was done by performing 29354 linear regression models, regressing the extent of the core immune cell infiltrate (test for trend) on each of the 29354 probes in the Illumina® DASL assay (please see Section 5.2). Unsupervised hierarchical clustering using the top ranked gene probes that were most significantly associated with the extent of the core immune cell infiltrate (Bonferroni-corrected p-value <0.05) was performed using Cluster 3.0. Figure 5.18 shows the resultant heat map, ranked from none to lots of immune cells within the core. Of the top 1288 genes, only 356 were inversely associated with an increasing extent of the core immune cell infiltrate. Unsurprisingly, the top 10 pathways that were upregulated in association with increasing amounts of immune cell infiltration (within the core) included immune pathways, particularly T- and B-cell signalling.

5.3.13 The extent of the core lymphocytic infiltrate and the transcriptome

The core immune cell infiltrate was composed of various immune cell subtypes, however, apart from lymphocytes and macrophages/melanophages, other immune cell subtypes were infrequently recorded within the core (Chapter 4). I decided to assess the association between the extent of the core lymphocytic infiltrate and the transcriptome because this was an independent predictor of survival in multivariable survival analyses and the macrophage/melanophage infiltrate was not (Chapter 4). Furthermore, arrowheads that had landed on lymphocytes within the core (using RandomSpot©) would have been incorporated into the POS calculation and, ultimately, I wanted to see if it was possible to distinguish which genes were associated with the core lymphocytes and which genes might be more likely to be related to other non-immune components. Of the top 1542 genes identified as being significantly associated with the extent of the core lymphocytic infiltrate, only 400 were downregulated.

Unsupervised clustering of the top ranked genes associated with the extent of the core lymphocytic infiltrate was performed in a similar way to that described above. Figure 5.19 shows the heat map, which is ranked according to increasing amounts (extent) of lymphocytic infiltrate within the cored region. Similar immune pathways were upregulated in association with an increasing extent of lymphocytic infiltrate, as had previously been identified in association with an increasing extent of immune cell infiltration within the core.

Figure 5.18 (on following page): Heat map and functional annotation for genes associated with the increasing extent of the core immune cell infiltrate

A) The gene dendrogram and heat map for genes associated with the increasing extent of the core immune cell infiltrate (test for trend) are shown. Going from left to right across the heat map, the tumours are ordered by an increasing extent of the core immune cell infiltrate. The genes in Cluster 1 were upregulated in melanomas with a low extent of core immune cells. The genes in Cluster 2 were upregulated in melanomas with a high extent of core immune cells. Red=gene upregulation. Green=gene downregulation.

Separate enrichment analyses were performed for genes within each of the two gene clusters, using MetaCore™. The top ten pathways for each gene cluster are shown (B and C). There were 356 genes within the first (uppermost) gene cluster, therefore, the pathways may not be reliable due to the relatively small number of genes for a MetaCore™ analysis. Melanomas in the second (lowermost) gene cluster (higher extent of core immune cell infiltrate) were enriched in immune pathways.

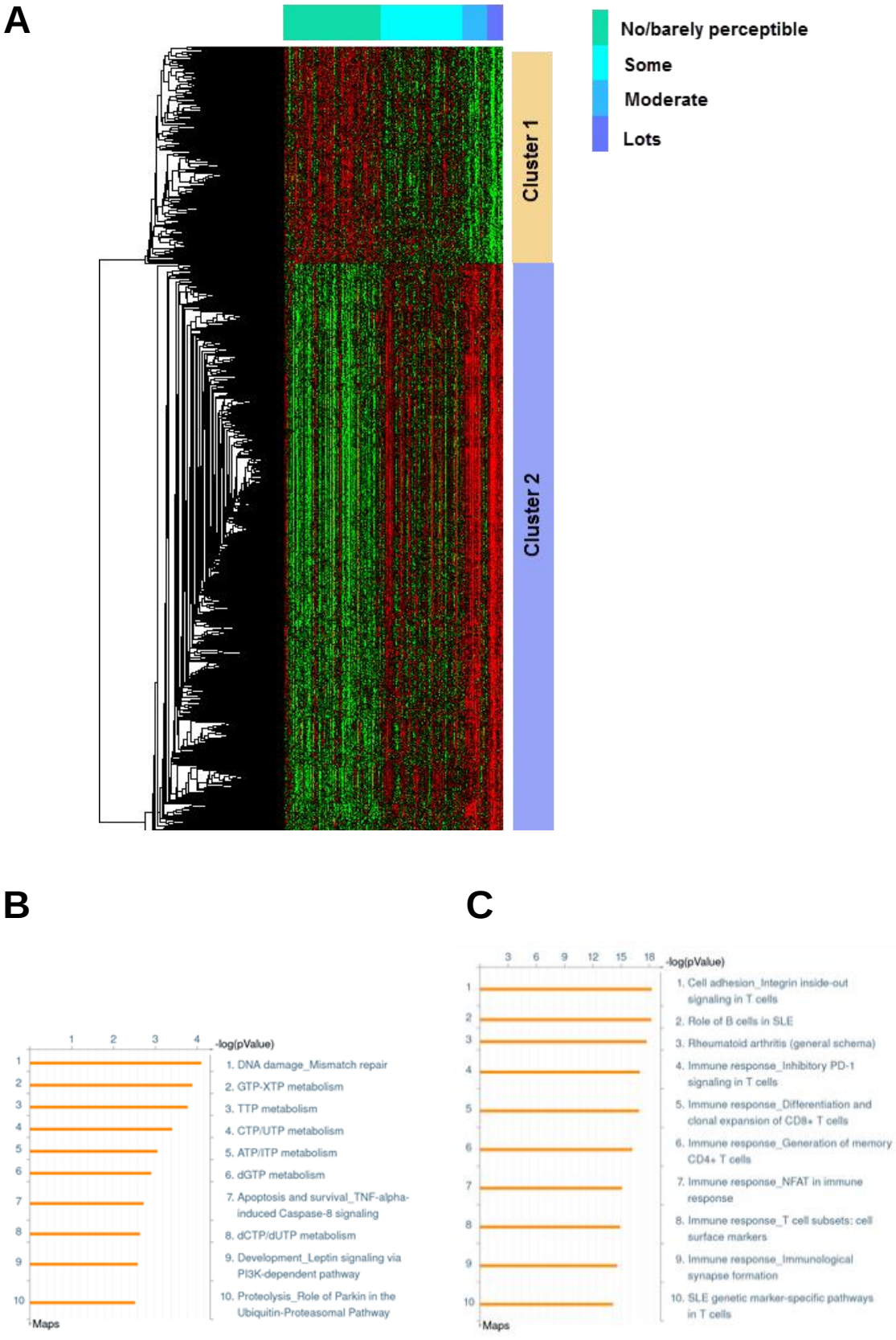
A
No/barely perceptible
Some
Moderate
Lots
Cluster 1
Cluster 2
B
1
2
3
4
-log(pValue)
1. DNA damage_Mismatch repair
2. GTP-XTP metabolism
3. TTP metabolism
4. CTP/UTP metabolism
5. ATP/ITP metabolism
6. dGTP metabolism
7. Apoptosis and survival_TNF-alpha-induced Caspase-8 signaling
8. dCTP/dUTP metabolism
9. Development_Leptin signaling via PI3K-dependent pathway
10. Proteolysis_Role of Parkin in the Ubiquitin-Proteasomal Pathway
Maps
C
3
6
9
12
15
18
-log(pValue)
1. Cell adhesion_Integrin inside-out signaling in T cells
2. Role of B cells in SLE
3. Rheumatoid arthritis (general schema)
4. Immune response_Inhibitory PD-1 signaling in T cells
5. Immune response_Differentiation and clonal expansion of CD8+ T cells
6. Immune response_Generation of memory CD4+ T cells
7. Immune response_NFAT in immune response
8. Immune response_T cell subsets: cell surface markers
9. Immune response_Immunological synapse formation
10. SLE genetic marker-specific pathways in T cells
Maps

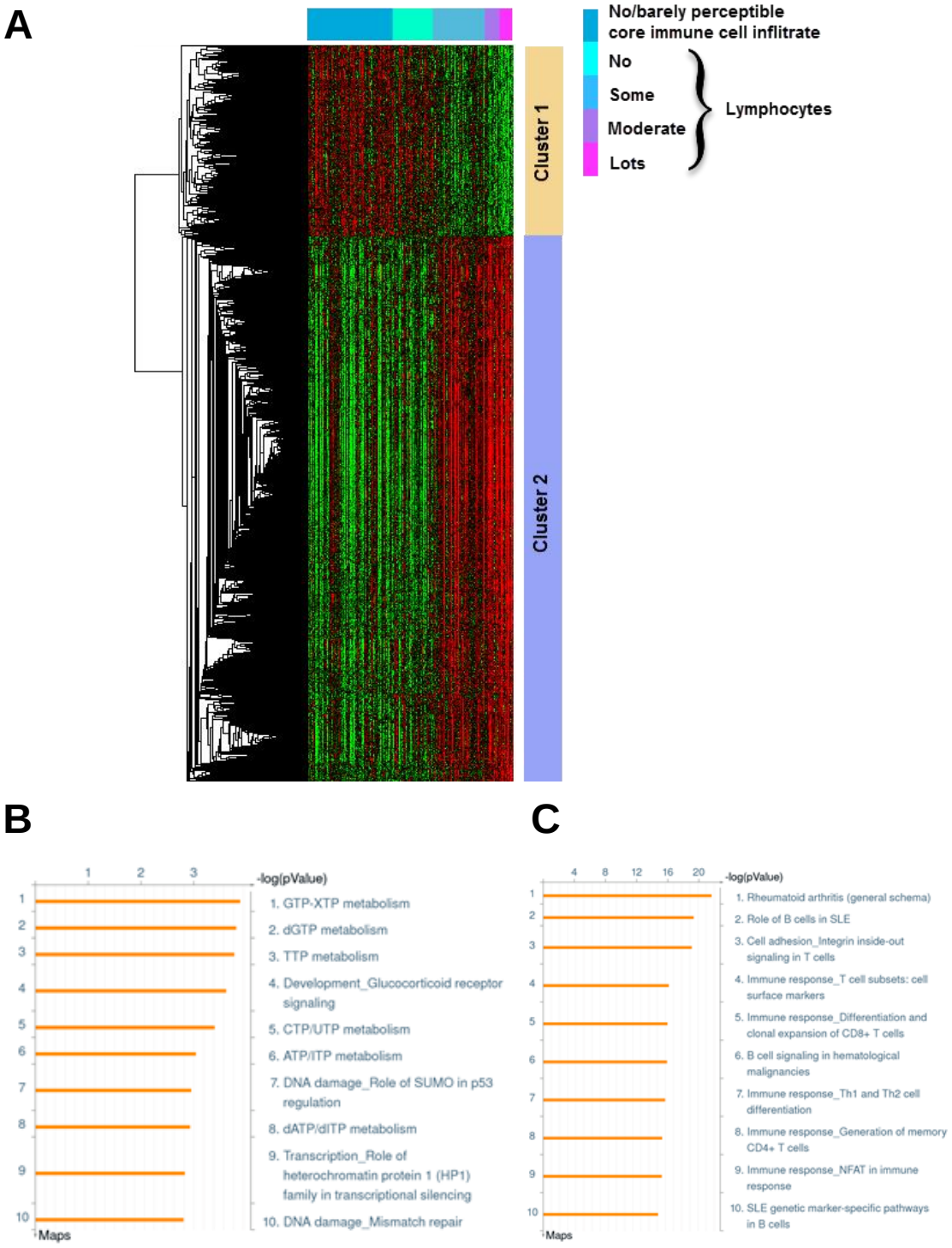

Figure 5.19: Heat map and functional annotation for genes associated with the increasing extent of the core lymphocytic infiltrate

A) The gene dendrogram and heat map for genes associated with the increasing extent of the core lymphocytic infiltrate (test for trend) are shown. Going from left to right across the heat map, there is an increasing extent of the core lymphocytic infiltrate. Red=gene upregulation. Green=gene downregulation.

(Figure 5.19 legend cont.) Separate enrichment analyses were performed for genes within each of the two gene clusters, using MetaCore™. The top ten pathways for each gene cluster are shown (B and C). There were 400 genes within Cluster 1 and, therefore, the pathways may not be reliable (due to the relatively small number of genes for a MetaCore™ analysis). Melanomas in Cluster 2 (higher extent of the core lymphocytic infiltrate) were enriched in immune pathways.

5.3.14 Comparative enrichment analysis for the percentage of stroma and the extent of the core immune cell and lymphocytic infiltrates using MetaCore™

MetaCore™ enrichment analyses of the top ranked genes for the POS and the extent of the core immune cell and lymphocytic infiltrates identified immune pathways as being significantly upregulated in association with each of these variables. In order to better understand the overlap in the pathways, I next performed a comparative enrichment experiment. Of the top 1000 genes for each of the POS and the extent of the core immune cell and lymphocytic infiltrates, one of the genes that was identified as being unique to the POS gene list was *stromal-derived factor 1* (*SDF1*; Figure 5.20).

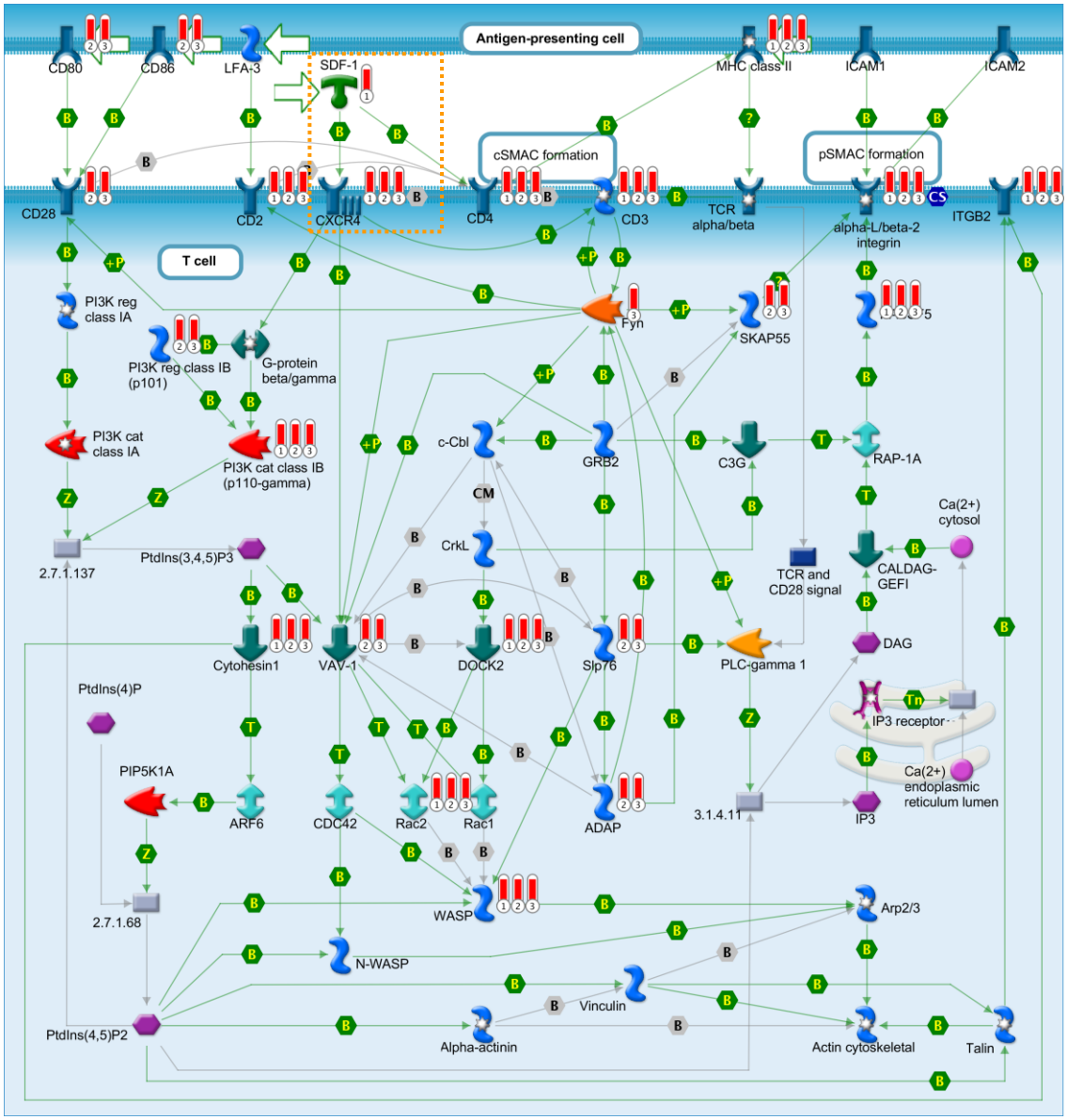

Figure 5.20: Image of the MetaCore™ immune response "immunological synapse formation" pathway

The pathway indicates which proteins are proposed to be mediating the signalling between the antigen presenting cell and the T lymphocyte. Red thermometers indicate upregulation of the corresponding gene in the transcriptome data set. There is upregulation of MHC class II, CD80 (a B-cell marker), CD86 (present on antigen presenting cells) and corresponding upregulation of T-cell markers, including CD3, CD4, CD2, and CD28.

Interestingly, *SDF1* (highlighted by orange hatched box) is uniquely upregulated in association with the POS (thermometer 1) but not with the extent of the core immune cell infiltrate (thermometer 2) or the core lymphocytic infiltrate (thermometer 3).

(Figure 5.20 legend cont.) There is also upregulation of its receptor, *C-X-C chemokine receptor 4* (CXCR4, also highlighed in orange hatched box) however this is not confined to the POS. Also upregulated in all three data sets are the integrins, ITGB2 and alpha-L/beta 2 integrin. T-cell activation occurs downstream of SDF1.

MetaCore™ Key: ADAP = adhesion and degranulation-promoter adapter protein. ARF6 = Adenosine diphosphate-ribosylation factor 6. ARP = actin-related protein 2 homolog. C3G (also known as RAPGEF1) = Rap Guanine nucleotide exchange factor 1. CALDAG-GEF = Calcium and diacylglycerol-related guanine nucleotide exchange factor. CBL = Cbl proto-oncogene. CD refers to cluster of differentiation. CrkL = Crk-like proto-oncogene. CDC42 = cell division control protein 42. DAG = diacylglycerol. DOCK2 = Dedicator of cytokinesis 2. Fyn = proto-oncogene tyrosine kinase. Grb2 = growth factor receptor-bound protein 2. ICAM = Intracellular adhesion molecule. IP3 = inositol triphosphate. ITGB2 = integrin beta 2. LFA3 = lymphocyte function-associated antigen 3 (also known as CD58). PI3K = phosphoinositide 3-kinase. PIP5K1A = phosphatidylinositol-4-phosphate 5-kinase type 1 alpha. PLC = phospholipase C. PtdIns = phosphatidylinositol. RAC (1 or 2) = Ras-related C3 botulinum toxin substrate (1 or 2). RAP1A = Ras-related protein Rap-1A. SKAP1: Src kinase-associated phosphoprotein 1. SLP76 = lymphocyte cytosolic protein 2. SMAC=Second mitochondrial-derived activator of caspase. TCR = T-cell receptor. VAV1 = Vav guanine nucleotide exchange factor. WASP = Wiskott-Aldrich Syndrome Protein. Interaction arrows: B, binding; +P, phosphorylation; T, transformation; Z, catalysis, ?, unspecified.

5.3.15 *Stromal-derived factor 1* and melanoma-specific death

In light of the strong association between *SDF1* and the POS, I was interested to assess whether or not *SDF1* expression might also influence survival, particularly due to conflicting reports in the literature (discussed later). Figure 5.21 shows the frequency distribution for the logged *SDF1* gene expression within 676 cases for which histopathological review and transcriptomic data were available.

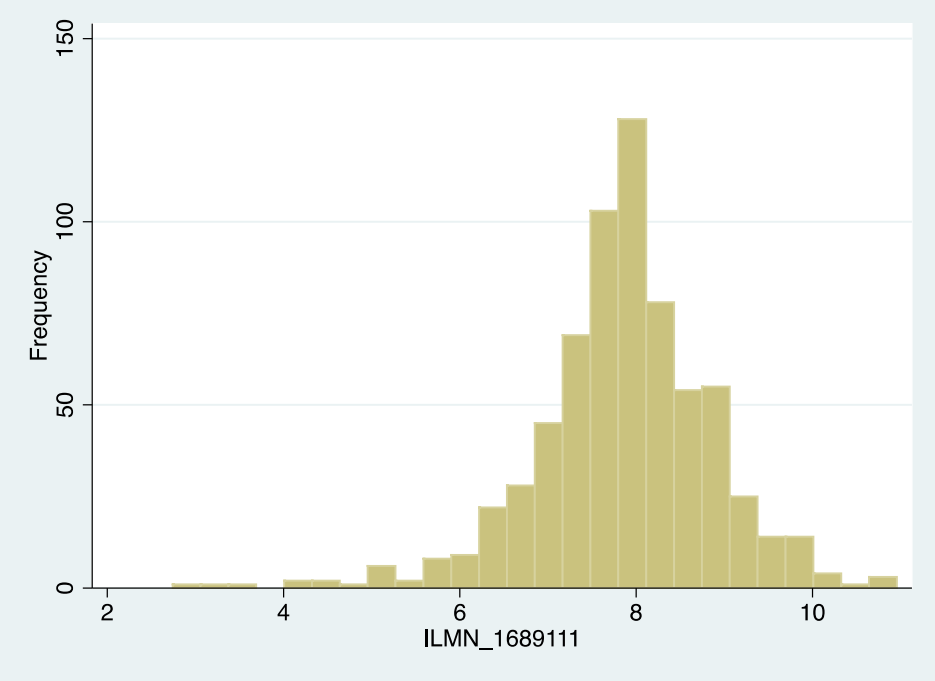

Figure 5.21 Histogram of *SDF1* gene expression (ILMN_1689111 probe)

The histogram shows the frequency distribution for the logged *SDF1* gene expression in 676 cases from the Leeds Melanoma Cohort Study. The mean expression was 7.9 (standard deviation 1.0).

In a univariable survival analysis, *SDF1* gene expression was significantly protective for melanoma-specific death (HR 0.79, 95% CI 0.69-0.90, Cox proportional hazards model, p=0.0005). Furthermore, in a multivariable model, adjusting for age, sex, site of primary, AJCC stage, the POS, melanoma cell structure and the extent of the core immune cell infiltrate, *SDF1* was an independent predictor of melanoma-specific death (HR 0.8, 95% CI 0.68-0.94, Cox proportional hazards model, p=0.005). To assess whether or not its receptors, *C-X-C chemokine receptor type 4* (*CXCR4*) and *C-X-C chemokine receptor type 7* (*CXCR7*), might also be prognostic, I performed survival analyses using their respective gene expression values. The findings revealed that *CXCR4* was protective in a univariable analysis for melanoma-specific death (HR 0.85, 95% CI 0.76-0.95, Cox proportional hazards model, p=0.005). *CXCR4* was also an independent predictor of survival in a multivariable analysis, adjusting for age, sex, site of primary, AJCC stage, melanoma cell structure and the extent of the core immune cell infiltrate (HR 0.86, 95% CI 0.76-0.99, Cox proportional hazards model, p=0.04) but it lost statistical significance after adjusting for the POS (Cox proportional hazards model, p=0.06). *CXCR7* was not significantly associated with melanoma-specific death in a univariable model (HR 0.92, 95% CI 0.82-1.03, Cox proportional hazards model, p=0.2).

5.4 Summary

My findings can be summarised as follows:

- The median POS within primary cutaneous melanomas in this study was 32.7%, consistent with findings of a smaller study, in which the average amount of stroma was reported to be 26% [145]. There was an inverse association between the POS and the following factors: age, AJCC stage, Breslow thickness, dominant nodule, microscopic ulceration and the number of core mitoses. The striking inverse association between the POS and several histopathological factors, which are considered to be predictive of poor survival, could reflect inadvertent sampling of some normal tissue in thinner tumours. The POS was lowest in *NRAS*-mutant tumours compared to *BRAF*-mutant and wild type melanomas. Increasing values for the POS were associated with female sex, increasing TIMs (borderline statistical significance), mixed stroma quality, dispersed melanoma cell structure, increasing melanoma cell pigmentation and an increasing extent of the core immune cell and lymphocytic infiltrates.
- The effect of combining the POS and AJCC stage was additive in terms of predicting either melanoma relapse or melanoma-specific death. The addition of the POS increased the power of prediction by 3% for both relapse and death.
- The POS was significantly associated with the immunome. Notably, immunome cluster 4, which contained the lowest expression of immune cell genes, also had the lowest value for the POS. The POS was significantly associated with each of ESTIMATE's scores, being positively associated with the ESTIMATE score, the immune and stromal scores and inversely associated with the tumour purity score. The POS and each of the ESTIMATE scores were independently prognostic in multivariable survival analyses and each of the ESTIMATE scores were more powerful predictors of melanoma-specific survival than the POS, with the ESTIMATE stromal score being the most significant. Therefore, although the POS is associated with ESTIMATE, it does not appear to simply be a reflection of the amount of immune cells present.
- Immune cell signalling pathways were upregulated and cell cycle pathways were downregulated in association with the POS. Similarly, immune cell pathways were enriched in association with the extent of the core immune cell and lymphocytic infiltrates. A comparative enrichment analysis revealed that *SDF1* was unique to the POS gene list. Moreover, *SDF1* was an independent prognostic factor, conferring a protective effect for melanoma-specific death. Its receptor *CXCR4* but not *CXCR7*, was protective for melanoma-specific death

but lost statistical significance in a multivariable model including the POS. There was no significant statistical interaction between the POS, the transcriptome and melanoma-specific survival.

5.5 Discussion

The POS was an independent prognostic factor (Chapter 4) and was associated with a number of interesting observations. The POS was significantly inversely associated with age and male sex, suggesting that it might reflect host factors associated with biological variation. Although melanomas with more aggressive histopathological characteristics have been reported to be associated with older age at diagnosis [7] and male sex [14], the explanation for this apparent disparity has not been fully elucidated. It is known that host factors, such as advancing age [260, 275] and smoking [276] contribute to changes in the tumour microenvironment that can promote cancer. Advancing age has been linked to decreased self-detection among melanoma patients [11]. That being the case, one might expect that melanomas at less visible sites might have had a lower POS. However, there was no significant association between the POS and the site of primary melanoma, although the median POS was lowest in truncal primaries. Ageing has also been linked to immunosenescence [12], which might account for the inverse association observed in association with the POS because core immune cells were incorporated into the calculation of the POS. A more detailed analysis of the histopathological factors associated with age would help to clarify this. It is well-recognised that females diagnosed with melanoma tend to have a better prognosis [22, 23]. As previously discussed, female sex was protective for melanoma-specific death in a univariable survival analysis but lost statistical significance in multivariable survival analyses (Chapter 4). Several hypotheses have been offered for the sex disparity, including effects mediated by hormones and host immunity [31]. Conversely, there does not appear to be a significant difference in the pattern of TILs in primary melanomas between the sexes [33, 64]. Nonetheless, it is possible that more subtle differences in the nature of the immune landscape could exist and may not be captured by this measure. Furthermore, the production of collagen might vary by sex, which could also be reflected in the POS. Oestrogen has been reported to increase collagen synthesis [277, 278], and a reduction in MMP activity has been linked to progesterone [277]. Moreover, androgens have been reported to impair wound healing due by alterations in MMP production [279]. The possibility that differences exist in the stromal composition of primary melanomas between men and women is an exciting prospect, worthy of further exploration.

The POS was inversely associated with Breslow thickness, ulceration and mitotic count, and, therefore, the observed differences by age and sex could reflect a more destructive primary tumour in these subgroups. In addition, cell cycle pathways were upregulated in cases with a low POS, suggesting that these tumours were more proliferative. Indeed, a criticism of my findings may be that the protective effect of the POS might reflect the reverse: that a lower POS might be a marker of a less proliferative, less aggressive tumour. However, the fact that the POS was an independent predictor of survival, after adjusting for age, sex and AJCC stage suggests that the POS might not simply be a read-out of the aggressiveness of the melanoma. The POS conferred an additional 3% predictive power, over and above AJCC stage (Figure 5.9 and Figure 5.10), indicating that the histopathological estimation of the POS as a prognostic marker would be worth evaluating in an independent cohort.

Furthermore, the POS was significantly associated with *BRAF/NRAS* mutation status, with a lower POS being recorded in melanomas harbouring an *NRAS* mutation. The results further support the notion that a biological explanation could underlie variations in the POS. *NRAS*-mutated melanomas are reported to be associated with adverse tumour characteristics [37], including nodular melanoma [280], however, no significant differences were observed in the proportions of nodular melanomas among cases with an *NRAS* mutation compared with a *BRAF* mutation (data not shown, analysis performed by Faye Elliott). A recent study has reported that brisk TILs are less likely to occur in *NRAS*-mutated primary melanomas [37], suggesting that a more immunosuppressive tumour microenvironment might exist in these tumours. The acquisition of resistance to *BRAF* inhibitor therapy has been reported to result in the increased production of MMPs [251]. Intriguingly, increased production of type I collagen has been described in association with *BRAF* inhibition, both in melanoma cell lines and in mice [281]. Conversely, variably increased expression of *SDF1* and *CXCR4* has been reported in dermal fibroblasts, grown in a medium conditioned with a *BRAF*-mutant melanoma cell line [282]. Therefore, although the reported findings are somewhat conflicting, the driver mutation status could shape not only the immune cell infiltrate but also the extent of collagen within primary melanomas, which might have therapeutic implications.

The observation that the POS was inversely associated with melanoma cell pigmentation is fascinating. As previously discussed, pigmentation is regarded to be a marker of melanocyte differentiation [111], therefore, it is possible that the nature of the tumour-stroma cross-talk might differ based on the level of melanocyte differentiation. Furthermore, melanoma cells with a high degree of pigmentation have been reported

to have reduced cell elasticity and, hence, an impaired capacity for invasion [114]. I would be keen to validate these findings in an independent data set.

A significant association was observed between the POS and the core immune cell variables, which is not surprising because these were included in the calculation of the POS. Furthermore, the downregulation of cell cycle pathways is indicative of the relative absence of melanoma cells within samples that had a high POS. Nonetheless, the consistent upregulation of immune cell and downregulation of cell cycle pathways is proof-of-concept that histopathological observations have transcriptomic correlates. Moreover, the POS remained an independent predictor of outcome, after adjusting for either the core immune cell or lymphocytic infiltrates in multivariable survival analyses (Chapter 4), indicating that although the POS reflects the presence of immune cells, the non-immune stromal constituents might also have a protective effect.

For the majority of cancers, studies indicate a hazardous role for increasing amounts of stroma. The reason for the contrasting findings of this project is not entirely clear. Melanoma is recognised as being one of the most highly immunogenic tumours [257], therefore, the immune cell infiltrate could have been responsible for the beneficial effects of the POS. One hypothesis is that stroma may promote or inhibit tumour growth, depending on the nature of that stroma and the cancer with which it is associated. Furthermore, many of the reported studies refer to cancers located at mucosal sites. Intrinsic differences might exist between the immune microenvironment of the skin and other tissues [268, 283] but further research could clarify this supposition.

The expression of MMPs has also been reported to vary according to site [284] and this might have contributed to differences in the effect of the POS on survival in various cancers. Moreover, Henriet *et al.* reported that fibrillar collagen inhibited the proliferation of melanoma cells *in vitro* [285], which suggests that the non-immune stroma could be contributing to the protective effect of the POS.

The region of tumour selected for analysis could also have influenced the results. In this study, I focused on a pre-defined region of the primary melanoma that was towards the invasive margin but was considered to be relatively deficient in immune and non-immune stromal cells. Inevitably some stromal “contamination” occurred. However, the conclusions drawn are appropriately based on comparisons within the sample set.

In contrast to the findings of Smolle *et al.*, who reported that an increased area of pre-existing collagen was hazardous in primary melanomas, this study showed that the POS was independently protective for melanoma-specific death [144]. However, there were notable differences in the approach used by Smolle *et al.*, for example, immune

cells were not recorded as part of their calculation [144]. In a recent study, Rashed *et al.* showed that the density of melanoma cells within the region of the Breslow thickness measurement was hazardous [270]. I found that ESTIMATE's tumour purity score was hazardous for melanoma-specific survival, lending further support to this discovery.

Desmoplastic melanoma is characterised by an abundance of collagenous stroma [286] and as such, is a biological example of the protective effects of the stroma within primary cutaneous melanoma, tending to present with more localised disease [100]. The nature of the stromal fibroblasts may be shaped by interactions with cancer cells, including the release of soluble factors, as well as cell-to-cell contact between cancer and stromal cells [247, 287]. Furthermore, there is evidence to suggest that physical force can activate normal fibroblasts, leading to alterations in the structure of fibronectin and in biochemical signalling [288], which could account for the inverse association between adverse features of the primary melanoma and the POS, as a more rapidly proliferating tumour might induce such changes in fibroblasts.

One of the strengths of the study is that all of the H&E sections were reviewed by Prof. Newton-Bishop and were marked for the purpose of TMA core sampling in a consistent way so that the data were comparable within the data set. Furthermore, a detailed histopathological assessment of a large number of melanomas collected from participants in a population-ascertained cohort, was performed by a single observer, with a high intra-observer reproducibility (Chapter 3). Moreover, transcriptomic data were available for the majority of these cases. By performing a comprehensive histopathological review of the cored region, it was possible to explore the corresponding transcriptomic correlates. This is the first study to utilise RandomSpot© to estimate the POS within a large cohort of primary melanomas and to explore its association with transcriptomic data derived from that region of the tumour.

The discovery that the POS was highly significantly protective for melanoma-specific death was surprising, in view of the abundance of literature in many cancers suggesting that the POS might be hazardous. A strong role for immune cells is implied by the consistent enrichment of immune cell pathways in association with a high stromal content. It was noteworthy that TILs within the whole tumour were not an independent prognostic factor in this study, although the core lymphocytic infiltrate was protective (Chapter 4). The revolutionary impact of immunotherapy in the treatment of advanced melanoma [216, 289] highlights the importance of anti-tumour immunity in melanoma. In spite of durable responses to immunotherapy [216, 289], the proportion of patients who respond is low and the potential toxicity high [290]. Identifying which factors reliably predict those who will benefit from immunotherapy is the focus of

intensive research in many centres. The POS included immune cells and, therefore, its protective effect is consistent with the observed clinical responses to immunotherapy. Moreover, ESTIMATE's immune score was significantly predictive of melanoma-specific survival (Table 5.4 and Table 5.5). In the future, the POS could be evaluated as a potential predictive biomarker of response to immunotherapy. Perhaps even more intriguing is the evidence to suggest that the non-immune stromal component of the POS might be protective. The POS remained an independent prognostic factor, after adjusting for the core immune cell infiltrate and the POS was significantly associated with not only the ESTIMATE immune score but also the stromal score, which indicates that the non-immune stromal component could be important. Moreover, the ESTIMATE stromal score was a more powerful predictor of survival. This work helps to inform the way histopathologists view melanoma and suggests that describing and quantifying the stromal constituents might be just as important as evaluating factors that relate to melanoma cell-specific features.

Comparative enrichment analyses between the POS and the extent of the core immune cell and lymphocytic infiltrates revealed a high degree of overlap. *SDF1* was upregulated in association with the POS but not with either the extent of the core immune cell infiltrate overall or the core lymphocytic infiltrate, suggesting that this might be a marker of the non-immune stromal compartment. Furthermore, survival analyses revealed that *SDF1* and its receptor, *CXCR4,* were protective for melanoma-specific death, with *SDF1* being an independent prognostic factor. Therefore, a synergy may exist between the non-immune and immune stromal constituents, which is worth exploring further. The possibility that *SDF1* was expressed by immune cells, or even by melanoma cells, cannot be ruled out, however, the strong association between the POS and *SDF1*, and not the extent of the core lymphocytic infiltrate or tumour percentage, suggests that this was not the case.

SDF1, also known as *CXCL12*, is a chemokine that is reported to induce chemotaxis of lymphocytes, monocytes and dendritic cells [291]. SDF1 protein expression has previously been demonstrated to be high in normal skin, particularly within fibroblasts, although it may also be expressed by other cell types, including immune, endothelial and cancer cells [292]. In an organotypic melanoma culture, *SDF1* expression by melanoma cells induced the migration of cytotoxic T lymphocytes towards them [241]. In mouse models of melanoma, colon and lung cancer, adenoviral gene transfer of *SDF1* resulted in the accumulation of dendritic cells and CD8+ T cells within the tumours, a corresponding reduction in tumour growth and increased survival [291]. Furthermore, in a melanoma mouse model, the injection of tumour cells expressing SDF1 led to tumour rejection in half of the mice and the tumours were heavily infiltrated

by lymphocytes [293]. In a study of 64 primary melanomas, McConnell *et al.* reported divergent effects for *SDF1* and its receptor, *CXCR4* [294]. The epidermal expression of SDF1 protein was protective for melanoma metastasis-free survival, whilst CXCR4 expression by melanoma cells was associated with increased metastases among AJCC stage II cases only [294]. They reported that the protein expression of CXCR7, an alternative receptor and scavenger for SDF1, was localised to vascular endothelial cells [294]. Their findings contrast with the results of my project, which revealed that both *SDF1* and *CXCR4* gene expression were protective for melanoma-specific death. In a study of 51 primaries and 52 melanoma metastases, Monteagudo *et al.* compared the mRNA expression ratio of *SDF1* and *CXCR4* [295]. The *SDF1/CXCR4* ratio was significantly higher in primary melanomas ≤1mm compared to melanomas >1mm in thickness, and in primary compared to metastatic melanomas, and the ratio was predictive of distant metastasis-free survival [295]. They noted SDF1 protein expression in melanoma, endothelial and dendritic cells, lymphocytes and fibroblasts and of CXCR4 in all of these cells apart from dendritic cells and fibroblasts [295]. Napolitano *et al.* studied peripheral blood lymphocytes in 195 stage I-III melanoma patients and found that cases with CD4+CD45RA+CXCR4+ lymphocyte levels comprising >25% of the peripheral blood lymphocytes, had a significantly longer disease-free survival [296].

Despite the evidence in favour of a protective role for *SDF1*, several studies also suggest a hazardous effect. An *in vitro* study found that high, but not low, levels of *SDF1* expression by melanoma cells repelled T cells, resulting in a decrease in the T-cell infiltration of tumours [297]. Furthermore, hypoxia has been shown to instigate the activation of dermal fibroblasts to myofibroblasts, capable of promoting melanoma cell invasion and displaying increased secretion of SDF1, vascular endothelial growth factor A and interleukin 6 [298]. D'Alterio *et al.* showed that mice, wild type or heterozygote for *CXCR4*, both developed lung metastases, following inoculation with melanoma cells but smaller metastases developed in heterozygote mice [299]. Treatment with a *CXCR4* inhibitor led to a reduction in lung metastases in both wild type and heterozygote mice [299]. *SDF1* has also been shown to promote melanoma cell invasion across an artificial membrane [300]. The expression of CXCR4 protein in primary melanomas has previously been shown to be associated with an increased risk of metastasis and death, however, the number of cases was small (n=40 and 71, respectively) and the median follow-up was short (32 and 38 months, respectively) [301, 302].

Further insight into the metastatic process could be gained by assessing the POS and SDF1 protein expression in primary cutaneous melanomas and matched metastases in

a large data set. The cellular source of SDF1 may be crucial. In the future, it may be possible to establish whether a higher POS in the primary tumour corresponds to a higher POS in the metastasis or if the POS tends to differ between cutaneous, nodal and visceral sites. Future work, recording the POS longitudinally in patients with metastases could inform therapeutic stratification and, perhaps, help in the identification of patients who would most likely benefit from early intervention with immunotherapy. The findings of this study suggest that TMA biopsies taken horizontally through the advancing edge of primary cutaneous melanomas, on average, consist of ~30% stroma. This information could be incorporated into an algorithm to inform the interpretation of transcriptomic data, in terms of the relative tumour and stromal fractions. Stromal “contamination” may also have implications for clinical mutation testing. New gene signatures could be developed that could be of even more prognostic significance, by refining the ESTIMATE gene lists and incorporating them into a single signature, tailored for use in melanoma. This study demonstrated that increasing POS conferred a decreased risk of melanoma-specific death, highlighting the need for further characterisation of fibroblasts and other stromal constituents within the melanoma microenvironment. The ratio of native dermal fibroblasts relative to cancer-associated fibroblasts may be important in determining the switch from an inhibitory microenvironment to one that is conducive to cancer growth, however, this was not possible to explore during my PhD. Further characterisation of the nature of the stroma and the basis of its profound protective effects in primary cutaneous melanomas may help to elucidate the key players in the non-immune stroma.

A limitation of the study was that the POS was measured within a segment of the primary melanoma rather than across the entire tumour. The amount of stroma could have varied from one region of the melanoma to another, particularly in view of the intrinsic heterogeneity of primary cutaneous melanoma [117, 222]. Although the phenotypic heterogeneity within primaries is well described [117], I argue that the manner in which the slides were marked for coring would have reduced this bias. Moreover, the POS consisted of several components, including collagen and immune cells, which makes it difficult to determine their respective contributions. The histopathological assessment focused on a virtual pathology image of the melanoma H&E section that had been taken prior to sampling with a TMA needle. Therefore, it is possible that the appearance (and the corresponding POS) of the estimated cored regions differed slightly from the TMA biopsy samples, due to inherent variation between serial H&E sections. Differences could also have occurred in the estimation of the cored region on the digital image relative to the TMA biopsy site or between the marking on the H&E section and the point of insertion of the TMA needle through the

tumour block. In addition, the histopathological assessment was based on a two-dimensional image of the cored region, whereas the TMA biopsy incorporated a three-dimensional piece of tissue, obtained through sampling the tumour horizontally. From a technical point of view, RandomSpot© software produces a set of arrows, the number of which can be selected by the user. Fifty arrows were allocated to each cored region on the basis of the results of pilot work (Appendix C). Due to the nature of the technique, it is possible that arrows could have landed more frequently on larger structures or nuclei, which might have led to overestimation of larger structures/cells. This is why a composite score was used for the POS, in preference to recording separate counts for each immune cell constituent. Nonetheless, it is possible that the technique could have produced inaccurate results for the POS, especially in view of the variation in melanoma cell size [117]. It is reassuring, however, that the average tumour purity determined by ESTIMATE [169] was ~70% (Figure 5.15). Finally, there was a bias towards sampling thicker primary melanomas and, therefore, it is not possible to ascertain whether or not similar results would have been obtained for melanomas <0.75mm thick. It is probable that thinner primary melanomas would have more stroma relative to thick tumours, however, this suspicion is as yet unconfirmed. Further work, looking at the POS across the entire primary melanoma, could help to clarify whether or not the findings pertaining to the cored region could be applied to the whole tumour. However, circumscription of the invasive margin of melanoma, followed by spot counting (using RandomSpot©) across the entire tumour, is less likely to be practicable in clinical work. This is because the advancing edge of melanoma tends to be convoluted as a result of nesting. It would be interesting to devise separate histopathological scores for the immune and non-immune cell components, to help to decipher their respective significance. Alternative techniques (to RandomSpot©), such as the use of disector frames, could be used to explore this [303]. This approach utilises counting frames, which adjust for the irregularity of the shapes of objects, thus reducing the possibility of over-estimating their frequency within a region of tissue [303]. Immunohistochemical studies were not performed in this study, as a limited number of tissue sections could be made from the tumour blocks, according to the ethical approval that is in place. In any case, conservation of the tumour blocks is crucial, to permit clinical mutation testing at a later date, in view of the fact that many of the study participants are still living. MetaCore™ enrichment analyses highlighted *SDF1* as being unique to the stroma gene list, among thousands of genes that were significantly associated with the POS. MetaCore™ produces results based on the literature and, therefore, there was an inherent bias towards identifying curated pathways as being significant.

In summary, I have provided strong evidence at both a histopathological and a transcriptomic level for the protective effects of a high percentage of stroma in primary melanomas. In the future, I would like to evaluate the POS in an independent data set to validate this compelling finding. In this study, the POS, ESTIMATE's scores and *SDF1* were each independent prognostic factors. Further research, to tease out the complex interactions between the tumour and host, and to explore the drivers of *SDF1* upregulation would be advantageous. As previously mentioned, although immunotherapy can produce durable effects [126, 289, 304], only a subset of patients will respond. Therefore, exploring whether or not the POS could assist in the identification of such individuals would be beneficial and alternative therapeutic strategies aimed at the non-immune stroma might also be worth evaluating. SDF1 levels have previously been shown to be quantifiable in the blood [305]. Therefore, in the future, studying the effects of circulating SDF1 levels and matched tumour samples in melanoma patients, could be worthwhile. I have shown that the POS is a highly reproducible parameter, both within and between observers (Chapter 3) and can be learned quickly. Although the ESTIMATE stromal score was a more powerful predictor, transcriptomic data are not readily available in clinical practice. The POS represents a histopathological measure that is inexpensive, reliable and can be measured using digital techniques, as in this study, or could be measured using a light microscope with a graticule (containing a grid). The results of this study suggest that the incorporation of the POS into the histopathological assessment of melanoma would be worthwhile. Furthermore, this work provides novel insights into the importance of the stromal compartment within primary melanomas and, in the future, how we might consider melanoma in terms of its microarchitecture and neighbouring cells.

Chapter 6 Histopathological changes associated with *BAP1* mutations or *ALK* fusions and the melanoma transcriptome

6.1 Introduction

The histopathology of melanoma is central to staging and underpins predictions of melanoma-specific survival [43].

There is growing evidence that histopathological characteristics might also help to identify patients whose tumours have particular somatic mutations and patients who have inherited genetic variation associated with risk, including familial cancer predisposition syndromes [159, 306]. Such genotype/phenotype correlations are important to elucidate because they could help to identify high-risk patients and to clarify the risk of other, associated cancers. This was of particular interest to me because the fundamental hypothesis of the thesis was that histopathological features might unveil characteristic transcriptomic signatures or associate with individual patient factors.

In this chapter, I will explore what is known about mutation of the *BRCA1 associated protein 1* (*BAP1*) gene in terms of cutaneous melanoma histopathology. This gene was identified as somatically mutated in lung cancer cell lines and breast cancer [307, 308]. Subsequently, somatic mutations and a germline mutation were reported in ocular melanoma [309]. Germline *BAP1* mutations were shown to be associated with increased risk of several cancer types, including ocular and cutaneous melanoma [159]. Cutaneous melanocytic lesions in individuals with germline *BAP1* mutations had an unusual appearance [159], however, similar findings could be identified in patients without such germline mutations [306, 310]. Moreover, unusual histopathological features were reported in lesions that behaved in a benign fashion, in families with germline *BAP1* mutations [159], and similar lesions were seen sporadically in the population [306]. Whether these lesions occurred in families with germline *BAP1* mutations or in the general population, it has not as yet proved possible to identify good prognostic markers, and such lesions are often known as “spitzoid tumours of uncertain malignant potential” (STUMP). In this chapter, I will describe work carried out in tumours excised from melanoma patients ascertained from the general population in the north of England, in whom variants in the *BAP1* gene were sought in the germline.

It has been reported that, at a somatic level, kinase fusions are relatively common in spitzoid lesions [311] and that melanocytic lesions with *Anaplastic lymphoma kinase*

(*ALK*) fusions have a characteristic histopathological appearance (typically reported as being exophytic with a plexiform growth pattern, consisting of fascicles of spindle cells) [158].

This chapter contains work that has recently been published [161] [312].

The aims of the project were to:-

- Determine the proportion of melanomas within the Leeds Melanoma Cohort Study (reviewed by me) that had histopathological features, which have previously been described in association with germline *BAP1* mutations.
- Determine the proportion of participants that carry germline *BAP1* mutations which have been predicted to be deleterious, in order to establish the predictive value of the histopathological features.
- Explore the relationship between the presence of a personal or family history of cancers and/or the presence of a germline *BAP1* mutation.
- Examine the association between the presence of characteristic *BAP1* histopathological features and the transcriptome, particularly with respect to *BAP1* and genes proposed to be involved in its signalling pathway.
- Determine the proportion of melanomas within the Leeds Melanoma Cohort Study (reviewed by me) that had histopathological features, which have previously been described in association with *ALK* fusions.
- Examine the association between the presence of characteristic *ALK* fusion-like histopathological features and the transcriptome, particularly with respect to *ALK* and genes proposed to be fusion partners for *ALK*.
- Explore the transcriptomic correlates of the histopathological appearances in cutaneous melanomas, which were suggestive of either a *BAP1* mutation or an *ALK* fusion, using an agnostic approach.

6.1.1 Germline *BAP1* mutations

The benefit of linking clinical, histopathological and genetic information is illustrated by the discovery of germline mutations in the *BAP1* gene.

There is some evidence from gene expression studies to suggest that two distinct molecular profiles might help to distinguish between primary uveal melanomas of different metastatic potential, with “class 1” and “class 2” signatures proposed to have a lower and a higher risk of metastasis, respectively [313]. In a study of uveal melanomas, Harbour *et al.* identified somatic *BAP1* mutations in 26/31 (84%) cases with a “class 2” gene expression signature, compared to 1/26 with a “class 1” signature [309]. All of the *BAP1* mutations were somatic, except for one case in which a germline

BAP1 mutation was also confirmed [309]. Wiesner *et al.* described a novel familial cancer predisposition syndrome in two families, which was associated with germline mutations in *BAP1* [159]. Loss of chromosome 3 or part of its short arm was found by array-based comparative genomic hybridization (aCGH) in 50% of the melanocytic lesions from three members in the first family described [159]. Massive parallel sequencing revealed a frameshift mutation in *BAP1* [159]. The wild type allele was noted to be somatically mutated, supporting the concept of *BAP1* as a tumour suppressor gene [159]. In the second family, the germline *BAP1* mutation abolished the acceptor splice site at the last exon, resulting in retention of the last intron [159]. Germline mutation carriers were predisposed to the development of multiple, pink, dome-shaped naevi from the second decade onwards, atypical Spitz tumours and both cutaneous and uveal melanomas [159]. Inheritance was reported to follow an autosomal dominant pattern.

It is estimated that germline *BAP1* mutations account for approximately 1-1.5% of cutaneous melanomas [163, 314]. In addition to cutaneous and uveal melanoma, subsequent reports have indicated that affected families appear to be at increased risk of several other cancers, including mesothelioma [315], meningioma [165], renal cell carcinoma [164] and basal cell carcinoma (BCC) [316, 317], among others. Tentative associations with cholangiocarcinoma [318], leukaemia [318], gastric [319] and thyroid cancer [320] have also been reported. Abdel-Rahman *et al.* additionally reported a positive family history of neuroendocrine carcinoma, breast cancer, colon cancer, lung and ovarian adenocarcinomas in such families [165], the significance of which is uncertain, considering that some of these cancers are not uncommon in the general population and could have been an incidental finding. An association with high-grade colorectal and renal cell carcinoma was reported in a recent meta-analysis, however, the studies (somewhat confusingly) included patients with somatic *BAP1* mutations [321].

6.1.2 The role of BAP1

BAP1 is located on chromosome 3p21 and it encodes a nuclear protein, BAP1 [322]. BAP1 acts as a deubiquitinating enzyme [308]. The part of the BAP1 protein, which confers its deubiquitinase activity, is referred to as the ubiquitin carboxy-terminal hydrolase (UCH) domain [308]. It is a member of the polycomb family of proteins, which are involved in silencing other genes. The BAP1 protein is thought to act as a tumour suppressor, to be involved in DNA repair and its nuclear localisation is crucial for its function in mice [323-325]. Kumar *et al.* reported that BAP1 may paradoxically

behave as a survival factor in some cutaneous melanomas, facilitating their proliferation [326]. A metabolic regulatory role has also been reported for BAP1 [327].

Loss of nuclear BAP1 expression is associated with a worse survival and increased risk of relapse in uveal melanoma [328], however, its impact on outcome in cutaneous melanoma is yet to be elucidated. Yeh *et al.* reported no evidence of relapse in 29 cases of cutaneous melanocytic lesions with isolated loss of chromosome 3 incorporating the *BAP1* locus, however, the mean follow-up time was just 16 months and the findings were limited to those with presumed somatic mutations [329]. A recent meta-analysis reported a worse outcome in association with inactivation of BAP1 for several cancers, except mesothelioma where it appears to confer a better prognosis [321]. It is noteworthy that the meta-analysis included studies which contained a mixture of cases with somatic and/or germline *BAP1* mutations [321].

6.1.3 Histopathological assessment of melanocytic lesions in association with germline *BAP1* mutations

Naevi, occurring in the context of an inherited *BAP1* mutation, although clinically bland, have been reported to display an unusual appearance on histopathological assessment [159]. At low power magnification, the lesions were symmetrical and strikingly dermal. At high power, the melanocytes were variably pleomorphic and were composed of a mixture of epithelioid melanocytes with abundant cytoplasm and prominent, eosinophilic nucleoli and in a subset, a population of round melanocytes with hyperchromatic nuclei [159]. Cutaneous melanocytic lesions, which had features that overlapped with melanoma, were regarded to be atypical Spitz tumours, the metastatic potential of which was uncertain [159]. Marusic *et al.* described a case series of six melanocytic lesions, including two primary cutaneous melanomas, in the setting of an inherited *BAP1* mutation [160]. Both melanomas were predominantly dermal and were flanked by adjacent naevus cells [160]. Five of the six cases had prominent nuclear pseudoinclusions and multinucleated melanocytes [160]. All cases showed adipocytic metaplasia [160]. Some of their findings, corroborated in this study, have been published [161].

6.1.4 Somatic *BAP1* mutations

The biological significance of somatic *BAP1* mutations in cutaneous melanoma has not been fully elucidated. Wiesner *et al.* reported that 5% (3/60) of sporadic cutaneous melanomas and 11% (2/18) of atypical Spitz tumours harboured somatic *BAP1* mutations [159]. They proposed that somatic *BAP1* mutations resulted in a distinctive histopathological appearance [159]. Both of the *BAP1*-mutated atypical Spitz tumours

in their study were reported to resemble those described in patients with inherited *BAP1* mutations [159]. The photomicrograph that was provided for a case of sporadic *BAP1*-mutated melanoma showed similar features [159]. Busam *et al.* reported similar histopathological features in 8 combined melanocytic lesions in 6 people without a germline *BAP1* mutation [310]. Yeh *et al.* reported one case of blue naevus-like melanoma, which occurred on the scalp of a 64-year-old woman and demonstrated loss of nuclear BAP1 staining on immunohistochemistry [329]. The authors reported the presence of a prominent lymphocytic infiltrate in half of the cases with biallelic loss of *BAP1*, some lesions containing larger melanocytes with a plasmacytoid appearance, in apposition to lymphocytes (which they referred to as “the kiss of death”) [329]. Loss of immunohistochemical nuclear staining for BAP1 appeared to correlate with biallelic loss of *BAP1* [159]. In a subsequent study of 32 atypical Spitz tumours, 28% (n=9) showed loss of nuclear BAP1 staining on immunohistochemistry (IHC), the majority (89%, 8/9) of which had concomitant *BRAF* mutations [306], which are unusual in Spitz naevi [330-332]. These lesions shared some features with those described in patients with germline *BAP1* mutations, including distinctive epithelioid melanocytes and the presence of multinucleated cells, although these features could also be appreciated to a variable degree in lesions where BAP1 was conserved [306]. Piris *et al.* reported that, in patients with germline *BAP1* mutations, 67% (20/30) of cutaneous melanocytic lesions showed combined *BRAF*V600E staining and loss of nuclear BAP1 staining, whereas nuclear BAP1 staining was conserved in most sporadic naevi and melanomas [332]. They reported loss of nuclear BAP1 staining in ~2.5% (2/80) sporadic primary melanomas, suggesting the possibility of somatic *BAP1* mutations, although the histopathological appearance of the sporadic melanomas was unremarkable (n=4) [332]. Murali *et al.* reported that the absence of nuclear BAP1 staining was higher (22%; 9/158) in desmoplastic melanomas, with loss of nuclear BAP1 staining in 6% (9/158) of melanomas overall [333].

6.1.5 Other molecular changes in spitzoid lesions

Apart from *BAP1* mutations, which are rare in cutaneous melanocytic lesions, several other molecular changes can occur in spitzoid lesions. A distinct subset of Spitz naevi with copy number gains in chromosome 11p, incorporating *HRAS*, has been noted [334]. These lesions tended to be intradermal and to consist of pleomorphic melanocytes, which were dispersed between collagen bundles at the base [334]. Intranuclear inclusions were also noted [334]. The histopathological appearance was similar in the 12 cases with gains in chromosome 11p, however, *HRAS* mutations were confirmed in 67% (n=8) of these cases [334].

In an effort to identify further putative molecular changes underlying spitzoid lesions, Wiesner *et al.* performed targeted DNA and RNA sequencing of 182 cancer genes and 162 kinase-related transcripts, respectively, on 30 Spitz naevi and 8 atypical Spitz tumours [311]. Kinase fusions were established in 60% of Spitz naevi and 75% of the atypical Spitz tumours [311]. In decreasing order of frequency, *ROS1*, *NTRK1*, *ALK*, *RET* and *BRAF* were identified in gene fusions [311]. These findings were replicated in 102 further spitzoid lesions and immunohistochemistry for the respective kinase was positive in cases with the corresponding gene fusions [311]. Such fusions could be potentially exploited therapeutically, where appropriate, by means of targeted inhibition [311]. Subsequently, *NTRK3* [335] and *MET* fusions [336] were identified.

STUMPs, sometimes referred to as atypical Spitz tumours, represent an entity which has uncertain biological behaviour and which displays some features of both a benign Spitz naevus and a cutaneous melanoma. Mutations involving the *TERT* promoter have been reported to predict a more aggressive biological behaviour in such lesions, associated with an increased likelihood of metastasis, although precise histopathological characteristics have not been ascribed to such lesions [337].

I was interested to establish whether or not there was a differential transcriptomic expression in *BAP1* between melanomas, which resembled the melanocytic lesions reported to occur in association with *BAP1* mutations and those melanomas, which did not display such features. In the absence of detectable differences in *BAP1* gene expression, I sought evidence for alternative molecular changes that have been reported in spitzoid lesions.

6.1.6 *ALK* fusions and ALK protein expression in melanoma

The *ALK* gene, located on chromosome 2p23, encodes a receptor tyrosine kinase called anaplastic lymphoma kinase, the activation of which leads to phosphorylation of intracellular kinases [338]. *ALK* fusions can lead to constitutive activation of the tyrosine kinase, resulting in uncontrolled proliferation [338]. *ALK* fusions have previously been identified in a spectrum of cancers, including lung cancer [339], inflammatory myofibroblastic tumours [340], lymphoma [341] and acral melanoma [342]. Kinase inhibitors, such as crizotinib, have been shown to be effective therapeutically [343, 344], although acquired resistance may develop [338]. Wiesner *et al.* reported *ALK* fusions in 10% (14/140) of spitzoid lesions overall, including 11% of Spitz naevi, 17% of atypical Spitz tumours and 3% of spitzoid melanomas in that series [311]. Busam *et al.* reported the histopathological characteristics of *ALK* fusions in a series of spitzoid melanocytic lesions, including 5 Spitz naevi and 12 atypical Spitz tumours [158]. Histopathological findings included a polypoid appearance and a

plexiform growth of fascicles, composed of spindle cells [158]. Of the 17 cases, 15 were amelanotic [158]. Melanocytes stained positive for ALK on immunohistochemistry (IHC) and fluorescence in situ hybridization (FISH) identified *tropomyosin 3* (*TPM3*) and *dynactin 1* (*DCTN1*) as the fusion partners in 11 and 6 cases, respectively [158]. Yeh *et al.* subsequently reported a series of 32 cases with *ALK* fusions, consisting of 6 Spitz naevi, 22 atypical Spitz tumours and 4 spitzoid melanomas [157]. Whilst the majority of the lesions were amelanotic, others were deeply pigmented [157]. The fusion partners included *NPM1*, *TPR*, *GTF3C2* and *CLIP1* [157]. The median thickness was 2.7mm and 16% of cases were ulcerated, whilst dermal mitoses were present in almost half of cases [157]. Lesions tended to be exophytic and were composed of fascicles of spindle cells [157]. More recently, Busam *et al.* reported immunoreactivity for ALK in 7/303 primary and 9/300 metastatic melanomas studied [345]. None of these lesions had *ALK* fusions but instead expressed the *ALK* isoform, *ALK alternative transcriptional initiation* (ALK^{ATI}) [345]. In contrast to *ALK* fusions, the lesions expressing ALK^{ATI} were composed predominantly of epithelioid melanocytes and 5/7 primary melanomas were of nodular subtype [345]. Others have suggested that *ALK* expression in melanoma is exceedingly rare [346]. The more recent discovery of ALK^{ATI} and its histopathological correlates were subsequent to the recording of my histopathological assessment. Therefore, henceforth, I report my findings with respect to possible *ALK* fusions rather than appearances associated with ALK^{ATI}.

6.2 Methods

6.2.1 Germline *BAP1* status testing

Germline *BAP1* testing was performed by the research group of Dr David Adams from the Sanger Institute on previously stored DNA extracted from blood samples from participants of the Leeds Melanoma Cohort Study. Samples were available for the majority of the cohort. Sorting Intolerant from Tolerant (SIFT) [347] and PolyPhen-2 [348] were packages used by the Sanger Institute to predict the pathogenicity of variants.

6.2.2 Deubiquitinase assays

The deubiquitinase function of BAP1 is considered to be central to its role as a tumour suppressor [323, 324]. The Sanger Institute, in collaboration with MISSION Therapeutics©, performed testing of the deubiquitinase function of BAP1 where a non-wild type variant was identified.

6.2.3 *BAP1*-like and *ALK* fusion-like histopathological characteristics

The FileMaker Pro® histopathology database in which I reported detailed histopathological assessment of primary melanomas contained a free-text box which allowed me to record additional details about each case reviewed, including features reported to be typical of *BAP1* mutations or kinase fusions. During the course of my assessment, I flagged cases with histopathological features associated with *BAP1* mutations using this comments box, in recognition of their potential significance. Examples of such features included a variable combination of: an intradermal melanocytic proliferation, epithelioid melanocytes, plasmacytoid melanocytes, round melanocytes with hyperchromatic nuclei, nuclear pleomorphism, and nuclear pseudoinclusions. I also highlighted cases, which had features suggestive of *ALK* fusions, e.g. mainly composed of plump, spindled melanocytes.

6.2.4 Cancer history

Participants recruited to the Leeds Melanoma Cohort Study were asked to list their personal and family history of cancer at recruitment, as part of a questionnaire. The extent of family cancer history and the level of detail provided varied across the cohort: participants were very variably aware of family history. The melanoma patients were asked to consider inviting their first-degree relatives to take part in the study and it was possible to confirm the cancer history in participating family members but not in other relatives. Data on personal and family cancer history were then extracted for analysis by Section staff.

Only first- or second- degree relatives were included in the analysis of family history of cancer. Cancer diagnoses in the probands and their first- and second-degree relatives were verified against Office of National Statistics data and wherever possible, pathology reports were obtained. In some cases, the proband provided additional information in the questionnaire free-text box, e.g. mesothelioma, which was more specific and more likely to reflect an accurate diagnosis than those recorded as “lung cancer”. For the most part, family history was recorded by category, e.g. kidney/bladder/ureter or lung or brain cancer. For instance, it was not possible to ascertain if “brain”, “lung” or “liver” cancers were primary or secondary unless it was explicitly stated.

For the purpose of analysis, I included cases with specific information about the type of cancer, i.e. “mesothelioma”, etc. I recorded the presence or absence of the following cancers previously reported to occur in families with germline *BAP1* mutations in the

proband and in the proband's first- or second-degree relatives: renal cancer, BCC, meningioma, mesothelioma, ocular melanoma or a family history of cutaneous melanoma. I elected to focus my analysis on these cancers because of the aforementioned evidence in the literature, and due to the nature of the cancer history database, in which information for several cancer types was recorded using broad categories. Therefore, it was not possible to distinguish between primary and secondary cancers, e.g. liver.

Where there was more than one case of cutaneous melanoma in the family, the proband was deemed to be the first case recruited (identified by having a lower study number) and the second melanoma case was recorded as a positive family history of cutaneous melanoma for the proband. The only exception was if each melanoma case within the same family had been recruited independently, in which circumstance, each melanoma case was regarded as a proband.

6.2.5 *BAP*-like phenotype

A proband was considered to have a *BAP*-like phenotype if he/she had a history of one or more of the following cancers: renal, BCC, meningioma, mesothelioma or ocular melanoma. This was called "*BAP*-like phenotype (proband)".

The "*BAP*-like phenotype (family)" was assigned if a first- or second-degree relative had a history of any of the above cancers. The "*BAP*-like phenotype (proband/family)" was assigned if either the proband or the proband's first- or second-degree relative(s) had a history of one of the aforementioned cancers.

The "*BAP*-like phenotype MM (family)" was assigned if a first- or second-degree relative had one or more of the above cancers or a history of cutaneous melanoma. The "*BAP*-like phenotype MM (proband/family)" was formed by either the proband having the "*BAP*-like phenotype (proband)" or the proband's first- or second-degree relative having the "*BAP*-like phenotype MM (family)".

6.2.6 Statistical analysis of cancer history data and *BAP1* variant type

Cancer history was analysed for the following cancers: renal, BCC, meningioma, mesothelioma, ocular melanoma (and a family history of cutaneous melanoma). Each cancer type was analysed as a dichotomous variable, i.e. as 0 or 1 (where 0=no and 1=yes), irrespective of the number of each cancer. By extension, the "*BAP*-like phenotype (family)" was equal to 1, even if more than one first- or second-degree relative had a cancer of interest, e.g. BCC.

Cross-tabulation of each cancer and variant type was performed for the proband and family. The Fisher's exact test p-value was reported if any cell value was <5. The Pearson's chi-squared test p-value was reported if there was no individual cell value <5. Cross-tabulation of each of these cancers was performed to compare 2 variant categories, i.e. "none" versus "benign" and "none" versus "deleterious".

Odds ratios were calculated for having a benign variant versus none and for having a deleterious variant versus none, to assess the effect of each variant compared to being wild type for *BAP1*. Exact 95% confidence intervals were calculated, unless there was a zero count in a cell, in which case the Cornfield approximation was used.

The Kruskal-Wallis test was performed to assess whether or not the age at diagnosis of melanoma differed by variant type.

6.2.7 Statistical analysis of *BAP*-like histopathology

Any comments in the histopathology database containing "BAP" were reviewed. If the comment suggested a *BAP*-like histopathological appearance in the primary melanoma, it was scored as "yes". All other reviewed cases lacking a comment about *BAP1* were scored as "no". This permitted analysis as a dichotomous variable, in a similar way to the classification of the cancer history data.

6.2.8 *BAP1* gene expression and transcriptomic analysis

The student's t-test was used to assess the association between *BAP*-like histopathology and gene expression for each of the 29,354 probes in the Illumina® WG-DASL HT12v14 assay. The False Discovery Rate (FDR) correction was performed to correct for multiple testing, to reduce the possibility of finding a significant association by chance. The ILMN_1768363 probe was used to measure *BAP1* gene expression from the melanoma tumour. This was the only probe for *BAP1* in the Illumina® WG-DASL HT12v14 assay. Where more than one probe was available for a single gene, the probe with the highest level of detection within the cohort was selected.

6.2.9 *ALK* gene expression and transcriptomic analysis

The student's t-test was used to assess the association between *ALK* fusion-like histopathology and gene expression for each of the 29,354 probes in the Illumina® WG-DASL HT12v14 assay. The FDR correction was performed to correct for multiple testing, as before. The ILMN_1753135 probe was used to measure *ALK* gene expression from the primary melanoma.

6.3 Results

6.3.1 Variants identified by germline *BAP1* testing

In total, there were 1977 cases from the Leeds Melanoma Cohort Study that had a stored, DNA sample for genetic testing by the Sanger Institute. Of these, 1868 had no variant and were named “none” in the analysis. One hundred cases had a variant that was predicted to be “tolerated” by SIFT or “benign” by PolyPhen-2. These were grouped together as “benign” for the purpose of analysis. Nine cases had a variant that was predicted to be “deleterious” by SIFT or “possibly damaging” or “probably damaging” by PolyPhen-2. These were grouped together as “deleterious” for analysis. Where SIFT and PolyPhen-2 results were divergent (e.g. “tolerated” by SIFT and “possibly damaging” by PolyPhen-2), the group with the more serious variant was assigned. This applied to 2/9 cases in the deleterious group. One splice acceptor variant, one frameshift variant and one case with both a missense and splice region variant were among the variants identified in the “deleterious” group, with the remaining cases in the group having missense variants.

6.3.2 Deubiquitinase assays

Eight of the nine variants that were predicted to be deleterious by SIFT or PolyPhen-2 were tested for deubiquitinase activity. The splice acceptor variant was presumed to result in *BAP1* loss-of-function but the deubiquitinase assay had not been performed, because the case was identified through a subsequent round of sequencing. A germline *BAP1* mutation was, however, confirmed in the proband through clinical testing. The frameshift variant and one of the missense variants showed loss of deubiquitinase activity. These three cases were regarded as having clear loss-of-function but the remaining 6 cases with variants predicted to be deleterious did not show any significant change in deubiquitinase activity.

6.3.3 Histopathological assessment of primary melanomas within the cohort with features associated with *BAP1* mutations

I completed a detailed histopathological assessment of 798 cases from the Leeds Melanoma Cohort Study. The majority of the 798 cases were those intended to be sampled for transcriptomic analysis. Of the 798 cases assessed, 64 (8%) had some histopathological features described as indicative of a *BAP1* mutation. Figure 6.1 shows some examples of melanomas with *BAP*-like histopathology.

Of the 798 cases, 713 had information on *BAP1* variants and cancer history data. 661/713 cases were not flagged as having histopathological features of a *BAP1* mutation, leaving 52 cases, which had suggestive histopathology and additional information about *BAP1* variant type and cancer data.

One of the families under follow-up in the melanoma clinic was recognised by Prof. Newton-Bishop as fitting the profile of a germline *BAP1* mutation (Figure 6.2). Clinical testing confirmed this suspicion. The proband and the proband's first- and second-degree relatives were invited to attend for genetic counselling. The proband was a participant of the Leeds Melanoma Cohort Study. Although sampling using a TMA core biopsy needle had not been performed on this primary melanoma because of its small size, a histopathological assessment was recorded. Family members attending the local melanoma/pigmented lesion clinics agreed to the review and description of their case histories and histopathological findings, which have since been reported [161]. Melanocytic lesions from first- and second-degree relatives were reviewed as part of the process, although only the assessment of the proband's melanoma was formally recorded in the histopathology database.

Figure 6.1 (on following 2 pages): Virtual pathology images of melanomas with *BAP*-like histopathology.

Histopathological findings show A) a melanocytic proliferation (x10 magnification) composed of epithelioid melanocytes, with relative sparing of the dermo-epidermal junction. Some multinucleated cells are highlighted by the black arrow; B) (x10 magnification) a predominantly dermal melanocytic proliferation with evidence of adipocytic metaplasia; C) High power view (x40 magnification) of the melanoma reveals intranuclear pseudoinclusions (a few of which have been highlighted with black arrows). D) Low power view (x4 magnification) of a melanocytic proliferation with relative sparing of the dermo-epidermal junction. E) High power view (x40 magnification) shows atypical melanocytes. The red arrows are pointing to multinucleated melanocytes and the black arrow is pointing to an intranuclear pseudoinclusion.

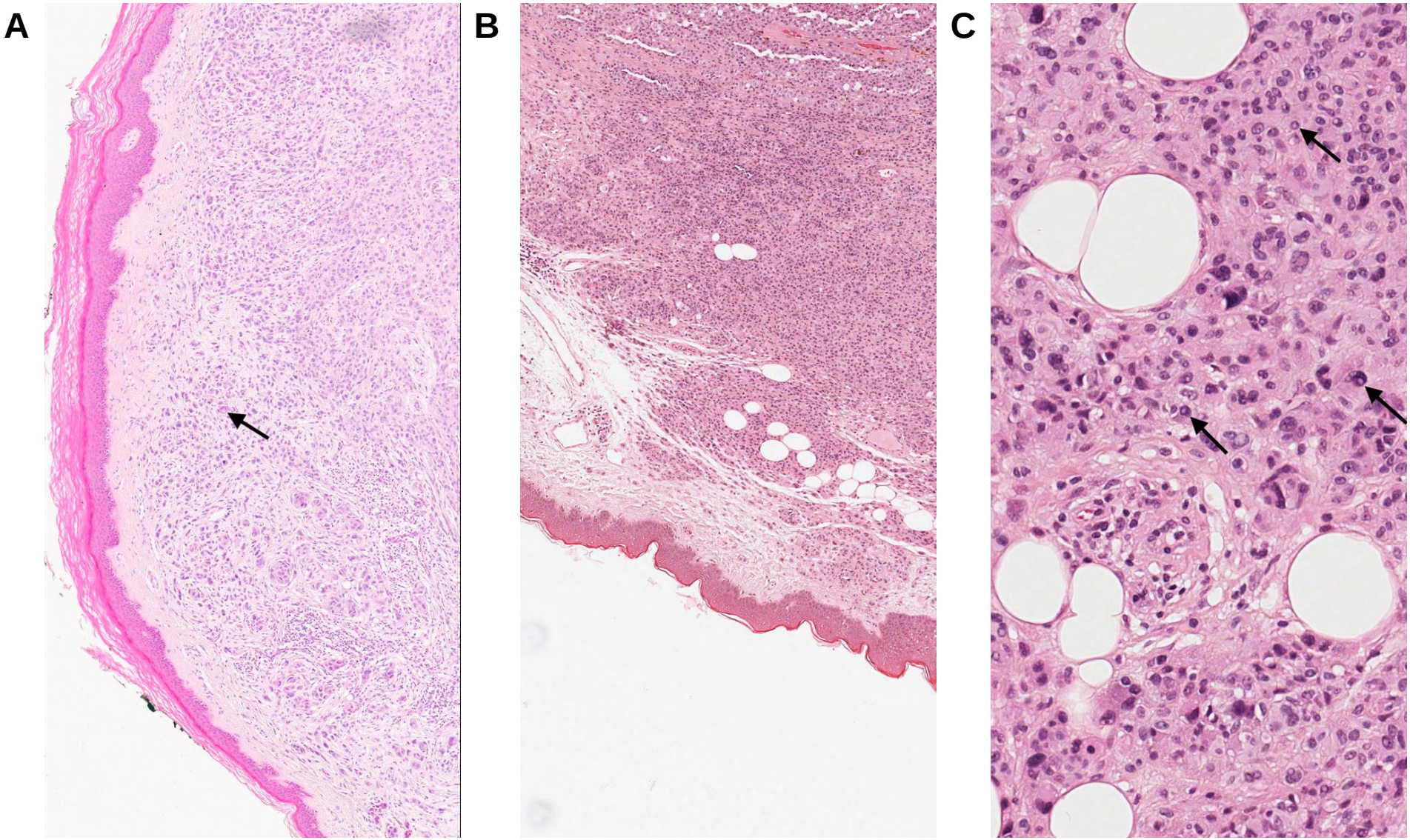
A
B
C

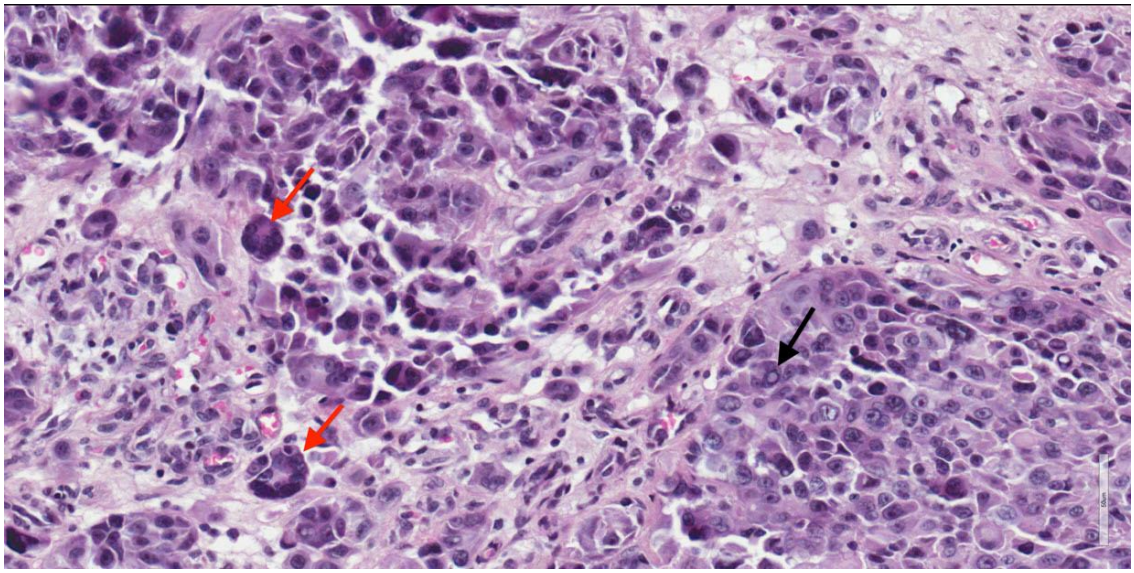

E

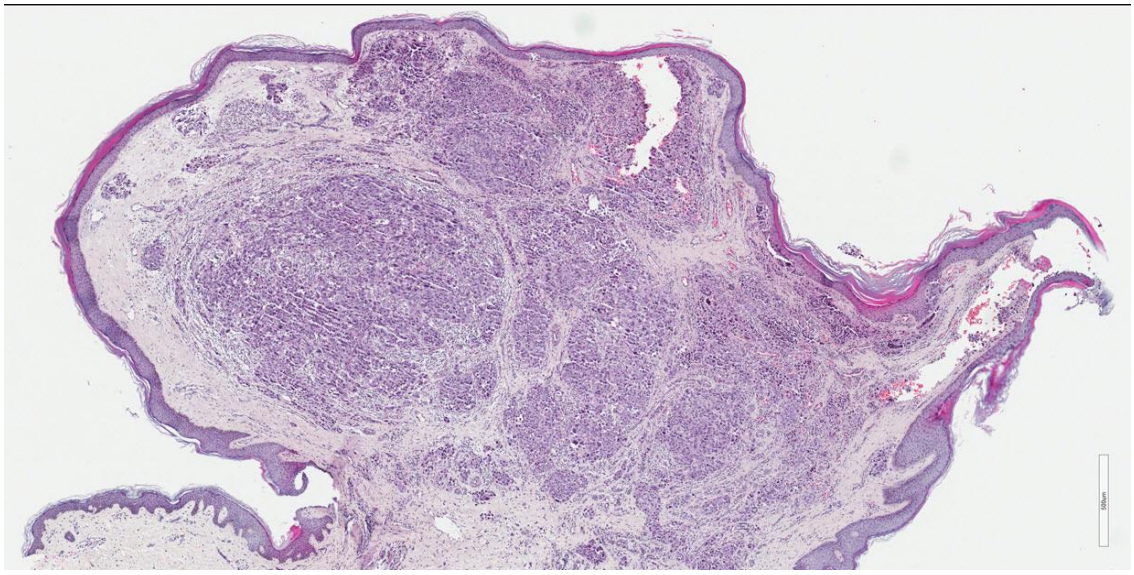

D

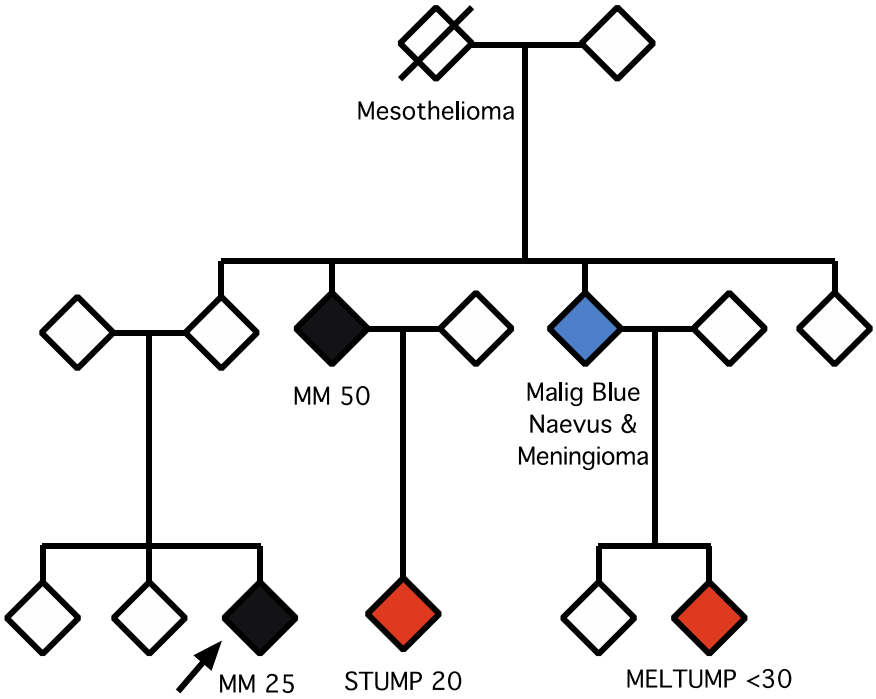

Figure 6.2: Pedigree for a family with a germline BAP1 mutation.

This family was identified by clinical testing. The proband is indicated by a black arrow. A splice acceptor site *BAP1* variant was identified in the proband. MM=melanoma. STUMP=Spitzoid tumour of uncertain malignant potential. MELTUMP=Melanocytic tumour of uncertain malignant potential. Malig Blue Naevus=Malignant blue naevus. Black diamonds represent cases of primary cutaneous melanoma. Red diamonds indicate cases of either STUMP or MELTUMP. The blue diamond indicates a case with a malignant blue naevus and a meningioma.

The proband had a melanocytic lesion, which was amelanotic, and clinically banal but was excised in view of a history of change. Initial histopathological assessment suggested a STUMP. This was diagnosed as a stage II melanoma at the melanoma multidisciplinary team meeting and was subsequently widely excised. A second-degree relative had a history of stage III melanoma (metastatic to a local lymph node basin, Figure 6.3A). Another second-degree relative had an unusual lesion on the scalp that had been curetted by the patient's general practitioner who suspected a cyst. The specimen had not been sent for histopathological assessment. The lesion subsequently recurred and was excised in the department of general surgery. This was diagnosed as a malignant blue naevus histopathologically and sadly the patient subsequently developed liver metastases. An incidental meningioma was diagnosed

on MRI brain. A third-degree relative had a history of asbestos exposure and was reported to have died of a pleural mesothelioma. Following clinical testing, the proband's remaining first- and second-degree relatives were invited for a skin examination. One of the proband's third-degree relatives reported a recent history of change in a long-standing pink lesion. The lesion was excised in view of this change. A STUMP was diagnosed. Subsequent wide local excision and sentinel lymph node biopsy were negative for melanoma. A further third-degree relative reported itch in a long-standing lesion, which had a reassuring clinical appearance but was diagnosed as a melanocytic tumour of uncertain malignant potential (MELTUMP) following histopathological examination.

Histopathological review of melanocytic lesions from this family revealed some features, which had previously been described in association with germline *BAP1* mutations [159, 160]. Namely, the primary melanomas from the proband and a second-degree relative were both amelanotic. The proband's melanoma was predominantly intradermal and was composed of pleomorphic, epithelioid melanocytes, some of which were multi-nucleated and had nuclear pseudoinclusions. A few benign melanocytic naevi had previously been excised from the proband, which were mainly intradermal, had a symmetrical appearance at low-power magnification and some pleomorphism at higher magnification. The second-degree relative's malignant blue naevus lacked an intraepidermal component but this may have been due to previous curettage (Figure 6.3B). The third-degree relative's STUMP was predominantly intradermal, consisting of a nodule composed of epithelioid melanocytes and an adjacent naevus-like component. Nuclear pseudoinclusions were numerous within the epithelioid nodule [161].

Figure 6.3 (following page): Photomicrographs of A) the melanoma lymph node metastasis in the proband's second-degree relative and B) the malignant blue naevus in the proband's second-degree relative.

A) Nuclear pleomorphism can be appreciated within melanoma cells (x40 magnification). The black arrow points to an epithelioid melanocyte, with a prominent eosinophilic nucleolus and abundant cytoplasm. An intranuclear pseudoinclusion is highlighted by the red arrow. B) Histopathological findings (x5 magnification) reveal a thick melanocytic tumour composed of fascicles of spindle cells. There is sparing of the dermo-epidermal junction. This lesion had previously been curetted.

A

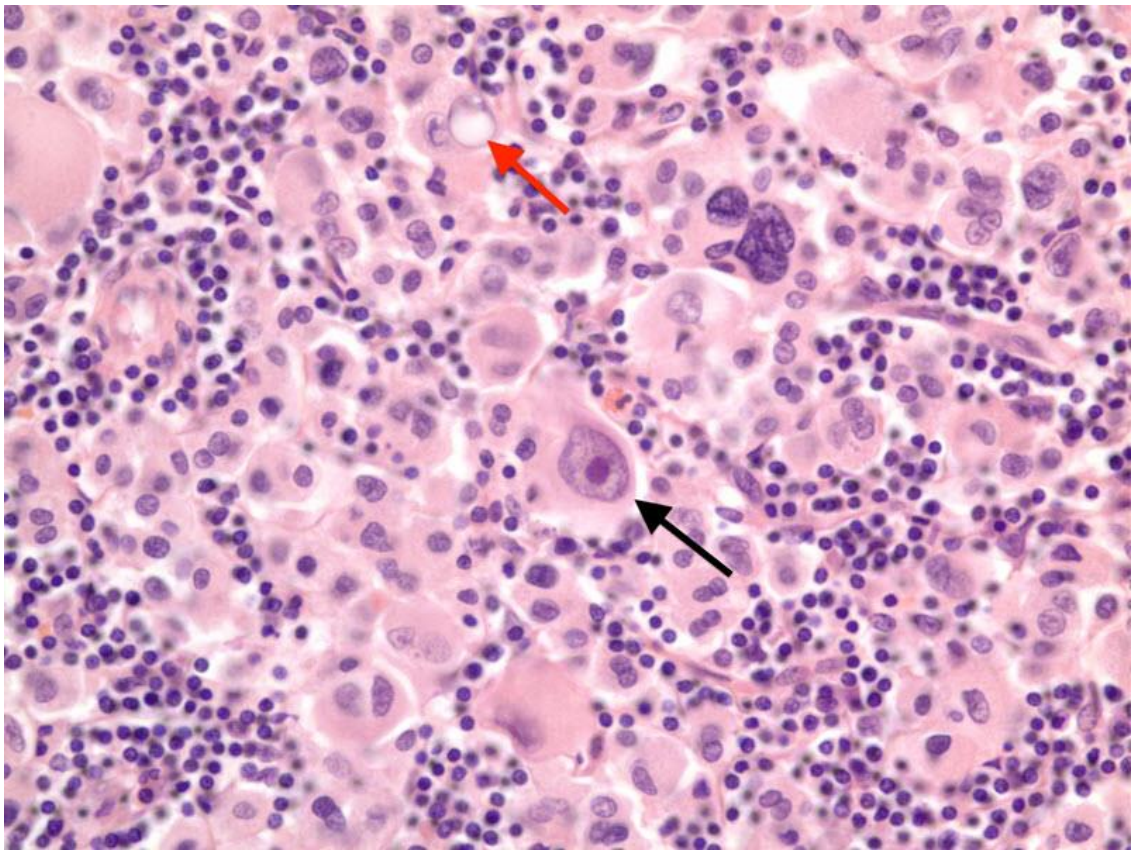

B

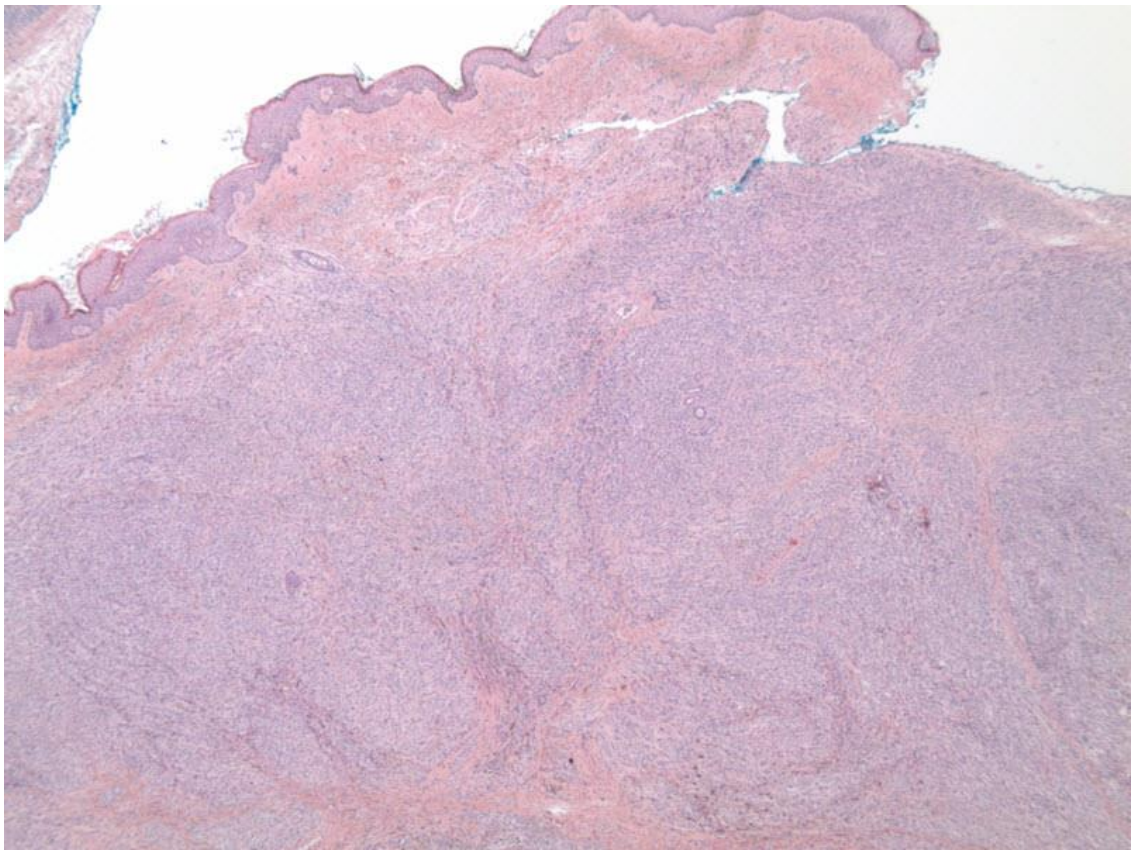

Eight other probands from the Leeds Melanoma Cohort Study were identified as having germline *BAP1* mutations which were predicted to be deleterious by the Sanger Institute. Their primary melanomas and pedigrees were reviewed. Of the remaining two probands with clear loss-of-function variants, one had an amelanotic, intradermal melanoma, whilst the other proband had an amelanotic melanoma that was otherwise difficult to distinguish from a melanoma in a person who was wild type for *BAP1*. In the other 6 cases with missense, germline *BAP1* variants which were predicted to be deleterious, the melanomas were unremarkable compared to other melanomas within the data set. Table 6.1 summarises the results for the 9 probands with *BAP1* variants that were predicted to be deleterious.

Table 6.1 (following page): Summary table of *BAP1* variants, deubiquitinase assay results, cancer history and *BAP*-like histopathology.

Cancer history is reported for melanoma probands (other than cutaneous melanoma) and for their family members (first- or second-degree relatives were considered only). The deubiquitinase assay was not done for the case with a splice acceptor site variant because it was detected in a second round of sequencing, however, it was predicted to be detrimental to *BAP1* function and clinical testing confirmed the presence of a germline *BAP1* mutation in the proband. Three of the nine variants that were predicted to be deleterious by SIFT or PolyPhen-2 were categorised as clear loss-of-function based on their deubiquitinase assay results (except for the splice acceptor variant, as aforementioned). LOF=loss-of-function. NA=not applicable.

Case	*BAP1* variant	Deubiquitinase assay	Category	Proband cancer history (other than cutaneous melanoma)	Family cancer history (1st & 2nd-degree relatives only)	*BAP*-like histopathology (Yes/No)
1	Splice acceptor site	Not done	Predicted deleterious, clear LOF	NA	Melanoma, malignant blue naevus, mesothelioma, meningioma	Yes
2	Frameshift	Abnormal	Predicted deleterious, clear LOF	NA	Melanoma, mesothelioma, bladder cancer	Yes
3	Missense	Abnormal	Predicted deleterious, clear LOF	BCC	Melanoma, renal, gastric cancer, cancer unknown site	No
4	Missense	Normal	Predicted deleterious	BCC, lymphoma	BCC, leukaemia, uterine cancer	No
5	Missense	Normal	Predicted deleterious	NA	Gastric, uterine cancer	No
6	Missense	Normal	Predicted deleterious	NA	BCC, colorectal cancer	No
7	Missense	Normal	Predicted deleterious	NA	Lung cancer	No
8	Missense	Normal	Predicted deleterious	NA	NA	No
9	Missense	Normal	Predicted deleterious	NA	NA	No

6.3.4 The association between histopathology, cancer frequency and germline *BAP1* mutations

Table 6.2 summarises the analysis of the family history for each of the cancers of interest within the proband, the proband's first- or second-degree relatives or the family overall (irrespective of whether the cancer occurred in the proband or in a first- or second-degree relative) by variant type and histopathological appearance in the proband's melanoma. Table 6.2 also shows the association between the presence of *BAP*-like histopathological features (in the proband's melanoma) and having a *BAP1* variant.

A reported history of mesothelioma or meningioma within either the proband or the family was significantly associated with the presence of a deleterious *BAP1* variant, compared to no variant (Table 6.2). The presence of a family history of one or more of the following cancers was associated with a deleterious *BAP1* variant: renal cancer, BCC, meningioma, mesothelioma or ocular melanoma ("*BAP*-like phenotype (in the family)"). It was notable that there were no cases of ocular melanoma within pedigrees in which a deleterious variant had been identified in the proband.

BAP-like histopathology was significantly associated with a history of mesothelioma in either the proband or the family (when taken together) but was not significantly associated with any of the other reported cancers. There was no significant association between the presence of *BAP*-like histopathological changes and the presence of a deleterious *BAP1* variant.

The mean age at diagnosis was lowest in cutaneous melanoma probands carrying a *BAP1* variant predicted to be deleterious (49.2 years compared to 57.3 years without a variant and 56.9 years in those cases with a benign variant) but this was not statistically significant (Kruskal-Wallis test p-value=0.7).

Table 6.2 (following page): Cancer history by *BAP1* variant type and histopathological appearance.

The cancer history among probands and their first- or second-degree relatives ("family") is reported for each of the following cancers, which are considered to be part of the spectrum of cancers seen in families with inherited *BAP1* mutations: renal cancer, basal cell carcinoma (BCC), meningioma, mesothelioma and ocular melanoma. The family history of cutaneous melanoma is also recorded. The reported cancer history is compared to the *BAP1* variant type (which was identified among probands by the Sanger Institute) and to the recorded histopathological appearance of the proband's melanoma (cases for which I had performed a histopathological review). The histopathological appearance ("*BAP*-like histology") was categorised as "Yes" or "No", for the presence of histopathological features suggestive of a *BAP1* mutation (including relative sparing of the dermo-epidermal junction by atypical melanocytes, epithelioid melanocytes, pleomorphic melanocytes, nuclear pseudoinclusions, multinucleated melanocytes and/or a naevoid component of melanocytes with hyperchromatic nuclei). The cancer history is reported separately for probands and their family members (first- or second-degree relatives). In addition, the cancer history for probands and their first- or second-degree family members ("family") was combined to increase statistical power, by assessing whether or not there was a cancer history in either the proband or their family (i.e. either a personal or a family history) for each cancer type. The "*BAP*-like phenotype" and the "*BAP*-like phenotype MM" (described in the Methods) are also compared to the *BAP1* variant type and the histopathological appearance of the proband's melanoma (*BAP*-like histopathology). Finally, a comparison between the "*BAP*-like histopathology" and the type of *BAP1* variant is reported. Fisher's exact test p-values (or Pearson's chi-squared test p-values, indicated by 'p') are reported. Fisher's exact test was used where a cell value was <5. Odds ratios (OR) and 95% confidence intervals (95% CI) for the likelihood of having a benign versus no variant; or of having a deleterious versus no variant, are reported. BCC=Basal cell carcinoma. NC=not calculable. NA=not applicable. N=number of cases. MM=melanoma.

	Presence of any *BAP1* variant in the proband (melanoma case)				Analysis by the type of *BAP1* variant					Analysis by the histopathological appearance		
					Any variant	Benign versus no variant		Predicted deleterious versus no variant		*BAP*-like histopathology (in the proband's melanoma for which central pathology review was available, total N=713)		
Cancer history in the proband and family	**None (N=1868)* (Row %)**	**Benign (N=100)* (Row %)**	**Predicted deleterious (N=9) (Row %)**	**Total N (%)**	**Fisher's exact P-value**	**Fisher's exact P-value**	**OR (95% CI)**	**Fisher's exact P-value**	**OR (95% CI)**	**No (N=661) (Column %)**	**Yes (N=52) (Column %)**	**Fisher's exact *P*-value**
Renal cancer (in the proband)	5 (71.4)	2 (28.6)	0 (0)	7 (100.0)	0.08	0.045	7.6 (0.7-47.0)	1	0 (0-174.3)	3 (0.5)	0 (0)	1
Renal cancer (in the family)	48 (90.6)	4 (7.5)	1 (1.9)	53 (100.0)	0.1	0.3	1.6 (0.4-4.4)	0.2	4.7 (0.1-36.5)	12 (1.8)	1 (1.9)	1
Renal cancer (in the proband or family)	53 (88.3)	6 (10.0)	1 (1.7)	60 (100.0)	0.06	0.07 p	2.2 (0.7-5.3)	0.2	4.3 (0.1-32.9)	15 (2.3)	1 (1.9)	1
BCC (in the proband)	261 (93.9)	14 (5.0)	3 (1.1)	278 (100.0)	0.3	0.99 p	1.0 (0.5-1.8)	0.1	3.1 (0.5-14.5)	99 (15.0)	8 (15.4)	0.9 p
BCC (in the family)	114 (93.4)	5 (4.1)	3 (2.5)	122 (100.0)	0.02	0.7 p	0.8 (0.3-2.0)	0.02	7.7 (1.2-36.5)	33 (5.0)	1 (1.9)	0.5
BCC (in the proband or family)	346 (94.5)	17 (4.7)	3 (0.8)	366 (100.0)	0.4	0.7 p	0.9 (0.5-1.6)	0.4	2.2 (0.4-10.4)	119 (18.0)	8 (15.4)	0.6 p
Meningioma (in the proband)	4 (100.0)	0 (0)	0 (0)	4 (100.0)	1	1	0 (0-18.1)	1	0 (0-219.4)	2 (0.3)	0 (0)	1
Meningioma (in the family)	0 (0)	0 (0)	1 (100.0)	1 (100.0)	0.005	NC	NC	0.005	NC	0 (0)	1 (1.9)	0.07
Meningioma (in the proband or family)	4 (80.0)	0 (0)	1 (20.0)	5 (100.0)	0.02	1	0 (0-18.1)	0.02	58.3 (1.1-670.5)	2 (0.3)	1 (1.9)	0.2

					Analysis by the type of *BAP1* variant					Analysis by the histopathological appearance		
	Presence of any *BAP1* variant in the proband (melanoma case)				Any variant	Benign versus no variant		Predicted deleterious versus no variant		*BAP*-like histopathology (in the proband's melanoma for which central pathology review was available, total N=713)		
Cancer history in the proband and family	**None (N=1868)* (Row %)**	**Benign (N=100)* (Row %)**	**Predicted deleterious (N=9) (Row %)**	**Total N (%)**	**Fisher's exact P-value**	**Fisher's exact P-value**	**OR (95% CI)**	**Fisher's exact P-value**	**OR (95% CI)**	**No (N=661) (Column %)**	**Yes (N=52) (Column %)**	**Fisher's exact *P*-value**
Mesothelioma (in the proband)	0 (0)	0 (0)	1 (100.0)	1 (100.0)	0.005	NC	NC	0.005	NC	1 (0.2)	0 (0)	1
Mesothelioma (in the family)	4 (66.7)	0 (0)	2 (33.3)	6 (100.0)	0.0004	1	0 (0-18.1)	0.0003	133.1 (10.1-1084.2)	1 (0.2)	2 (3.9)	0.02
Mesothelioma (in the proband or family)	4 (57.1)	0 (0)	3 (42.9)	7 (100.0)	0.000003	1	0 (0-18.1)	0.000003	233 (26.7-1660.1)	2 (0.3)	2 (3.9)	0.03
Cutaneous melanoma (in the family)	146 (93.0)	8 (5.1)	3 (1.9)	157 (100.0)	0.049	0.95 p	1.03 (0.4-2.2)	0.03	5.9 (0.9-27.9)	47 (7.1)	4 (7.7)	0.8
Ocular melanoma (in the proband)	0 (0)	0 (0)	0 (0)	0 (0)	NC	NC	NC	NC	NC	0 (0)	0 (0)	NC
Ocular melanoma (in the family)	2 (100.0)	0 (0)	0 (0)	2 (100.0)	1	1	0 (0-36.1)	1	0 (0-439.1)	1 (0.2)	0 (0)	1
Ocular melanoma (in the proband or family)	2 (100.0)	0 (0)	0 (0)	2 (100.0)	1	1	0 (0-36.1)	1	0 (0-439.1)	1 (0.2)	0 (0)	1
BAP-like phenotype (in the proband)	267 (93.4)	16 (5.6)	3 (1.0)	286 (100.0)	0.2	0.6 p	1.1 (0.6-2.0)	0.1	3.0 (0.5-14.1)	102 (15.4)	8 (15.4)	1 p
BAP-like phenotype (in the family)	166 (93.3)	8 (4.5)	4 (2.2)	178 (100.0)	0.01	0.8 p	0.9 (0.4-1.9)	0.006	8.2 (1.6-38.4)	46 (7.0)	3 (5.8)	1
BAP-like phenotype MM (in the family)	289 (93.5)	16 (5.2)	4 (1.3)	309 (100.0)	0.08	0.9 p	1.04 (0.6-1.8)	0.04	4.4 (0.9-20.4)	85 (12.9)	5 (9.6)	0.5 p

					Analysis by the type of *BAP1* variant					**Analysis by the histopathological appearance**		
	Presence of any *BAP1* variant in the proband (melanoma case)				**Any variant**	**Benign versus no variant**		**Predicted deleterious versus no variant**		***BAP*-like histopathology (in the proband's melanoma for which central pathology review was available, total N=713)**		
Cancer history in the proband and family	**None (N=1868)* (Row %)**	**Benign (N=100)* (Row %)**	**Predicted deleterious (N=9) (Row %)**	**Total N (%)**	**Fisher's exact P-value**	**Fisher's exact P-value**	**OR (95% CI)**	**Fisher's exact P-value**	**OR (95% CI)**	**No (N=661) (Column %)**	**Yes (N=52) (Column %)**	**Fisher's exact *P*-value**
BAP-like phenotype (in the proband or family)	397 (94.1)	21 (5.0)	4 (0.9)	422 (100.0)	0.2	0.95 p	0.98 (0.6-1.6)	0.1	3.0 (0.6-13.8)	132 (20.0)	10 (19.2)	0.9 p
BAP-like phenotype MM (in the proband or family)	496 (94.1)	27 (5.1)	4 (0.8)	527 (100.0)	0.5	0.9 p	1.02 (0.6-1.6)	0.3	2.2 (0.4-10.3)	163 (24.7)	12 (23.1)	0.8 p
BAP-like histopathology present (in the proband's melanoma for which a histopathology review was completed, N=713)	49 (94.2)	1 (1.9)	2 (3.9)	52 (100.0)	0.1	0.7	0.4 (0.01-2.6)	0.1	3.6 (0.4-19.8)	NA	NA	NA

6.3.5 The relationship between *BAP*-like histopathology and *BAP1* gene expression

Figure 6.4 shows the distribution for *BAP1* gene expression within the data set. The mean (logged) gene expression for *BAP1* (as measured by the ILMN_1768363 probe) was 7.8 (standard deviation (S.D.) 0.6).

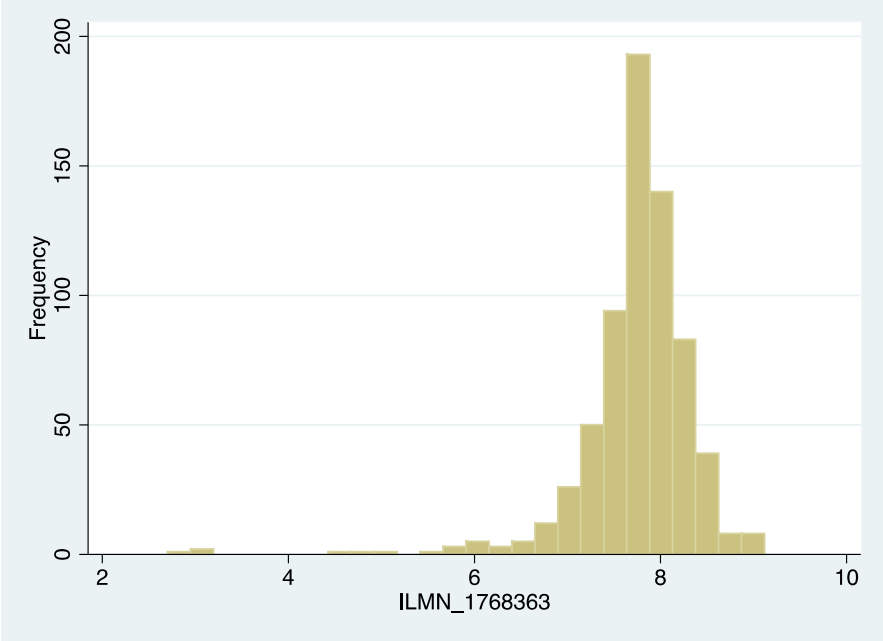

Figure 6.4: Histogram of *BAP1* gene expression.

The histogram shows the frequency distribution for *BAP1* gene expression of (ILMN_1768363 probe) in 676 cases from the Leeds Melanoma Cohort Study

BAP1 gene expression (as measured by the ILMN_1768363 probe) was available for 676 of the 798 cases reviewed, with 53 (7.8%) of these cases having *BAP*-like histopathology. *BAP1* gene expression was similar in cases with (mean (unlogged) expression=214.6) and without features of *BAP*-like histopathology (mean (unlogged) expression=226.5; FDR-corrected p-value=1.0) (Figure 6.5 and Table 6.3). It is important to note that gene expression data were only available for 3 of the 9 cases with variants which had been predicted to be deleterious and this may have affected the results. Each of the three variants was a missense variant and *BAP1* (logged) gene expression values were as follows: 7.97, 8.40 and 9.03 (Figure 6.6). Neither *BAP*-like histopathology nor *BAP1* gene expression was significantly associated with melanoma-specific death (data not shown).

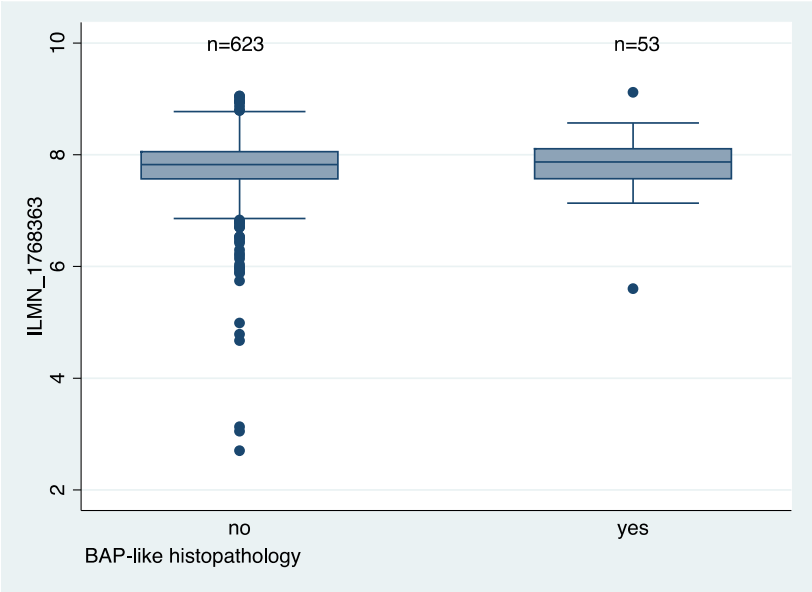

Figure 6.5 Box and whisker plots of *BAP1* expression in cases with and without *BAP*-like histopathology.

The mean (logged) *BAP1* (ILMN_1768363 probe) gene expression (and standard deviation) was 7.7 (0.6) and 7.8 (0.5) for cases without and with a *BAP*-like histopathology, respectively. The mean gene expression for genes proposed to be implicated in the *BAP1* pathway and the corresponding t-test p-values are summarised in Table 6.3.

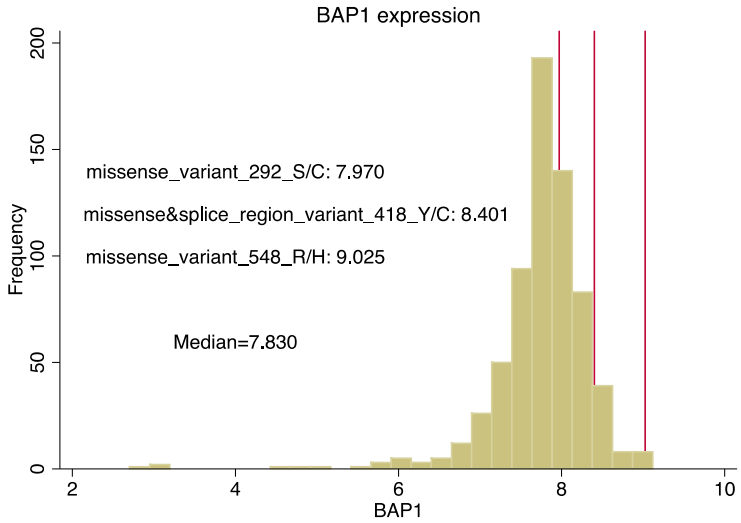

Figure 6.6: Histogram of *BAP1* (logged) gene expression.

The histogram shows the frequency distribution for *BAP1* gene expression in 676 cases from the Leeds Melanoma Cohort. Three variants, which were predicted to be deleterious by SIFT or PolyPhen-2 and for which gene expression and histopathological data were available, are highlighted on the histogram by three red lines.

6.3.6 The relationship between *BAP*-like histopathology and gene expression of other genes implicated in the BAP1 pathway and spitzoid lesions

The expression of several genes in the putative BAP1 pathway (Figure 6.7) was also analysed, comparing cases with and without histopathology suggestive of a *BAP1* mutation (Table 6.3). There was no significant difference in the gene expression of any of the following genes, which are implicated in the putative BAP1 pathway: *BARD1*, *HCFC1*, *E2F1*, *ASXL1*, *RAD51*, *YY1* or *PRC1* (Table 6.3) [349]. *Host cell factor C1* (*HCFC1)*, which is involved in the regulation of the *E2F* transcription factors [350], is deubiquitinated by BAP1 leading to modulation of cell proliferation [351]. ASXL1 forms a complex with BAP1 and has been implicated in its activation [352], however, they appear to have divergent effects on downstream gene regulation [353].

Figure 6.7 (on following page): (Adapted from Ladanyi *et al.* [349]) The putative role of BAP1 in: A) transcription factor regulation, B) chromatin modification and C) double-strand DNA break repair.

A) HCFC1 is a binding partner of BAP1, which interacts with transcription factors and is involved in chromatin modification. It is involved in the demethylation of a lysine residue in H4 and the methylation of a lysine residue in H3. YY1 is a transcription factor that binds HCFC1 and BAP1. B) PRC2 is involved in the methylation of a lysine residue in H3, which leads to the recruitment of PRC1. This results in the addition of a ubiquitin moiety to lysine 119 of H2A, provoking the repression of chromatin and gene silencing. The ubiquitylated H2A may complex with and be regulated by BAP1 and ASXL1, leading to the removal of the ubiquitin moiety. This state of flux is proposed to influence the expression of PRC target genes. C) BAP1 is thought to be involved in DNA repair, the mechanism for which has not been fully elucidated. It may associate with BRCA1 and BARD1 or it might regulate proteins downstream of RAD51. ASXL1, Additional sex combs like 1; ATM, Ataxia telangiectasia mutated; BAP1, BRCA1-associated protein-1; BARD1, BRCA1-associated RING domain protein 1; BRCA1, Breast cancer 1; BRCA2, Breast cancer 2, DNA, deoxyribonucleic acid; E2F1, E2F Transcription Factor 1; HCFC1, Host-cell factor C1; H2A, Histone 2A; H4, Histone 4; H3, Histone 3; me, methyl group; P, phosphate; P53, Tumour protein p53; PRC1, Polycomb repressive complex 1; PRC2, Polycomb repressive complex 2; RAD51, RAD51 recombinase; Ub, Ubiquitin; YY1, Ying yang 1.

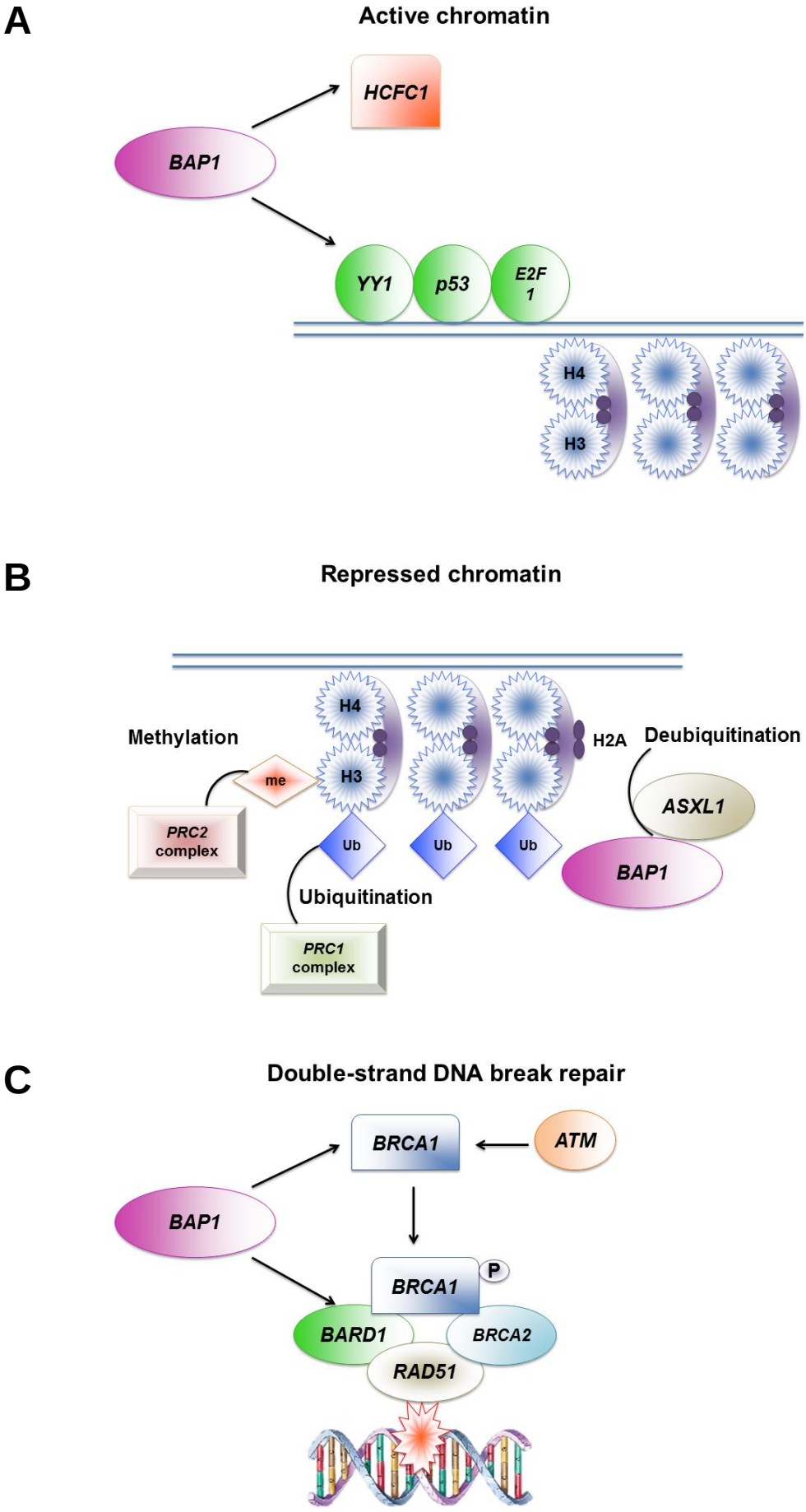
A
Active chromatin
HCFC1
BAP1
YY1
p53
E2F 1
H4
H3
B
Repressed chromatin
H4
H3
Methylation
me
PRC2 complex
H2A
Deubiquitination
ASXL1
BAP1
Ub
Ub
Ub
Ubiquitination
PRC1 complex
C
Double-strand DNA break repair
BRCA1
ATM
BAP1
BRCA1
P
BARD1
BRCA2
RAD51

As previously discussed, *BRAF* is reported to be mutated in the majority of *BAP1*-mutated melanocytic lesions [332]. Therefore, I also tested for differential expression in *BRAF* between cases with and without *BAP*-like histopathology. There was no significant difference in *BRAF* expression in the presence or absence of *BAP*-like histopathology (Table 6.3).

Both *BAP1* and *USP16* deubiquitinate H2A-Ub: *BAP1* modulates homologous repair, while *USP16* is involved in DNA double strand break-induced transcriptional silencing [354]. It is not entirely clear whether or not *BAP1* and *USP16* act independently of one another [354]. To explore whether or not the *BAP*-like histopathological changes might reflect an alternative but similar mechanism, I assessed *USP16* expression in cases with and without *BAP*-like histopathology. *USP16* expression was not significantly different between cases with and without consistent histopathology (Table 6.3).

As previously discussed, spitzoid lesions composed of epithelioid melanocytes, a desmoplastic response and some intranuclear inclusions have been reported in association with amplification of chromosome 11p and/or *HRAS* mutations [334]. Therefore, I also checked the gene expression of *HRAS* (ILMN_1773751 probe), however, *HRAS* expression was similar in cases with and without *BAP*-like histopathology (Table 6.3).

The histopathological appearance of spitzoid lesions with *TERT* promoter mutations have not been elucidated, however, the presence of such mutations has been reported to be associated with a more aggressive clinical course [337]. Therefore, recognition of the corresponding histopathological appearance could be beneficial. Therefore, I decided to explore the possibility that *TERT* might be implicated in melanomas with *BAP1*-like histopathological features, by comparing *TERT* gene expression in cases with and without such changes. However, there was no statistically significant difference in *TERT* gene expression in cases with and without *BAP1*-like histopathological features (Table 6.3).

6.3.7 Melanomas with histopathological features suggestive of *ALK* fusions and the relationship with gene expression of *ALK* and its potential fusion partners

Forty-six (5.8%) cases had histopathological features consistent with an *ALK* fusion, including a plexiform growth pattern and plump, spindle-shaped melanocytes. An example is shown in Figure 6.8.

Table 6.3: Mean gene expression (unlogged and logged) for some genes implicated in the putative *BAP1* pathway or in spitzoid lesions for cases with and without *BAP*-like histopathology.

The student's t-test p-values are reported for the differential expression (False discovery rate (FDR)-corrected for multiple testing). *BAP1, BRCA1-associated protein 1.* Please see abbreviations for details of other gene names.

Gene	Probe	Mean gene expression in cases without *BAP*-like histopathology (unlogged)	Mean gene expression in cases with *BAP*-like histopathology (unlogged)	Mean gene expression in cases without *BAP*-like histopathology (logged)	Mean gene expression in cases with *BAP*-like histopathology (logged)	T-test FDR corrected p-value
ASXL1	ILMN_1726025	231.1	222.6	7.9	7.8	1.0
BAP1	ILMN_1768363	214.6	226.5	7.7	7.8	1.0
BARD1	ILMN_2074258	192.5	172.8	7.6	7.4	1.0
BRAF	ILMN_1652472	219.4	251.3	7.8	8.0	1.0
BRCA1	ILMN_1738027	209.8	186.9	7.8	7.7	1.0
E2F1	ILMN_2051469	228.2	228.8	7.8	7.8	1.0
HCFC1	ILMN_1732705	218.0	207.1	7.8	7.7	1.0
HRAS	ILMN_1773751	235.9	222.4	7.8	7.8	1.0
PRC1	ILMN_1728934	227.6	202.0	7.8	7.7	1.0
RAD51	ILMN_2363027	231.0	205.2	7.8	7.8	1.0
TP53	ILMN_1779356	217.3	201.5	7.8	7.7	1.0
TERT	ILMN_2373119	261.7	213.3	8.1	7.8	1.0
USP16	ILMN_2397230	219.0	202.7	7.8	7.7	1.0
YY1	ILMN_2181540	223.8	214.8	7.8	7.7	1.0

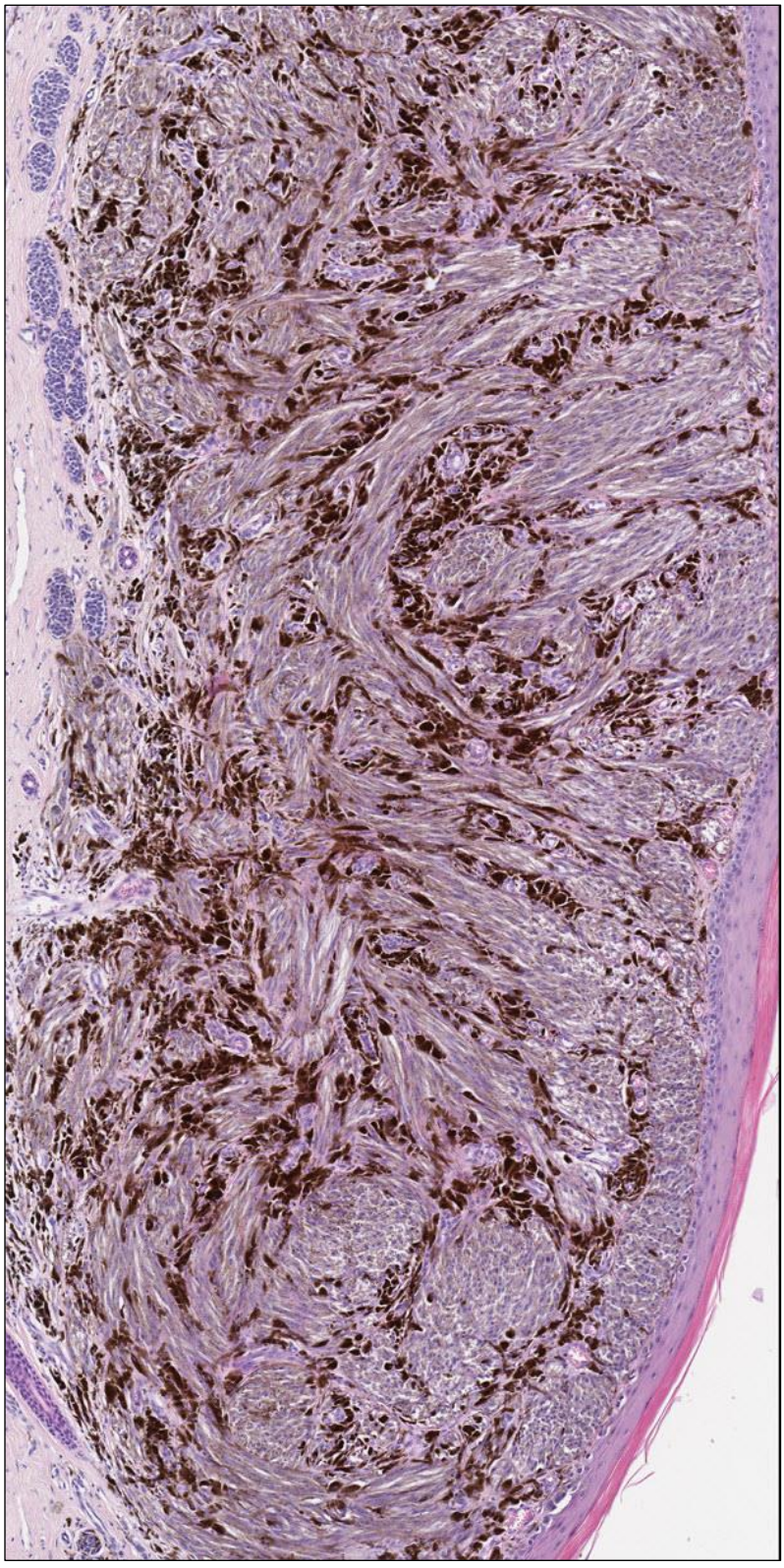

Figure 6.8: Virtual pathology image of a melanoma with *ALK* fusion-like histopathology

Histopathological findings (x10 magnification) reveal a melanoma with a plexiform growth pattern, composed of fascicles of plump, pigmented spindle cells. Melanophages can also be seen within the tumour.

Of the 798 cases reviewed, 676 had gene expression data and 41 (6.1%) of these cases had histopathological changes suggestive of an *ALK* fusion. The distribution for *ALK* gene expression is shown in Figure 6.9. The mean (logged) gene expression for *ALK*, in the 676 cases for which gene expression was available, was 7.8 (S.D. 1.1).

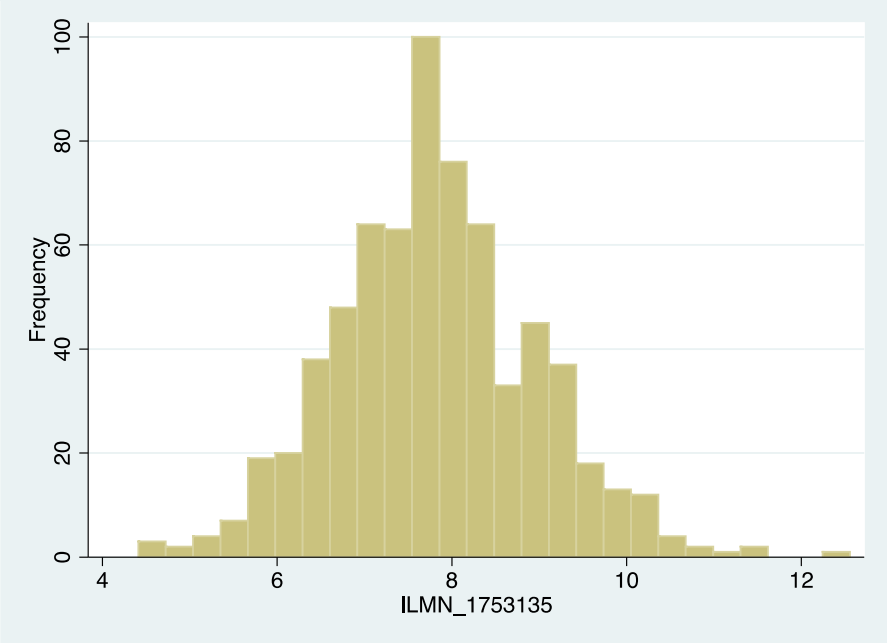

Figure 6.9: Histogram of the expression of the ILMN_1753135 probe (*ALK*) in 676 cases from the Leeds Melanoma Cohort Study.

Unexpectedly, the mean gene expression for *ALK* was lower in cases with histopathological features of an *ALK* fusion compared to cases without but this was not statistically significant (Table 6.4).

The relationship between *ALK* fusion-like histopathology and the expression of the following genes, reported to be *ALK* fusion partners, was assessed: *TPM3*, *DCTN1* [158, 311], *NPM1*, *TPR*, *GTF3C2*, *CLIP1* [157] (Table 6.4). I also explored The Cancer Genome Atlas (TCGA) fusion gene database [355] for other potential *ALK* fusion partners. I assessed for the differential expression of some of its potential fusion partners: *KCNQ5* (melanoma), *TPM1* (bladder cancer), *EML4* (lung adenocarcinoma, thyroid carcinoma), *C2ORF61* (ovarian serous cystadenocarcinoma), *STRN* (thyroid carcinoma) (Table 6.4).

6.3.8 The relationship between *ALK* fusion-like histopathology and gene expression of other kinases implicated in fusions

There was no strong evidence, at a gene expression level, to support the presence of an *ALK* fusion in cases with suggestive histopathology. It appeared that there could be a degree of overlap in the histopathological features of spitzoid lesions between *ALK* and other kinase fusions [311]. Therefore, I assessed whether or not there were differences in the gene expression of other kinases (namely *BRAF*, *MET*, *NTRK1*, *NTRK3*, *RET, ROS1*) among cases with and without *ALK* fusion-like histopathology (Table 6.4). *TERT* expression was also assessed, as before.

Transcriptomic analysis revealed a single gene, *Crystallin Mu* (*CRYM*), that was significantly upregulated in lesions that had *ALK* fusion-like histopathology (Table 6.4). Figure 6.10 shows the distribution for *CRYM* gene expression in 676 cases for which gene expression data were available.

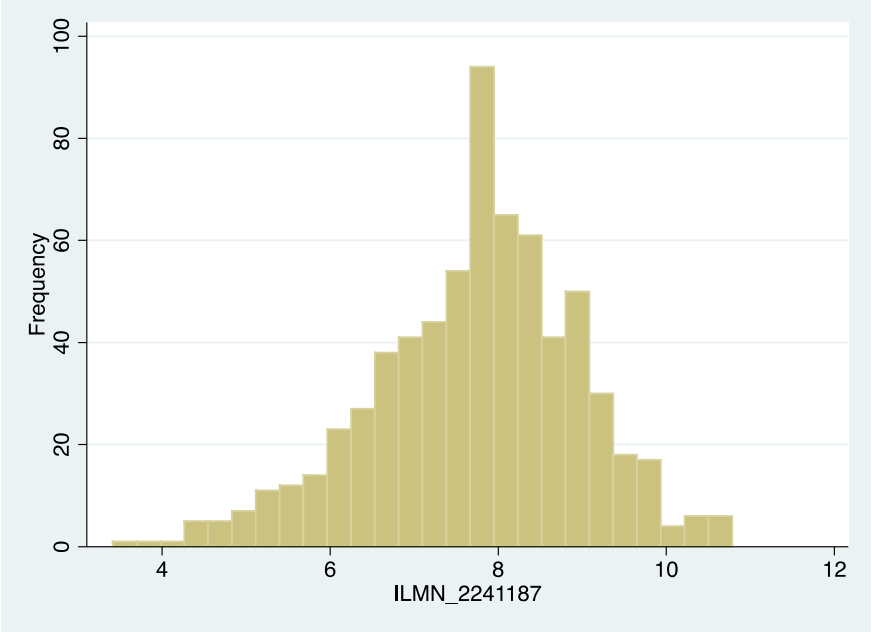

Figure 6.10: Histogram of the distribution of the *CRYM* probe (ILMN_2241187).

Table 6.4 (following page): Mean gene expression (unlogged and logged) for some genes implicated in spitzoid lesions, including kinase fusions and their binding partners, for cases with and without *ALK* fusion-like histopathology.

The student's t-test p-values are reported for the differential expression (FDR-corrected for multiple testing). *ALK=Anaplastic lymphoma kinase.* FDR=False discovery rate. Please see abbreviations for other gene names.

Gene	Probe	Mean gene expression in cases without *ALK* fusion-like histopathology (unlogged)	Mean gene expression in cases with *ALK* fusion-like histopathology (unlogged)	Mean gene expression in cases without *ALK* fusion-like histopathology (logged)	Mean gene expression in cases with *ALK* fusion-like histopathology (logged)	T-test FDR corrected p-value
ALK	ILMN_1753135	229.1	184.4	7.8	7.5	0.9
BRAF	ILMN_1652472	222.1	216.8	7.8	7.8	1.0
C2ORF61	ILMN_1790070	226.4	237.6	7.8	7.9	1.0
CLIP1	ILMN_2404085	214.1	231.1	7.7	8.0	1.0
CRYM	ILMN_2241187	204.1	405.1	7.7	8.7	0.01
DCTN1	ILMN_2412807	229.8	235.2	7.8	7.8	1.0
EML4	ILMN_1718297	229.6	226.7	7.8	7.8	1.0
GTF3C2	ILMN_2356574	222.8	220.9	7.8	7.8	1.0
KCNQ5	ILMN_2060268	266.2	312.5	8.1	8.3	0.9
MET	ILMN_1715175	231.7	222.7	7.9	7.8	1.0
NPM1	ILMN_2379762	220.8	186.2	7.8	7.5	0.8
NTRK1	ILMN_1731777	243.1	209.6	7.9	7.7	0.9
NTRK3	ILMN_1687967	263.4	303.2	8.0	8.2	0.9
RET	ILMN_1706301	237.6	267.5	7.8	7.9	0.9
ROS1	ILMN_1811234	255.6	258.3	8.0	8.0	1.0
STRN	ILMN_1749882	228.1	215.2	7.8	7.7	0.9
TERT	ILMN_2373119	270.2	280.4	8.1	8.1	1.0
TPM1	ILMN_2360710	220.1	223.2	7.8	7.6	1.0
TPM3	ILMN_1697567	225.3	204.3	7.8	7.8	0.8
TPR	ILMN_1730999	223.6	216.1	7.8	7.8	1.0

The mean (unlogged) gene expression of *CRYM* in cases with *ALK* fusion-like histopathology was almost twice that of cases without such features (Table 6.4**,** FDR-corrected p-value=0.01). Figure 6.11 shows the box and whisker plot for *ALK* fusion-like histopathology by *CRYM* gene expression. Neither *ALK* fusion-like histopathology nor *CRYM* gene expression was significantly associated with melanoma-specific death (data not shown).

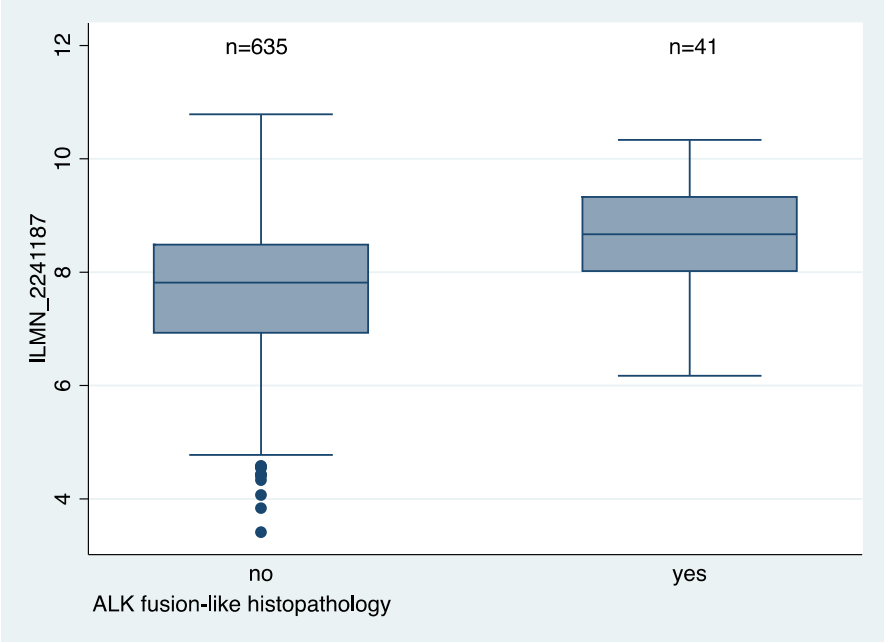

Figure 6.11: Box and whisker plots showing the gene expression for *CRYM* (ILMN_2241187 probe) by the presence or absence of *ALK* fusion-like histopathology.

6.4 Discussion

Only 9/1977 cases within the Leeds Melanoma Cohort had *BAP1* variants predicted to be deleterious by SIFT or PolyPhen-2, indicating that *BAP1* mutations are rare in cutaneous melanoma probands. Deubiquitinase assays were performed by the Sanger Institute. Loss of deubiquitinase activity was confirmed in two of the three cases with clear loss-of-function mutations. The deubiquitinase assay was not performed for the case with a splice acceptor site variant, however, there was strong a priori evidence to suppose that BAP1 function would be affected and a germline *BAP1* mutation was confirmed on clinical testing. The remaining 6 cases with *BAP1* variants that were predicted to be deleterious did not display a detectable loss of deubiquitinase function. The role of *BAP1* beyond its deubiquitinase activity continues to be explored [356].

This might explain why some variants were predicted to be deleterious but did not alter deubiquitinase activity. It is also possible that some *BAP1* variants fell below the threshold of detection of the assay. The other possible explanation is that these variants might not be deleterious, even though the software had predicted them to be as such.

A limitation of the cancer history analysis is that cancer subtypes might have been under-represented, e.g. mesothelioma could have been recorded as “lung” cancer and would not have been included in the analysis. A further limitation is that although the cancer data were entered as a positive history of cancer it was not possible to calculate the number of affected versus unaffected family members or to account for the size of the pedigree. This could have led to an over-representation of cancers in larger families and an under-representation in smaller pedigrees. Recall bias could have occurred, so that more detailed medical information could have been available in some families. Family dynamics around disclosure of cancers among relatives could not be accounted for. Educational levels achieved by the probands could also have influenced the level of detail provided in the survey. Inevitably adoption or estrangement within the family occurred and could not be accounted for.

Information from pedigrees was, however, informative in predicting carriers of germline *BAP1* mutations. The presence of a history of meningioma or mesothelioma in cutaneous melanoma probands or their first- and second-degree relatives in particular, was associated with an increased likelihood of a deleterious *BAP1* variant. It was interesting to note that none of the families with a deleterious *BAP1* variant in this study had a history of ocular melanoma. Of the nine cases with deleterious *BAP1* variants, the family cancer history was more persuasive for the presence of a germline *BAP1* mutation in the three cases with clear loss-of-function variants, compared with the other six cases.

BAP-like histopathology was not significantly associated with the presence of a deleterious *BAP1* variant, compared to no *BAP1* variant. In addition, *BAP*-like histopathology was not significantly associated with any of the following cancers (reported in association with the *BAP1* tumour predisposition syndrome) or with the “*BAP*-like phenotype”: renal cancer, basal cell carcinoma, meningioma, ocular melanoma or a family history of cutaneous melanoma. There was, however, a significant association between *BAP*-like histopathology and the presence of a history of mesothelioma in either the proband or the family, when taken together. The findings might reflect the small numbers of cases with such cancer histories. Alternatively, cases with *BAP*-like histopathological features could have somatic rather than germline *BAP1* mutations. This was not possible to verify during my PhD but could be explored

in future work, pending ethical approval. It is also possible that the *BAP*-like histopathological features are non-specific and, therefore, may not reliably identify cases with either somatic or germline *BAP1* mutations. Sequencing of the melanoma tumour for somatic mutations might help to clarify this.

There was no significant association between the presence or absence of *BAP*-like histopathology and *BAP1* gene expression. Furthermore, gene expression data were available for only 3 of the 9 cases with variants predicted to be deleterious and surprisingly, *BAP1* gene expression was above average in these cases. In early reports of cutaneous lesions in *BAP1* mutation carriers, loss of heterozygosity (LOH) was demonstrated [159]. Therefore, loss of the wild type allele in germline *BAP1* mutation carriers and a corresponding reduction in *BAP1* gene expression would have been anticipated. There were three cases with clear loss-of-function *BAP1* variants; however, their melanomas had not been sampled with a TMA biopsy needle. It would have been interesting to assess for LOH in all 9 cases with variants predicted to be deleterious, however, this was not possible due to a lack of tumour tissue for all cases.

Previous reports describe a high frequency of *BRAF* mutations in *BAP1*-mutant cutaneous melanocytic lesions [306, 332]. The mean expression of *BRAF* was slightly higher in cases with *BAP*-like histopathology but did not reach statistical significance. This observation of course does not preclude the presence of mutations. Furthermore, somatic *BRAF* mutations commonly occur in primary melanomas within the general population, irrespective of germline *BAP1* mutation status [357]. Transcriptomic analysis did not reveal any variation in alternative genes that could be implicated in association with the *BAP*-like histopathological appearance. Conclusions relating to the gene expression results in the context of *BAP1*, are limited by the fact that a minority (3/9) of cases with variants predicted to be deleterious had gene expression data available for analysis and these were cases with the least compelling pedigrees and type of variant (missense).

The frequency of *BAP*-like histopathology was relatively high within the cases analysed (~8%, 53/676), compared to the low frequency of *BAP1* variants predicted to be deleterious. This could indicate that such histopathological findings are less specific than currently presumed [159]. The database used to record the histopathological features with respect to *BAP*-like and *ALK* fusion-like changes was not designed with the intent of recording such features systematically. It is therefore possible that the features were not recorded consistently throughout the study. The high number of cases identified with *BAP*-like histopathology, however, would suggest that the features were assessed frequently.

There was no significant association between the presence of *ALK* fusion-like histopathology and *ALK* gene expression. The expression of its proposed fusion partners, *CLIP1* and *NPM1*, were not significantly altered in cases with *ALK* fusion-like histopathology. Although not statistically significant, *ALK* expression was decreased rather increased in cases with *ALK* fusion-like histopathological features. The gene expression data did not support the presence of an alternative kinase fusion in such cases. Previous studies which reported kinase fusions in spitzoid lesions, utilized targeted DNA sequencing, RT-PCR and fluorescence in situ hybridisation (FISH) to establish their presence [311]. These methods were not explored in the thesis. *CRYM* gene expression was notably increased in cases with *ALK* fusion-like histopathology.

The role of *CRYM* in melanocytic lesions has not yet been determined. *CRYM* has been identified as a candidate substrate for *Protein Kinase A* (*PKA*), *Mitogen-activated protein kinase 1* (*MAPK1*), *Protein Kinase N* (*PKN*), *LCK*/*YES novel tyrosine kinase* (*LYN*) and *FYN* [358]. *CRYM* encodes a type of protein called crystallin, which has been implicated in maintenance of the transparency of the ocular lens [359] and in binding thyroid hormone, which may be important in thyroid hormone signalling in other tissues [360]. Mutations in *CRYM* have been reported in association with inherited deafness [361]. The cBioPortal database (based on the Cancer Genome Atlas Network data set, which includes metastatic melanoma cases) reports that somatic *CRYM* mutations occur in approximately 1% of melanomas [362]. Although, its biological role in melanoma has not been fully elucidated, *CRYM* mutations have been reported to occur in other cancers including prostate cancer [363], metastatic uterine leiomyosarcoma [364] and has been shown to be predictive of treatment failure in head and neck squamous cell carcinoma [365].

In summary, in this study of population-ascertained cutaneous melanoma cases, there was an association between a family history of mesothelioma, meningioma and BCC and the presence of a deleterious, germline *BAP1* variant. The cancer history was particularly strong for three cases with germline *BAP1* variants for which there was compelling evidence for loss-of-function. We did not identify uveal melanomas in these pedigrees. In the original reports of families with germline *BAP1* mutations, ascertainment was for families with mixed cancers, in addition to uveal cancers. The fact that uveal melanomas were not found probably reflects a bias of ascertainment, both for the original uveal melanoma families and for our study. Clarity about the risk of various cancers is crucial to provide information to families with inherited *BAP1* mutations. This study reflects a lack of data in this regard. In the future, the identification of probands using cancer gene panels or exome sequencing may produce less biased estimates of cancer risk.

Six germline variants were identified by the Sanger Institute that were predicted to be deleterious but had apparently normal deubiquitinase activity. In these families, there was a personal or family history of either BCC, haematological malignancies, uterine or gastrointestinal tract cancers. One case of lung cancer occurred in an elderly relative of one of these probands. The significance of the cancer history in these cases is uncertain. Unfortunately, it was not possible to perform BAP1 immunohistochemistry or to test for loss of the wild type allele in the primary tumours because of lack of FFPE tumour tissue.

BAP-like histopathology was not associated with the presence of a deleterious *BAP1* variant overall, although 2 of the 3 tumours from families with clear loss-of-function mutations did have “typical” changes, such as lack of an origin from the epidermis and lack of pigmentation. The presence of *BAP*-like histopathology in the proband’s melanoma was significantly associated with a history of mesothelioma in the proband or family. The observations in these 2 families suggest then that the unusual histopathological appearances of the cutaneous tumours described by Wiesner *et al.* are associated with deleterious germline mutations. The lack of association between the histopathological appearances and germline status overall, however, suggests that the association is weak: i.e. that these appearances are poorly predictive of germline status, not being specific to germline genetic variation.

The factors underlying the *BAP1*-like histopathological features at a somatic level are unknown. There was no significant difference in *BAP1* gene expression in cases with and without *BAP*-like histopathology, and three cases with missense variants (predicted to be deleterious) had *BAP1* gene expression that was equivalent to or higher than the average in the cases studied. Moreover, there was no significant association between a *BAP*-like histopathology and the expression of other genes that have been proposed to be involved in its signalling pathway.

There was no evidence to support the presence of kinase fusions in melanomas that appeared to resemble spitzoid lesions with *ALK* fusion-like histopathology. The number of cases with such features was small and the methods used curtailed the further exploration of such findings. However, a novel candidate gene, *CRYM*, was identified through transcriptomic analysis, which associated with the *ALK* fusion-like histopathological changes. The mechanism underlying the putative role of *CRYM* in such cases requires further elucidation. Sequencing would help to clarify whether or not overexpression was due to either amplification or mutation of *CRYM*. Immunohistochemistry for CRYM, performed on control samples and melanomas with and without increased *CRYM* gene expression would be worthwhile to evaluate CRYM protein expression in the context of its corresponding gene expression. Furthermore,

examining pedigrees of such cases and sequencing of matched blood and tumour samples for *CRYM* mutations, would be worthwhile in assessing for germline *CRYM* mutations. The work presented in this chapter shows proof-of-principle that histopathological appearances could have biological correlates (albeit somewhat variable), which is the foundation of my thesis.

Chapter 7 Final discussion

The American Joint Committee on Cancer (AJCC) staging system is a powerful tool in predicting survival from cutaneous melanoma [43]. Breslow thickness, microscopic ulceration, mitoses (7th edition), microsatellites and the burden of nodal or distant metastases are central to this classification [43]. The most informative cut-off points for Breslow thickness continue to be debated, such that these have now been amended in the pending 8th edition of the AJCC staging system (in press), with the proposed new cut-off point for stage IA of 0.8mm now approximating the original thickness that had been reported by Breslow (0.76mm) to differentiate between cases that are capable of metastasis [45]. Although mitotic count had been incorporated into the 7th edition of the AJCC staging, to distinguish stage IA from stage IB cutaneous melanoma [43], it has not been retained in the forthcoming 8th edition (in press). The results reported in this thesis are based on the 7th edition of the AJCC staging system [43]. Consistent with the AJCC 7th edition, Breslow thickness, microscopic ulceration and the number of core mitoses were among the most highly reproducible and prognostic parameters recorded in my study. Furthermore, an increasing extent (width) of ulceration was hazardous for melanoma-specific death in univariable survival analyses. The literature reports various prognostic cut-off points for the width of ulceration [53-56]. In my project, there was a trend in the hazard ratios for an increasing extent of ulceration and a non-parametric test for trend was significantly associated with melanoma-specific death, suggesting that there might be a benefit to measuring the extent of ulceration on a continuous scale. Tumour-infiltrating lymphocytes (TILs) have been shown to be an independent prognostic factor in some studies [27, 60-63, 212], while others have failed to demonstrate an independent prognostic effect [64, 65, 67] or found TILs to be of borderline statistical significance [69]. Nonetheless, the recording of TILs could be important, particularly in this era of immunotherapy [216, 289]. I found that TILs (with respect to the whole tumour) were of borderline statistical significance in univariable survival analysis and were not an independent predictor of melanoma-specific death. It was notable that, in this study, there was an inherent bias towards thicker melanomas, from which a TMA core biopsy could be obtained without destroying the clinical block. Previous studies have shown that brisk TILs tend to decrease with increasing Breslow thickness [27, 61, 64]. Interobserver agreement for TILs using the virtual pathology protocol was moderate, whereas previously published studies have shown varying strengths of agreement between observers [27, 199-201], reflecting the subjective nature of the measure. Remarkably, the extent of the lymphocytic infiltrate within the cored region was significantly and independently protective for melanoma-specific

death. This measure was based on an “eyeballed” estimation, however, precise counting of lymphocytes could be performed in the future. The role of regression in melanoma is controversial, with some studies reporting a protective effect [74, 79], while others indicate a more sinister role [82-84]. Similarly, in this thesis, the presence of tumour loss and its increasing depth were significantly hazardous in univariable survival analysis. In addition, cases that had both deep and superficial tumour loss were at increased risk of melanoma-specific death. Nonetheless, the test for trend for the increasing depth of tumour loss was not an independent predictor of outcome. It is dogma that regression results from host-mediated anti-tumour immunity [71]. However, an alternative hypothesis is that regression represents an intrinsic event within the tumour, leading to tumour cell death and the selection of more aggressive tumour cells in the evolution of the melanoma [73]. Further research is required to elucidate this association. Although there was moderate to perfect inter- and intraobserver agreement for the intensity and pattern of tumour-infiltrating melanophages, neither of these measures significantly influenced melanoma-specific death. Unfortunately, it was not possible to further characterise the polarization of the macrophages/melanophages during my PhD.

At the beginning of my PhD, I noted that primary melanomas were as visually captivating when viewed with a microscope, as they are to the naked eye, displaying remarkable diversity of cell shape, variation in pigmentation and contrasting architectural arrangements, e.g. nests. These striking characteristics have long been described by pathologists but were of uncertain prognostic significance. I was keen to explore this further. Early studies suggested that cutaneous melanoma relapses tended to occur more frequently in association with epithelioid melanocytes within the primary melanoma [101], and that spindle cell melanomas had a better prognosis [103]. Furthermore, desmoplastic melanomas, which display a markedly spindled melanoma cell shape, have a tendency to recur locally but metastasise less frequently [99, 100]. Additionally, *in vitro* cell migration assays have shown that melanoma cells with a rounded or “amoeboid” appearance degraded type I collagen more efficiently than cells with a “mesenchymal” phenotype [105]. This prompted me to investigate the role of melanoma cell-specific features more closely. The grading of melanoma cell pigmentation was highly reproducible within and between observers, yet, it was of no prognostic significance. There was moderate to substantial agreement for melanoma cell shape, yet, the vast majority of cases had a round/ovoid/epithelioid appearance and the number of cases in the other categories was small. There was no significant effect for melanoma cell shape in survival analyses. Weaker inter- and intraobserver reproducibility was noted for melanoma cell structure. Nonetheless, melanoma cell “sheets” corresponded to an increased risk of melanoma-specific death in univariable

analysis but lost significance in multivariable survival analyses, adjusting for age, sex, site of primary, AJCC stage and the extent of either the core immune cell or lymphocytic infiltrates. The dispersed cell structure was independently hazardous for melanoma-specific death in the same multivariable analyses, although the number of cases in this category was small. Therefore, although these features are visually intriguing, they did not appear to be of any consequence from a prognostication point of view, in this study of over 700 primary tumours.

In spite of the lack of predictive power, it would appear that these morphological distinctions might indicate somatic or germline mutations. Viros *et al.* showed that *BRAF*-mutated melanomas tended to have large, round, pigmented cells [108]. I was interested to assess whether or not the histopathological changes that had been reported to occur in association with either a *BAP1* mutation or an *ALK* fusion were predictive of differential gene expression in *BAP1* or *ALK*, respectively. *BAP*-like histopathology was recorded in 8% of cases in this data set, a rate that is higher than would be expected, in comparison to the rarity of germline *BAP1* mutations [314]. This begs the question whether or not these melanomas had acquired somatic *BAP1* mutations, however, there was no demonstrable difference in *BAP1* gene expression between cases with and without a *BAP*-like histopathological appearance. It is noteworthy that no transcriptomic data were available for the three cases with the most compelling evidence for *BAP1* loss-of-function variants. Unfortunately, it was not possible to explore this further with BAP1 immunohistochemistry or to assess for loss of heterozygosity due to the limited amount of tissue that could be sampled (as previously discussed). Initial reports of cutaneous melanocytic lesions in cases harbouring a germline *BAP1* mutation were presented as having a characteristic histopathological appearance [159] but, subsequently, melanomas with somatic *BAP1* mutations were noted to adopt a similar appearance [306]. Although the features were recorded in spitzoid lesions, some of the cases could not be distinguished from melanoma and, therefore, I recorded the presence or absence of such features for cases in the Leeds Melanoma Cohort Study. There was no significant association between a *BAP*-like histopathology and the presence of a predicted deleterious *BAP1* variant. Therefore, these histopathological features appeared to be poorly predictive of germline *BAP1* mutations in this study. Data for the personal and/or family history of cancers, which had been reported to be associated with germline *BAP1* mutations, were extracted. Due to the nature of the recorded cancer history, I focused my analysis on specific categories, e.g. mesothelioma, as opposed to lung cancer. There was a significant association between the presence of a predicted deleterious *BAP1* variant and the presence of a family history of either mesothelioma or meningioma. *BAP*-like histopathology was significantly associated with the presence of mesotheliomas in the

pedigrees. A deubiquitinase assay was used to confirm the biological effects in cases harbouring predicted deleterious variants. Unfortunately, this failed to detect expected changes in function in 6 cases, possibly as a consequence of a lack of sensitivity. This was a large study, in which the prevalence of germline *BAP1* mutations, corresponding pedigrees and histopathology of melanomas in the probands were assessed. Nonetheless, a larger scale study is necessary to inform decisions about clinical testing for germline *BAP1* mutations and screening for cancers among affected probands and their family members. Similarly, *ALK* fusion-like histopathology was not associated with a significant difference in *ALK* gene expression, or in its proposed binding partners. However, the Illumina® probes did not bind across the proposed fusion sites, which could account for the lack of association between the *ALK* fusion-like histopathological appearance and the *ALK* (and binding partners) gene expression results. Alternatively, the histopathological appearance might be non-specific. It was not possible to perform ALK immunohistochemistry, due to the need to conserve the tumour blocks for clinical testing. Regardless, the identification of an association between *ALK* fusion-like histopathology and *CRYM* gene expression serves as a proof-of-concept that histopathological appearances have transcriptomic correlates. The biological significance of this finding will be explored in future research.

This project was unique in several ways. The study was based on a large data set for which detailed clinical, histopathological and transcriptomic data were available. The median follow-up of participants was 7 years, enabling me to be confident in assessing the impact of my recorded histopathology measures on relapse and survival. Furthermore, the histopathological assessment was detailed and was performed by a single observer with high intraobserver reproducibility. I developed a robust protocol, in tandem with the accumulation of knowledge and skills. The virtual pathology platform contributed significantly to the originality of the project. This facilitated the development of a novel approach, combining a comprehensive histopathological assessment of the tumour as a whole but also, importantly, to evaluate the cored regions in detail. This enabled me to assess whether or not the microscopic appearance of melanoma could have transcriptomic correlates, which could potentially be useful clinically.

The results of inter- and intraobserver studies provide evidence that the protocol was reproducible, although some parameters were more variably reported within or between observers, e.g. the presence of tumour loss, the quality of the stroma and the number of core blood vessels. It is reassuring that the Breslow thickness and microscopic ulceration, which are regarded to be the cornerstones of staging and for which the highest interobserver agreement is reported [190, 191, 195, 196], were also highly reproducible in my thesis. Moreover, the majority of the newly developed

measures pertaining to the cored regions were highly reproducible. The solid groundwork had now been laid for analyses of the impact of such factors on melanoma-specific relapse and death, aspects that were particularly important to me as a dermatologist.

Nonetheless, it was surprising that TILs were of borderline statistical significance, particularly as they had been an independent prognostic factor in interim analyses (data not shown), and because immunotherapy has revolutionised the treatment of metastatic melanoma [289, 290, 304, 366]. The results could be a reflection of the biased data set that I studied, in that these tumours were inherently thicker because they had been sampled using a TMA needle. I enumerated mitoses within the cored region. Substantial inter- and intraobserver agreement was demonstrable and the number of core mitoses was a significant prognostic factor in univariable analysis. This suggests the possibility that, in the future, pathologists could focus on a pre-defined region of the melanoma, instead of searching for the most mitotically-active region (or "hot spot") [43] within the tumour. I would speculate that this would be likely to save time and to be more highly reproducible between observers.

Survival analyses revealed that Breslow thickness and ulceration status were hazardous for melanoma-specific survival. Several other histopathological factors were of prognostic significance. There was a convincing trend in the hazard ratios for an increasing extent of ulceration, suggesting that not only its presence is important in determining outcome but also its extent. Similarly, an increasing depth of tumour loss was associated with a worse prognosis, highlighting the importance of recording its measurement in millimetres. ROC curve analyses showed that the combination of AJCC stage and the percentage of stroma (POS) increased the area under the curve, compared to AJCC stage alone. The extent of the core immune cell and lymphocytic infiltrates were associated with a better prognosis, indicating that grading the immune cell infiltrate, particularly lymphocytes, within the advancing melanoma margin which has the least immune cell infiltrate would be worthwhile. Such factors could be considered for inclusion in melanoma prediction models in the future.

Stemming from my research of the cored regions, I discovered that the POS within the core was a highly significant, independent prognostic factor. Furthermore, it was powerfully protective for melanoma-specific death, such that for every percentage increase in stroma, there was a corresponding 1% decrease in melanoma-specific death. In addition, ROC curve analyses revealed that the POS added a further 3% predictive power to AJCC stage, both for melanoma relapse and death. This contrasted starkly with many studies in other cancers inferring a hazardous role for the POS [131, 134, 135, 137-142, 261, 262]. The POS tended to parallel those factors that are known

to be associated with a good outcome, such as younger age at diagnosis [6, 7, 367-369], female sex [14, 15, 19] and early AJCC stage [43]. The corollary was also true, that the POS was inversely associated with factors predictive of a poor outcome, namely Breslow thickness [43, 45], microscopic ulceration [43, 48, 53, 54, 56, 370], increasing mitoses (albeit measured within the core) and/or more aggressive tumours, e.g. *NRAS*-mutations [37]. Moreover, there was a significant association between the POS and the increasing extent of both the core immune cell and lymphocytic infiltrates. The beneficial effects of the POS could be due to several factors. It could simply be a reflection of a less aggressive primary melanoma: that is that very proliferative tumours may destroy or push aside the stroma. Alternatively, the core immune cells could be responsible for the survival advantage. Another possibility is that the non-immune stroma is mediating the protective effect associated with the POS. Lastly, a combination of these factors could be at play, e.g. the non-immune stromal cells might be working in harmony with immune cells by facilitating their infiltration and by warding off the tumour via physical rigidity. It is difficult to untangle the evidence because the POS was a combined measure of the immune and non-immune stromal components (due to technical reasons discussed in Chapter 5). At a transcriptomic level, the POS was associated with the expression of both immune and non-immune stromal genes. Survival analyses of the ESTIMATE scores revealed a highly significant prognostic role for both the immune and non-immune compartments. This suggests the possibility that a synergy exists between the non-immune and immune stromal cells. The ESTIMATE tumour purity score was hazardous for melanoma-specific death and, therefore, it is still possible that a high POS could be the result of a less aggressive tumour. MetaCore™ enrichment analyses revealed immune cell pathways to be upregulated in association with the POS and similarly for the extent of the core immune cell and lymphocytic infiltrates. Cell cycle pathways were downregulated in cases with a high POS, which might reflect tumour cell “dilution”. Thousands of genes were significantly associated with the POS (data not shown). A MetaCore™ comparative enrichment analysis of the top 1000 genes associated with each of the POS and the extent of the core immune cell and lymphocytic infiltrates, identified *SDF1* as being uniquely upregulated in association with the POS. *SDF1* is a chemokine that is known to promote the chemotaxis of lymphocytes, monocytes and dendritic cells [291]. Fibroblasts are the main source of *SDF1* in the skin, although it can be expressed by a variety of cell types, including lymphocytes, endothelial cells and even cancer cells [292]. I found that *SDF1* expression was independently protective for melanoma-specific death. Furthermore, expression of its receptor *CXCR4* but not *CXCR7* (a decoy receptor for *SDF1*) [294], was significantly protective, although it lost statistical significance after the addition of the POS to the multivariable model. This is a

controversial finding, bearing in mind that the literature contains numerous conflicting studies about the prognostic role of both *SDF1* and *CXCR4,* not only in melanoma [241, 293-302] but also for other cancers [291, 371-375]. The fact that the POS, the ESTIMATE stromal score and *SDF1* were each independently protective for melanoma-specific death, suggests that primary melanomas with more abundant stroma have a better prognosis than do melanomas with sparse amounts of stroma. Moreover, that this protective effect may result from the chemotaxis of immune cells consequent upon release of chemokines by fibroblasts. This finding warrants further research, particularly in view of the fact that I focused on a pre-defined region within the melanoma and the amount of stroma could have varied across the tumour.

A limitation of the study is that virtual pathology is not yet in widespread clinical use in the UK, which could affect the translation of some of these measures into clinical practice. Furthermore, the cored region variables were based on a pre-determined region of the melanoma. It is not known how this could relate to the rest of the tumour, especially in view of the fact that melanoma is a highly heterogeneous tumour [117, 222]. Moreover, the reproducibility of the selection of the region of tumour at the invasive margin, relatively deficient in immune cells and collagen, has not been assessed. In addition, the extent to which the histopathological description is a true reflection of the three-dimensional core is not known. From a practical point of view, there were some special considerations in the use FFPE archival specimens for transcriptomic studies: RNA degradation [177] had been anticipated due to the time that had elapsed between obtaining the original tumour block and the RNA extraction. The WG-DASL® assay was designed to overcome these issues [178]. High quality results have previously been shown using the WG-DASL® assay (now retired) for RNA extracted from melanoma samples [175]. Unfortunately, two plates of RNA failed owing to reagent degradation (more than 900 samples were sent to the service provider). A further limitation is that inter- and intraobserver agreement could be studied for only a small number of cases. Ideally, I would have liked to have assessed the reproducibility of the new protocol between 3 independent observers. Furthermore, the POS was a composite score of both the immune and non-immune stromal constituents. This led to subsequent difficulties in unravelling their relative contributions. Finally, although I had access to a large data set, the study was underpowered to provide definitive answers in relation to *BAP1* germline mutations, due to their rarity in primary cutaneous melanoma [314].

The strengths of the study were that the virtual pathology protocol was highly reproducible between and within observers. Survival analyses revealed several highly significant prognostic measures, both established and new. Among these, the POS

was identified as a novel biomarker, which was independently protective for melanoma-specific death. Moreover, the results of transcriptomic analysis independently support the view that the stroma is protective. This is the largest study to date of the prevalence of germline *BAP1* mutations within a population-ascertained, cutaneous melanoma cohort, which combined pedigree and histopathological assessment of primary cutaneous melanomas in the probands. The project has produced new hypotheses that will be explored in the future, in this rich data set.

Appendix A : Definitions

Definitions used throughout the report are listed below in alphabetical order.

Term	Definition
Acceptor splice site	The splice site at the end of an intron.
Acral	Affecting the hand or foot.
Acral lentiginous melanoma	A subtype of cutaneous melanoma occurring in the volar or subungual skin. The intraepidermal component is usually lentiginous in pattern with a “moth eaten” appearance [5].
Adenoviral gene transfer	The use of a vector (adenovirus) to deliver genetic material to a cell.
Adhesion molecule	A cell surface protein that is involved in the attachment of cells to the extracellular matrix.
Adipocytic (fatty) degeneration	The abnormal accumulation of fat within the cytoplasm of a cell.
Adipocytic (fatty) metaplasia	The replacement of normal tissue by fat cells (adipocytes) where they are not normally found.
Agnostic	Unbiased.
Algorithm	A computer-based set of rules for calculations.
ALK fusion-like histopathology	The histopathological appearance of a melanocytic proliferation, consisting of plump spindle-shaped melanocytes arranged in a plexiform growth pattern and tending to have a polypoid silhouette.
Allele	One of a number of forms of the same gene.
Amelanotic	Lacking pigment.
Amoeboid (cell movement)	A description given to a type of cell movement that has a rounded appearance in vitro [105].
Angiogenesis	The development of new blood vessels.
Apoptosis	Programmed cell death.
Array-based comparative genomic hybridization	A molecular technique for analysing the copy number variations relative to the number of copies of chromosomes within the cell in a test sample compared to a reference sample. Fluorescent probes are used for labelling.
Atypical Spitz (spitzoid) tumour	A melanocytic lesion which displays some features of both a Spitz naevus and of melanoma, such that its behaviour cannot be reliably predicted [376]. The term is controversial but is considered to be interchangeable with Spitzoid Tumour of Uncertain Malignant Potential for the purpose of this thesis.

Term	Definition
Azan trichrome stain	A histology stain that is formed from a mixture of 3 coloured dyes, which stains collagen, basement membrane and mucin blue; nuclei are stained red and muscle and red blood cells are stained orange to red.
BAP-like histopathology	The histopathological appearance of a melanocytic (often spitzoid) proliferation, consisting of epithelioid melanocytes and/or naevoid melanocytes, with a tendency towards epidermal sparing, intranuclear pseudoinclusions and multinucleated melanocytes.
Benign melanocytic naevus	A mole (of the skin).
Biallelic	Referring to both alleles.
Binary variable	A variable that has 2 categories.
Biobank	A large collection of tissue samples and/or data retained for research.
Bioinformatics	The science of analysing complex biological data.
Biomarker	A molecule, gene or characteristic that is capable of identifying the presence of a disease or a particular characteristic of a disease.
Bonferroni correction	A statistical method of p-value adjustment made for simultaneous multiple testing.
Breslow thickness (in mm)	The measurement between the top of the granular layer of the epidermis and the deepest point of invasion of melanoma, or where epidermal ulceration is present (and involves the thickest region of tumour), the measurement between the base of the ulcer and the deepest point of melanoma invasion. The measurement excludes melanoma cells apposed to adnexal structures or lying within vessels and microsatellites, where present [51].
Cancer-associated fibroblasts	A subpopulation of fibroblasts that promote tumour growth, angiogenesis and metastasis.
Carcinogen	An agent that has the capacity to cause cancer.
Categorical variable	A variable that has ≥2 categories.
Censoring	A statistical method of curtailing a time-to-event analysis to a fixed point in time, where study participants may be lost to follow-up or where the event of interest (relapse or death) has not yet occurred within the selected follow-up time period.
Chemokine	A small, chemotactic cytokine.
Chemoresistance	The resistance of cancer cells to inhibition by a chemical substance.
Chemotaxis	The movement of a cell towards a secreted substance.
Chip	A type of micro-array carrying large numbers of genetic probes.

Term	Definition
Clark level I	Melanoma confined to the epidermis.
Clark level II	Melanoma begins to encroach on but does not fill the papillary dermis.
Clark level III	Melanoma fills and expands the papillary dermis.
Clark level IV	Melanoma invades the reticular dermis.
Clark level V	Melanoma invades the subcutaneous fat.
Collagen	The principal structural protein in connective tissue.
Confidence interval	A range of values within which the true effect size or statistic is likely to lie based on probability.
Connective tissue	Tissue that supports other tissues or organs.
Continuous variable	A variable with an infinite number of possible values.
Copy number variation	The number of copies in sections of the genome, which vary between individuals.
Cox proportional hazards model	A statistical method for examining the effect of one or more predictor variables on the risk of event per time unit and how it changes over time.
Crisis	A state of extreme telomere dysfunction, precipitated by chromosomal abnormalities and leading to cell death.
Curated pathway	A biological pathway that has been constructed or edited by a person with expertise in the area.
Curette	A surgical instrument that can be used to remove the superficial part of a skin lesion and often results in a fragmented specimen.
Cytokine	A substance that is secreted by a cell (typically an immune cell) and has an effect on other cells.
Cytoplasm	The material within a cell, excluding the nucleus.
Degrees of freedom	The number of independent values of a statistic that are free to vary.
Dendritic cell	A professional antigen-presenting cell.
Dermo-epidermal junction	The junction between the lower epidermis and the upper dermis of the skin.
Desmoplasia	Growth of fibrous or connective tissue.
Desmoplastic melanoma	A subtype of cutaneous melanoma that is ill-defined and variably cellular. It is composed of spindle cells associated with dense collagen, and usually occurs on sun-damaged skin [5]. Lentigo maligna may be seen in association.
Deubiquitinating enzyme	An enzyme that removes ubiquitin from other molecules.
Dichotomous	Two different categories.
Discontiguous ulcers	Ulcers that are separated by normal intervening epidermis.

Term	Definition
DNA double-strand break	Both strands of the DNA double helix structure have been cut.
DNA methylation	The addition of methyl groups to DNA, which may alter its activity.
DNA ploidy	The DNA content within cells, with normal somatic cells having 2 copies of each chromosome.
Driver mutation	A somatic mutation that confers a growth advantage to the cancer cell which carries it and has been positively selected during cancer evolution [377].
Dyscohesive response	The tendency for cells in the upper dermis to segregate in response to early ulceration.
Eosinophil	A white blood cell whose nucleus stains with eosin.
Eosinophilic	Stains readily with eosin.
Epidermal atrophy	Thinning of the epidermis due to a reduction in keratinocytes, which may be accompanied by flattening of the rete ridges.
Epithelial-mesenchymal transition	A process whereby an epithelial cell gains the ability to invade and adopt the properties of a mesenchymal stem cell.
Epithelioid melanocyte	A melanocyte with a round nucleus, a prominent, pink nucleolus and variably eosinophilic and often abundant cytoplasm [97].
Event	In the context of Cox proportional hazards models, an event refers to the occurrence of either melanoma relapse or melanoma-specific death (pertaining to the statistical analysis).
Exogenous	Originating outside of the body.
Exome sequencing	A technique of sequencing all of the expressed genes.
Exon	The coding part of the RNA transcript or its corresponding DNA sequence.
Exophytic	Related to the outward growth of a tumour.
Expansile	Related to expansion.
Extracapsular extension	The extension of melanoma beyond the capsule of the lymph node.
Extracellular matrix	A structure that provides support to surrounding cells and is composed of extracellular molecules, including collagen, proteoglycans and elastin.
Eyepiece graticule	A glass disc that contains a fine scale and is inserted into the eyepiece of a microscope to allow measurements to be made.
False discovery rate correction	A statistical method of p-value adjustment that reduces the number of false positives when performing multiple testing.
Fibroblast	A cell that synthesises collagen.
Fibrocyte	An inactive mesenchymal cell.
Fibrosis	The thickening and scarring of connective tissue.

Term	Definition
FISH	A technique that uses fluorescent probes to label specific regions of chromosomes.
Fold-change	Describes how much a measure changes from an initial value to a final value, calculated using the ratio of the final value divided by the initial value.
Frameshift mutation	A genetic mutation caused by the insertion or deletion of nucleotides in a DNA sequence that is not divisible by three.
Fusion	A combination of two previously separate genes.
Gene ontology	A bioinformatics approach to deduce the molecular function and biological processes of genes.
Genome	The complete set of genes within a cell.
Genomics	The study of the structure or function of the genome (the complete set of genes within an organism).
Germ cell	A cell that is capable of reproduction by uniting with a similar cell from the opposite sex to form an individual.
Germline	A mutation that occurs in germ cells, which can be transmitted to offspring.
Granular cell layer	A layer of the epidermis, also known as the stratum granulosum.
Haematopoiesis	The production of blood cells and platelets.
Hazard ratio	A statistical ratio that describes the risk of a particular event, taking into account the time-to-event.
Heat map	A graphical representation of data using colours, especially for transcriptomic data.
Heterozygote	An organism that has two different alleles of the same gene.
Histological subtype	The category that defines the type of melanoma; largely grouped as follows: nodular, superficial spreading, acral lentiginous and lentigo maligna melanoma (please see Chapter 2 for more details).
Homologous recombination repair	A mechanism of DNA double-strand break repair where the genetic information is duplicated from the opposite sister chromatid, i.e. the other copy of the duplicated chromosome.
Immunosenescence	Gradual decline in immune cell function in association with age.
In situ (melanoma)	Melanoma cells are confined to the epidermis.
In vitro	An experiment performed in a controlled environment outside of a living organism.
Interphase	A phase in cell cycle in which the cell copies its DNA in preparation for mitosis.
Interquartile range	Calculated as the 75^{th} minus the 25^{th} percentile of the frequency distribution of a continuous variable.
Intron	The non-coding section of an RNA transcript or its corresponding DNA.

Term	Definition
Isoform	Messenger RNAs produced at the same locus but differing in the protein coding DNA sequences, which may affect gene function.
Kamino body	An eosinophilic, spherical structure (“globoid”) that is often found at the dermo-epidermal junction of Spitz naevi.
Kaplan-Meier curve(s)	A graphical representation of the time to failure, e.g. death.
Kinase	An enzyme that transfers phosphate to another molecule.
Kruskal-Wallis test	A non-parametric statistical test to assess whether three or more variables have the same distribution (non-parametric version of “analysis of variance”).
Laser capture microdissection	A method of isolating cells or small pieces of tissue by using a laser to dissect a microscopic region of interest.
Lateral	The part (of the melanoma) that is furthest from the centre.
Lentigo maligna	The *in situ* phase of lentigo maligna melanoma (i.e. radial growth phase; peri-adnexal involvement is frequent).
Lentigo maligna melanoma	A subtype of cutaneous melanoma characterised by epidermal atrophy, a prominent intraepidermal lentiginous component, accompanied by evidence of actinic damage or solar elastosis and frequently involving adnexal structures [5].
Leukocyte methylation score	A score that indicates the extent of DNA methylation in leukocytes (white blood cells).
Likelihood ratio test	A test of two hypotheses in frequentist statistical methods.
Linear regression	A statistical method used to examine whether an independent continuous variable is a linear predictor of a continuous outcome measure.
Loss of heterozygosity	Loss of a gene and its surrounding chromosomal region.
Lymphocyte	A white blood cell with a single nucleus, occurring mainly in the lymphatic system.
Lymphovascular invasion	The presence of melanoma cells within lymphatic or blood vessels.
Macrometastasis	A clinically-detectable lymph node metastasis, confirmed on lymphadenectomy or when there is gross extracapsular extension [51], i.e. a palpable lymph node due to the secondary spread of melanoma.
Macrophage	A white blood cell with the capacity to engulf foreign substances and debris.
Massive parallel sequencing	Also known as next generation sequencing. This is a process of DNA sequencing in which thousands or millions of DNA sequences are produced simultaneously.
Matrix metalloproteinase	An enzyme that breaks down extracellular proteins, such as collagen or elastin.

Term	Definition
Maturation	The tendency of melanocytes to become smaller towards the base of a benign melanocytic lesion.
Maximum microscopic diameter (in mm)	The distance between the most lateral epidermal nest at either side of the melanoma, or where nests are absent, the distance between the furthest edges of the invasive component of the tumour. (This definition was developed following discussion with Dr W. Merchant).
Median	A value that lies at the midpoint of a distribution.
Melanocyte	A cell that produces melanin pigment.
Melanoma-specific death	Death due to melanoma.
Melanoma-specific survival	The interval between melanoma diagnosis and the time of melanoma-specific death (event) or death due to other causes (censored), or the interval between melanoma diagnosis and censoring and there is no record of death.
Melanophage	A pigment-laden macrophage.
Melanosome	A specialised structure within a melanocyte that is responsible for making, storing and transporting melanin pigment.
MELTUMP	A melanocytic lesion which displays some features of both a benign melanocytic naevus and of melanoma but falls short of a diagnosis of melanoma. Its behaviour cannot be reliably predicted.
Mesenchymal (phenotype/cell movement)	A description given to a type of cell movement that has an elongated appearance *in vitro* [105].
Mesenchymal cell	A cell that has the capacity to develop into tissues of the lymphatic, circulatory or connective tissues.
Mesothelioma	A cancer of the mesothelium.
Mesothelium	The lining of the pleural and peritoneal cavities.
MetaCore™	A bioinformatics package that can be used to input several genes and to compute an enrichment analysis, thus providing information on biological pathways that are altered in the data set.
Metastasis(-es)	The development of secondary cancer(s) at a site(s) distant to the primary cancer.
Metastasis-free survival	The interval between melanoma diagnosis and the time of melanoma metastasis (event) or death (censored), or the interval between melanoma diagnosis and censoring and there is no record of metastasis.
Microarray	DNA sequences for all of the genes in an organism, arranged in a grid for genetic testing.

Term	Definition
Micrometastasis	A metastasis detected microscopically, on sentinel lymph node biopsy or completion lymphadenectomy, in the absence of any clinical abnormality [51].
Microsatellite	The presence of a discontinuous nest of metastatic cells >0.05mm in diameter, deep to the invasive melanoma and separated by normal dermis of at least 0.3mm [43].
Microscopic ulceration	A full thickness epidermal defect, accompanied by reactive changes (including neutrophils and fibrin) and surrounding epidermal thinning or hyperplasia, in the absence of trauma or surgery [51].
Mini-wall	A large digital screen display, consisting of 3 computer screens orientated adjacent to each other and linked to a single computer. It can be used to view a single item across three screens in unison or to display separate items on each parallel screen at the same time.
Missense mutation	A mutation where a single nucleotide change results in coding for a different amino acid.
Mitosis (-es)	The process of cell division (occurring within the nucleus), where a parent cell divides to form two daughter cells.
Mitotic rate (per mm^2)	The number of dermal mitoses within $1mm^2$ region of the “hot spot” (or area of apparently most numerous dermal mitoses), or in the absence of a hot spot, the number of dermal mitoses within $1mm^2$ of a representative dermal mitosis [43].
Molecular profile	A pattern based on gene expression signatures or mutation status or genomic characteristics of the tumour.
Molecule	A group of atoms bonded together, being the smallest part in a chemical element.
Monocyte	The largest type of white blood cell. It is capable of differentiating into a macrophage.
Multinucleated	Having multiple nuclei.
Multivariable	In statistical modelling, multivariable implies that multiple predictor variables are included in the model.
Mutation	A structural change in a gene, resulting in a variant form.
Myofibroblast	An atypical fibroblast that has features of a fibroblast and a smooth muscle cell.
Naevus/naevi	A benign melanocytic lesion (mole).
Neutrophil	A white blood cell with a role in innate immunity (rudimentary response to foreign substances) and a multi-lobed nucleus.
Nodular melanoma	A subtype of cutaneous melanoma characterised by a predominant vertical growth phase, with the lateral intraepidermal component extending no more than 3 rete ridges beyond the vertical growth phase component. (Please see Table 2.1).

Term	Definition
Non-parametric test	A statistical test that can be performed on a continuous variable without making any assumptions about its distribution.
Nuclear hyperchromasia	A darkly staining nucleus.
Nuclear pleomorphism	Nuclei that vary in size and shape.
Nuclear pseudoinclusion	A bleb of cytoplasm, prolapsed into the nucleus.
Nucleolus (-i)	A structural component of the nucleus.
Nucleotide	A molecule, which is a subunit of DNA or RNA.
Nucleus (-i)	A structure within a cell that contains the genetic material.
Ocular micrometre	A glass disc containing a ruled scale, which can be inserted into the eyepiece of a microscope to make measurements.
Ordinal variable	A type of categorical variable, where individual categories are ordered.
Organotypic culture	The culture of 2 or more cell types from a complex tissue or organ.
Overall survival	The length of time that patients live after the date of diagnosis (of cancer).
Pagetoid spread	The upward spread of atypical melanocytes into the epidermis.
Pairwise analysis	A statistical comparison between 2 variables.
Papillary dermis	The uppermost layer of the dermis.
Paucicellular	Having few cells.
Perineural invasion	The presence of melanoma cells surrounding a nerve.
Peritoneum	The serous membrane that forms the abdominal cavity.
Phenotype	The physical characteristics of an individual resulting from the interaction between the individual's genetic make-up (genotype) and the environment.
Plasma	The liquid component of blood in which the blood cells are suspended.
Plasma cell	A white blood cell (fully differentiated B cell) that secretes antibodies.
Plasmacytoid	Resembling a plasma cell.
Pleomorphism	The variability in size and shape of cells or their nuclei.
Pleura	One of the membranes around the lungs.
Plexiform	Resembling a plexus (or complex network).
Prognosis	The likely course of a medical condition.
Promoter	A segment of DNA that initiates the transcription of a gene.

Term	Definition
Pyrosequencing	A DNA sequencing method that depends upon the release of pyrophosphate during DNA synthesis. A series of enzymatic reactions then result in the release of light that is proportional to the number of incorporated nucleotides.
Quantile normalisation	A statistical method of making two distributions identical.
Quartile	Any of 4 equal groups.
Quintile	Any of 5 equal groups.
Radial growth phase (*in situ*)	The presence of intraepidermal melanoma cells, singly or in nests [182].
Radial growth phase (microinvasive)	The presence of intraepidermal melanoma with involvement of the papillary dermis but which does not meet the criteria for vertical growth phase [182].
Radial growth phase (RGP) melanoma	Predominantly intraepidermal melanoma, or if present, dermal nests consist of <15 cells, are no larger than intraepidermal nests and dermal mitoses are absent [5]. (Please see Table 2.1).
Reference category (baseline)	The category that is used as the baseline in a statistical model, against which other categories are compared.
Regression	Replacement of melanoma cells by a variable lymphocytic infiltrate, melanophages, telangiectasia and fibrosis and often accompanied by epidermal atrophy [77]. • Stage 1 regression: some loss of dermal melanoma but preservation of the epidermal component [77]. • Stage 2 regression: loss of all dermal melanoma but a residual junctional component remains [77]. • Stage 3 regression: loss of junctional and dermal components of melanoma, with resultant dermal scarring [77]. • Partial regression: loss of part of the tumour mass without complete replacement of tumour by inflammatory cells and fibrosis [75]. • Segmentary regression: complete regression of a segment of melanoma [75].
Relapse	Evidence of recurrence of melanoma.
Relapse survival time	The interval between melanoma diagnosis and the time of melanoma relapse (event) or death (censored), or the interval between melanoma diagnosis and censoring and there is no record of relapse.
Relative tumour loss	The Breslow thickness divided by the depth of tumour loss in millimetres.
Rete ridges	Thickened extensions of the epidermis that protrude into the dermis.

Term	Definition
Reticular dermis	The layer of dermis that lies beneath the papillary dermis and is composed of dense connective tissue.
ROC curve analysis	A method of evaluating the true positive and the true negative rate.
RT-PCR	A technique used to detect RNA, through a process involving the amplification of complementary DNA.
Senescence	The loss of a cell's ability to divide and grow.
Sentinel lymph node biopsy	A surgical procedure used to evaluate whether or not cancer (melanoma) has spread to the first draining lymph node(s).
Septum (-a)	A partition between two chambers or structures.
Silencing	Repressing the expression of a gene.
Singular value decomposition	A statistical method (similar to a principal components analysis), which describes the structure of the data.
Solar elastosis	The presence of elastotic fibres in the dermis, which may occur singly or may form clumps or amorphous masses [183].
Somatic cell	A cell of a living organism that is not a reproductive cell.
Somatic mutation	A mutation that occurs in somatic cells and is capable of being transmitted to daughter cells in the process of cell division.
Spearman correlation	A statistical method of assessing the dependence between the ranking of two variables.
Spindle-shaped melanocyte	A melanocyte with an elongated, fusiform or cigar-like shape.
Spitz naevus	A type of benign melanocytic naevus that was described by Sophie Spitz. It is typically pink in colour, although may be pigmented. On histopathological assessment, vertical nests of epithelioid and spindle cells may be seen. Kamino bodies may also be noted.
Spitz tumours	Melanocytic lesions with an appearance reminiscent of a Spitz naevus. This may refer to Spitz naevi, atypical Spitz tumours (lesions which have features that are not typical of a naevus but do not fulfil the criteria for melanoma) or spitzoid melanomas. The lesions consist of epithelioid/spindle cells with abundant cytoplasm and often lack pigment.
Spitzoid	Displaying features of a Spitz naevus.
Spitzoid Tumour of Uncertain Malignant Potential	Please see "Atypical Spitz tumour".
Splice site	The site at which splicing takes place.
Splicing	The process in which introns are removed and exons are joined together.
Sporadic	Not inherited.
Squamous epithelium	The surface covering of the skin, which consists of flattened highly differentiated keratinocytes.

Term	Definition
Statistical interaction	In a statistical model, the effect of one predictor variable on outcome depends on the value of another predictor variable, i.e. the effects of two predictor variables on the outcome variable are not additive or multiplicative.
Stem cell	An undifferentiated cell that is capable of limitless cell division and which can give rise to other types of cells.
Stroma	The supportive tissue of an organ or tumour, consisting of connective tissue, blood vessels and immune cells.
Subcutaneous	Under the skin.
Subcutis	The tissue underlying the dermis of the skin, which consists mainly of fat.
Superficial spreading melanoma	A subtype of melanoma characterised by a predominantly nested pattern of melanoma but may sometimes contain a dermal nodule with a lateral intraepidermal component extending more than 3 rete ridges beyond the vertical growth phase melanoma. Pagetoid spread is common in this subtype. (Please see Table 2.1).
T cell exhaustion	A state of T cell dysfunction, characterised by poor T cell effector function, which may occur in cancer.
Targeted DNA sequencing	A technique that involves sequencing a specific region of DNA at a high resolution.
Telomerase	A protein that adds telomere sequences to the 3' end of the telomere.
Telomere	Repetitive nucleotide sequences at the ends of chromosomes that protect them from fusion with other chromosomes.
Tertile	Any of 3 equal groups.
Time-to-event analysis	Pertaining to survival analyses, considering the time to the event (either melanoma relapse or melanoma-specific death) or the time to the censoring point for participants not having the event or not known to have had the event.
Transcription	A process whereby part of the DNA of a gene is copied into RNA.
Transcriptome	The messenger RNA expressed by the genes of an organism.
Tumour implant	The insertion of tumour into a host (e.g. a mouse).
Tumour-infiltrating lymphocytes (TILs)	Lymphocytes in the vertical growth phase that surround and disrupt melanoma cells [181]. • Absent TILs: no lymphocytes or if present, they do not infiltrate the vertical growth phase melanoma [60]. • Non-brisk TILs: lymphocytes infiltrate the invasive melanoma but only focally [60]. • Brisk TILs: lymphocytes diffusely infiltrate the entire base or the entire invasive component [60].

Term	Definition
Tumour-infiltrating melanophages	Macrophages/melanophages that infiltrate or are closely apposed to the VGP melanoma.
Tumour loss	A clear deficit within the silhouette of the melanoma at 4x magnification and composed of a variable presence of lymphocytes, melanophages and/or fibrous tissue.
Ubiquitin	A small regulatory protein.
Univariable	Involving one predictor variable in a statistical model with one outcome.
Unsupervised hierarchical clustering	A computerised method of grouping objects that are similar together in a cluster, without any pre-conditions.
UV signature	A distinct pattern of somatic mutations that develops as a consequence of exposure to ultraviolet radiation and typically leads to the formation of pyrimidine dimers involving cytosine-thymine or cytosine-cytosine to thymine-thymine [378].
Variant	A difference in the DNA between an individual and most people.
Vector	An organism that does not cause disease but transfers a pathogen to another host.
Vertical growth phase (VGP) melanoma	Melanoma that invades the dermis and dermal melanoma nests show a growth advantage over intraepidermal nests, or are >15 cells and/or dermal mitoses are present [5].
Virtual pathology	The use of digitised pathology images and computerised techniques for the assessment of histological sections.
Visceral	Relating to an internal organ.
Wilcoxon rank-sum (Mann Whitney U) test	A non-parametric test to assess whether two variables come from two different distributions or from the same distribution; the extension to 3 or more variables is termed the Mann Whitney U test.

Appendix B : Prof. Cook Protocol

B.1 Prof. Cook Protocol

Review data were recorded in a FileMaker Pro® Database designed and implemented by the Section of Epidemiology and Biostatistics. Below are a series of screen shots showing the data fields used in accordance with the protocol developed by Professor M. Cook.

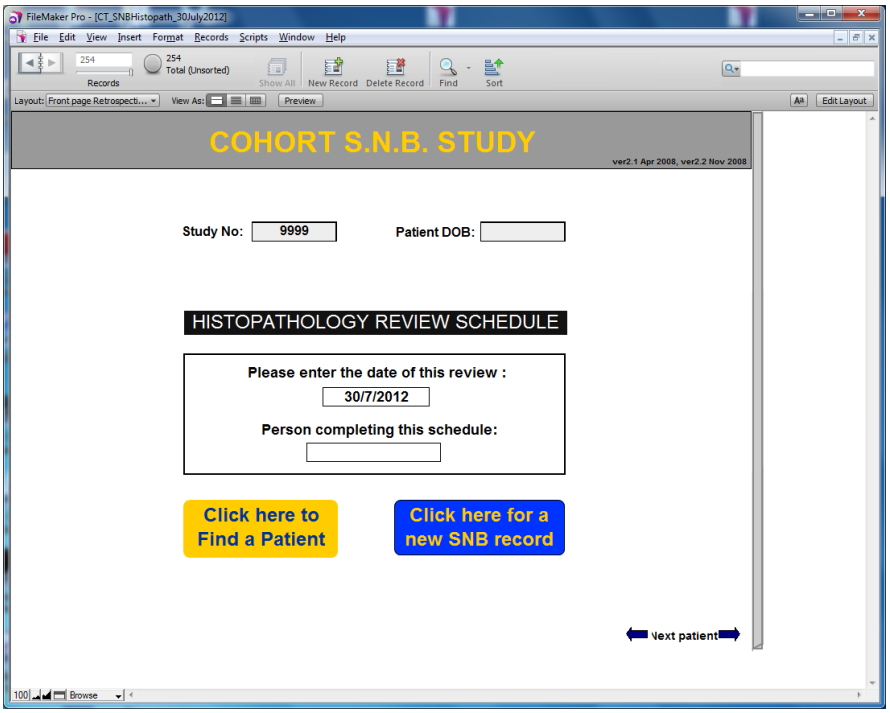

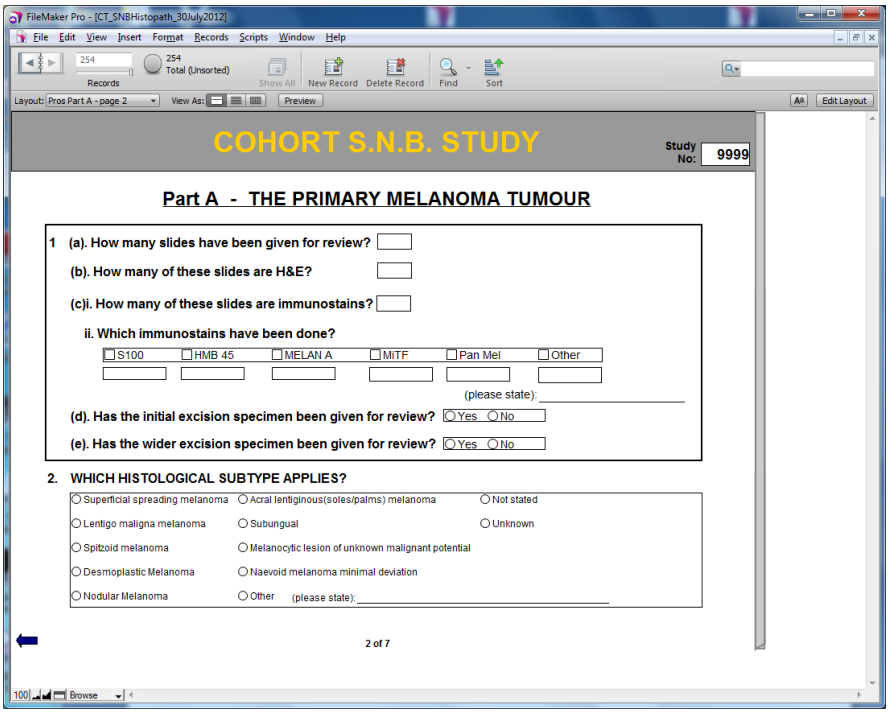

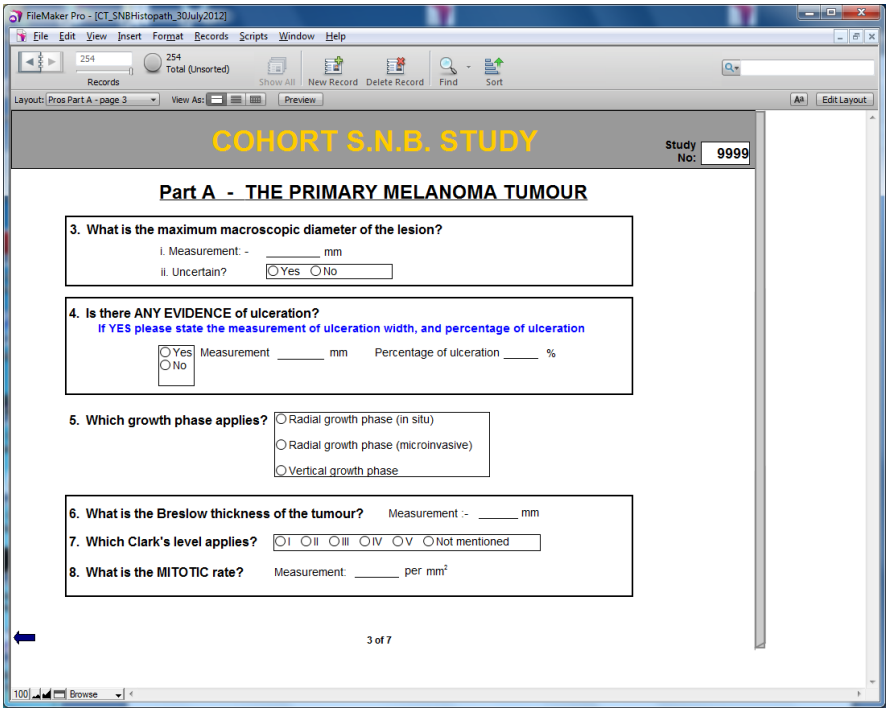

FileMaker Pro - [CT_SNBHistopath_30July2012]

File Edit View Insert Format Records Scripts Window Help

Layout: Pros Part A - page 3 | Preview | Edit Layout

COHORT S.N.B. STUDY — Study No: 9999

Part A - THE PRIMARY MELANOMA TUMOUR

3. What is the maximum macroscopic diameter of the lesion?

i. Measurement: - _____ mm

ii. Uncertain? ○ Yes ○ No

4. Is there ANY EVIDENCE of ulceration?

If YES please state the measurement of ulceration width, and percentage of ulceration

○ Yes ○ No Measurement _____ mm Percentage of ulceration _____ %

5. Which growth phase applies?

○ Radial growth phase (in situ)
○ Radial growth phase (microinvasive)
○ Vertical growth phase

6. What is the Breslow thickness of the tumour? Measurement :- _____ mm

7. Which Clark's level applies? ○ I ○ II ○ III ○ IV ○ V ○ Not mentioned

8. What is the MITOTIC rate? Measurement: _____ per mm^2

3 of 7

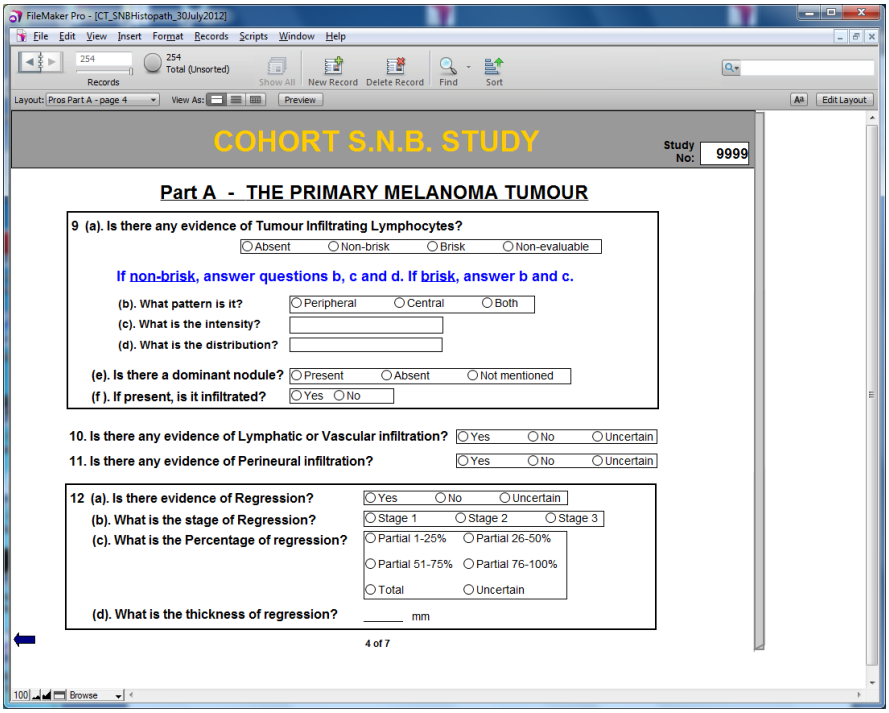

FileMaker Pro - [CT_SNBHistopath_30July2012]

File Edit View Insert Format Records Scripts Window Help

Layout: Pros Part A - page 4 | Preview | Edit Layout

COHORT S.N.B. STUDY — Study No: 9999

Part A - THE PRIMARY MELANOMA TUMOUR

9 (a). Is there any evidence of Tumour Infiltrating Lymphocytes?

○ Absent ○ Non-brisk ○ Brisk ○ Non-evaluable

If non-brisk, answer questions b, c and d. If brisk, answer b and c.

(b). What pattern is it? ○ Peripheral ○ Central ○ Both

(c). What is the intensity?

(d). What is the distribution?

(e). Is there a dominant nodule? ○ Present ○ Absent ○ Not mentioned

(f). If present, is it infiltrated? ○ Yes ○ No

10. Is there any evidence of Lymphatic or Vascular infiltration? ○ Yes ○ No ○ Uncertain

11. Is there any evidence of Perineural infiltration? ○ Yes ○ No ○ Uncertain

12 (a). Is there evidence of Regression? ○ Yes ○ No ○ Uncertain

(b). What is the stage of Regression? ○ Stage 1 ○ Stage 2 ○ Stage 3

(c). What is the Percentage of regression?

○ Partial 1-25% ○ Partial 26-50%
○ Partial 51-75% ○ Partial 76-100%
○ Total ○ Uncertain

(d). What is the thickness of regression? _____ mm

4 of 7

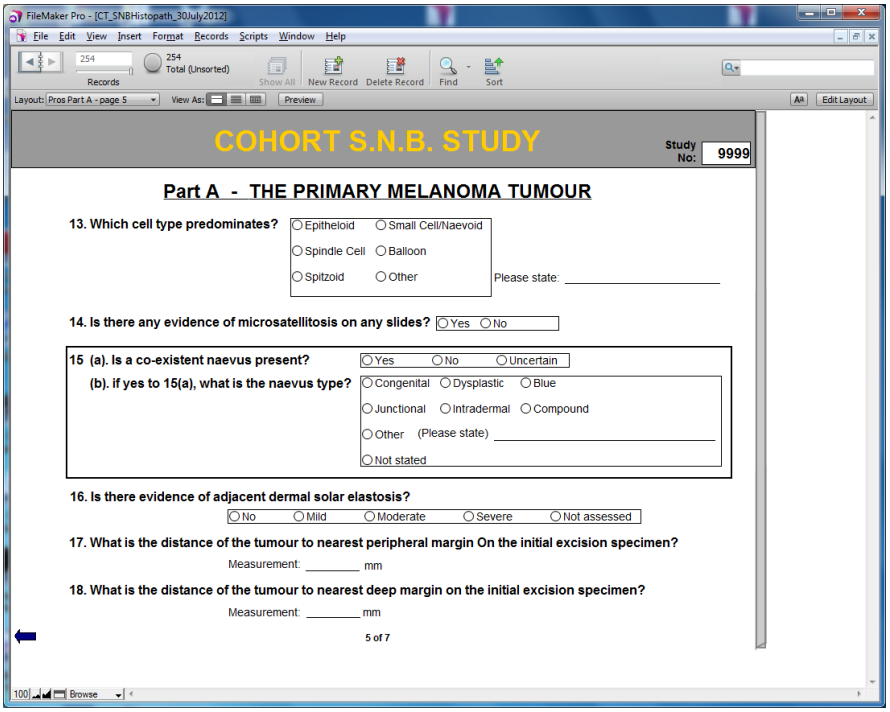

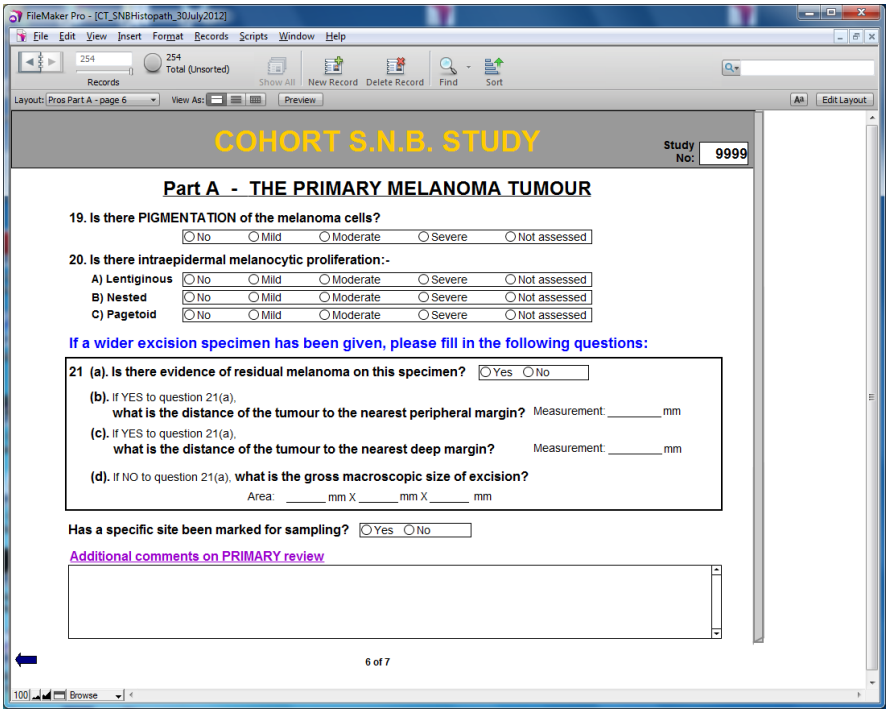

B.2 Descriptive statistics of 158 cases of primary melanoma

The table below summarises the scoring of variables used in the Prof. Cook protocol for 158 cases of primary melanoma.

Measure	Feature	N	Statistic	Value
Number of H&E slides		158	Median (range)	1 (1-4)
Histological subtype	Superficial spreading	158	N (%)	115 (72.78)
	Nodular			14 (8.86)
	Lentigo maligna (melanoma)			1 (0.63)
	Acral lentiginous			3 (1.9)
	Naevoid melanoma minimal deviation			6 (3.8)
	Spitzoid			1 (0.63)
	Subungual			1 (0.63)
	Lentigo maligna (in situ)			2 (1.27)
	Melanoma in situ			1 (0.63)
	Metastasis			1 (0.63)
	Other			8 (5.06)
	Unknown			5 (3.16)
Maximum diameter (mm)		158	Median (range)	7 (1.7-23.8)
Growth phase	Radial growth phase (*in situ*)	158	N (%)	5 (3.16)
	Radial growth phase (microinvasive)			7 (4.43)
	Vertical growth phase			146 (92.41)
Clark's level	I	158	N (%)	4 (2.53)
	II			7 (4.43)
	III			11 (6.96)
	IV			121 (76.58)
	V			4 (2.53)
	Base absent			7 (4.43)
	Unknown			4 (2.53)
Breslow thickness (mm)		158	Median (range)	1.37 (0-9)
Ulceration	Yes	158	N (%)	30 (18.99)
	No			128 (81.01)
Diameter of ulceration (mm)		29	Median (range)	1.6 (0.1-15)
Percentage ulceration (%)		29	Median (range)	20 (1.38-87.5)
Traumatic ulceration	Yes	158	N (%)	22 (13.92)
	No			32 (20.25)
	Unknown			104 (65.82)
Erosion only	Yes	158	N (%)	3 (1.9)
	No			29 (18.35)
	Unknown			126 (79.75)
Epidermis absent	Yes	158	N (%)	1 (0.63)
	No			41 (25.95)
	Unknown			116 (73.42)

Measure	Feature	N	Statistic	Value
Mitotic rate/mm²	0	158	N (%)	39 (24.68)
	1-5			87 (55.06)
	≥6			31 (19.62)
	Unknown			1 (0.63)
TILs	Absent	158	N (%)	8 (5.06)
	Non-brisk			100 (63.29)
	Brisk			30 (18.99)
	Non-evaluable			19 (12.03)
	Unknown			1 (0.63)
TILs location	Central	158	N (%)	2 (1.27)
	Peripheral			3 (1.9)
	Both			125 (79.11)
	Unknown			28 (17.72)
TILs intensity	Scanty	158	N (%)	76 (48.1)
	Moderate			40 (25.32)
	Dense			14 (8.86)
	Unknown			28 (17.72)
TILs distribution	Focal	158	N (%)	2 (1.27)
	Multifocal			96 (60.76)
	Segmental			30 (18.99)
	Unknown			30 (18.99)
Dominant nodule infiltrated by TILs	Yes	158	N (%)	70 (44.3)
	No			3 (1.9)
	Unknown			85 (53.8)
Regression	Yes	158	N (%)	6 (3.8)
	No			144 (91.14)
	Uncertain			8 (5.06)
Stage of regression	No regression	158	N (%)	144 (91.14)
	Stage 1			7 (4.43)
	Stage 2			5 (3.16)
	Stage 3			1 (0.63)
	Unknown stage			1 (0.63)
Thickness of regression (mm)		13	Median (range)	0.72 (0.2-1.4)
Microsatellites	Yes	158	N (%)	2 (1.27)
	No			155 (98.1)
	Unknown			1 (0.63)
Lymphovascular invasion	Yes	158	N (%)	12 (7.59)
	No			142 (89.87)
	Uncertain			4 (2.53)

Measure	Feature	N	Statistic	Value
Perineural invasion	Yes	158	N (%)	2 (1.27)
	No			154 (97.47)
	Uncertain			2 (1.27)
Distance to peripheral margin (mm)		158	Median (range)	1.71 (0-19)
Distance to deep margin (mm)		158	Median (range)	4 (0-18)
Coexistent naevus	Yes	158	N (%)	23 (14.56)
	No			117 (74.05)
	Uncertain			18 (11.39)
Naevus type	Compound	158	N (%)	2 (1.27)
	Intradermal			36 (22.78)
	Dysplastic			1 (0.63)
	Congenital			1 (0.63)
	Unknown			118 (74.68)
Main cell type	Epithelioid	158	N (%)	94 (59.49)
	Small/ Naevoid			31 (19.62)
	Spindle			15 (9.49)
	Spitzoid			4 (2.53)
	Balloon			1 (0.63)
	Other			6 (3.8)
	Unknown			7 (4.43)
Giant tumour cells	Yes	158	N (%)	15 (9.49)
	No			59 (37.34)
	Unknown			84 (53.16)
Intercellular clefting	Yes	158	N (%)	24 (15.19)
	No			50 (31.65)
	Unknown			84 (53.16)
Spitzoid features	Yes	158	N (%)	20 (12.66)
	No			55 (34.81)
	Unknown			83 (52.53)

Appendix C : Virtual Pathology Protocol

C.1 Virtual pathology protocol

Review data were recorded in a FileMaker Pro® Database designed and implemented by the Section of Epidemiology and Biostatistics. On the following two pages are a series of screen shots showing the data fields used in accordance with the virtual pathology protocol (Figure B1.1).

C.2 Pilot work to quantify stromal content in primary melanomas using virtual pathology imaging

The average proportion of stromal content in each tumour and matching core was plotted after the addition of each scored arrow to give a moving average plot. This was done in order to assess the variance across the scored arrow count and to evaluate the optimum number of arrows that would give a meaningful estimation of the proportion of stroma (Figure B1.2).

A) **B)**

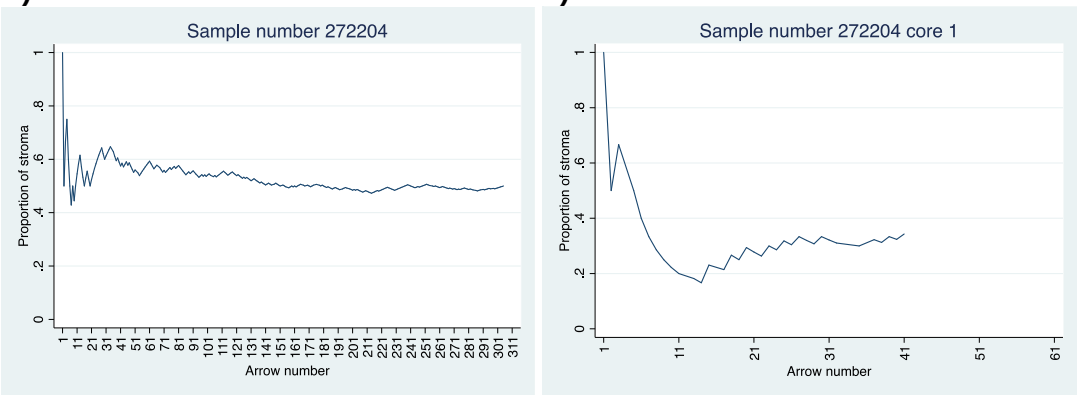

Figure B1.1 The moving average for the proportion of stroma by arrow count

A) The moving average for the proportion of stroma by arrow count across a representative area of tumour for sample 272204. The graph shows the proportion of stroma, beginning with the first arrow and then increasing in number. The “true” proportion of stroma is approximately 0.5, over 300 arrows. The proportion of stroma varies a lot when the sample is small, reflected by fluctuations in the graph. The graph reaches a steady state after 145 arrows. After 50 arrows, the proportion of stroma is approximately 0.55 which reflects about 10% error. B) The moving average for the proportion of stroma by arrow count in core 1 of sample 272204. The estimated proportion of stroma is approximately 0.3.

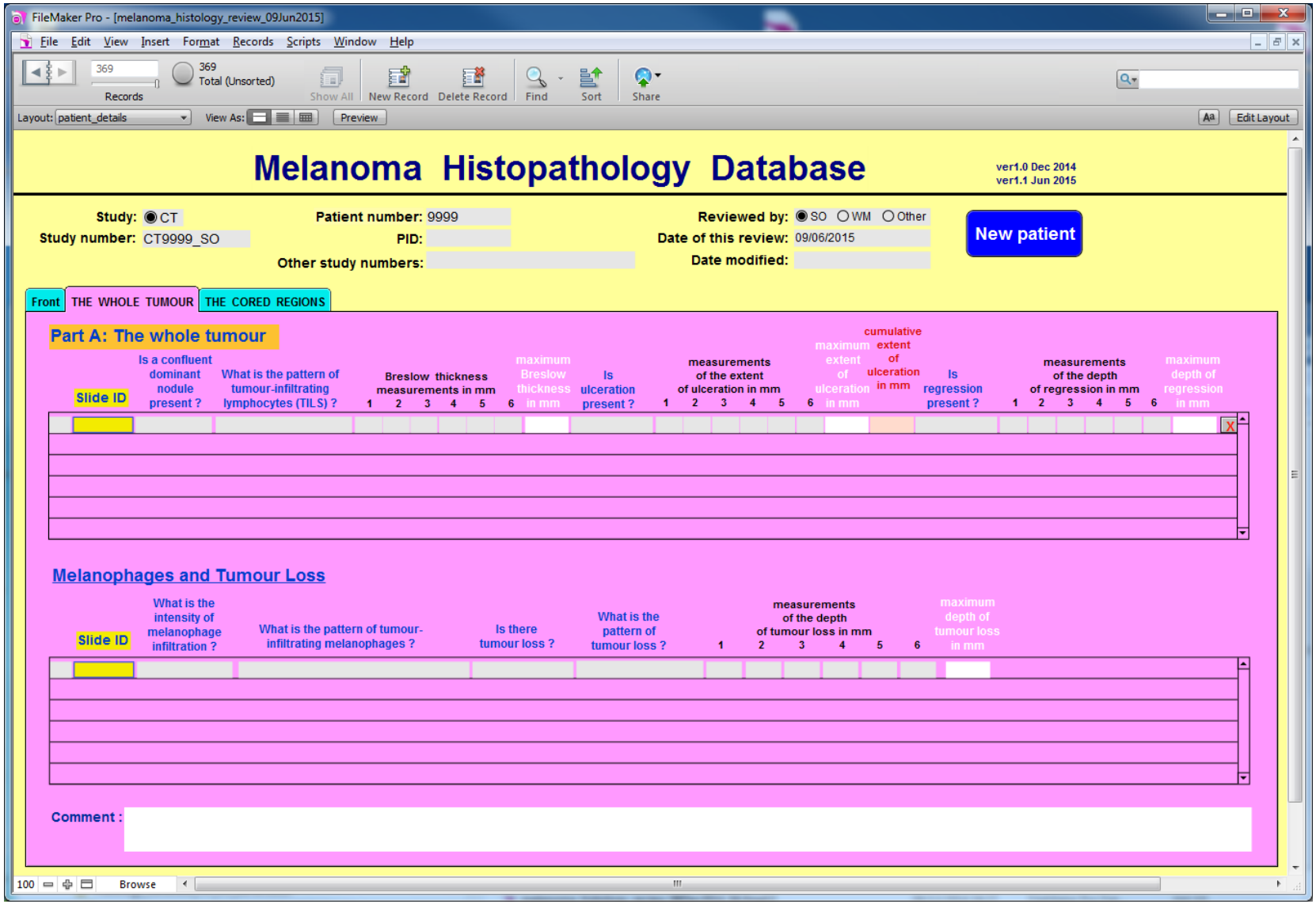
FileMaker Pro - [melanoma_histology_review_09Jun2015]
File Edit View Insert Format Records Scripts Window Help
Records
369 Total (Unsorted)
Show All
New Record
Delete Record
Find
Sort
Share
Layout: patient_details
View As:
Preview
Edit Layout
Melanoma Histopathology Database
ver1.0 Dec 2014
ver1.1 Jun 2015
Study: CT
Study number: CT9999_SO
Patient number: 9999
PID:
Other study numbers:
Reviewed by: SO WM Other
Date of this review: 09/06/2015
Date modified:
New patient
Front
THE WHOLE TUMOUR
THE CORED REGIONS
Part A: The whole tumour
Slide ID
Is a confluent dominant nodule present ?
What is the pattern of tumour-infiltrating lymphocytes (TILS) ?
Breslow thickness measurements in mm
1 2 3 4 5 6
maximum Breslow thickness in mm
Is ulceration present ?
measurements of the extent of ulceration in mm
1 2 3 4 5 6
maximum extent of ulceration in mm
cumulative extent of ulceration in mm
Is regression present ?
measurements of the depth of regression in mm
1 2 3 4 5 6
maximum depth of regression in mm
Melanophages and Tumour Loss
Slide ID
What is the intensity of melanophage infiltration ?
What is the pattern of tumour-infiltrating melanophages ?
Is there tumour loss ?
What is the pattern of tumour loss ?
measurements of the depth of tumour loss in mm
1 2 3 4 5 6
maximum depth of tumour loss in mm
Comment :
100
Browse

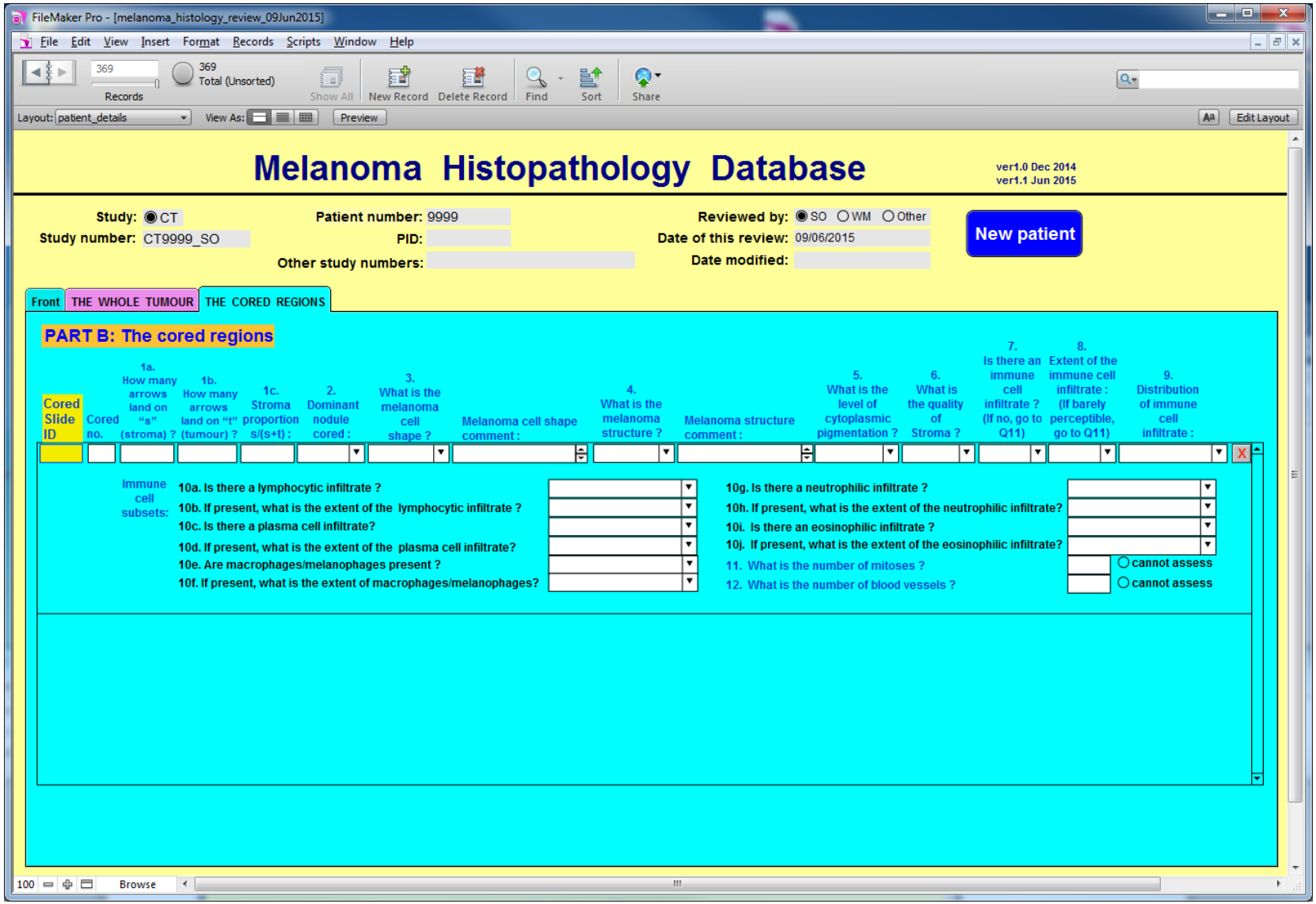
FileMaker Pro - [melanoma_histology_review_09Jun2015]
File Edit View Insert Format Records Scripts Window Help
Records
369 Total (Unsorted)
Show All
New Record
Delete Record
Find
Sort
Share
Layout: patient_details
View As:
Preview
Edit Layout
Melanoma Histopathology Database
ver1.0 Dec 2014
ver1.1 Jun 2015
Study: CT
Study number: CT9999_SO
Patient number: 9999
PID:
Other study numbers:
Reviewed by: SO WM Other
Date of this review: 09/06/2015
Date modified:
New patient
Front
THE WHOLE TUMOUR
THE CORED REGIONS
PART B: The cored regions
Cored Slide ID
Cored no.
1a. How many arrows land on "s" (stroma) ?
1b. How many arrows land on "t" (tumour) ?
1c. Stroma proportion s/(s+t) :
2. Dominant nodule cored :
3. What is the melanoma cell shape ?
Melanoma cell shape comment :
4. What is the melanoma structure ?
Melanoma structure comment :
5. What is the level of cytoplasmic pigmentation ?
6. What is the quality of Stroma ?
7. Is there an immune cell infiltrate ? (If no, go to Q11)
8. Extent of the immune cell infiltrate : (If barely perceptible, go to Q11)
9. Distribution of immune cell infiltrate :
Immune cell subsets:
10a. Is there a lymphocytic infiltrate ?
10b. If present, what is the extent of the lymphocytic infiltrate ?
10c. Is there a plasma cell infiltrate?
10d. If present, what is the extent of the plasma cell infiltrate?
10e. Are macrophages/melanophages present ?
10f. If present, what is the extent of macrophages/melanophages?
10g. Is there a neutrophilic infiltrate ?
10h. If present, what is the extent of the neutrophilic infiltrate?
10i. Is there an eosinophilic infiltrate ?
10j. If present, what is the extent of the eosinophilic infiltrate?
11. What is the number of mitoses ?
cannot assess
12. What is the number of blood vessels ?
cannot assess
100
Browse

C.3 Comparison of representative tumour with tumour core

The table below gives the mean and standard deviation of the proportion of stroma in the representative tumours compared with the cores, by sample number, and the corresponding p-values from two-tailed T-tests. The results show that for some cases (e.g. 272254 and 272309), the estimated proportion of stroma within the core was similar to the estimated proportion of stroma within the representative tumours. However, for others (e.g. 272204 and 272279), the estimated proportion of stroma within the core appeared to differ from the estimated proportion of stroma within the representative tumour.

	Proportion of stroma in representative tumours		Proportion of stroma in cores		
Sample number	Median (range)	Mean (s.d)	Median (range)	Mean (s.d)	T-test p-value
272204	0.50 (0.43-1)	0.53 (0.05)	0.31 (0.17-1)	0.33 (0.15)	<0.00005
272254	0.18 (0.15-1)	0.21 (0.11)	0.22 (0-0.28)	0.20 (0.07)	0.3419
272279	0.25 (0-0.5)	0.24 (0.08)	0.57 (0.46-1)	0.57 (0.09)	<0.00005
272288	0.36 (0-0.5)	0.35 (0.04)	0.17 (0-0.32)	0.19 (0.06)	<0.00005
272305	0.41 (0.39-1)	0.43 (0.06)	0.32 (0-0.42)	0.32 (0.06)	<0.00005
272308	0.29 (0-0.31)	0.27 (0.04)	0.27 (0-0.31)	0.24 (0.06)	<0.00005
272309	0.52 (0-0.58)	0.51 (0.06)	0.5 (0.41-1)	0.52 (0.10)	0.5196
272314	0.27 (0-0.31)	0.25 (0.07)	0.27 (0-0.35)	0.25 (0.07)	0.6458
272318	0.33 (0-0.75)	0.34(0.08)	0.33 (0-0.4)	0.32(0.07)	0.0495
272320	0.43 (0.3-1)	0.43 (0.04)	0.46 (0-0.53)	0.45 (0.07)	0.0218

C.4 Comparison of percentage stroma by eyeball estimate versus arrow count

% agreement for percentage stroma by estimate vs. arrow count was 57.89% (11/19).

	Stroma % arrow count					
Stroma % estimate	0	1-24%	25-49%	50-74%	≥75%	Total
0	0 (0)	0 (0)	0 (0)	0 (0)	0 (0)	0 (0)
1-24%	0 (0)	4 (66.67)	4 (36.36)	1 (50.00)	0 (0)	9 (47.37)
25-49%	0 (0)	2 (33.33)	7 (63.64)	1 (50.00)	0 (0)	10 (52.63)
50-74%	0 (0)	0 (0)	0 (0)	0 (0)	0 (0)	0 (0)
≥75%	0 (0)	0 (0)	0 (0)	0 (0)	0 (0)	0 (0)
Total	0 (0)	6 (100)	11 (100)	2 (100)	0 (0)	19 (100)

C.5 Comparison of percentage of stroma by eyeball estimate versus an eyeball estimate using categories

% agreement for percentage stroma by estimate vs. stroma category was 73.68% (14/19).

	Stroma category				
Stroma % estimate	**None**	**Some**	**Moderate**	**Lots**	**Total**
0	0 (0)	0 (0)	0 (0)	0 (0)	0 (0)
1-24%	0 (0)	5 (100)	4 (30.77)	0 (0)	9 (47.37)
25-49%	0 (0)	0 (0)	9 (69.23)	1 (100)	10 (52.63)
50-74%	0 (0)	0 (0)	0 (0)	0 (0)	0 (0)
≥75%	0 (0)	0 (0)	0 (0)	0 (0)	0 (0)
Total	0 (0)	5 (100)	13 (100)	1 (100)	19 (100)

Appendix D : Core Comparisons

D.1 Comparison of Core 1 and Core 2

The table below summarises the results comparing core 1 and core 2.

The Spearman correlation coefficient (rho), percentage (%) agreement, kappa statistic, 95% confidence intervals (95%CI), p-value and the strength of agreement are shown for factors recorded using the virtual pathology protocol within the first and second cored regions. Missing values were excluded from the calculation of the percentage agreement. NA=not applicable. NC=not calculable.

Cored region measures					
	Analysis of core 1 versus core 2				
Factor	**Spearman rho**	**% Agreement**	**Kappa (95%CI)**	**p-value**	**Strength of agreement**
Percentage of stroma	0.7			$2x10^{-58}$	NA
Quality of the stroma		92	0.41 (0.25-0.57)	$<1x10^{-16}$	Moderate
Melanoma cell shape		89	0.61 (0.5-0.69)	$<1x10^{-16}$	Substantial
Melanoma cell structure		74	0.58 (0.51-0.64)	$<1x10^{-16}$	Moderate
Melanoma cell pigmentation		88	0.64 (0.55-0.72)	$<1x10^{-16}$	Substantial
Presence or absence of immune cell infiltrate		93	0.47 (0.31-0.64)	$<1x10^{-16}$	Moderate
Extent of immune cell infiltrate		61	0.39 (0.31-0.45)	$<1x10^{-16}$	Fair
Location of immune cell infiltrate		61	0.42 (0.36-0.49)	$<1x10^{-16}$	Moderate
Presence or absence of lymphocytic infiltrate		67	0.47 (0.39-0.54)	$<1x10^{-16}$	Moderate
Extent of lymphocytic infiltrate		57	0.36 (0.3-0.44)	$<1x10^{-16}$	Fair
Presence or absence of plasma cell infiltrate		75	0.54 (0.46-0.62)	$<1x10^{-16}$	Moderate
Extent of plasma cell infiltrate		75	0.53 (0.45-0.61)	$<1x10^{-16}$	Moderate
Presence or absence of macrophage/melanophage infiltrate		73	0.56 (0.49-0.62)	$<1x10^{-16}$	Moderate

Cored region measures					
	Analysis of core 1 versus core 2				
Factor	**Spearman rho**	**% Agreement**	**Kappa (95%CI)**	**p-value**	**Strength of agreement**
Extent of macrophage/melanophage infiltrate		63	0.46 (0.39-0.52)	$<1x10^{-16}$	Moderate
Presence or absence of neutrophilic infiltrate		75	0.51 (0.43-0.58)	$<1x10^{-16}$	Moderate
Extent of neutrophilic infiltrate		75	0.51 (0.43-0.59)	$<1x10^{-16}$	Moderate
Presence or absence of eosinophilic infiltrate		76	0.52 (0.45-0.6)	$<1x10^{-16}$	Moderate
Core mitoses (tertiles)		55	0.32 (0.26-0.41)	$<1x10^{-16}$	Fair
Core blood vessels		55	0.28 (0.22-0.36)	$2x10^{-15}$	Fair

References

1. Burns, T., Breathnach, S., Cox, N. and Griffiths, C., ed. *Rook's Textbook of Dermatology*. Eighth ed. 2010.
2. Cancer Research UK. *Skin cancer incidence statistics*. 2016. [cited 8th December 2016]; Available from: http://www.cancerresearchuk.org/health-professional/cancer-statistics/statistics-by-cancer-type/skin-cancer/incidence.
3. National Cancer Intelligence Network. *Mortality, incidence and gender - Malignant melanoma*. 2012. [cited 8th December 2016]; Available from: http://www.ncin.org.uk/publications/data_briefings/mortality_incidence_and_gender_malignant_melanoma.
4. Rigel, D. S., et al., *ABCDE--an evolving concept in the early detection of melanoma.* Archives of Dermatology, 2005. **141**(8): p. 1032-4.
5. Mooi, W. J. K., T., ed. *Pathology of Melanocytic Disorders*. 2nd ed. Vol. 17. 2007, CRC Press.
6. Balch, C. M., et al., *Age as a prognostic factor in patients with localized melanoma and regional metastases.* Ann Surg Oncol, 2013. **20**(12): p. 3961-8.
7. Balch, C. M., et al., *Age as a predictor of sentinel node metastasis among patients with localized melanoma: an inverse correlation of melanoma mortality and incidence of sentinel node metastasis among young and old patients.* Ann Surg Oncol, 2014. **21**(4): p. 1075-81.
8. Weiss, S. A., et al., *Impact of aging on host immune response and survival in melanoma: an analysis of 3 patient cohorts.* J Transl Med, 2016. **14**(1): p. 299.
9. Hoejberg, L., et al., *Trends in melanoma in the elderly in Denmark, 1980-2012.* Acta Oncol, 2016. **55 Suppl 1**: p. 52-8.
10. Olazagasti Lourido, J. M., et al., *Increasing Incidence of Melanoma in the Elderly: An Epidemiological Study in Olmsted County, Minnesota.* Mayo Clin Proc, 2016. **91**(11): p. 1555-1562.
11. Trolle, L., R. Henrik-Nielsen, and R. Gniadecki, *Ability to self-detect malignant melanoma decreases with age.* Clin Exp Dermatol, 2011. **36**(5): p. 499-501.
12. Derhovanessian, E., et al., *Immunity, ageing and cancer.* Immun Ageing, 2008. **5**: p. 11.
13. Cancer Research UK. *Skin cancer mortality statistics*. 2016. [cited 8th December 2016]; Available from: http://www.cancerresearchuk.org/health-professional/cancer-statistics/statistics-by-cancer-type/skin-cancer/mortality#heading-One.

14. Lasithiotakis, K., et al., *Age and gender are significant independent predictors of survival in primary cutaneous melanoma.* Cancer, 2008. **112**(8): p. 1795-804.
15. Vranova, J., et al., *Malignant melanoma in the Czech Republic: Incidence and mortality according to sex, age and disease stage.* Biomed Pap Med Fac Univ Palacky Olomouc Czech Repub, 2012.
16. Richardson, B. S., et al., *The age-specific effect modification of male sex for ulcerated cutaneous melanoma.* JAMA Dermatol, 2014. **150**(5): p. 522-5.
17. Joosse, A., et al., *Sex Differences in Melanoma Survival are Not Related to Mitotic Rate of the Primary Tumor.* Ann Surg Oncol, 2014.
18. Hajdarevic, S., et al., *Coping styles in decision-making among men and women diagnosed with malignant melanoma.* J Health Psychol, 2013. **18**(11): p. 1445-55.
19. Joosse, A., et al., *Gender differences in melanoma survival: female patients have a decreased risk of metastasis.* J Invest Dermatol, 2011. **131**(3): p. 719-26.
20. Gupta, S., et al., *Gender Disparity and Mutation Burden in Metastatic Melanoma.* J Natl Cancer Inst, 2015. **107**(11).
21. Haluza, D., et al., *Gender aspects of recreational sun-protective behavior: results of a representative, population-based survey among Austrian residents.* Photodermatol Photoimmunol Photomed, 2016. **32**(1): p. 11-21.
22. Speijers, M. J., et al., *Tumor mitotic rate added to the equation: melanoma prognostic factors changed? : a single-institution database study on the prognostic value of tumor mitotic rate for sentinel lymph node status and survival of cutaneous melanoma patients.* Ann Surg Oncol, 2015. **22**(9): p. 2978-87.
23. Thompson, J. F., et al., *Prognostic significance of mitotic rate in localized primary cutaneous melanoma: an analysis of patients in the multi-institutional American Joint Committee on Cancer melanoma staging database.* J Clin Oncol, 2011. **29**(16): p. 2199-205.
24. Azimi, F., et al., *Tumor-infiltrating lymphocyte grade is an independent predictor of sentinel lymph node status and survival in patients with cutaneous melanoma.* J Clin Oncol, 2012. **30**(21): p. 2678-83.
25. Eriksson, H., et al., *Prognostic factors in localized invasive primary cutaneous malignant melanoma: results of a large population-based study.* Br J Dermatol, 2015. **172**(1): p. 175-86.
26. Mandala, M., et al., *Mitotic rate correlates with sentinel lymph node status and outcome in cutaneous melanoma greater than 1 millimeter in thickness: A multi-institutional study of 1524 cases.* J Am Acad Dermatol, 2016.

27. Thomas, N. E., et al., *Tumor-infiltrating lymphocyte grade in primary melanomas is independently associated with melanoma-specific survival in the population-based genes, environment and melanoma study.* J Clin Oncol, 2013. **31**(33): p. 4252-9.
28. Egger, M. E., et al., *Prognostic factors in melanoma patients with tumor-negative sentinel lymph nodes.* Surgery, 2016. **159**(5): p. 1412-21.
29. MacKie, R. M. and C. A. Bray, *Hormone replacement therapy after surgery for stage 1 or 2 cutaneous melanoma.* Br J Cancer, 2004. **90**(4): p. 770-2.
30. Karagas, M. R., et al., *A pooled analysis of 10 case-control studies of melanoma and oral contraceptive use.* Br J Cancer, 2002. **86**(7): p. 1085-92.
31. Nosrati, A. and M. L. Wei, *Sex disparities in melanoma outcomes: The role of biology.* Arch Biochem Biophys, 2014.
32. Burton, A. L., et al., *Prognostic factors in young women with cutaneous melanoma.* Am J Surg, 2014. **207**(1): p. 102-8.
33. Mandala, M., et al., *Clinical and histopathological risk factors to predict sentinel lymph node positivity, disease-free and overall survival in clinical stages I-II AJCC skin melanoma: outcome analysis from a single-institution prospectively collected database.* Eur J Cancer, 2009. **45**(14): p. 2537-45.
34. Callender, G. G., et al., *Prognostic implications of anatomic location of primary cutaneous melanoma of 1 mm or thicker.* Am J Surg, 2011. **202**(6): p. 659-64; discussion 664-5.
35. Platz, A., et al., *Human cutaneous melanoma; a review of NRAS and BRAF mutation frequencies in relation to histogenetic subclass and body site.* Mol Oncol, 2008. **1**(4): p. 395-405.
36. Curtin, J. A., et al., *Somatic activation of KIT in distinct subtypes of melanoma.* J Clin Oncol, 2006. **24**(26): p. 4340-6.
37. Thomas, N. E., et al., *Association Between NRAS and BRAF Mutational Status and Melanoma-Specific Survival Among Patients With Higher-Risk Primary Melanoma.* JAMA Oncol, 2015. **1**(3): p. 359-68.
38. Duarte, C. A., et al., *Survival of acral lentiginous melanoma in the National Cancer Institute of Colombia.* J Eur Acad Dermatol Venereol, 2016.
39. Sanlorenzo, M., et al., *Melanoma of the lower extremities: foot site is an independent risk factor for clinical outcome.* Int J Dermatol, 2015. **54**(9): p. 1023-9.
40. Sanchez, A., et al., *Primary genitourinary melanoma: Epidemiology and disease-specific survival in a large population-based cohort.* Urol Oncol, 2016. **34**(4): p. 166 e7-14.

41. Tchelebi, L., A. Guirguis, and H. Ashamalla, *Rectal melanoma: epidemiology, prognosis, and role of adjuvant radiation therapy.* J Cancer Res Clin Oncol, 2016. **142**(12): p. 2569-2575.
42. Kalkhoran, S., et al., *Historical, clinical, and dermoscopic characteristics of thin nodular melanoma.* Archives of Dermatology, 2010. **146**(3): p. 311-8.
43. Balch, C. M., et al., *Final version of 2009 AJCC melanoma staging and classification.* J Clin Oncol, 2009. **27**(36): p. 6199-206.
44. Gimotty, P. A., et al., *A population-based validation of the American Joint Committee on Cancer melanoma staging system.* J Clin Oncol, 2005. **23**(31): p. 8065-75.
45. Breslow, A., *Thickness, cross-sectional areas and depth of invasion in the prognosis of cutaneous melanoma.* Ann Surg, 1970. **172**(5): p. 902-8.
46. Balch, C. M., et al., *Prognostic factors analysis of 17,600 melanoma patients: validation of the American Joint Committee on Cancer melanoma staging system.* J Clin Oncol, 2001. **19**(16): p. 3622-34.
47. Balch, C. M., et al., *Final version of the American Joint Committee on Cancer staging system for cutaneous melanoma.* J Clin Oncol, 2001. **19**(16): p. 3635-48.
48. McGovern, V. J., et al., *Ulceration and prognosis in cutaneous malignant melanoma.* Histopathology, 1982. **6**(4): p. 399-407.
49. Jewell, R., et al., *The clinicopathological and gene expression patterns associated with ulceration of primary melanoma.* Pigment Cell Melanoma Res, 2015. **28**(1): p. 94-104.
50. Storr, S. J., et al., *Objective assessment of blood and lymphatic vessel invasion and association with macrophage infiltration in cutaneous melanoma.* Mod Pathol, 2012. **25**(4): p. 493-504.
51. Slater, D. and M. Walsh, *Standards and data sets for reporting cancers. Data set for the histological reporting of primary cutaneous malignant melanoma and regional lymph nodes.* Royal College of Pathologists, 2014.
52. Spatz, A., et al., *Interobserver reproducibility of ulceration assessment in primary cutaneous melanomas.* Eur J Cancer, 2003. **39**(13): p. 1861-5.
53. In 't Hout, F. E., et al., *Prognostic importance of the extent of ulceration in patients with clinically localized cutaneous melanoma.* Ann Surg, 2012. **255**(6): p. 1165-70.
54. Grande Sarpa, H., et al., *Prognostic significance of extent of ulceration in primary cutaneous melanoma.* Am J Surg Pathol, 2006. **30**(11): p. 1396-400.

55. Day, C. L., Jr., et al., *Malignant melanoma. Prognostic significance of "microscopic satellites" in the reticular dermis and subcutaneous fat.* Ann Surg, 1981. **194**(1): p. 108-12.

56. Bonnelykke-Behrndtz, M. L., et al., *Prognostic stratification of ulcerated melanoma: not only the extent matters.* Am J Clin Pathol, 2014. **142**(6): p. 845-56.

57. Scolyer, R. A., et al., *Interobserver reproducibility of histopathologic prognostic variables in primary cutaneous melanomas.* Am J Surg Pathol, 2003. **27**(12): p. 1571-6.

58. Roach, B. A., et al., *Does mitotic rate predict sentinel lymph node metastasis or survival in patients with intermediate and thick melanoma?* Am J Surg, 2010. **200**(6): p. 759-63; discussion 763-4.

59. Baker, J. J., et al., *Prognostic significance of tumor mitotic rate in T2 melanoma staged with sentinel lymphadenectomy.* J Surg Oncol, 2015. **111**(6): p. 711-5.

60. Clark, W. H., Jr., et al., *Model predicting survival in stage I melanoma based on tumor progression.* J Natl Cancer Inst, 1989. **81**(24): p. 1893-904.

61. Clemente, C. G., et al., *Prognostic value of tumor infiltrating lymphocytes in the vertical growth phase of primary cutaneous melanoma.* Cancer, 1996. **77**(7): p. 1303-10.

62. van Houdt, I. S., et al., *Favorable outcome in clinically stage II melanoma patients is associated with the presence of activated tumor infiltrating T-lymphocytes and preserved MHC class I antigen expression.* Int J Cancer, 2008. **123**(3): p. 609-15.

63. Tuthill, R. J., et al., *Risk assessment in localized primary cutaneous melanoma: a Southwest Oncology Group study evaluating nine factors and a test of the Clark logistic regression prediction model.* Am J Clin Pathol, 2002. **118**(4): p. 504-11.

64. Taylor, R. C., et al., *Tumor-infiltrating lymphocytes predict sentinel lymph node positivity in patients with cutaneous melanoma.* J Clin Oncol, 2007. **25**(7): p. 869-75.

65. Thorn, M., et al., *Clinical and histopathologic predictors of survival in patients with malignant melanoma: a population-based study in Sweden.* J Natl Cancer Inst, 1994. **86**(10): p. 761-9.

66. Larsen, T. E. and T. H. Grude, *A retrospective histological study of 669 cases of primary cutaneous malignant melanoma in clinical stage I. 3. The relation between the tumour-associated lymphocyte infiltration and age and sex, tumour cell type, pigmentation, cellular atypia, mitotic count, depth of invasion,*

ulceration, tumour type and prognosis. Acta Pathol Microbiol Scand A, 1978. **86A**(6): p. 523-30.

67. Barnhill, R. L., et al., *Predicting five-year outcome for patients with cutaneous melanoma in a population-based study.* Cancer, 1996. **78**(3): p. 427-32.
68. Wong, S. L., et al., *Results of sentinel lymph node biopsy in patients with thin melanoma.* Ann Surg Oncol, 2006. **13**(3): p. 302-9.
69. Weiss, S. A., et al., *Immunologic heterogeneity of tumor-infiltrating lymphocyte composition in primary melanoma.* Hum Pathol, 2016. **57**: p. 116-125.
70. Rao, U. N., et al., *Presence of tumor-infiltrating lymphocytes and a dominant nodule within primary melanoma are prognostic factors for relapse-free survival of patients with thick (t4) primary melanoma: pathologic analysis of the e1690 and e1694 intergroup trials.* Am J Clin Pathol, 2010. **133**(4): p. 646-53.
71. Rubinstein, J. C., et al., *Regression in thin melanoma is associated with nodal recurrence after a negative sentinel node biopsy.* Cancer Med, 2016. **5**(10): p. 2832-2840.
72. Ribero, S., et al., *Association of Histologic Regression in Primary Melanoma With Sentinel Lymph Node Status: A Systematic Review and Meta-analysis.* JAMA Dermatol, 2015. **151**(12): p. 1301-1307.
73. Bastian, B. C., *Hypothesis: a role for telomere crisis in spontaneous regression of melanoma.* Arch Dermatol, 2003. **139**(5): p. 667-8.
74. Ribero, S., et al., *Favourable prognostic role of regression of primary melanoma in AJCC stage I-II patients.* Br J Dermatol, 2013. **169**(6): p. 1240-5.
75. Zurac, S., et al., *Spectrum of morphologic alterations of regression in cutaneous melanoma--potential for improving disease prognosis.* Rom J Intern Med, 2012. **50**(2): p. 145-53.
76. Ribero, S., et al., *Regression in cutaneous melanoma: a comprehensive review from diagnosis to prognosis.* J Eur Acad Dermatol Venereol, 2016.
77. Kaur, C., et al., *The correlation of regression in primary melanoma with sentinel lymph node status.* J Clin Pathol, 2008. **61**(3): p. 297-300.
78. Maurichi, A., et al., *Prediction of survival in patients with thin melanoma: results from a multi-institution study.* J Clin Oncol, 2014. **32**(23): p. 2479-85.
79. Morris, K. T., et al., *Primary cutaneous melanoma with regression does not require a lower threshold for sentinel lymph node biopsy.* Ann Surg Oncol, 2008. **15**(1): p. 316-22.
80. Burton, A. L., et al., *Regression does not predict nodal metastasis or survival in patients with cutaneous melanoma.* Am Surg, 2011. **77**(8): p. 1009-13.
81. Botella-Estrada, R., et al., *Correlation of histologic regression in primary melanoma with sentinel node status.* JAMA Dermatol, 2014. **150**(8): p. 828-35.

82. Ronan, S. G., et al., *Thin malignant melanomas with regression and metastases.* Arch Dermatol, 1987. **123**(10): p. 1326-30.
83. Slingluff, C. L., Jr., et al., *Lethal "thin" malignant melanoma. Identifying patients at risk.* Ann Surg, 1988. **208**(2): p. 150-61.
84. Sondergaard, K. and K. Hou-Jensen, *Partial regression in thin primary cutaneous malignant melanomas clinical stage I. A study of 486 cases.* Virchows Arch A Pathol Anat Histopathol, 1985. **408**(2-3): p. 241-7.
85. Blessing, K., et al., *Thin malignant melanomas (less than 1.5 mm) with metastasis: a histological study and survival analysis.* Histopathology, 1990. **17**(5): p. 389-95.
86. Guitart, J., et al., *Histological characteristics of metastasizing thin melanomas: a case-control study of 43 cases.* Arch Dermatol, 2002. **138**(5): p. 603-8.
87. Egger, M. E., et al., *Lymphovascular invasion as a prognostic factor in melanoma.* Am Surg, 2011. **77**(8): p. 992-7.
88. Schmidt, C. R., et al., *An increased number of sentinel lymph nodes is associated with advanced Breslow depth and lymphovascular invasion in patients with primary melanoma.* Ann Surg Oncol, 2009. **16**(4): p. 948-52.
89. Tas, F. and K. Erturk, *Histological lymphovascular invasion is associated with nodal involvement, recurrence, and survival in patients with cutaneous malignant melanoma.* Int J Dermatol, 2016.
90. Rose, A. E., et al., *Clinical relevance of detection of lymphovascular invasion in primary melanoma using endothelial markers D2-40 and CD34.* Am J Surg Pathol, 2011. **35**(10): p. 1441-9.
91. Petersson, F., et al., *Immunohistochemical detection of lymphovascular invasion with D2-40 in melanoma correlates with sentinel lymph node status, metastasis and survival.* J Cutan Pathol, 2009. **36**(11): p. 1157-63.
92. Hennessy, J. and M. Ethunandan, *Perineural invasion in malignant melanoma.* Br J Oral Maxillofac Surg, 2012. **50**(4): p. 378.
93. Croker, J., B. Burmeister, and M. Foote, *Neurotropic melanoma: the management of localised disease.* J Skin Cancer, 2012. **2012**: p. 706452.
94. Newlin, H. E., et al., *Neurotropic melanoma of the head and neck with clinical perineural invasion.* Am J Clin Oncol, 2005. **28**(4): p. 399-402.
95. Chen, J. Y., et al., *Desmoplastic neurotropic melanoma: a clinicopathologic analysis of 128 cases.* Cancer, 2008. **113**(10): p. 2770-8.
96. National Cancer Intelligence Network. *COSD Pathology*. 2015. [cited 17th December 2016]; Available from: http://www.ncin.org.uk/collecting_and_using_data/data_collection/cosd_downloads_v6?upid=389.

97. McKee, P. H., *Pathology of the skin with Clinical Correlation.* 1996, London: Mosby-Wolfe.

98. Crowson, A. N., C. M. Magro, and M. C. Mihm, *Prognosticators of melanoma, the melanoma report, and the sentinel lymph node.* Mod Pathol, 2006. **19 Suppl 2**: p. S71-87.

99. Lens, M. B., J. A. Newton-Bishop, and A. P. Boon, *Desmoplastic malignant melanoma: a systematic review.* Br J Dermatol, 2005. **152**(4): p. 673-8.

100. Feng, Z., et al., *Incidence and survival of desmoplastic melanoma in the United States, 1992-2007.* J Cutan Pathol, 2011. **38**(8): p. 616-24.

101. Ascierto, P. A., et al., *Epithelioid cell-type melanoma as a prognostic factor of poor response to immunological treatment.* Ann Oncol, 2000. **11**(11): p. 1504.

102. Chi, H. I., et al., *Epithelioid cell melanomas have greater DNA ploidy abnormalities than spindle cell melanomas: cytological evidence for a higher malignant potential of the former.* Arch Dermatol Res, 1993. **285**(7): p. 410-4.

103. Larsen, T. E. and T. H. Grude, *A retrospective histological study of 669 cases of primary cutaneous malignant melanoma in clinical stage I. 2. The relation of cell type, pigmentation, atypia and mitotic count to histological type and prognosis.* Acta Pathol Microbiol Scand A, 1978. **86A**(6): p. 513-22.

104. Sanz-Moreno, V. and C. J. Marshall, *The plasticity of cytoskeletal dynamics underlying neoplastic cell migration.* Curr Opin Cell Biol, 2010. **22**(5): p. 690-6.

105. Orgaz, J. L., et al., *Diverse matrix metalloproteinase functions regulate cancer amoeboid migration.* Nat Commun, 2014. **5**: p. 4255.

106. Sanz-Moreno, V., et al., *Rac activation and inactivation control plasticity of tumor cell movement.* Cell, 2008. **135**(3): p. 510-23.

107. Sanz-Moreno, V., et al., *ROCK and JAK1 signaling cooperate to control actomyosin contractility in tumor cells and stroma.* Cancer Cell, 2011. **20**(2): p. 229-45.

108. Viros, A., et al., *Improving melanoma classification by integrating genetic and morphologic features.* PLoS Med, 2008. **5**(6): p. e120.

109. Yin, Z., et al., *A screen for morphological complexity identifies regulators of switch-like transitions between discrete cell shapes.* Nat Cell Biol, 2013. **15**(7): p. 860-71.

110. Barnhill, R. L., *The Spitzoid lesion: rethinking Spitz tumors, atypical variants, 'Spitzoid melanoma' and risk assessment.* Mod Pathol, 2006. **19 Suppl 2**: p. S21-33.

111. Brozyna, A. A., et al., *Melanogenesis affects overall and disease-free survival in patients with stage III and IV melanoma.* Hum Pathol, 2013. **44**(10): p. 2071-4.

112. Rigel, D. S., et al., *ABCDE--an evolving concept in the early detection of melanoma.* Arch Dermatol, 2005. **141**(8): p. 1032-4.
113. Pizzichetta, M. A., et al., *Dermoscopic diagnosis of amelanotic/hypomelanotic melanoma.* Br J Dermatol, 2016.
114. Sarna, M., et al., *Cell elasticity is an important indicator of the metastatic phenotype of melanoma cells.* Exp Dermatol, 2014. **23**(11): p. 813-8.
115. Brozyna, A. A., et al., *Melanin content in melanoma metastases affects the outcome of radiotherapy.* Oncotarget, 2016. **7**(14): p. 17844-53.
116. Pinner, S., et al., *Intravital imaging reveals transient changes in pigment production and Brn2 expression during metastatic melanoma dissemination.* Cancer Res, 2009. **69**(20): p. 7969-77.
117. Banerjee, S. S. and M. Harris, *Morphological and immunophenotypic variations in malignant melanoma.* Histopathology, 2000. **36**(5): p. 387-402.
118. Somasundaram, R., J. Villanueva, and M. Herlyn, *Intratumoral heterogeneity as a therapy resistance mechanism: role of melanoma subpopulations.* Adv Pharmacol, 2012. **65**: p. 335-59.
119. Harbst, K., et al., *Multiregion Whole-Exome Sequencing Uncovers the Genetic Evolution and Mutational Heterogeneity of Early-Stage Metastatic Melanoma.* Cancer Res, 2016. **76**(16): p. 4765-74.
120. Harbst, K., et al., *Molecular and genetic diversity in the metastatic process of melanoma.* J Pathol, 2014. **233**(1): p. 39-50.
121. Sanborn, J. Z., et al., *Phylogenetic analyses of melanoma reveal complex patterns of metastatic dissemination.* Proc Natl Acad Sci U S A, 2015. **112**(35): p. 10995-1000.
122. Bastian, B. C., *The molecular pathology of melanoma: an integrated taxonomy of melanocytic neoplasia.* Annu Rev Pathol, 2014. **9**: p. 239-71.
123. Bramhall, R. J., K. Mahady, and A. H. Peach, *Spontaneous regression of metastatic melanoma - clinical evidence of the abscopal effect.* Eur J Surg Oncol, 2014. **40**(1): p. 34-41.
124. Harris, J., S. Bines, and T. Das Gupta, *Therapy of disseminated malignant melanoma with recombinant alpha 2b-interferon and piroxicam: clinical results with a report of an unusual response-associated feature (vitiligo) and unusual toxicity (diffuse pulmonary interstitial fibrosis).* Med Pediatr Oncol, 1994. **22**(2): p. 103-6.
125. MacKie, R. M., R. Reid, and B. Junor, *Fatal melanoma transferred in a donated kidney 16 years after melanoma surgery.* N Engl J Med, 2003. **348**(6): p. 567-8.
126. Hodi, F. S., et al., *Improved survival with ipilimumab in patients with metastatic melanoma.* N Engl J Med, 2010. **363**(8): p. 711-23.

127. Min, L. and F. S. Hodi, *Anti-PD1 following ipilimumab for mucosal melanoma: durable tumor response associated with severe hypothyroidism and rhabdomyolysis.* Cancer Immunol Res, 2014. **2**(1): p. 15-8.
128. Brahmer, J. R., et al., *Safety and activity of anti-PD-L1 antibody in patients with advanced cancer.* N Engl J Med, 2012. **366**(26): p. 2455-65.
129. Ji, R. R., et al., *An immune-active tumor microenvironment favors clinical response to ipilimumab.* Cancer Immunol Immunother, 2012. **61**(7): p. 1019-31.
130. Criscitiello, C., A. Esposito, and G. Curigliano, *Tumor-stroma crosstalk: targeting stroma in breast cancer.* Curr Opin Oncol, 2014. **26**(6): p. 551-5.
131. Moorman, A. M., et al., *The prognostic value of tumour-stroma ratio in triple-negative breast cancer.* Eur J Surg Oncol, 2012. **38**(4): p. 307-13.
132. Ruiter, D., et al., *Melanoma-stroma interactions: structural and functional aspects.* Lancet Oncol, 2002. **3**(1): p. 35-43.
133. Wiesner, T., et al., *NF1 Mutations Are Common in Desmoplastic Melanoma.* Am J Surg Pathol, 2015. **39**(10): p. 1357-62.
134. Zhang, T., et al., *Tumor-stroma ratio is an independent predictor for survival in NSCLC.* Int J Clin Exp Pathol, 2015. **8**(9): p. 11348-55.
135. Lv, Z., et al., *Tumor-stroma ratio is a prognostic factor for survival in hepatocellular carcinoma patients after liver resection or transplantation.* Surgery, 2015. **158**(1): p. 142-50.
136. Downey, C. L., et al., *The prognostic significance of tumour-stroma ratio in oestrogen receptor-positive breast cancer.* Br J Cancer, 2014. **110**(7): p. 1744-7.
137. Huijbers, A., et al., *The proportion of tumor-stroma as a strong prognosticator for stage II and III colon cancer patients: validation in the VICTOR trial.* Ann Oncol, 2013. **24**(1): p. 179-85.
138. Labiche, A., et al., *Stromal compartment as a survival prognostic factor in advanced ovarian carcinoma.* Int J Gynecol Cancer, 2010. **20**(1): p. 28-33.
139. Park, J. H., et al., *The relationship between tumour stroma percentage, the tumour microenvironment and survival in patients with primary operable colorectal cancer.* Ann Oncol, 2014. **25**(3): p. 644-51.
140. Wang, K., et al., *Tumor-stroma ratio is an independent predictor for survival in esophageal squamous cell carcinoma.* J Thorac Oncol, 2012. **7**(9): p. 1457-61.
141. West, N. P., et al., *The proportion of tumour cells is an independent predictor for survival in colorectal cancer patients.* Br J Cancer, 2010. **102**(10): p. 1519-23.

142. Wu, Y., et al., *Comprehensive genomic meta-analysis identifies intra-tumoural stroma as a predictor of survival in patients with gastric cancer.* Gut, 2013. **62**(8): p. 1100-11.
143. Smolle, J., et al., *Quantitative morphology of collagen fibers in cutaneous malignant melanoma and melanocytic nevus.* American Journal of Dermatopathology, 1996. **18**(4): p. 358-63.
144. Smolle, J., et al., *Incorporation of pre-existing collagen bundles in primary cutaneous melanoma.* Melanoma Research, 1998. **8**(2): p. 161-5.
145. Webster, J. D., et al., *Quantifying histological features of cancer biospecimens for biobanking quality assurance using automated morphometric pattern recognition image analysis algorithms.* J Biomol Tech, 2011. **22**(3): p. 108-18.
146. Yajima, I., et al., *RAS/RAF/MEK/ERK and PI3K/PTEN/AKT Signaling in Malignant Melanoma Progression and Therapy.* Dermatol Res Pract, 2012. **2012**: p. 354191.
147. Sensi, M., et al., *Mutually exclusive NRASQ61R and BRAFV600E mutations at the single-cell level in the same human melanoma.* Oncogene, 2006. **25**(24): p. 3357-64.
148. Mitra, A., et al., *Melanoma sentinel node biopsy and prediction models for relapse and overall survival.* Br J Cancer, 2010. **103**(8): p. 1229-36.
149. Jonsson, G., et al., *Gene expression profiling-based identification of molecular subtypes in stage IV melanomas with different clinical outcome.* Clin Cancer Res, 2010. **16**(13): p. 3356-67.
150. Harbst, K., et al., *Molecular profiling reveals low- and high-grade forms of primary melanoma.* Clin Cancer Res, 2012. **18**(15): p. 4026-36.
151. Nsengimana, J., et al., *Independent replication of a melanoma subtype gene signature and evaluation of its prognostic value and biological correlates in a population cohort.* Oncotarget, 2015. **6**(13): p. 11683-93.
152. Gerami, P., et al., *Development of a prognostic genetic signature to predict the metastatic risk associated with cutaneous melanoma.* Clin Cancer Res, 2015. **21**(1): p. 175-83.
153. Cancer Genome Atlas Network. Electronic address, i. m. o. and N. Cancer Genome Atlas, *Genomic Classification of Cutaneous Melanoma.* Cell, 2015. **161**(7): p. 1681-96.
154. Lawrence, M. S., et al., *Discovery and saturation analysis of cancer genes across 21 tumour types.* Nature, 2014. **505**(7484): p. 495-501.
155. Broekaert, S. M., et al., *Genetic and morphologic features for melanoma classification.* Pigment Cell Melanoma Res, 2010. **23**(6): p. 763-70.

156. Poynter, J. N., et al., *BRAF and NRAS mutations in melanoma and melanocytic nevi.* Melanoma Res, 2006. **16**(4): p. 267-73.

157. Yeh, I., et al., *Clinical, Histopathologic, and Genomic Features of Spitz Tumors With ALK Fusions.* Am J Surg Pathol, 2015. **39**(5): p. 581-91.

158. Busam, K. J., et al., *Clinical and pathologic findings of Spitz nevi and atypical Spitz tumors with ALK fusions.* Am J Surg Pathol, 2014. **38**(7): p. 925-33.

159. Wiesner, T., et al., *Germline mutations in BAP1 predispose to melanocytic tumors.* Nat Genet, 2011. **43**(10): p. 1018-21.

160. Marusic, Z., M. Buljan, and K. J. Busam, *Histomorphologic Spectrum Of Bap1 Negative Melanocytic Neoplasms In A Family With Bap1-Associated Cancer Susceptibility Syndrome.* J Cutan Pathol, 2015.

161. O'Shea, S. J., et al., *Histopathology of melanocytic lesions in a family with an inherited BAP1 mutation.* J Cutan Pathol, 2016. **43**(3): p. 287-9.

162. Carbone, M., et al., *BAP1 cancer syndrome: malignant mesothelioma, uveal and cutaneous melanoma, and MBAITs.* J Transl Med, 2012. **10**: p. 179.

163. Njauw, C. N., et al., *Germline BAP1 inactivation is preferentially associated with metastatic ocular melanoma and cutaneous-ocular melanoma families.* PLoS One, 2012. **7**(4): p. e35295.

164. Popova, T., et al., *Germline BAP1 mutations predispose to renal cell carcinomas.* Am J Hum Genet, 2013. **92**(6): p. 974-80.

165. Abdel-Rahman, M. H., et al., *Germline BAP1 mutation predisposes to uveal melanoma, lung adenocarcinoma, meningioma, and other cancers.* J Med Genet, 2011. **48**(12): p. 856-9.

166. O'Shea, S. J., et al., *A population-based analysis of germline BAP1 mutations in melanoma.* Human Molecular Genetics, 2017. **26**(4): p. 717–728.

167. Eggermont, A. M., et al., *Long term follow up of the EORTC 18952 trial of adjuvant therapy in resected stage IIB-III cutaneous melanoma patients comparing intermediate doses of interferon-alpha-2b (IFN) with observation: Ulceration of primary is key determinant for IFN-sensitivity.* Eur J Cancer, 2016. **55**: p. 111-21.

168. Rakosy, Z., et al., *Integrative genomics identifies gene signature associated with melanoma ulceration.* PLoS One, 2013. **8**(1): p. e54958.

169. Yoshihara, K., et al., *Inferring tumour purity and stromal and immune cell admixture from expression data.* Nat Commun, 2013. **4**: p. 2612.

170. Ladanyi, A., *Prognostic and predictive significance of immune cells infiltrating cutaneous melanoma.* Pigment Cell Melanoma Res, 2015. **28**(5): p. 490-500.

171. Angelo, M., et al., *Multiplexed ion beam imaging of human breast tumors.* Nat Med, 2014. **20**(4): p. 436-42.

172. Feng, Z., et al., *Multispectral imaging of formalin-fixed tissue predicts ability to generate tumor-infiltrating lymphocytes from melanoma.* J Immunother Cancer, 2015. **3**: p. 47.

173. Rehg, J. E., D. Bush, and J. M. Ward, *The utility of immunohistochemistry for the identification of hematopoietic and lymphoid cells in normal tissues and interpretation of proliferative and inflammatory lesions of mice and rats.* Toxicol Pathol, 2012. **40**(2): p. 345-74.

174. Bindea, G., et al., *Spatiotemporal dynamics of intratumoral immune cells reveal the immune landscape in human cancer.* Immunity, 2013. **39**(4): p. 782-95.

175. Conway, C., et al., *Gene expression profiling of paraffin-embedded primary melanoma using the DASL assay identifies increased osteopontin expression as predictive of reduced relapse-free survival.* Clin Cancer Res, 2009. **15**(22): p. 6939-46.

176. Jewell, R., et al., *Patterns of expression of DNA repair genes and relapse from melanoma.* Clin Cancer Res, 2010. **16**(21): p. 5211-21.

177. April, C. S. and J. B. Fan, *Gene expression profiling in formalin-fixed, paraffin-embedded tissues using the whole-genome DASL assay.* Methods Mol Biol, 2011. **784**: p. 77-98.

178. April, C., et al., *Whole-genome gene expression profiling of formalin-fixed, paraffin-embedded tissue samples.* PLoS One, 2009. **4**(12): p. e8162.

179. Du, P., W. A. Kibbe, and S. M. Lin, *lumi: a pipeline for processing Illumina microarray.* Bioinformatics, 2008. **24**(13): p. 1547-8.

180. Lauss, M., et al., *Monitoring of technical variation in quantitative high-throughput data sets.* Cancer Inform, 2013. **12**: p. 193-201.

181. College of American Pathologists. *Protocol for the Examination of Specimens From Patients With Melanoma of the Skin*. [PDF] 2015. [cited 17th December 2016]; Available from: http://www.cap.org/apps/docs/committees/cancer/cancer_protocols/2013/SkinMelanoma_13protocol_3300.pdf.

182. Crowson, A. N., Magro, C. M and Mihm Jr, M. C., *The Melanocytic Proliferations. A Comprehensive Textbook of Pigmented Lesions*. First ed.: Wiley Blackwell.

183. Karagas, M. R., et al., *Measures of cumulative exposure from a standardized sun exposure history questionnaire: a comparison with histologic assessment of solar skin damage.* Am J Epidemiol, 2007. **165**(6): p. 719-26.

184. Luo, S., A. Sepehr, and H. Tsao, *Spitz nevi and other Spitzoid lesions part I. Background and diagnoses.* J Am Acad Dermatol, 2011. **65**(6): p. 1073-84.

185. Wright, A. I., H. I. Grabsch, and D. E. Treanor, *RandomSpot: A web-based tool for systematic random sampling of virtual slides.* J Pathol Inform, 2015. **6**: p. 8.

186. StataCorp, *Stata Statistical Software: Release 12*, 2011: College Station, TX: StataCorp LP.

187. Scolyer, R. A., G. V. Long, and J. F. Thompson, *Evolving concepts in melanoma classification and their relevance to multidisciplinary melanoma patient care.* Mol Oncol, 2011. **5**(2): p. 124-36.

188. StataCorp, *Stata Statistical Software: Release 14*, 2015: College Station, TX: StataCorp LP

189. de Hoon, M. J., et al., *Open source clustering software.* Bioinformatics, 2004. **20**(9): p. 1453-4.

190. Heenan, P. J., et al., *Inter-observer variation between pathologists in the classification of cutaneous malignant melanoma in western Australia.* Histopathology, 1984. **8**(5): p. 717-29.

191. Murali, R., et al., *Interobserver variation in the histopathologic reporting of key prognostic parameters, particularly clark level, affects pathologic staging of primary cutaneous melanoma.* Ann Surg, 2009. **249**(4): p. 641-7.

192. Colloby, P. S., K. P. West, and A. Fletcher, *Observer variation in the measurement of Breslow depth and Clark's level in thin cutaneous malignant melanoma.* J Pathol, 1991. **163**(3): p. 245-50.

193. Prade, M., et al., *Difficulties encountered in the application of Clark classification and the Breslow thickness measurement in cutaneous malignant melanoma.* Int J Cancer, 1980. **26**(2): p. 159-63.

194. Patrawala, S., et al., *Discordance of histopathologic parameters in cutaneous melanoma: Clinical implications.* J Am Acad Dermatol, 2016. **74**(1): p. 75-80.

195. Eriksson, H., et al., *Interobserver variability of histopathological prognostic parameters in cutaneous malignant melanoma: impact on patient management.* Acta Derm Venereol, 2013. **93**(4): p. 411-6.

196. Corona, R., et al., *Interobserver variability on the histopathologic diagnosis of cutaneous melanoma and other pigmented skin lesions.* J Clin Oncol, 1996. **14**(4): p. 1218-23.

197. Lock-Andersen, J., et al., *Observer variation in histological classification of cutaneous malignant melanoma.* Scand J Plast Reconstr Surg Hand Surg, 1995. **29**(2): p. 141-8.

198. Krieger, N., et al., *Inter-observer variability among pathologists' evaluation of malignant melanoma: effects upon an analytic study.* J Clin Epidemiol, 1994. **47**(8): p. 897-902.

199. Monshizadeh, L., et al., *A critical review of melanoma pathology reports for patients referred to the Western Australian Melanoma Advisory Service.* Pathology, 2012. **44**(5): p. 441-7.

200. Urso, C., et al., *Interobserver reproducibility of histological features in cutaneous malignant melanoma.* J Clin Pathol, 2005. **58**(11): p. 1194-8.

201. Busam, K. J., et al., *Histologic classification of tumor-infiltrating lymphocytes in primary cutaneous malignant melanoma. A study of interobserver agreement.* Am J Clin Pathol, 2001. **115**(6): p. 856-60.

202. Schimming, T. T., et al., *pHH3 immunostaining improves interobserver agreement of mitotic index in thin melanomas.* Am J Dermatopathol, 2012. **34**(3): p. 266-9.

203. Niebling, M. G., et al., *Reproducibility of AJCC staging parameters in primary cutaneous melanoma: an analysis of 4,924 cases.* Ann Surg Oncol, 2013. **20**(12): p. 3969-75.

204. Garbe, C., et al., *Mitotic rate in primary melanoma: interobserver and intraobserver reliability, analyzed using H&E sections and immunohistochemistry.* J Dtsch Dermatol Ges, 2016. **14**(9): p. 910-5.

205. Santillan, A. A., et al., *Pathology review of thin melanoma and melanoma in situ in a multidisciplinary melanoma clinic: impact on treatment decisions.* J Clin Oncol, 2010. **28**(3): p. 481-6.

206. Piepkorn, M. W., et al., *The MPATH-Dx reporting schema for melanocytic proliferations and melanoma.* J Am Acad Dermatol, 2014. **70**(1): p. 131-41.

207. Carney, P. A., et al., *Achieving consensus for the histopathologic diagnosis of melanocytic lesions: use of the modified Delphi method.* J Cutan Pathol, 2016. **43**(10): p. 830-7.

208. Lott, J. P., et al., *Evaluation of the Melanocytic Pathology Assessment Tool and Hierarchy for Diagnosis (MPATH-Dx) classification scheme for diagnosis of cutaneous melanocytic neoplasms: Results from the International Melanoma Pathology Study Group.* J Am Acad Dermatol, 2016. **75**(2): p. 356-63.

209. Viera, A. J. and J. M. Garrett, *Understanding interobserver agreement: the kappa statistic.* Fam Med, 2005. **37**(5): p. 360-3.

210. Patrick, R. J., S. Corey, and L. F. Glass, *The use of sequential serial sectioning of thin melanomas in determining maximum Breslow depth.* J Am Acad Dermatol, 2007. **57**(5 Suppl): p. S127-8.

211. Robsahm, T. E., et al., *Sex differences in rising trends of cutaneous malignant melanoma in Norway, 1954-2008.* Melanoma Res, 2013. **23**(1): p. 70-8.

212. Schatton, T., et al., *Tumor-infiltrating lymphocytes and their significance in melanoma prognosis.* Methods Mol Biol, 2014. **1102**: p. 287-324.

213. McClain, S. E., et al., *Outcome of sentinel lymph node biopsy and prognostic implications of regression in thin malignant melanoma.* Melanoma Res, 2012. **22**(4): p. 302-9.
214. Socrier, Y., et al., *Histological regression in primary melanoma: not a predictor of sentinel lymph node metastasis in a cohort of 397 patients.* Br J Dermatol, 2010. **162**(4): p. 830-4.
215. Tas, F. and K. Erturk, *Presence of histological regression as a prognostic factor in cutaneous melanoma patients.* Melanoma Res, 2016. **26**(5): p. 492-6.
216. Lebbe, C., et al., *Survival follow-up and ipilimumab retreatment of patients with advanced melanoma who received ipilimumab in prior phase II studies.* Ann Oncol, 2014. **25**(11): p. 2277-84.
217. Iles, M. M., et al., *The effect on melanoma risk of genes previously associated with telomere length.* J Natl Cancer Inst, 2014. **106**(10).
218. National Cancer Intelligence Network. *Mortality, Incidence and gender - Malignant Melanoma*. 2012. [cited; Available from: http://www.ncin.org.uk/publications/data_briefings/mortality_incidence_and_gender_malignant_melanoma.
219. Arce, P. M., et al., *Is sex an independent prognostic factor in cutaneous head and neck melanoma?* Laryngoscope, 2014. **124**(6): p. 1363-7.
220. Shen, S., et al., *Characteristics and associations of high-mitotic-rate melanoma.* JAMA Dermatol, 2014. **150**(10): p. 1048-55.
221. Mar, V., et al., *Nodular melanoma: a distinct clinical entity and the largest contributor to melanoma deaths in Victoria, Australia.* J Am Acad Dermatol, 2013. **68**(4): p. 568-75.
222. Shannan, B., et al., *Heterogeneity in Melanoma.* Cancer Treat Res, 2016. **167**: p. 1-15.
223. Ladstein, R. G., et al., *Tumor necrosis is a prognostic factor in thick cutaneous melanoma.* Am J Surg Pathol, 2012. **36**(10): p. 1477-82.
224. Grivennikov, S. I., F. R. Greten, and M. Karin, *Immunity, inflammation, and cancer.* Cell, 2010. **140**(6): p. 883-99.
225. Waugh, K. A., S. M. Leach, and J. E. Slansky, *Tolerance of Tumor-Specific T cells in Melanoma Metastases.* J Clin Cell Immunol, 2016. **7**(2).
226. Mueller, M. M. and N. E. Fusenig, *Friends or foes - bipolar effects of the tumour stroma in cancer.* Nat Rev Cancer, 2004. **4**(11): p. 839-49.
227. Han, J. S., et al., *Primary cutaneous balloon cell melanoma: a very rare variant.* Int J Dermatol, 2014. **53**(11): p. e535-6.
228. Kao, G. F., E. B. Helwig, and J. H. Graham, *Balloon cell malignant melanoma of the skin. A clinicopathologic study of 34 cases with histochemical,*

immunohistochemical, and ultrastructural observations. Cancer, 1992. **69**(12): p. 2942-52.

229. Martinez-Casimiro, L., J. L. Sanchez Carazo, and V. Alegre, *Balloon cell naevus.* J Eur Acad Dermatol Venereol, 2009. **23**(2): p. 236-7.
230. Magro, C. M., A. N. Crowson, and M. C. Mihm, *Unusual variants of malignant melanoma.* Mod Pathol, 2006. **19 Suppl 2**: p. S41-70.
231. Moreau, J. F., J. L. Weissfeld, and L. K. Ferris, *Characteristics and survival of patients with invasive amelanotic melanoma in the USA.* Melanoma Res, 2013. **23**(5): p. 408-13.
232. Nielsen, P. S., et al., *Automated quantification of proliferation with automated hot-spot selection in phosphohistone H3/MART1 dual-stained stage I/II melanoma.* Diagn Pathol, 2016. **11**: p. 35.
233. Villanueva, J. and M. Herlyn, *Melanoma and the tumor microenvironment.* Curr Oncol Rep, 2008. **10**(5): p. 439-46.
234. Zhou, L., et al., *Perspective of Targeting Cancer-Associated Fibroblasts in Melanoma.* J Cancer, 2015. **6**(8): p. 717-26.
235. Tan, K. W., et al., *Tumor stroma and chemokines control T-cell migration into melanoma following Temozolomide treatment.* Oncoimmunology, 2015. **4**(2): p. e978709.
236. Hutchenreuther, J., et al., *CCN2 Expression by Tumor Stroma Is Required for Melanoma Metastasis.* J Invest Dermatol, 2015.
237. Frame, M. C. and A. Serrels, *FAK to the rescue: activated stroma promotes a "safe haven" for BRAF-mutant melanoma cells by inducing FAK signaling.* Cancer Cell, 2015. **27**(4): p. 429-31.
238. Tiago, M., et al., *Fibroblasts protect melanoma cells from the cytotoxic effects of doxorubicin.* Tissue Eng Part A, 2014. **20**(17-18): p. 2412-21.
239. Pierard, G. E., C. Pierard-Franchimont, and P. Delvenne, *Malignant melanoma and its stromal nonimmune microecosystem.* J Oncol, 2012. **2012**: p. 584219.
240. Flach, E. H., et al., *Fibroblasts contribute to melanoma tumor growth and drug resistance.* Mol Pharm, 2011. **8**(6): p. 2039-49.
241. Zhang, T., et al., *CXC chemokine ligand 12 (stromal cell-derived factor 1 alpha) and CXCR4-dependent migration of CTLs toward melanoma cells in organotypic culture.* J Immunol, 2005. **174**(9): p. 5856-63.
242. Pankova, D., et al., *Cancer-associated Fibroblasts Induce a Collagen Cross-link Switch in Tumor Stroma.* Mol Cancer Res, 2015.
243. Kalluri, R. and M. Zeisberg, *Fibroblasts in cancer.* Nat Rev Cancer, 2006. **6**(5): p. 392-401.

244. Akerfelt, M., et al., *Automated tracking of tumor-stroma morphology in microtissues identifies functional targets within the tumor microenvironment for therapeutic intervention.* Oncotarget, 2015. **6**(30): p. 30035-56.

245. Hirata, E., et al., *Intravital imaging reveals how BRAF inhibition generates drug-tolerant microenvironments with high integrin beta1/FAK signaling.* Cancer Cell, 2015. **27**(4): p. 574-88.

246. Moffitt, R. A., et al., *Virtual microdissection identifies distinct tumor- and stroma-specific subtypes of pancreatic ductal adenocarcinoma.* Nat Genet, 2015. **47**(10): p. 1168-78.

247. Yamaguchi, H. and R. Sakai, *Direct Interaction between Carcinoma Cells and Cancer Associated Fibroblasts for the Regulation of Cancer Invasion.* Cancers (Basel), 2015. **7**(4): p. 2054-62.

248. Kraman, M., et al., *Suppression of antitumor immunity by stromal cells expressing fibroblast activation protein-alpha.* Science, 2010. **330**(6005): p. 827-30.

249. Kim, E., et al., *Senescent fibroblasts in melanoma initiation and progression: an integrated theoretical, experimental, and clinical approach.* Cancer Res, 2013. **73**(23): p. 6874-85.

250. Zhou, L., et al., *Dermal fibroblasts induce cell cycle arrest and block epithelial-mesenchymal transition to inhibit the early stage melanoma development.* Cancer Med, 2016. **5**(7): p. 1566-79.

251. Sandri, S., et al., *Vemurafenib resistance increases melanoma invasiveness and modulates the tumor microenvironment by MMP-2 upregulation.* Pharmacol Res, 2016. **111**: p. 523-33.

252. Hofmann, U. B., et al., *Matrix metalloproteinases in human melanoma.* J Invest Dermatol, 2000. **115**(3): p. 337-44.

253. Nikkola, J., et al., *High serum levels of matrix metalloproteinase-9 and matrix metalloproteinase-1 are associated with rapid progression in patients with metastatic melanoma.* Clin Cancer Res, 2005. **11**(14): p. 5158-66.

254. Hanahan, D. and R. A. Weinberg, *Hallmarks of cancer: the next generation.* Cell, 2011. **144**(5): p. 646-74.

255. Izar, B., et al., *Bidirectional cross talk between patient-derived melanoma and cancer-associated fibroblasts promotes invasion and proliferation.* Pigment Cell Melanoma Res, 2016. **29**(6): p. 656-668.

256. Ohtani, H., et al., *Defining lymphocyte-predominant breast cancer by the proportion of lymphocyte-rich stroma and its significance in routine histopathological diagnosis.* Pathol Int, 2015. **65**(12): p. 644-51.

257. Dany, M., et al., *Advances in immunotherapy for melanoma management.* Hum Vaccin Immunother, 2016: p. 1-11.
258. Robert, C., et al., *Ipilimumab plus dacarbazine for previously untreated metastatic melanoma.* N Engl J Med, 2011. **364**(26): p. 2517-26.
259. Wolchok, J. D., et al., *Nivolumab plus ipilimumab in advanced melanoma.* N Engl J Med, 2013. **369**(2): p. 122-33.
260. Kaur, A., et al., *sFRP2 in the aged microenvironment drives melanoma metastasis and therapy resistance.* Nature, 2016. **532**(7598): p. 250-4.
261. Mesker, W. E., et al., *Presence of a high amount of stroma and downregulation of SMAD4 predict for worse survival for stage I-II colon cancer patients.* Cell Oncol, 2009. **31**(3): p. 169-78.
262. Chen, Y., et al., *Prognostic Significance of the Tumor-Stroma Ratio in Epithelial Ovarian Cancer.* Biomed Res Int, 2015. **2015**: p. 589301.
263. Pandey, S., et al., *IL-4/CXCL12 loop is a key regulator of lymphoid stroma function in follicular lymphoma.* Blood, 2017.
264. Demarchi, L. M., et al., *Prognostic values of stromal proportion and PCNA, Ki-67, and p53 proteins in patients with resected adenocarcinoma of the lung.* Mod Pathol, 2000. **13**(5): p. 511-20.
265. Downey, C. L., et al., *Prognostic significance of tumour stroma ratio in inflammatory breast cancer.* Springerplus, 2015. **4**: p. 68.
266. Unlu, M., et al., *The prognostic value of tumor-stroma proportion in laryngeal squamous cell carcinoma.* Turk Patoloji Derg, 2013. **29**(1): p. 27-35.
267. Pongsuvareeyakul, T., et al., *Prognostic evaluation of tumor-stroma ratio in patients with early stage cervical adenocarcinoma treated by surgery.* Asian Pac J Cancer Prev, 2015. **16**(10): p. 4363-8.
268. Devaud, C., et al., *Tissues in different anatomical sites can sculpt and vary the tumor microenvironment to affect responses to therapy.* Mol Ther, 2014. **22**(1): p. 18-27.
269. Mesker, W. E., et al., *Comment on: The prognostic significance of tumour-stroma ratio in oestrogen receptor-positive breast cancer.* Br J Cancer, 2015. **112**(11): p. 1832-3.
270. Rashed, H., et al., *Breslow density is a novel prognostic feature in cutaneous malignant melanoma.* Histopathology, 2016.
271. Smolle, J., et al., *Pathology of tumor-stroma interaction in melanoma metastatic to the skin.* Human Pathology, 1995. **26**(8): p. 856-61.
272. Aran, D., M. Sirota, and A. J. Butte, *Systematic pan-cancer analysis of tumour purity.* Nat Commun, 2015. **6**: p. 8971.

273. Carter, S. L., et al., *Absolute quantification of somatic DNA alterations in human cancer.* Nat Biotechnol, 2012. **30**(5): p. 413-21.

274. Hoek, K., et al., *Expression profiling reveals novel pathways in the transformation of melanocytes to melanomas.* Cancer Res, 2004. **64**(15): p. 5270-82.

275. Simpson, R. M., et al., *Age-related changes in pericellular hyaluronan organization leads to impaired dermal fibroblast to myofibroblast differentiation.* Am J Pathol, 2009. **175**(5): p. 1915-28.

276. Salem, A. F., et al., *Cigarette smoke metabolically promotes cancer, via autophagy and premature aging in the host stromal microenvironment.* Cell Cycle, 2013. **12**(5): p. 818-25.

277. Kanda, N. and S. Watanabe, *Regulatory roles of sex hormones in cutaneous biology and immunology.* J Dermatol Sci, 2005. **38**(1): p. 1-7.

278. Stevenson, S. and J. Thornton, *Effect of estrogens on skin aging and the potential role of SERMs.* Clin Interv Aging, 2007. **2**(3): p. 283-97.

279. Gilliver, S. C., et al., *Androgens influence expression of matrix proteins and proteolytic factors during cutaneous wound healing.* Lab Invest, 2007. **87**(9): p. 871-81.

280. Pracht, M., et al., *Prognostic and predictive values of oncogenic BRAF, NRAS, c-KIT and MITF in cutaneous and mucous melanoma.* J Eur Acad Dermatol Venereol, 2015. **29**(8): p. 1530-8.

281. Jenkins, M. H., et al., *The BRAF(V600E) inhibitor, PLX4032, increases type I collagen synthesis in melanoma cells.* Matrix Biol, 2015. **48**: p. 66-77.

282. Whipple, C. A. and C. E. Brinckerhoff, *BRAF(V600E) melanoma cells secrete factors that activate stromal fibroblasts and enhance tumourigenicity.* Br J Cancer, 2014. **111**(8): p. 1625-33.

283. Duluc, D., et al., *Transcriptional fingerprints of antigen-presenting cell subsets in the human vaginal mucosa and skin reflect tissue-specific immune microenvironments.* Genome Med, 2014. **6**(11): p. 98.

284. Kahlert, C., et al., *Tumour-site-dependent expression profile of angiogenic factors in tumour-associated stroma of primary colorectal cancer and metastases.* Br J Cancer, 2014. **110**(2): p. 441-9.

285. Henriet, P., et al., *Contact with fibrillar collagen inhibits melanoma cell proliferation by up-regulating p27KIP1.* Proc Natl Acad Sci U S A, 2000. **97**(18): p. 10026-31.

286. Busam, K. J., et al., *Cutaneous desmoplastic melanoma: reappraisal of morphologic heterogeneity and prognostic factors.* Am J Surg Pathol, 2004. **28**(11): p. 1518-25.

287. Albrengues, J., G. Meneguzzi, and C. Gaggioli, *Analysis of collective invasion of carcinoma cells in a 3D organotypic model.* Methods Mol Biol, 2013. **961**: p. 243-52.

288. Ao, M., et al., *Stretching fibroblasts remodels fibronectin and alters cancer cell migration.* Sci Rep, 2015. **5**: p. 8334.

289. Topalian, S. L., et al., *Survival, durable tumor remission, and long-term safety in patients with advanced melanoma receiving nivolumab.* J Clin Oncol, 2014. **32**(10): p. 1020-30.

290. Hodi, F. S., et al., *Combined nivolumab and ipilimumab versus ipilimumab alone in patients with advanced melanoma: 2-year overall survival outcomes in a multicentre, randomised, controlled, phase 2 trial.* Lancet Oncol, 2016. **17**(11): p. 1558-1568.

291. Fushimi, T., T. P. O'Connor, and R. G. Crystal, *Adenoviral gene transfer of stromal cell-derived factor-1 to murine tumors induces the accumulation of dendritic cells and suppresses tumor growth.* Cancer Res, 2006. **66**(7): p. 3513-22.

292. Quan, C., et al., *Dermal fibroblast expression of stromal cell-derived factor-1 (SDF-1) promotes epidermal keratinocyte proliferation in normal and diseased skin.* Protein Cell, 2015. **6**(12): p. 890-903.

293. Dunussi-Joannopoulos, K., et al., *Efficacious immunomodulatory activity of the chemokine stromal cell-derived factor 1 (SDF-1): local secretion of SDF-1 at the tumor site serves as T-cell chemoattractant and mediates T-cell-dependent antitumor responses.* Blood, 2002. **100**(5): p. 1551-8.

294. McConnell, A. T., et al., *The prognostic significance and impact of the CXCR4-CXCR7-CXCL12 axis in primary cutaneous melanoma.* Br J Dermatol, 2016.

295. Monteagudo, C., et al., *CCL27-CCR10 and CXCL12-CXCR4 chemokine ligand-receptor mRNA expression ratio: new predictive factors of tumor progression in cutaneous malignant melanoma.* Clin Exp Metastasis, 2012. **29**(6): p. 625-37.

296. Napolitano, M., et al., *CD4(+)CD45RA(+)CXCR4 (+) lymphocytes are inversely associated with progression in stages I-III melanoma patients.* Cancer Immunol Immunother, 2010. **59**(4): p. 511-7.

297. Vianello, F., et al., *Murine B16 melanomas expressing high levels of the chemokine stromal-derived factor-1/CXCL12 induce tumor-specific T cell chemorepulsion and escape from immune control.* J Immunol, 2006. **176**(5): p. 2902-14.

298. Comito, G., et al., *Stromal fibroblasts synergize with hypoxic oxidative stress to enhance melanoma aggressiveness.* Cancer Lett, 2012. **324**(1): p. 31-41.

299. D'Alterio, C., et al., *Inhibition of stromal CXCR4 impairs development of lung metastases.* Cancer Immunol Immunother, 2012. **61**(10): p. 1713-20.

300. Bartolome, R. A., et al., *Stromal cell-derived factor-1alpha promotes melanoma cell invasion across basement membranes involving stimulation of membrane-type 1 matrix metalloproteinase and Rho GTPase activities.* Cancer Res, 2004. **64**(7): p. 2534-43.

301. Longo-Imedio, M. I., et al., *Clinical significance of CXCR3 and CXCR4 expression in primary melanoma.* Int J Cancer, 2005. **117**(5): p. 861-5.

302. Scala, S., et al., *Expression of CXCR4 predicts poor prognosis in patients with malignant melanoma.* Clin Cancer Res, 2005. **11**(5): p. 1835-41.

303. Mouton, P. R., *Unbiased stereology. A concise guide*. 2011: The Johns Hopkins University Press.

304. Robert, C., et al., *Pembrolizumab versus Ipilimumab in Advanced Melanoma.* N Engl J Med, 2015. **372**(26): p. 2521-32.

305. Xiao, Q., et al., *SDF1 gene variation is associated with circulating SDF1alpha level and endothelial progenitor cell number: the Bruneck Study.* PLoS One, 2008. **3**(12): p. e4061.

306. Wiesner, T., et al., *A distinct subset of atypical Spitz tumors is characterized by BRAF mutation and loss of BAP1 expression.* Am J Surg Pathol, 2012. **36**(6): p. 818-30.

307. Jensen, D. E. and F. J. Rauscher, 3rd, *Defining biochemical functions for the BRCA1 tumor suppressor protein: analysis of the BRCA1 binding protein BAP1.* Cancer Lett, 1999. **143 Suppl 1**: p. S13-7.

308. Jensen, D. E. and F. J. Rauscher, 3rd, *BAP1, a candidate tumor suppressor protein that interacts with BRCA1.* Ann N Y Acad Sci, 1999. **886**: p. 191-4.

309. Harbour, J. W., et al., *Frequent mutation of BAP1 in metastasizing uveal melanomas.* Science, 2010. **330**(6009): p. 1410-3.

310. Busam, K. J., et al., *Combined BRAF(V600E)-positive melanocytic lesions with large epithelioid cells lacking BAP1 expression and conventional nevomelanocytes.* Am J Surg Pathol, 2013. **37**(2): p. 193-9.

311. Wiesner, T., et al., *Kinase fusions are frequent in Spitz tumours and spitzoid melanomas.* Nat Commun, 2014. **5**: p. 3116.

312. O'Shea, S. J., Robles-Espinoza, C.D., McLellan, L., Harrigan, J., Jacq, X., Hewinson, J., Iyer, V., Merchant, W., Elliott, F., Harland, M., Bishop, D.T., Newton-Bishop, J.A., Adams, D.J., *A population-based analysis of germline BAP1 mutations in melanoma.* Human Molecular Genetics, 2017. **26**(4): p. 717–728.

313. Onken, M. D., et al., *Collaborative Ocular Oncology Group report number 1: prospective validation of a multi-gene prognostic assay in uveal melanoma.* Ophthalmology, 2012. **119**(8): p. 1596-603.
314. Champine, M. K., W.; Leachman S.A., *Genetic counseling and testing for hereditary melanoma: an updated guide for dermatologists.* Hereditary Genetics, 2013(S2).
315. Testa, J. R., et al., *Germline BAP1 mutations predispose to malignant mesothelioma.* Nat Genet, 2011. **43**(10): p. 1022-5.
316. Mochel, M. C., et al., *Loss of BAP1 Expression in Basal Cell Carcinomas in Patients With Germline BAP1 Mutations.* Am J Clin Pathol, 2015. **143**(6): p. 901-4.
317. de la Fouchardiere, A., et al., *Germline BAP1 mutations predispose also to multiple basal cell carcinomas.* Clin Genet, 2015. **88**(3): p. 273-7.
318. Klebe, S., et al., *BAP1 hereditary cancer predisposition syndrome: a case report and review of literature.* Biomark Res, 2015. **3**: p. 14.
319. Busam, K. J., M. Wanna, and T. Wiesner, *Multiple epithelioid Spitz nevi or tumors with loss of BAP1 expression: a clue to a hereditary tumor syndrome.* JAMA Dermatol, 2013. **149**(3): p. 335-9.
320. McDonnell, K. J., et al., *A novel BAP1 mutation is associated with melanocytic neoplasms and thyroid cancer.* Cancer Genet, 2016. **209**(3): p. 75-81.
321. Luchini, C., et al., *Different prognostic roles of tumor suppressor gene BAP1 in cancer: A systematic review with meta-analysis.* Genes Chromosomes Cancer, 2016. **55**(10): p. 741-9.
322. Soura, E., et al., *Hereditary melanoma: Update on syndromes and management: Emerging melanoma cancer complexes and genetic counseling.* J Am Acad Dermatol, 2016. **74**(3): p. 411-20; quiz 421-2.
323. Ismail, I. H., et al., *Germline mutations in BAP1 impair its function in DNA double-strand break repair.* Cancer Res, 2014. **74**(16): p. 4282-94.
324. Ventii, K. H., et al., *BRCA1-associated protein-1 is a tumor suppressor that requires deubiquitinating activity and nuclear localization.* Cancer Res, 2008. **68**(17): p. 6953-62.
325. Kadariya, Y., et al., *Bap1 Is a Bona Fide Tumor Suppressor: Genetic Evidence from Mouse Models Carrying Heterozygous Germline Bap1 Mutations.* Cancer Res, 2016. **76**(9): p. 2836-44.
326. Kumar, R., et al., *BAP1 has a survival role in cutaneous melanoma.* J Invest Dermatol, 2015. **135**(4): p. 1089-97.
327. Baughman, J. M., et al., *NeuCode Proteomics Reveals Bap1 Regulation of Metabolism.* Cell Rep, 2016. **16**(2): p. 583-95.

328. Kalirai, H., et al., *Lack of BAP1 protein expression in uveal melanoma is associated with increased metastatic risk and has utility in routine prognostic testing.* Br J Cancer, 2014. **111**(7): p. 1373-80.

329. Yeh, I., et al., *Ambiguous melanocytic tumors with loss of 3p21.* Am J Surg Pathol, 2014. **38**(8): p. 1088-95.

330. Da Forno, P. D., et al., *BRAF, NRAS and HRAS mutations in spitzoid tumours and their possible pathogenetic significance.* Br J Dermatol, 2009. **161**(2): p. 364-72.

331. Fullen, D. R., et al., *BRAF and NRAS mutations in spitzoid melanocytic lesions.* Mod Pathol, 2006. **19**(10): p. 1324-32.

332. Piris, A., M. C. Mihm, Jr., and M. P. Hoang, *BAP1 and BRAFV600E expression in benign and malignant melanocytic proliferations.* Hum Pathol, 2014.

333. Murali, R., et al., *BAP1 expression in cutaneous melanoma: a pilot study.* Pathology, 2013. **45**(6): p. 606-9.

334. Bastian, B. C., P. E. LeBoit, and D. Pinkel, *Mutations and copy number increase of HRAS in Spitz nevi with distinctive histopathological features.* Am J Pathol, 2000. **157**(3): p. 967-72.

335. Yeh, I., et al., *NTRK3 kinase fusions in Spitz tumours.* J Pathol, 2016.

336. Yeh, I., et al., *Activating MET kinase rearrangements in melanoma and Spitz tumours.* Nat Commun, 2015. **6**: p. 7174.

337. Lee, S., et al., *TERT Promoter Mutations Are Predictive of Aggressive Clinical Behavior in Patients with Spitzoid Melanocytic Neoplasms.* Sci Rep, 2015. **5**: p. 11200.

338. Zhao, Z. V., V.; Zhang, M., *Anaplastic lymphoma kinase: Role in cancer and therapy perspective.* Can Biol Ther, 2015. **16**(12): p. 1691-1701.

339. Soda, M. C., Y.L.; Enomoto, M.; Takada, S.; Yamashita, Y.; Ishikawa, S.; Fujiwara, S.; Watanabe, H.; Kurashina, K.; Hatanaka, H.; Bando, M.; Ohno, S.; Ishikawa, Y.; Aburatani, H.; Niki, T.; Sohara, Y.; Sugiyama, Y.; Mano, H., *Identification of the transforming EML4-ALK fusion gene in non-mall-cell lung cancer.* Nature, 2007. **448**: p. 561-566.

340. Lawrence, B. P.-A., A.; Hibbard, M.K.; Rubin, B.P.; Dal Cin, P.; Pinkus, J.L.; Pinkus, G.S.; Xiao, S.; Yi, E.S.; Fletcher, C.D.M.; Fletcher, J.A., *TPM3-ALK and TPM4-ALK oncogenes in inflammatory myofibroblastic tumours.* Am J Pathol, 2000. **157**(2): p. 377-384.

341. Lamant, L. D., N.; Pulford, K.; Delsol, G.; Mariame, B., *A new fusion gene TPM3-ALK in anaplastic large cell lymphoma created by a (1;2)(q25;p23) translocation.* Blood, 1999. **93**(9): p. 3088-3095.

342. Niu, H. Z., Q.; Wang, F.; Shao, Q.; Guan, Y.; Wen, X.; Chen, L.; Feng, Q.; Li, W.; Zeng, Y.; Zhang, X., *Identification of anaplastic lymphoma kinase break points and oncogenic mutation profiles in acral/mucosal melanomas.* PCMR, 2013. **26**(5): p. 646-653.

343. Shaw, A. T. K., D.W.; Nakagawa, K.; Seto, T.; Crino, L.; Ahn, M.J.; De Pas, T.; Besse, B.; Solomon, B.J., Blackhall, F.; Wu, Y.;Thomas, M.; O'Byrne, K.J.; Moro-Sibilot, D.; Camidge D.R.; Mok, T.; Hirsh, V.; Riely, G.J.; Iyer, S.; Tassell, V.; Polli, A.; Wilner, K.D.; Janne, P.A., *Crizotinib versus chemotherapy in advanced ALK-positive lung cancer.* N Engl J Med, 2013. **368**(25): p. 2385-94.

344. Solomon, B. J. M., T.; Kim, D.; Wu, Y.; Nakagawa, K.; Mekhail, T.; Felip, E.; Cappuzzo, F.; Paolini, J.; Usari, T.; Iyer, S.; Reisman, A.; Wilner, K.D.; Tursi, J.; Blackhall, F., *First-line crizotinib versus chemotherapy in ALK-positive lung cancer.* N Engl J Med, 2014. **371**(23): p. 2167-2177.

345. Busam, K. J. V., R.E.; Lum, T.; Busam, J.A.; Hollmann, T.J.; Saw, R.P.M.; Coit, D.C.; Scolyer, R.A.; Wiesner, T., *Primary and metastatic cutaneous melanomas express ALK through alternative transcriptional initiation.* Am J Surg Pathol, 2016. **40**(6): p. 786-795.

346. Uguen, A., Uguen, M.; Guibourg, B., *ALK expression in melanomas. Looking for a needle in a haystack.* Am J Surg Pathol, 2016. **40**(10): p. 1437.

347. Ng, P. C. H., S., *SIFT: predicting amino acid changes that affect protein function.* Nucleic Acids Res, 2003. **31**(13): p. 3812-4.

348. Adzhubei, I. A. J., D.M.; Sunyaev, S.R., *Predicting functional effect of human missense mutations using PolyPhen-2*, in *Curr Protoc Hum Genet*, 2013.

349. Ladanyi, M., et al., *New strategies in pleural mesothelioma: BAP1 and NF2 as novel targets for therapeutic development and risk assessment.* Clin Cancer Res, 2012. **18**(17): p. 4485-90.

350. Eletr, Z. M., L. Yin, and K. D. Wilkinson, *BAP1 is phosphorylated at serine 592 in S-phase following DNA damage.* FEBS Lett, 2013. **587**(24): p. 3906-11.

351. Machida, Y. J., et al., *The deubiquitinating enzyme BAP1 regulates cell growth via interaction with HCF-1.* J Biol Chem, 2009. **284**(49): p. 34179-88.

352. Sahtoe, D. D., et al., *BAP1/ASXL1 recruitment and activation for H2A deubiquitination.* Nat Commun, 2016. **7**: p. 10292.

353. LaFave, L. M., et al., *Loss of BAP1 function leads to EZH2-dependent transformation.* Nat Med, 2015. **21**(11): p. 1344-9.

354. Kee, Y. and T. T. Huang, *Role of Deubiquitinating Enzymes in DNA Repair.* Mol Cell Biol, 2016. **36**(4): p. 524-44.

355. *TCGA Fusion Gene Data Portal. Landscape of cancer-associated fusions using Pipeline for RNA sequencing Data Analysis*. [cited; Available from: http://54.84.12.177/PanCanFusV2/.

356. Rai, K., et al., *Comprehensive review of BAP1 tumor predisposition syndrome with report of two new cases.* Clin Genet, 2015.

357. Ellerhorst, J. A., et al., *Clinical correlates of NRAS and BRAF mutations in primary human melanoma.* Clin Cancer Res, 2011. **17**(2): p. 229-35.

358. Amano, M. H., T.; Hasanuzzaman Shohag, Md.; Kozawa, K.; Kato, K.; Zhang, X.; Yura, Y.; Matsuura, Y.; Kataoka, C.; Nishioka, T.; Kaibuchi, K., *Kinase-interacting substrate screening is a novel method to identify kinase substrates.* J Cell Biol, 2015. **209**(6): p. 895-912.

359. Graw, J., *Genetics of crystallins: cataracts and beyond.* Experimental Eye Research, 2009. **88**: p. 173-189.

360. Suzuki, S. S., N.; Mori, J.' Oshima, A.; Usami, S.; Hashizume, K., *Mu-crystalin as an intracellular 3,5,3'-triiodothyronine holder in vivo.* Mol Endocrinol, 2007. **21**(4): p. 885-894.

361. Oshima, A. S., S.; Takumi, Y.; Hashizume, K.; Abe, S.; Usami, S., *CRYM mutations cause deafness through thyroid hormone binding properties in the fibrocytes of the cochlea.* J Med Genet, 2006. **43**(e25).

362. cBioPortal. *CBioPortal for cancer genomics*. 2016. [cited 18th December 2016]; Available from: http://www.cbioportal.org.

363. Malinowska, K. C., I.T.; Susani, M.; Wrulich, O.A.; Uberall, F.; Kenner, L.; Culig, Z., *Identification of mu-crystallin as an androgen-regulated gene in human prostate cancer.* The Prostate, 2009. **69**: p. 1109-1118.

364. Davidson, B. A., W.M.; Forsund, M.; Holth, A.; Yang, Y.; Kobayashi, Y.; Chen, L.; Kristensent, G.B.; Shih, I.; Wang, T., *Gene expression signatures of primary and metastatic uterine leiomyosarcoma.* Human Pathology, 2014. **45**: p. 691-700.

365. Reddy, R. B. B., A.R.; James, B.L.; Govindan, S.V.; Mathew, R.; Dr, R.; Hedne, N.; Illiayaraja, J.; Kekatpure, V.; Khora, S.S.; Hicks, W.; Tata, P.; Kuriakose, M.A.; Suresh, A., *Meta-analyses of microarray data sets identifies ANO1 and FADD as prognostic markers of head and neck cancer.* PLoS One, 2016. **11**(1): p. e0147409.

366. Robert, C., et al., *Nivolumab in previously untreated melanoma without BRAF mutation.* N Engl J Med, 2015. **372**(4): p. 320-30.

367. Fleming, N. H., et al., *Impact of age on the management of primary melanoma patients.* Oncology, 2013. **85**(3): p. 173-81.

368. Kretschmer, L., et al., *Age as a key factor influencing metastasizing patterns and disease-specific survival after sentinel lymph node biopsy for cutaneous melanoma.* Int J Cancer, 2011. **129**(6): p. 1435-42.

369. Page, A. J., et al., *Increasing Age Is Associated with Worse Prognostic Factors and Increased Distant Recurrences despite Fewer Sentinel Lymph Node Positives in Melanoma.* Int J Surg Oncol, 2012. **2012**: p. 456987.

370. Munsch, C., et al., *Breslow thickness, clark index and ulceration are associated with sentinel lymph node metastasis in melanoma patients: a cohort analysis of 612 patients.* Dermatology, 2014. **229**(3): p. 183-9.

371. Mirisola, V., et al., *CXCL12/SDF1 expression by breast cancers is an independent prognostic marker of disease-free and overall survival.* Eur J Cancer, 2009. **45**(14): p. 2579-87.

372. Mego, M., et al., *CXCR4-SDF-1 interaction potentially mediates trafficking of circulating tumor cells in primary breast cancer.* BMC Cancer, 2016. **16**: p. 127.

373. Wu, W., et al., *Prognostic significance of CXCL12, CXCR4, and CXCR7 in patients with breast cancer.* Int J Clin Exp Pathol, 2015. **8**(10): p. 13217-24.

374. Rave-Frank, M., et al., *Prognostic value of CXCL12 and CXCR4 in inoperable head and neck squamous cell carcinoma.* Strahlenther Onkol, 2016. **192**(1): p. 47-54.

375. Scala, S., et al., *CXC chemokine receptor 4 is expressed in uveal malignant melanoma and correlates with the epithelioid-mixed cell type.* Cancer Immunol Immunother, 2007. **56**(10): p. 1589-95.

376. Cho-Vega, J. H., *A diagnostic algorithm for atypical spitzoid tumors: guidelines for immunohistochemical and molecular assessment.* Mod Pathol, 2016. **29**(7): p. 656-70.

377. Stratton, M. R., *Journeys into the genome of cancer cells.* EMBO Mol Med, 2013. **5**(2): p. 169-72.

378. Alexandrov, L. B. and M. R. Stratton, *Mutational signatures: the patterns of somatic mutations hidden in cancer genomes.* Curr Opin Genet Dev, 2014. **24**: p. 52-60.